UNIVERSIDAD NACIONAL AUTÓNOMA DE MÉXICO

PROGRAMA DE POSGRADO EN CIENCIAS DE LA TIERRA

INSTITUTO DE GEOLOGÍA

Registro y Condiciones Paleoambientales de Eventos Anóxicos Oceánicos del Cretácico en el Margen Occidental del proto-Atlántico Norte: Norte y Centro de México

---

Record and paleoenvironmental conditions of Cretaceous Oceanic Anoxic Events on the western margin of the proto-North Atlantic Ocean: North and Central Mexico

Que para optar por el grado de Doctor en Ciencias de la Tierra

PRESENTA:

Fernando Núñez Useche

COMITÉ TUTOR

Dr. Ricardo Barragán Manzo (Director), Instituto de Geología-UNAM
Dr. Madhavaraju Jayagopal, Instituto de Geología-UNAM
Dra. Elena Centeno García, Instituto de Geología-UNAM

JURADO EXAMINADOR

Dr. Martín Merino Ibarra, Instituto de Ciencias del Mar y Limnología-UNAM
Dr. José Manuel Grajales Nishimura, Instituto de Geología-UNAM
Dr. Rubén López Doncel, Universidad Autónoma de San Luis Potosí
Dr. Carles Canet, Instituto de Geofísica-UNAM
Dr. Ricardo Barragán Manzo, Instituto de Geología-UNAM

México, Ciudad de México, Mayo de 2016

Núñez-Useche, F., 2016. Registro y Condiciones Paleoambientales de Eventos Anóxicos Oceánicos del Cretácico en el Margen Occidental del proto-Atlántico Norte: Norte y Centro de México. Tesis de Doctorado. Universidad Nacional Autónoma de México.

La realización de esta tesis fue posible gracias al apoyo de:

BECA PARA ESTUDIOS DE DOCTORADO

PROYECTO CONACyT-SEP 177510

PROYECTO PAPIIT IN 109912, DGAPA, UNAM

PROYECTO PAPIIT IN 101914, DGAPA, UNAM

BECA PARA ESTUDIOS DE DOCTORADO

APOYO LOGÍSTICO PARA EL DESARROLLO DEL PROYECTO

INSTITUTO MEXICANO DEL PETRÓLEO

PATROCINIO DE ANÁLISIS GEOQUÍMICOS

Generalitat de Catalunya

PROYECTO 2009 GR-0044

BECA PARA INVESTIGACIÓN OTORGADA AL AUTOR

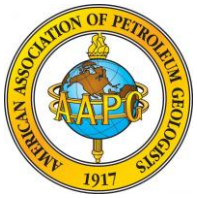

BECA CONMEMORATIVA DANA RUSSEL PARA INVESTIGACIÓN OTORGADA AL AUTOR

Para ustedes:
Luz Dary, Fernando,
Angélica y Jeisson

Agradecimientos

Aprecio de forma sincera y profunda el apoyo económico otorgado por varias instituciones para mi manutención y para el desarrollo de este proyecto. Igualmente, la guía dada por mi tutor, Ricardo Barragán, quien jugó un papel sustancial para que este trabajo llegara a buen puerto. También agradezco a Carles Canet por su importante ayuda y confianza.

Los datos presentados en esta trabajo fueron posible gracias al valioso apoyo de Josep Moreno, Teresa Pi, Ana Luisa Carreño, Eliza Fitz, Priyadarsi Debajyoti, Fabián Durán, Griselda Abascal, Mario Ramos, Rafael López, Blanca Estela Buitrón, David Zamudio, Edith Cienfuegos, Francisco Javier Otero, Rafael Puente, Margarita Reyes, Sonia Ángeles, Yolanda Hornelas, Carlos Linares, Kumiko Shimada, Lucy Mora, Isaac Hernández, Gabriela Solís, Gerardo Arrieta, Teodoro Hernández, Jaime Díaz y Martha Lagunas.

Agradezco los acertados comentarios hechos a los manuscritos por Miguel Company, Hugh Jenkyns, Hermann Darío Bermúdez, Michel Moullade Bruno Granier, Phil Salvador, Florentin Maurrasse, Alexis Godet, José Manuel Castro, Karl Föllmi, Thierry Corrège y Patriz Zell. Sin duda, sus críticas ayudaron a mejorar la calidad de los artículos.

Gracias totales a mi familia, amigos y maestros, de aquí, de allí y de allá, por alentarme a dar cada paso y soportarme.

La presente tesis está conformada por 5 manuscritos (publicados/sometidos) en revistas arbitradas e indizadas de carácter nacional e internacional. A continuación se describe la contribución del autor a cada uno de ellos:

1) Mexican archives for the major Cretaceous Oceanic Anoxic Events

-Autores: Fernando Núñez-Useche, Ricardo Barragán, Josep Anton Moreno-Bedmar y Carles Canet

-Revista: Boletín de la Sociedad Geológica Mexicana.

-Estatus: publicado

-Contribución: concepción y diseño del estudio; revisión y análisis bibliográfico y redacción del artículo.

2) A negative carbon isotope excursion within the Dufrenoyia furcata Zone: proposal for a new episode for chemostratigraphic correlation in the Aptian

-Autores: Fernando Núñez-Useche, Josep Anton Moreno-Bedmar, Miguel Company y Ricardo Barragán

-Revista: Carnets de Géologie [Notebooks on Geology]

-Estatus: publicado

-Contribución: revisión y análisis bibliográfico y redacción del artículo.

3) Geochemical and paleoenvironmental record of the early to early late Aptian major episodes of accelerated change

-Autores: Fernando Núñez-Useche, Ricardo Barragán, Josep Anton Moreno-Bedmar y Carles Canet.

-Revista: Sedimentary Geology

-Estatus: publicado

-Contribución: parte de la concepción y diseño del estudio; trabajo de campo; análisis sedimentológico y de microfacies; preparación de muestras para análisis geoquímicos y de láminas doblemente pulidas; adquisición de datos de conteo y tamaño de framboides, análisis e interpretación de datos y redacción del artículo.

4) Record of upper Aptian–lower Albian environmental perturbation in northeastern Mexico

-Autores: Fernando Núñez-Useche, Ricardo Barragán, Carles Canet y Rafael Antonio López-Martínez

-Revista: Journal of South American Earth Sciences

-Estatus: sometido

-Contribución: concepción y diseño del estudio, preparación de muestras para análisis geoquímicos, análisis e interpretación de datos y redacción del artículo.

5) Bioevents and redox conditions around the Cenomanian–Turonian anoxic event in Central Mexico

-Autores: Fernando Núñez-Useche, Carles Canet, Ricardo Barragán y Pura Alfonso.

-Revista: Palaeogeography, Palaeoclimatology, Palaeoecology

-Estatus: publicado

-Contribución: concepción y diseño del estudio; trabajo de campo; análisis sedimentológico y de microfacies; preparación de muestras para análisis geoquímicos; identificación de bioeventos, adquisición de datos de microsonda y microscopio electrónico; conteo y medición de framboides, análisis e interpretación de datos y redacción del artículo.

RESUMEN

La aplicación de un estudio integral en rocas carbonatadas del Cretácico en México provee información sobre el registro y las condiciones paleoambientales de episodios de cambio global acelerado. En el norte de México, el Evento Anóxico Oceánico 1a (Aptiano temprano) está registrado en las facies lagunares y de barras de ooides de la unidad Cupidito (parte superior de la Formación Cupido) , y en su parte inferior corresponde a sedimentos enriquecidos en materia orgánica (hasta 5.15%) . Este evento se asocia con una excursión isotópica negativa de carbono de 2.86‰ seguida de un variación positiva de 3.25‰. Las fases previa e inicial del OAE 1a tuvieron lugar durante intervalos intermitentes de condiciones más cálidas y húmedas que activaron la llegada de material detrítico y nutrientes a la laguna Cupidito. Esto elevó la productividad marina y causó condiciones redox de fondo variables. La parte final del OAE 1a estuvo asociada a una fase de alcalinidad y condiciones climáticas menos extremas. Mientras varias plataformas carbonatadas en el Tetis desaparecieron y fueron ahogadas, la plataforma Cupido sobrevivió al OAE 1a. Hacia la cima de la Formación Cupido se encuentra una excursión isotópica negativa de carbono de 0.7‰ que es correlacionable con el evento IFNE (Intra-Furcata Negative Excursion; Aptiano temprano tardío) , propuesto como un nuevo marcador quimio-estratigráfico global para el Aptiano. La parte baja de la Formación La Peña contiene el registro de los niveles Aparein (final del Aptiano temprano) y Noire (Aptiano tardío temprano) , correspondientes con intervalos ricos en materia orgánica (hasta 8.72% y 18.39%, respectivamente) . El primero está asociado con condiciones eutróficas climáticamente inducidas, posible estancamiento de la columna de agua y un régimen anóxico-disóxico de fondo. El segundo está también relacionado con condiciones eutróficas pero vinculadas a la acción de un sistema local de surgencia y anoxia marina en el fondo. En la parte media de la Formación La Peña está registrado el OAE 1b (Aptiano-Albiano) . Este evento corresponde a una excursión isotópica negativa de carbono de 2.09‰ que ocurre a lo largo de un intervalo enriquecido en materia orgánica (hasta 7.5%) . Durante este evento tuvo lugar un pico climático extremo de condiciones húmedas y cálidas que aumentaron el arribo de material detrítico y causó estratificación de la columna de agua y condiciones de fondo empobrecidas en oxígeno.

En el centro de México, el OAE 2 (Cenomaniano-Turoniano) está registrado en las facies pelágicas de la Formación Agua Nueva. El intervalo equivalente a este evento presenta una mayor concentración de materia orgánica marina (hasta 3.32%) y fue reconocido mediante la identificación de bioeventos, principalmente del cambio en la abundancia de foraminíferos planctónicos del género *Heterohelix* y del evento de filamentos, ambos reportados por primera vez en México. La alta productividad marina, controlada parcialmente por la caída de ceniza volcánica en la cuenca, desencadenó condiciones anóxicas-disóxicas de fondo durante el evento anóxico y más oxigenadas luego de su ocurrencia. El máximo valor de fraccionamiento isotópico de azufre (72.2‰) dentro del OAE 2 está asociado a un mayor enterramiento de materia orgánica y disponibilidad de sulfato. Esto reafirma la propuesta de un mecanismo global que controló la composición isotópica del azufre durante este evento.

ABSTRACT

The application of an integrated study provides information about the record and paleoenvironmental conditions of episodes of accelerated global change. In northern Mexico, the Oceanic Anoxic Event (OAE) 1a (early Aptian) is recorded within the lagoonal and ooids shoal facies of the Cupidito unit (upper part of the Cupido Formation) , and its lower part corresponds to sediments enriched in organic matter (up to 5.15%) . This event is associated with a negative carbon isotope excursion of 2.86‰ followed by a positive variation of 3.25‰. Previous and initial phases of this event took place during intermittent intervals characterized by warmer and more humid conditions that triggered the arrival of detrital material and nutrients to the Cupidito lagoon. This enhanced the marine productivity and resulted in variable bottom-water redox conditions. The final part of the OAE 1a was related to a phase of alkalinity and less extreme climate conditions. Whereas several tethyan carbonate platforms experienced demise and drowning during OAE 1a, the Cupido platform survived this event. Toward the top of the Cupido Formation there is a negative carbon isotope excursion of 0.7‰ that is correlatable with the IFNE (Intra-Furcata Negative Excursion; late early Aptian) , proposed herein as a new global chemostratigraphic marker for the Aptian record. The lower part of the La Peña Formation contains the record of the Aparein (latest early Aptian) and Noire (early late Aptian) levels, corresponding to stratigraphic intervals enriched in organic matter (up to 8.72% y 18.39%, respectively) . The first one is associated with climatically induced eutrophic marine conditions, water column stratification and anoxic-dysoxic settings. The second one is also related to eutrophic marine conditions but linked to a local upwelling system and bottom-water anoxia. The middle part of the La Peña Formation contains the record of the OAE 1b (Aptian-Albian) . Such event corresponds to a long-term negative carbon isotope excursion of 2.09‰ through an interval enriched in organic matter (up to 7.5%) . During this event, a peak of extreme warm and humid climate conditions that increased the arrival of detrital material and caused water column stratification and oxygen-depleted bottom-water conditions took place.

In central Mexico, the OAE 2 (Cenomanian-Turonian) is recorded within the organic-rich pelagic facies of the Agua Nueva Formation (Tampico-Misantla Basin) . The OAE 2 time-equivalent interval shows a higher concentration of organic matter (up to 3.32%) and was herein recognized through the identification of characteristic bioevents, mainly the increase in abundance of planktonic foraminifera of genus *Heterohelix* (*Heterohelix* shift) and the filament event, both reported for the first time in Mexico. High marine productivity, partially controlled by intrabasinal vocanic ash-fall, favored anoxic-dysoxic bottom-water conditions during the anoxic event, and more oxygenated waters thereafter. Maximum value of sulfur isotope fractionation (72.2‰) within the OAE 2 is related to a higher organic matter burial and sulfate availability. This fact confirms the proposal of a global mechanism that controlled the sulfur isotope signature during this event.

ÍNDICE GENERAL

El planeta durante el Cretácico (hace 105 Ma)

CAPÍTULO 1

INTRODUCCIÓN

INTRODUCCIÓN

El Cretácico –conocido como el mundo del efecto invernadero– es un periodo durante el que diversos y significativos cambios globales en el sistema litósfera-océano-atmósfera impactaron profundamente y de forma única la evolución del planeta (Föllmi et al., 2006; Weissert y Erba, 2004; Méhay et al., 2009; Föllmi, 2012; Erba et al. 2015) . Dichas transformaciones desencadenaron una serie de prominentes eventos de cambio global acelerado asociados con extremas perturbaciones climáticas, alteración de los ciclos biogeoquímicos de varios elementos, variación de los patrones evolutivos de flora y fauna marina y continental, y significativas modificaciones en los ambientes sedimentarios (Menegatti et al., 1998; Leckie et al., 2002; Erba et al., 2010; Herrle et al., 2004; Föllmi, 2012) . En el marco de algunos de estos intensos periodos de cambio global surgieron los Eventos Anóxicos Oceánicos (OAEs) (Schlanger y Jenkyns, 1976; Arthur y Schlanger, 1979) , a modo de efectivas válvulas reguladoras que permitieron acentuar gradualmente sus efectos. Durante estos episodios tuvieron lugar considerables variaciones en el ciclo del carbono y un marcado aumento en el depósito de sedimentos enriquecidos en materia orgánica en varias cuencas oceánicas. Dicha acumulación, casi sincrónica, estuvo vinculada con un incremento en la productividad marina, una lenta circulación oceánica y el empobrecimiento en oxígeno de la masa de agua intermedia y de fondo (Schlanger y Jenkyns, 1976; Leckie et al., 2002; Núñez-Useche et al., 2015; Sabatino et al., 2015) .

1.1 EL ESCENARIO DEL CRETÁCICO Y SU RELACIÓN CON LOS EVENTOS ANÓXICOS OCEÁNICOS

El rompimiento de Pangea al final del Triásico-inicio del Jurásico resultó en diversos bloques continentales separados por cuencas oceánicas en nacimiento. La separación y deriva de bloques durante el Cretácico puede considerarse como el principal evento conductor de los cambios litotectónicos, oceanográficos y climáticos ocurridos durante este periodo (Figs. 1 y 2) . Como resultado de la apertura del Atlántico, a partir del Aptiano comenzó una enorme producción de corteza oceánica en las dorsales y se incrementó dramáticamente la actividad volcánica en el interior y los límites de las placas (Larson, 1991a, b) . Mientras el promedio de la tasa de producción de corteza oceánica en los últimos 70–80 millones de años ha sido 18–20 × 10^6 km^3/Ma, hace 120–125 millones de años la producción se incrementó hasta 35 × 10^6 km^3/Ma y se mantuvo así por cerca de 40 millones de años. Según Skelton (2003) , puesto que la tasa de expansión del suelo oceánico más alta durante el Cretácico fue de 17 cm/año – cifra similar a la tasa más rápida que se observa actualmente en la dorsal Pacífico-Nazca– antes que a una exageradamente rápida expansión del suelo oceánico, este incremento se asoció a una longitud anormalmente extensa de dorsales con expansión rápida. Otro factor que

contribuyó a este aumento en la producción de corteza oceánica fue el extraordinario ascenso de enormes plumas de magma provenientes del manto; hecho que ocasionó erupciones volcánicas submarinas masivas y el emplazamiento de las Grandes Provincias Ígneas en el Océano Pacífico y el sur del Océano Índico (Larson, 1991a; Snow y Duncan, 2005; Kidder y Worsley, 2010; Föllmi 2012; Erba et al., 2015) . Las erupciones asociadas a la construcción de estas mesetas submarinas liberaron enormes cantidades volátiles y partículas sólidas, así como elementos mayores, menores y trazas al sistema océano-atmósfera mediante la desgasificación magmática y el intercambio hidrotermal agua-roca. Esto causó un importante impacto en las condiciones climáticas, geoquímicas y bióticas de los océanos.

La intensa actividad volcánica durante el Cretácico promovió la liberación a la atmósfera de inmensas concentraciones de CO_2. Por ejemplo, Méhay et al. (2009) estiman que el emplazamiento de la meseta de Ontong-Java durante el Barremiano tardío-Aptiano temprano (la provincia ígnea más gran del mundo con una extensión de 1.9×10^6 km^2 y un volumen de 44.4×10^6 km^3) resultó en la liberación de casi 9 600 Gt de CO_2. En general, las concentraciones se elevaron hasta 1200–4800 ppm (Berner, 1994; Bergman et al., 2004; Kidder y Worsley, 2012; Wang et al., 2013) . Estos valores, entre 4 y 16 veces mayores que los niveles pre-industriales y actuales (280–400 ppm) , y similares a los que se calculan para el año 2100 (Meehl et al., 2007) , incrementaron la temperatura global, ocasionaron el establecimiento de condiciones de efecto invernadero y generaron un débil gradiente latitudinal de la temperatura que ocasionó la ausencia de cubiertas de hielo y el surgimiento de extensos bosques en las zonas polares (Chumakov et al., 1995; Beerling y Royer, 2002; Harland et al., 2007) . La temperatura promedio de la superficie terrestre y marina llegaron a estar 15°C y 10°C por encima de la actual, respectivamente (Skelton, 2003) . Sin embargo, valores máximos en la superficie marina se alcanzaron durante el Turoniano con valores promedio de 33–34°C (hasta 42°C) en las zonas tropicales y 30–32°C (hasta 20°C) en el Atlántico Sur subpolar (Bice y Norris, 2002; Keller, 2008; Hay y Floegel, 2012; van Helmond, 2013) . Para este tiempo, la temperatura promedio de la masa de agua profunda y de fondo excedió los 10°C, llegando a 20°C en el Atlántico Norte (Brass et al., 1982; Huber et al., 1999) . Algunas investigaciones (Frakes, 1999; Weissert y Lini, 1991; Steuber et al. 2005; Li et al., 2015) sugieren que a pesar de la existencia de fases cálidas de larga duración, dichas condiciones climáticas fueron en general inestables y se interrumpieron por episodios cortos de enfriamiento global. Estos estudios incluso sugieren que condiciones sub-congelantes y congelantes, favorables para la formación de capas de hielo, debieron existir en ciertas áreas de las altas latitudes durante determinados periodos de tiempo. Por ejemplo, temperaturas de hasta 4°C han sido calculadas para la superficie marina del Atlántico subtropical durante el Aptiano-Albiano (Herrle et al., 2015) . Este enfriamiento pudo ser inducido por la ceniza volcánica y los gases expulsados a la atmósfera, la disminución periódica de los niveles de CO_2 asociados con la alta tasa de intemperismo de rocas silicatadas y el enterramiento de materia orgánica (Sinninghe Damsté et al., 2010; Jarvis et al., 2011) .

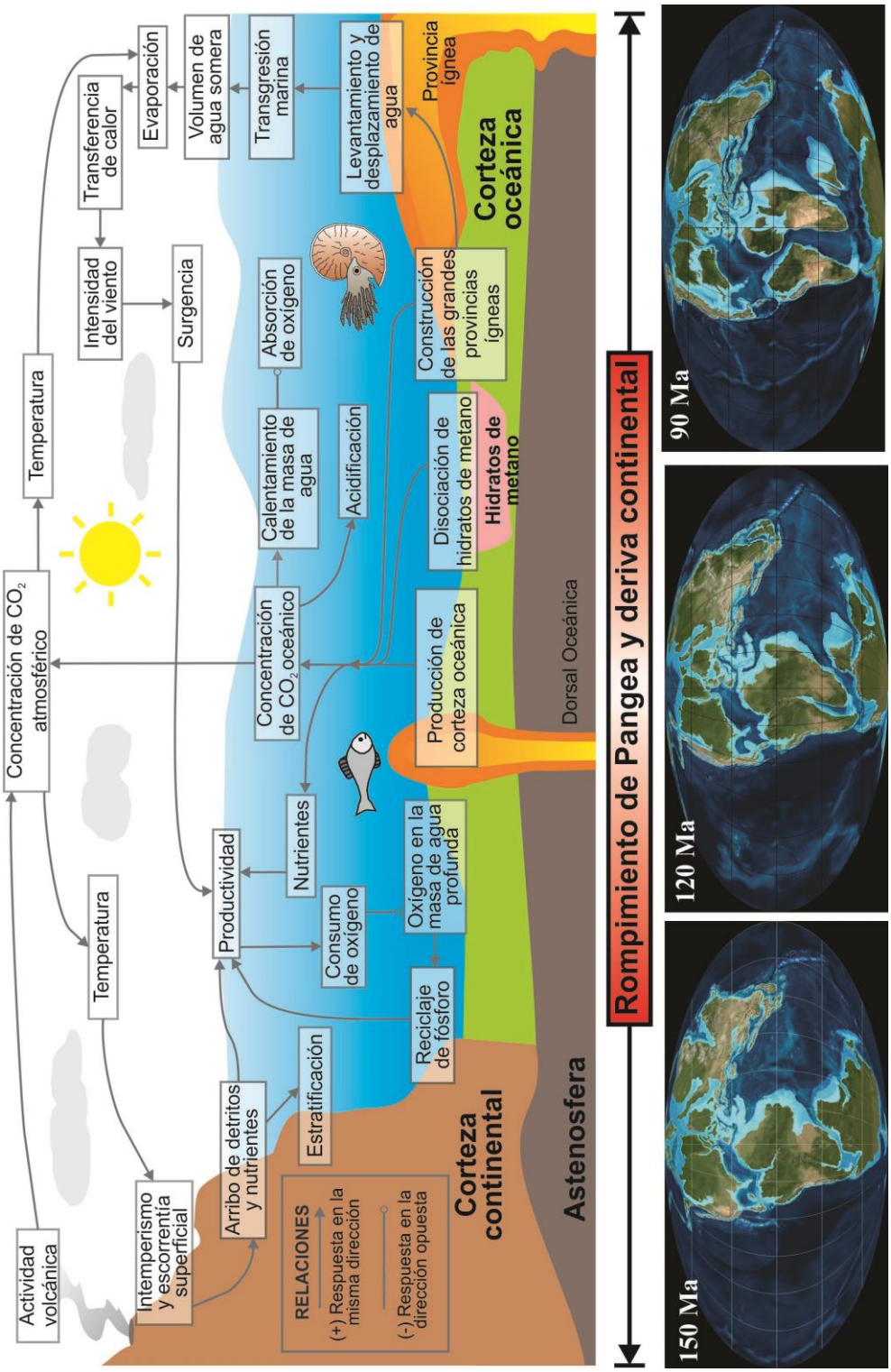

Figura 1. Diagrama resumiendo la relación entre los distintos factores litosféricos, oceánicos y atmosféricos que propiciaron la acumulación de materia orgánica en los sedimentos marinos durante los Eventos Anóxicos Oceánicos del Cretácico. Núñez-Useche (2016) : Basado en Meyers y Kump (2008) y Westermann et al. (2013) .

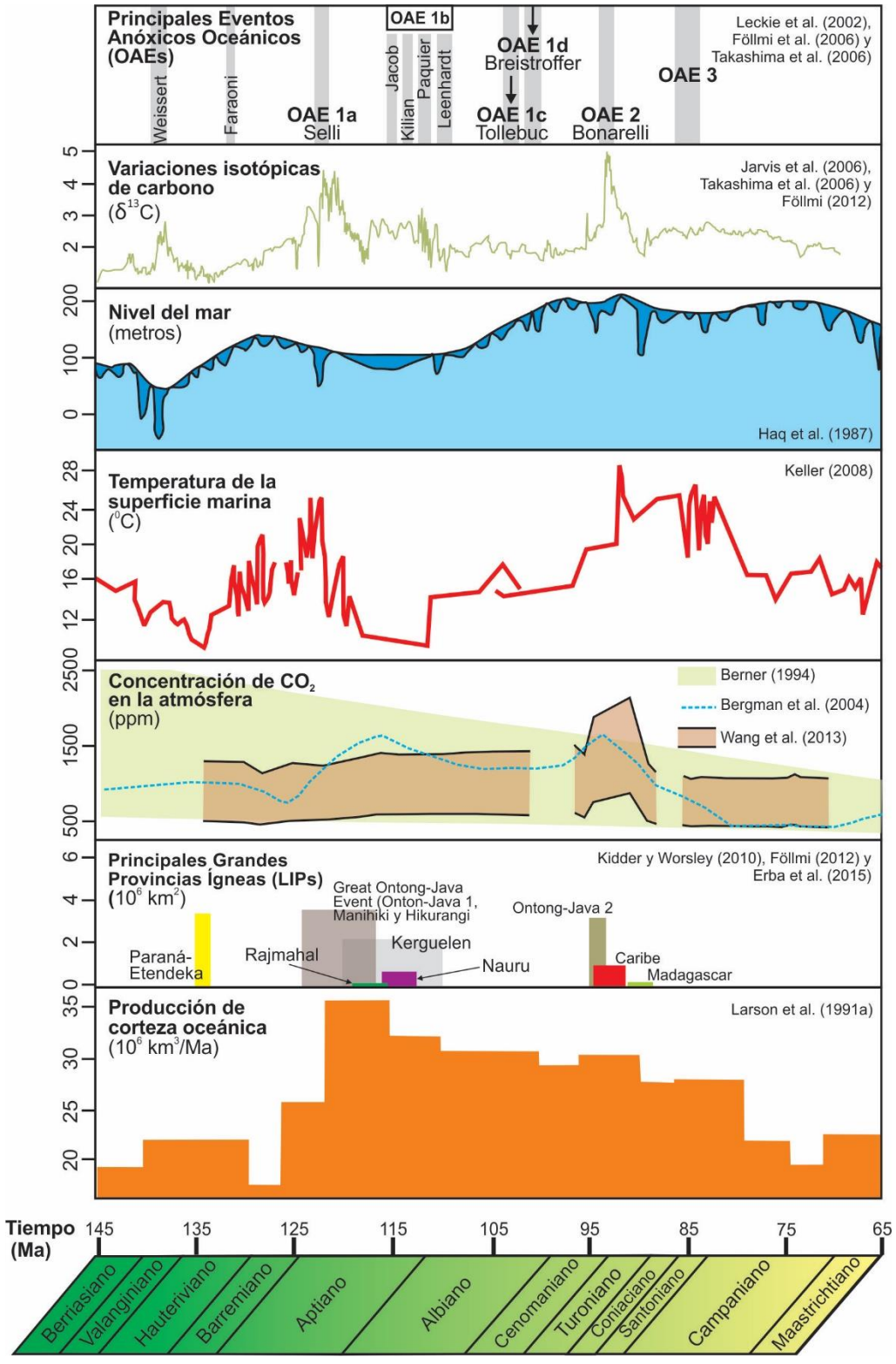

Figura 2. Principales cambios en diferentes geosferas durante el Cretácico y Eventos Anóxicos Oceánicos.

El calentamiento generalizado de la masa de agua oceánica y presumiblemente la rápida epirogénesis y disminución de la presión hidrostática relacionadas con el emplazamiento de las superplumas submarinas causaron a la vez la desestabilización de hidratos de gas metano de origen termogénico y biogénico. Estos se encontraban congelados bajo el suelo oceánico de los márgenes continentales, y su catastrófica liberación a la masa de agua y atmósfera ocurrió en varios pulsos intermitentes (Jahren, 2002; Wagner et al., 2007; Méhay et al., 2009; Bottini et al. 2012) . Simulaciones numéricas de Wagner et al. (2007) sugieren que durante el Albiano temprano se liberaron cerca de 1.15×10^{18} g de metano, cifra que se encuentra en el rango de las emisiones actuales de este gas en el suelo oceánico ($1–10 \times 10^{18}$ g; Milkov, 2004) . Una vez liberado, el metano reforzó los altos niveles de CO_2 y el calentamiento planetario. Además, su oxidación en la columna de agua contribuyó a disminuir la solubilidad del oxígeno y crear condiciones anóxicas-disóxicas sobre el fondo marino.

El aumento global de la temperatura trajo consigo un clima más húmedo y vigoroso, la aceleración del ciclo hidrológico y un incremento en las tasa de intemperismo en las zonas continentales. Handond y Lenton (2003) calculan que la tasa de intemperismo aumentó hasta un 20–25% hace 120–100 millones de años. Este escenario también intensificó la precipitación y escorrentía superficial, al igual que el arribo de material detrítico, nutrientes y materia orgánica continental a las cuencas oceánicas (Takashima et al., 2006; Meyers, 2006; Föllmi, 2012; Núñez-Useche et al., 2015) . Condiciones más fértiles en la masa de agua superficial estimularon una alta productividad marina, incrementando a la vez la demanda de oxígeno en la parte intermedia de la columna de agua. Esto propició el desarrollo de zonas de mínimo oxígeno a escala regional y global, favorables para la preservación de materia orgánica en los sedimentos (Leckie et al., 2002; Meyer y Kump, 2008; Adams et al., 2010; Trabucho Alexandre et al., 2010; Núñez-Useche et al., 2015; Reolid et al., 2015) . Adicionalmente, las altas temperaturas de la superficie marina disminuyeron la capacidad de absorción y retención de oxígeno de la columna de agua. Bajo estas condiciones, las cuencas marinas aisladas se volvieron aún más anóxicas y se transformaron en sumideros para el depósito de materia orgánica (Zimmerman et al., 1987; Poulsen, 2001) .

Como resultado de las elevadas temperaturas y del desplazamiento de enormes volúmenes de agua por la acción de las extensas dorsales oceánicas y el marcado crecimiento de superplumas asociadas a promontorios en el fondo marino, el nivel del mar aumentó, las áreas inundadas en los márgenes continentales se expandieron y tuvo lugar la formación de grandes mares epicontinentales (Arthur et al., 1987; Schlanger et al., 1987; Leckie et al., 2002) . Datos de Haq et al. (1987) y Hardenbol et al. (1998) revelan que durante el Cretácico el nivel del mar alcanzó 200 m por encima del nivel actual. Las transgresiones y las permanencias altas del nivel del mar fueron clave para inundar las zonas costeras, ampliar geográficamente la extensión de las plataformas carbonatadas someras y amplificar las zonas de mínimo oxígeno. Bigg (2003) estima que cerca del 20%

de las áreas costeras actuales fueron inundadas durante el Cretácico, favoreciendo el retrabajo de los sedimentos y suelos y el arribo de nutrientes a las zonas costeras. Además, los altos niveles de CO_2 atmosférico ocasionaron acidificación oceánica (Méhay et al., 2009; Kidder y Worsley, 2010; Hay y Floegel, 2012; Erba et al., 2015) , fenómeno oceanográfico que afectó la saturación de carbonato y su exportación a los sedimentos marinos (Kędzierski et al., 2012; Gambacorta et al., 2015) y contribuyó a la desaparición y rápida tasa evolutiva de varias formas de vida (Leckie et al., 2002; Weissert y Erba, 2004; Erba y Tremolada, 2004; Erba et al., 2010) . Por ejemplo, durante el Cenomaniano-Turoniano, todos estos cambios ocasionaron la séptima extinción masiva más grande de los últimos 250 millones de años en la que desaparecieron cerca del 26% de los géneros (Sepkoski, 1989) . Por otro lado, las altas temperaturas también promovieron la evaporación excesiva en zonas tropicales y subtropicales y la respectiva formación de masas de agua densas, salinas y empobrecidas en oxígeno. Esto activó una circulación halotermal en la que estas masas de agua se hundieron y retornaron a la superficie tanto en zonas ecuatoriales como de latitud alta (Poulsen et al., 2001: Bigg, 2003; Hay et al., 2006) . Este escenario difirió significativamente de la circulación termohalina actual gobernada por la formación y hundimiento de masas de agua fría y densa en los polos y su ascenso en las zonas tropicales. Al formar parte de la masa de agua profunda, las masas de agua cretácicas produjeron bajas tasas de ventilación del fondo oceánico, reforzando nuevamente las condiciones anóxicas y euxínicas, principalmente en las partes profundas de las cuencas aisladas como el Atlántico Norte y Sur (de Graciansky et al., 1984; Zimmerman et al., 1987) . Adicionalmente, el depósito a gran escala de evaporitas en el Atlántico Sur (Wortmann y Chernyavsky, 2007) parece haber cambiado en balance salino del océano creando menos agua salina, lo que ocasionó una lenta circulación (Hay et al., 2006) .

Algunos autores (Schlanger y Jenkyns, 1976; Erbacher et al., 2001; Leckie et al., 2002; van Helmond et al., 2013) sugieren que indistintamente del tipo de circulación marina existente durante el Cretácico, el débil gradiente latitudinal de temperatura debió implicar una lenta circulación marina y por lo tanto una limitada ventilación del suelo oceánico y el estancamiento de la columna en algunas cuencas marinas. Este último factor pudo ser intensificado por la descarga de agua dulce y material detrítico del continente. Otros sugieren (Erbacher et al., 1996; Leckie et al., 2002) que las altas temperaturas generaron condiciones apropiadas para la generación de grandes tasas de surgencia vertical y advección lateral de masas de agua ricas en nutrientes. Además, aunque el bajo gradiente latitudinal de la temperatura debió reducir la fuerza de los vientos, la intensa evaporación del agua en zonas tropicales y la respectiva transferencia de calor a la atmósfera causaron un incremento de la velocidad del viento que estimuló la surgencia costera, la disponibilidad de nutrientes en la zona fótica y el sostenimiento de la productividad marina (Peterson y Calvert, 1990; Jenkyns, 1999) .

En el marco de este convulso contexto cretácico de cambios paleoambientales surgen los Eventos Anóxicos Oceánicos (OAEs) . Estos episodios de cambio global acelerado tuvieron un inicio relativamente abrupto y una corta duración (usualmente entre 0.5 y 1 Ma) , y fueron casi simultáneos y/o inmediatamente posteriores a las repentinas transformaciones en el sistema litósfera-océano-atmósfera. El rasgo más distintivo de estos eventos fue el extenso depósito de sedimentos oscuros enriquecidos en materia orgánica y con una fábrica laminada, favorecido tanto por las condiciones de alta productividad en la superficie marina como por el empobrecimiento en oxígeno de la masa de agua intermedia y profunda de varias cuencas oceánicas (Schlanger y Jenkyns, 1976; Arthur y Schlanger, 1979; Leckie et al., 2012; Takashima et al., 2006; Föllmi , 2012; Núñez-Useche et al., 2015, 2016; Sabatino et al., 2015) . De esta forma, los OAEs actuaron como un efectivo mecanismo planetario que reguló las elevadas temperaturas mediante el secuestro de CO_2 y la disminución de sus altas concentraciones. Estos eventos también resultaron en una multitud de diferentes y extraordinarias perturbaciones en diversos entornos, cuyo registro estratigráfico, geoquímico y biológico se encuentra impreso en los sedimentos. Por ejemplo, los OAEs ocasionaron excursiones isotópicas de carbono positivas y/o negativas, variaciones en la composición isotópica del azufre en el agua de mar y los sedimentos; cambios en la tasa de enterramiento de elementos mayores, trazas y tierras raras; formación de nuevos minerales singenéticos y diagenéticos, extinciones y rápidas transformaciones evolutivas de los organismos marinos; alteraciones ecológicas y morfológicas en las plataformas carbonatadas y fases de ahogamiento; así como otros fenómenos tanto en el ambiente marino como continental (Leckie et al., 2002; Snow y Duncan, 2005; Méhay et al., 2009; Erba et al., 2010, 2015; Adams et al., 2010; Trabucho Alexandre et al., 2010; Gambacorta et al., 2015) .

1.2 PRINCIPALES CONTROLES EN LA ACUMULACIÓN DE MATERIA ORGÁNICA EN LOS SEDIMENTOS MARINOS

La materia orgánica preservada en los depósitos sedimentarios constituye el origen de todos los combustibles fósiles, es una importante ventana a la historia del planeta y una de las últimas fuentes de prácticamente todo el oxígeno (Berner y Canfield, 1989) . Determinar su contenido y tipo es fundamental para descifrar los procesos paleoceanográficos y las condiciones paleoambientales que tuvieron lugar durante su acumulación. En los sedimentos, estos parámetros están controlado por el clima; la temperatura y su interacción con la atmósfera, biosfera y masa continental; los procesos tectónicos que controlan la creación del relieve; el ciclo hidrológico y el arribo de detritos y nutrientes a las cuencas oceánicas; la producción y el empaquetamiento fecal; así como por las variaciones eustáticas del nivel del mar y las condiciones energéticas y redox en la columna de agua y la interfase sedimento-agua (Pedersen y Calvert, 1990; Kuypers et al., 2002; Killops y Killops, 2005; Piper y Calvert, 2009) . De manera general, estas variables se agrupan en tres principales factores relacionados entre sí: la producción fotosintética, la tasa de

sedimentación/dilución y la descomposición microbiana (Emerson y Hedges, 1988; Arthur y Sageman, 1994; Sageman et al., 2003; Piper y Calvert, 2009) (Fig. 3) . Estos factores determinan la tasa de fijación y exportación de carbono orgánico desde la masa de agua superficial, la rapidez a la cual la materia orgánica es remineralizada y su tasa de enterramiento en los sedimentos. Aunque no existe un consenso general sobre la importancia relativa de cada uno, estos factores dan lugar a dos modelos fundamentales –preservacionista y productivista- que tratan de explicar la formación actual y pasada de depósitos ricos en materia orgánica.

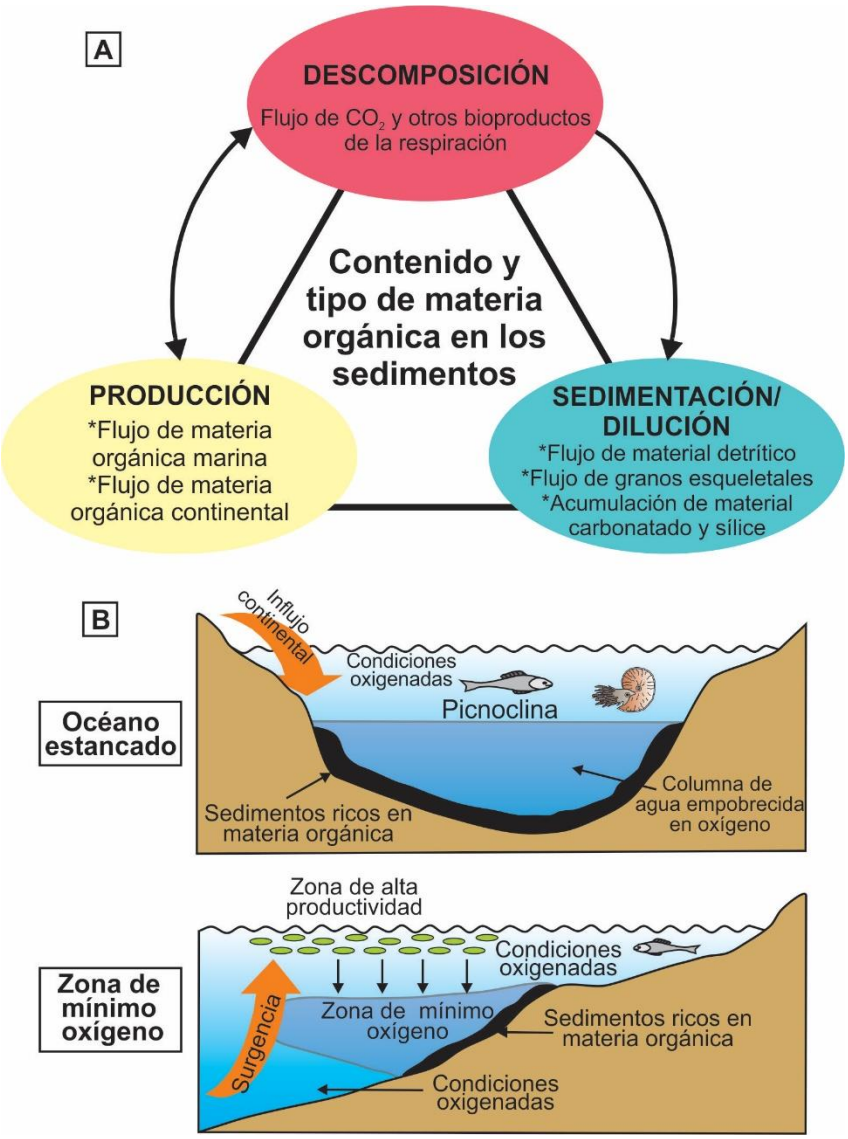

Figura 3. (A) Factores que controlan el contenido y tipo de materia orgánica en los sedimentos. Modificado de Sageman et al. (2003) . (B) Diagramas simplificados de los modelos de formación de los depósitos ricos en materia orgánica. Modificado de Brumsack (2006) y Takashima et al. (2006) .

1.2.1 Modelo preservacionista: océano estancado

En condiciones oxidantes la materia orgánica es inestable y rápidamente remineralizada a CO_2. Bajo este régimen redox, el porcentaje de materia orgánica que alcanza el fondo marino, usualmente el 10%, está regido directamente por la cantidad y calidad de la materia orgánica inicialmente producida, la profundidad de depósito que controla el tiempo de exposición a la oxidación microbiana y la tasa de sedimentación (Suess, 1980; Betzer et al., 1984; Emerson y Hedges, 1988; Thunell et al., 2000; Goñi et al., 2003; Piper y Calvert, 2009) . Su degradación es rápida en la zona fótica, continúa en la columna de agua durante el descenso de las partículas orgánicas y se incrementa en la interfase sedimento-agua. Según el modelo preservacionista, el enriquecimiento de materia orgánica en los sedimentos ocurre gracias a su mejorada conservación, asociada con la deficiencia de oxígeno debido a la fuerte estratificación y subsecuente estancamiento de la columna de agua (Schlanger y Jenkyns, 1976; Demaison y Moore, 1980; Erbacher et al., 2001; Brumsack, 2006) . El surgimiento de una fuerte picnoclina resulta del influjo de material detrítico y agua dulce y el posterior desarrollo de una capa superficial de baja salinidad. Este estancamiento debilita la difusión del oxígeno y la mezcla de agua, evitando la reposición del oxígeno disuelto consumido en la oxidación de la materia orgánica. En consecuencia, la concentración de oxígeno disminuye dramáticamente por debajo de la picnoclina, y la columna de agua, la masa de agua de fondo y el agua de poro del sedimento se empobrecen en oxígeno, favoreciendo la preservación de la materia orgánica (Fig. 3) . En estas condiciones la productividad marina depende esencialmente del arribo de nutrientes procedentes del continente, e incluso una baja productividad puede generar condiciones anóxicas en la parte profunda de la masa de agua.

Puesto que en el océano actual la circulación termohalina funciona como una eficiente cinta transportadora de oxígeno para su re-equilibrio, el desarrollo de condiciones oceánicas estancadas solo se presenta en áreas relativamente restringidas como el Mar Báltico (Boesen y Postma, 1988) , la cuenca de Cariaco (Lyons et al., 2003; Piper y Calvert, 2009) y el Mar negro (Arthur y Sageman, 1994; Brumsack, 2006) . Estas cuencas están aisladas de la circulación oxigenada y su masa de agua profunda tiene un tiempo de residencia de cientos a miles de años (Piper y Calvert, 2009) . Sin embargo, durante el Cretácico, condiciones estancadas propicias para el desarrollo de anoxia fueron más fácilmente logradas en varias cuencas marinas debido a su configuración estrecha y cerrada que las mantuvo relativamente aisladas; el acelerado ciclo hidrológico y la inundación de las zonas costeras que aumentó el arribo de material detrítico a las zonas costeras y la lenta circulación oceánica y la circulación halotermal que acentuó la deficiencia de oxígeno. A su vez, el aumento de la escorrentía superficial elevó de forma simultánea la llegada de nutrientes a la superficie marina y disparó la fertilidad (Leckie et al., 2002; Wagner et al., 2007)

En oposición a este modelo, algunas investigaciones (Henrichs y Reeburgh, 1987; Canfield, 1989; Calvert y Pedersen, 1992; Hetzel et al., 2009) sugieren que el contenido de

oxígeno es irrelevante para la conservación de la materia orgánica en los sedimentos. Si bien el oxígeno es el principal agente oxidante de la materia orgánica, no es el único. Basados en mediciones experimentales, estos estudios encontraron que la tasa de descomposición de la materia orgánica en condiciones oxigenadas no excede en gran medida a la que ocurre en condiciones anóxicas. En el caso del Cretácico, datos de Hetzel et al. (2009) sugieren que una mejorada preservación antes que una excepcionalmente alta productividad explica satisfactoriamente el contenido similar de materia orgánica de sedimentos depositados en varios lugares del sur del Atlántico Norte durante el OAE 2. Mediante simulaciones numéricas, estos autores estimaron que las tasas de productividad primaria en estos lugares fueron varios órdenes de magnitud inferiores a las que se reportan actualmente en zonas afectadas por corrientes de surgencia.

1.2.2 Modelo productivista: zona de mínimo oxígeno

La producción fotosintética realizada por el fitoplancton es considerada como la principal fuente de materia orgánica en el océano actual y del Mesozoico. Durante este proceso, la luz solar es usada para transformar el carbono orgánico disuelto y los nutrientes minerales en materia orgánica viviente. Justamente, el modelo productivista enfatiza que el intenso incremento en la producción primaria de fitoplancton en la zona fótica genera tal cantidad de materia orgánica que su degradación sobrepasa la capacidad oxidativa de la masa de agua inmediatamente subyacente. Estas condiciones conllevan al agotamiento de la concentración de oxígeno en la masa de agua intermedia y generan una zona de oxígeno mínimo en cuya intersección con el suelo oceánico surgen condiciones anóxicas favorables para la preservación de la materia orgánica (Pedersen y Calvert, 1990; Wilson y Norris, 2001; Leckie et al., 2002; Meyers, 2006; Takashima et al., 2006) (Fig. 3) .En este modelo, la masa de agua que se encuentra por encima y por debajo de la zona de oxígeno mínimo contiene una mayor concentración de oxígeno disuelto, controlada por el intercambio de la superficie con la atmósfera y la circulación lateral del agua (Karstensen et al., 2008) .

Este modelo está basado en las condiciones que se observan actualmente en varias zonas costeras como los márgenes continentales de Perú, Namibia y el Golfo de California (Böning et al., 2004; Brumsack., 2006; Piper y Calvert, 2009; Núñez-Useche et al., 2014) . En dichas áreas, la estratificación de la masa de agua es débil y corrientes de surgencia permanentes o estacionales, que se hundieron en zonas de latitud alta y acumularon nutrientes durante su advección, afloran y originan condiciones eutróficas en la superficie marina que incrementan las tasas de productividad y contribuyen a la creación y expansión de la zona de mínimo oxígeno. El área de suelo oceánico que hoy experimenta una severa deficiencia de oxígeno como resultado de este proceso oceanográfico se estima en aproximadamente el 0.1–0.2%, y se distribuye principalmente a lo largo del margen continental oeste de norte y Suramérica, el suroeste de África y el noreste del Océano

Índico (Helly y Levin, 2004; Brumsack, 2006; Meyers, 2006) . En el escenario del Cretácico, diversos procesos diferentes al intemperismo y escorrentía superficial dispararon la productividad marina e incrementaron el consumo de oxígeno en la masa de agua intermedia: las altas tasas de surgencia vertical y advección lateral de masas de aguas ricas en nutrientes (Erbacher et al., 1996; Leckie et al., 2002; Poulsen et al., 2003) ; la actividad volcánica submarina, especialmente aquella asociada al emplazamiento de las Grandes Provincias Ígneas, que introdujo grandes cantidades de elementos biolimitantes al océano (Larson, 1991a; Snow y Duncan, 2005; Föllmi, 2012; Erba et al., 2015) ; la dispersión y caída de ceniza volcánica que fertilizó la superficie marina (Anbar y Knoll, 2002) , y el reciclaje de fósforo desde los sedimentos anóxicos (Kuypers et al., 2004; Mort et al., 2007) . Según Meyers (2006) , aunque la anoxia marina fue sin duda un factor muy importante durante los OAEs, el alto contenido de materia orgánica de algunos sedimentos asociados con estos eventos solo puede explicarse mediante una elevada productividad marina, sostenida por una regeneración activa de nutrientes.

1.3 MOTIVACIÓN, OBJETIVOS Y METODOLOGÍA

Registrar y caracterizar las condiciones paleoambientales relacionadas con los episodios cretácicos de cambio global acelerado son tareas clave para entender y profundizar en el conocimiento sobre los mecanismos globales y locales que les dieron origen. Esta comprensión es vital considerando que aunque las condiciones climáticas y oceanográficas del Cretácico distan claramente de las actuales, modelos predictivos sugieren que si las emisiones antropogénicas de CO_2 continúan al mismo ritmo, circunstancias similares podrían experimentarse en el próximo siglo. Tal como los expresan Hay et al. (2006) , el Cretácico es un laboratorio para probar ideas sobre las causas y consecuencias del cambio climático global, uno de los principales retos científicos de la humanidad. En este contexto, estos episodios sirven como modelos potenciales para entender mejor el impacto en el ciclo del carbono y advertir posibles desequilibrios con influencia directa en la biosfera, particularmente aquellos fenómenos naturales que puedan amenazar la actividad humana. Además, puesto que durante el lapso de tiempo de ocurrencia de los Eventos Anóxicos Oceánicos (OAEs) se depositó el mayor volumen conocido de rocas generadoras de hidrocarburos (Arthur y Schlanger, 1979; Klemme y Ulmishek, 1991; Núñez-Useche et al., 2014) , el estudio de estos eventos es también significativo desde el punto de vista económico ya que es crítico para comprender la forma en que las condiciones paleoambientales influenciaron el depósito de materia orgánica y así orientar mejor las tareas de exploración y explotación de estos georrecursos.

Gran parte del conocimiento actual sobre los episodios cretácicos de cambio global acelerado proviene de su extensa documentación y estudio en los sedimentos marinos depositados principalmente en el Tetis y el Atlántico Oriental (ej. Menegatti et al., 1998; Herrle et al., 2004; Jarvis et al., 2006; Erba et al., 2010; Kędzierski et al., 2012; Westermann

et al., 2013; Gambacorta et al., 2015; Reolid et al., 2015) . A pesar de que existe un número significativo de publicaciones centradas en secciones del Atlántico Occidental (ej. Snow y Ducan, 2005; Hetzel et al., 2009; Trabucho Alexandre et al., 2010; Gaona-Narvaez et al., 2013; Phelps et al., 2015) , aún es poco lo que se conoce sobre estos episodios en México (Hernández-Romano et al., 1997; Duque-Botero et al., 2009; Elrick et al., 2009; Ifrim et al., 2011; Madhavaraju et al., 2013; Blanco-Piñón et al., 2014) , área clave del margen occidental del proto-Atlántico Norte que marcó la entrada al Mar Interior Occidental y representó condiciones de transición entre un mar epicontinental y la cuenca oceánica abierta. Precisamente, esta tesis está centrada en los sedimentos calcáreos y ricos en materia orgánica de las formaciones Cupido (Barremiano-Aptiano) y la Peña (Aptiano-Albiano) en el noreste de México, y de la Formación Agua Nueva (Cenomaniano-Turoniano) en el centro del país. Tiene como objetivos (i) identificar los episodios de cambio global acelerado registrados durante el depósito de estas unidades, particularmente los OAEs 1a, 1b y 2, (ii) realizar su correlación con facies equivalentes depositadas en otras cuencas sedimentarias, (iii) descifrar las condiciones paleoambientales/paleocenográficas existentes durante su ocurrencia, y (iv) evaluar los factores globales/locales que les dieron origen. Estos se logra mediante una caracterización integral que combina múltiples indicadores sedimentológicos, mineralógicos, petrográficos, paleontológicos, bioestratigráficos, cronoestratigráficos y geoquímicos, que se encuentran detallados en cada uno de los artículos aceptados/enviados que conforman esta tesis.

El primer capítulo introduce a las condiciones paleoambientales y paleocenográficas que predominaron durante el Cretácico y que favorecieron el surgimiento de los episodios de cambio global acelerado, y a los modelos que tratan de explicar el enriquecimiento de materia orgánica en los sedimentos marinos. Con base en la información disponible, el segundo capítulo ofrece un panorama general de los principales Eventos Anóxicos Oceánicos del Cretácico, integra y resume su estado del arte en México y realiza una revisión de las unidades estratigráficas más propicias para encontrar su registro, considerando su edad, litología y ambiente de depósito. Este capítulo constituye el punto de partida para la búsqueda de dichos eventos. Considerando la información publicada del Barremiano–Aptiano en depósitos sedimentarios del Dominio Prebético en España, en el tercer capítulo se discute y propone una nueva subdivisión del segmento isotópico de carbono C7 de Menegatti et al. (1998) . Además, se enfatiza que una excursión isotópica negativa menor en la base del segmento C7 y dentro de la Biozona de amonites *Dufrenoyia furcata* (Intra-Furcata Negative Excursion, IFNE) se puede observar en varias secciones estratigráficas de diferentes partes del mundo, incluyendo México; por lo que puede ser considerada como un potencial marcador quimio-estratigráfico para el Aptiano.

En el cuarto capítulo, datos publicados de bioestratigrafía de amonites se combinan con estratigrafía isotópica de carbono para documentar diferentes episodios de cambio global acelerado (OAE 1a, IFNE, posible Nivel Aparein y Nivel Noire) en los depósitos del Aptiano de las formaciones Cupido y La Peña en el noreste de México. Integrando información de facies sedimentarias, contenido de materia orgánica y abundancia de foraminíferos

bentónicos y planctónicos, y datos de elementos redox-sensibles, contenido mineralógico y abundancia y tamaño de framboides de pirita se descifran las condiciones paleoambientales y los mecanismos que propiciaron estos eventos globales, y particularmente, el depósito de sedimentos ricos en materia orgánica en las unidades estudiadas. También se analiza la respuesta de la plataforma carbonatada Cupido ante el OAE 1a, los factores que determinaron el ahogamiento final de este importante elemento paleogeográfico y la diacronía de la cima de la Formación Cupido. El quinto capítulo está enfocado en el uso de bioestratigrafía de colomiélidos, edades numéricas derivadas de estratigrafía isotópica de estroncio y cronoestratigrafía isotópica de carbono para registrar el OAE 1b en la parte media de la Formación La Peña en el noreste de México. Mediante datos de contenido mineral y de carbono orgánico total, en este capítulo también se analizan las condiciones paleoambientales asociadas a este evento. En el sexto capítulo se estudian los depósitos ricos en materia orgánica del Cenomaniano-Turoniano de la Formación Agua Nueva en la cuenca de Tampico-Misantla, centro de México. Mediante la definición de bioeventos, principalmente relacionados con foraminíferos planctónicos, y geocronología U-Pb en circones magmáticos se constriñe la edad de una sección estratigráfica e identifican las facies equivalentes al OAE 2. En ese capítulo se estudian y analizan las variaciones de las facies sedimentarias y de determinados componentes esqueletales; los cambios en el contenido y tipo de materia orgánica, nitrógeno total, componentes minerales y elementos redox-sensibles; la señal isotópica del carbono, la distribución de la abundancia y tamaño de los framboides de pirita; y la firma isotópica del azufre y la composición elemental de granos de pirita; todo ello con el objetivo de determinar las cambios en las condiciones de oxigenación y productividad, encontrar las causas de dichas fluctuaciones y construir un modelo depositacional. Finalmente, en el séptimo capítulo se presentan los principales resultados y conclusiones generales.

REFERENCIAS

Anbar, A.D., Knoll, A.H., 2002. Proterozoic ocean chemistry and evolution: a bioinorganic bridge? Science 297, 1137–1142.

Arthur, M.A., Sageman, B.B., 1994. Marine black shales: depositional mechanisms and environments of ancient deposits. Annual Review of Earth and Planetary Sciences 22, 499–551.

Arthur, M.A., Schlanger, S.O., 1979. Cretaceous "Oceanic Anoxic Events" as causal factors in development of reef-reservoired giant oil fields. American Association of Petroleum Geologists Bulletin 63, 870–885.

Adams, D.D., Hurtgen, M.T., Sageman, B.B., 2010. Volcanic triggering of a biogeochemical cascade during Oceanic Anoxic Event 2. Nature Geoscience 3, 201–204.

Berner, 1994. GEOCARB II: A revised model of atmospheric CO_2 over Phanerozoic time. American Journal of Science 294, 56–91.

Bergman, N.M., Lenton, T.M., Watson, A.J., 2004. COPSE: a new model of biogeochemical cycling over Phanerozoic time. American Journal of Science 304, 397–437.

Beerling, D.J., Royer, D.L., 2002. Fossil plants as indicators of the Phanerozoic global carbon cycle. Annual Review of Earth and Planetary Sciences 30, 527–556.

Berner, R.A., Canfield, D.E., 1989. A new model for atmospheric oxygen over Phanerozoic time. American Journal of Science 289, 333–361.

Betzer, P., Showers, W., Laws, E., Winn, C., DiTullio, G., Kroopnick, P., 1984. Primary production and particle fluxes on a transect of the equator at 1538Win the Pacific Ocean. Deep-Sea Research 31, 1–11.

Bice, K.L., Norris, R.D., 2002. Possible atmospheric CO_2 extremes of the warm mid-Cretaceous (late Albian–Turonian) . Paleoceanography 17, 1070.

Bigg G.R., 2003. The oceans and Climate. Cambridge University Press, United Kingdom (273 pp.) .

Blanco-Piñón, A., Maurrasse, F.J.-M.R., Zavala Díaz-de la Serna, F.J., López-Doncel, R.A., Ángeles-Trigueros, S.A., Hernández-Avila, J., Juárez Arriaga, E., 2014. Evidencias petrográficas de estructuras de origen algal/bacteriano en carbonatos de la Formación Agua Nueva (Cenomaniano/Turoniano: Cretácico Superior) en Xilitla, S. L. P. México Central. Boletín de la Sociedad Geológica Mexicana 66, 397–412.

Boesen, C., Postma, D., 1988. Pyrite formation in anoxic environments of the Baltic. American Journal of Science, 288(6) , 575–603.

Böning, P., Brumsack, H.J., Böttcher, M.E., Schnetger, B., Kriete, C., Kallmeyer, J., Borchers, S.L., 2004. Geochemistry of Peruvian near-surface sediments. Geochimica et Cosmochimica Acta 68, 4429–4451.

Bottini, C., Cohen, A.S., Erba, E., Jenkyns, H.C., Coe, A.L., 2012. Osmium isotope evidence for volcanism, weathering and ocean mixing during the early Aptian OAE 1a. Geology 40, 583–586.

Brass, G.W., Southam, J.R., Peterson, W.H., 1982. Warm saline bottom water in the ancient ocean. Nature 296, 620–923.

Brumsack, H.J., 2006. The trace metal content of recent organic carbon rich sediments: implications for Cretaceous black shale formation. Palaeogeography, Palaeoclimatology, Palaeoecology 232, 344–361.

Calvert, S.E., Pedersen, T.F., 1992. Organic carbon accumulations and preservation in marine sediments: how important is anoxia? En: Whelan, J.K., Farrington, J.W. (Eds.) , Productivity, accumulation and preservation of organic matter in recent and ancient sediments. Columbia University Press, New York, NY, 231–263.

Canfield, D. E., 1989, Sulfate reduction and oxic respiration in marine sediments: implications for organic carbon preservation in euxinic environments: Deep-Sea Research 6, 121–138.

Chumakov, N.M., Zharkov, M.A., Herman, A.B., Doludenko, M.P., Kalandadze, N.M., Lebedev, E.L., Ponomareko, A.G., Rautian, A.S., 1995. Climatic belts of mid-Cretaceous time. Stratigraphy and Geological Correlation 3, 241–260.

de Graciansky, P.C., Deroo, G., Herbin, J.P., Montadert, L., Müller, C., Schaaf, A., Sigal, J., 1984. Ocean-wide stagnation episode in the Late Cretaceous. Nature 308, 346–349.

Demaison, G.J., Moore, G.T., 1980. Anoxic environments and oil source bed genesis. American Association of Petroleum Geologists Bulletin 64, 1179–1209.

Duque-Botero, F., Maurrasse, F.J-M-R., Hickey-Vargas, R., Melinte, M., Jaffe, R., Lopez-Oliva, J.G., 2009. Microspheroids accumulation and geochemistry of an anoxic basin of the Cenomanian/Turonian: The record of the Indidura Formation, NE Mexico. Geologic Problem Solving with Microfossils: A Volume in Honor of Garry D. Jones. Society for Sedimentary Geology, Society of Sedimentary Geology Special Publication 93, 171–186.

Elrick, M., Molina-Garza, R., Duncan, R., Snow L., 2009. C-isotope stratigraphy and paleoenvironmental changes across OAE 2 (mid-Cretaceous) from shallow-water platform carbonates of southern Mexico. Earth and Planetary Science Letters 277, 295–306.

Emerson, S., Hedges, J.I., 1988. Processes controlling the organic carbon content of open ocean sediments. Paleoceanography 3, 621– 634.

Erba, E., Bottini, C., Weissert, J.H., Keller, C.E., 2010, Calcareous nannoplankton response to surface-water acidification around Oceanic Anoxic Event 1a: Science 329, 428–432.

Erba, E., Duncan, R.A., Bottini, C., Tiraboschi, D., Weissert, H., Jenkyns, H.C., Malinverno, A., 2015. Environmental consequences of Ontong Java Plateau and Kerguelen Plateau volcanism. En: Neal, C.R., Sager, W.W., Sano, T., Erba, E. (Eds.) , The Origin, Evolution, and Environmental Impact of Oceanic Large Igneous Provinces. Geological Society of America Special Paper 511.

Erba, E., Tremolada, F. 2004. Nannofossil carbonate fluxes during the Early Cretaceous: Phytoplankton response to nutrification episodes, atmospheric CO_2, and anoxia. Paleoceanography 19, PA1008.

Erbacher J., Thurow J., Littke R., 1996. Evolution patterns of radiolaria and organic matter variations: A new approach to identify sea-level changes in mid-Cretaceous pelagic environments. Geology 24, 499–502.

Erbacher, J., Huber, B.T., Norris, R.D., Markey, M., 2001. Increased thermohaline stratification as a possible cause for an ocean anoxic event in the Cretaceous period. Nature 409, 325–327.

Föllmi, K.B., 2012. Early Cretaceous life, climate and anoxia. Cretaceous Research 35, 230–257.

Föllmi, K.B., Godet, A., Bodin, S., Linder, P., 2006. Interactions between environmental change and shallow water carbonate buildup along the northern Tethyan margin and their impact on the Early Cretaceous carbon isotope record. Paleoceanography 21 (PA4211) , 4211–4216.

Frakes, L.A., 1999. Estimating the global thermal state from Cretaceous sea surface and continental temperature data. En: Barrera, E., Johnson, C.C. (Eds.) , Evolution of the Cretaceous Ocean-Climate System. Geological Society of America, Special Paper 332, 49–57.

Gaona-Narvaez, T., Florentin, J.-M.R., Etayo-Serna, F., 2013. Geochemistry, palaeoenvironments and timing of Aptian organic-rich beds of the Paja Formation (Curití, Eastern Cordillera, Colombia) . Geological Society, London, Special Publications 382, 31-48.

Gambacorta, G., Jenkyns, H.C., Russo, F., Tsikos, H., Wilson, P.A., Faucher, G., Erba, E., 2015. Carbon-and oxygen-isotope records of mid-Cretaceous Tethyan pelagic sequences from the Umbria–Marche and 972 Belluno Basins (Italy) . Newsletters on Stratigraphy 48, 299–323.

Goñi, M.G., Heather, L.A., Thunell, R.C., Tappa, E., Black, D., Astor, Y., Varela, R., Müller-Karger, F., 2003. Biogenic fluxes in the Cariaco Basin: a combined study of sinking particulates and underlying sediments. Deep-Sea Research 50, 781–807.

Haq, B.U., Hardenbol, J., Vail, P.R., 1987. Chronology of fluctuating sea levels since the Triassic. Science 235, 1156–1167.

Hardenbol, J., Thierry, J., Farley, M.B., de Graciansky, P.C., Vail, P.P., 1998. Mesozoic and Cenozoic sequence chronostratigraphic framework of European basins. En: de Graciansky, P.C., Hardenbol, J., Jacquin, T., Vail, P.P. (Eds.) , Mesozoic and Cenozoic Sequence 1409 Stratigraphy of European Basins. Society of economic paleontologists and mineralogists Special Publication 60, 3–13.

Hay, W. W., Floegel, S., 2012. New thoughts about the Cretaceous climate and oceans. Earth-Science Reviews 115, 262–272.

Handoh, I.C., Lenton, T.M., 2003. Periodic mid-Cretaceous oceanic anoxic events linked by oscillations of the phosphorus and oxygen biogeochemical cycles. Global Biogeochemical Cycles 17, 1902.

Harland, M., Francis, J.E., Brentnall, S.J., Beerling, D.J., 2007. Cretaceous (Aptian-Albian) conifer wood from Northern Hemisphere high latitudes: Forest composition and palaeoclimate. Review of Palaeobotany and Palynology 143, 167–196.

Hay, W.W., Migdisov, A., Balukhovsky, A.N., Wold, C.N., Flögel, S., Söding, E., 2006. Evaporites and the salinity of the ocean during the Phanerozoic: implications for climate, ocean circulation and life. Palaeogeography, Palaeoclimatology, Palaeoecology 240, 3–46.

Helly, J.J., Levin, L.A., 2004. Global distribution of naturally occurring marine hypoxia on continental margins. Deep-Sea Research Part I 51, 1159– 1168.

Henrichs, S.M., Reeburgh, W.S., 1987. Anaerobic mineralization of marine sediment organic matter: rates and the role of anaerobic processes in the oceanic carbon economy. Geomicrobiology Journal 5, 191– 238.

Hernández-Romano, U., Aguilera-Franco, N., Martínez-Medrano, M., Barceló-Duarte, J., 1997. Guerrero-Morelos Platform drowning at the Cenomanian–Turonian boundary, Huitziltepec area, Guerrero State, southern Mexico. Cretaceous Research 18, 661–686.

Herrle, J.O., Kößler, P., Friedrich, O., Erlenkeuser, H., Hemleben, C., 2004. High-resolution carbon isotope records of the Aptian to Lower Albian from SE France and the Mazagan Plateau (DSDP Site 545) : a stratigraphic tool for paleoceanographic and paleobiologic reconstruction. Earth and Planetary Science Letters 218, 149–161.

Herrle, J.O., Schröder-Adams, C.J., Davis, W., Pugh, A.T., Galloway, J.M., Fath, J., 2015. Mid-Cretaceous High Arctic stratigraphy, climate, and Oceanic Anoxic Events. Geology 43, 403–406.

Hetzel, A., Böttcher, M.E., Wortmann, U.G., Brumsack, H.J., 2009. Paleo-redox conditions during OAE2 reflected in Demerara Rise sediment geochemistry (ODP Leg 207) . Palaeogeography, Palaeoclimatology, Palaeoecology 273, 302–328.

Huber, B.T., Macleod, K.G., & Wing, S.L., 2000. Warm climates in earth history. Cambridge University Press, 79–131.

Ifrim, C., Götz, S., Stinnesbeck, W., 2011. Fluctuations of the oxygen minimum zone at the end of Oceanic Anoxic Event 2 reflected by benthic and planktic fossils. Geology 39, 1043–1046.

Jarvis, I., Gale, A.S., Jenkyns, H.C., Pearce, M.A., 2006. Secular variation in Late Cretaceous carbon isotopes: a new δ13C carbonate reference curve for the Cenomanian–Campanian (99.6–70.6 Ma) . Geological Magazine 142, 561–608.

Jarvis, I., Lignum, J.S., Gröcke, D.R., Jenkyns, H.C., and Pearce, M.A., 2011, Black shale deposition, atmospheric CO2 drawdown, and cooling during the Cenomanian-Turonian Oceanic Anoxic Event: Paleoceanography, v. 26, PA3201.

Jahren A.H., 2002. The biogeochemical consequences of the mid-Cretaceous superplume. Journal of Geodynamics 34, 177–191.

Jenkyns, H.C., 1999. Mesozoic anoxic events and paleoclimate. Zentralblatt Geologische Palaöntologie Teil, 943–949.

Karstensen, J., Stramma, L., Visbeck, M., 2008. Oxygen minimum zones in the eastern tropical Atlantic and Pacific oceans. Progress in Oceanography 77, 331–350.

Kędzierski, M., Machaniec, E., Rodríguez-Tovar, F.J., Uchman, A., 2012. Bio-events, foraminiferal and nannofossil biostratigraphy of the Cenomanian/Turonian boundary interval in the Subsilesian Nappe, Rybie section, Polish Carpathians. Cretaceous Research 35, 181–198.

Keller, G., 2008. Cretaceous climate, volcanism, impacts, and biotic effects. Cretaceous Research 29, 754–771.

Kidder, D.L., Worsley, T.R., 2010. Phanerozoic Large Igneous Provinces (LIPs) , HEATT (Haline Euxinic Acidic Thermal Transgression) episodes, and mass extinctions. Palaeogeography, Palaeoclimatology, Palaeoecology 295, 162–191.

Kidder, D.L.,Worsley, T.R., 2012. Human-induced hothouse climate? Geological Society of America Today 22, 4–11.

Killops, S.D., Killops, V., 2005. Introduction to Organic Geochemistry Second ed. Blackwell, Publishing Ltd., MA, USA (391 pp) .

Kuypers, M.M.M., Pancost, R.D., Nijenjuis, I.A., Sinninghe Damste, J.S., 2002. Enhanced productivity led to increased organic carbon burial in the euxinic North Atlantic basin during the late Cenomanian oceanic anoxic event. Paleoceanography 17, PA000569.

Kuypers, M.M.M, van Breugel, Y., Schouten, S., Erba, E., Sinninghe Damsté, J.S., 2004. N_2-fixing cyanobacteria supplied nutrient N for Cretaceous oceanic anoxic events. Geology 32, 853–856.

Larson, R. L., 1991a. Geological consequences of superplumes. Geology 19, 963-966.

Larson, R. L., 1991b. Latest pulse of Earth: Evidence for a mid-Cretaceous superplume. Geology 19, 547–550.

Leckie, R.M., Bralower, T.J., Cashman, R., 2002. Oceanic anoxic events and plankton evolution: biotic response to tectonic forcing during the mid-Cretaceous. Paleoceanography 17 , 1–29.

Li, X., Wei, Y., Li, Y., Zhang, C., 2015. Carbon isotope records of the early Albian oceanic anoxic event (OAE) 1b from eastern Tethys (southern Tibet, China) . Cretaceous Research, en prensa. doi:10.1016/j.cretres.2015.08.015.

Lyons, T.W., Werne, J.P., Hollander, D.J., Murray, R.W., 2003. Contrasting sulfur geochemistry and Fe/Al and Mo/Al ratios across the last oxic-to-anoxic transition in the Cariaco Basin, Venezuela. Chemical Geology 195, 131–157.

Madhavaraju, J., Lee, Y.I., León, C.M. G., 2013. Diagenetic significance of carbon, oxygen and strontium isotopic compositions in the Aptian-Albian Mural Formation in Cerro Pimas area, northern Sonora, Mexico. Journal of iberian geology 39, 73–88.

Méhay, S., Keller, C.E., Bernasconi, S.M., Weissert, H., Erba, E., Bottini, C., Hochuli, P.A., 2009. A volcanic CO_2 pulse triggered the Cretaceous oceanic anoxic event 1a and a biocalcification crisis. Geology 37, 819–822.

Menegatti, A.P.,Weissert, H., Brown, R.S., Tyson, R.V., Farrimond, P., Strasser, A., Caron,M., 1998. High-resolution $\delta^{13}C$ stratigraphy through the early Aptian "Livello Selli" of the Alpine Tethys. Paleoceanography 13, 530–545.

Meyers, P.A., 2006. Paleoceanographic and paleoclimatic similarities between Mediterranean sapropels and Cretaceous black shales. Palaeogeography, Palaeoclimatology, Palaeoecology 235, 305–320.

Meyer, K., Kump, L., 2008. Oceanic euxinia in earth history: Causes and consequences, Annual Reviews of Earth and Planetary Sciences 36, 251–288.

Milkov A.V., 2004. Global estimates of hydrate-bound gas in marine sediments: how much is really out there? Earth-Science Reviews 66 (3–4) , 183–197.

Mort, H. P., Adatte, T., Föllmi, K. B., Keller, G., Steinmann, P., Matera, V., Berner, Z., Stüben, D., 2007. Phosphorus and the roles of productivity and nutrient recycling during oceanic anoxic event 2. Geology 35, 483-486.

Núñez-Useche, F., Barragán, R., Canet, C., 2014, Sedimentación carbonatada, silícica y otros sedimentos químicos en los ambientes marinos profundos, En: Low, A., Peters, E (Eds.) : La Frontera Final: El Océano Profundo, ISBN: 978-607-8246-70-0, México, D.F, 57-85.

Núñez-Useche, Barragán, R., Moreno-Bedmar, J.A., Canet, C., 2015. Geochemical and paleoenvironmental record of the early to early late Aptian major episodes of

accelerated change: Evidence from Sierra del Rosario, Northeast Mexico. Sedimentary Geology 324, 47–66.

Núñez-Useche, F., Canet C., Barragán, R., Alfonso, P., 2016. Bioevents and redox conditions around the Cenomanian–Turonian anoxic event in Central Mexico. Palaeogeography, Palaeoclimatology, Palaeoecology, en prensa. doi:10.1016/j.palaeo.2016.01.035.

Pedersen, T.F., Calvert, S.E., 1990. Anoxia vs. productivity: What controls the formation of organic-carbon-rich sediments and sedimentary rocks. American Association of Petroleum Geologists Bulletin 74, 454–466.

Phelps, R.M., Kerans, C., Da-Gama, R.O., Jeremiah, J., Hull, D., Loucks, R.G., 2015. Response and recovery of the Comanche carbonate platform surrounding multiple Cretaceous oceanic anoxic events, northern Gulf of Mexico. Cretaceous Research 54, 117–144.

Piper, D.Z., Calvert, S.E., 2009. A marine biogeochemical perspective on black shale deposition. Earth-Science Reviews 95, 63–96.

Poulsen C.L., Barron E.J., Arthur M.A., Peterson W.H., 2001. Response of mid-Cretaceous global oceanic circulation to tectonic and CO_2 forcings. Paleoceanography 16, 576–592.

Poulsen, C.J., Gendaszek, A.S., Jacob, R.L., 2003. Did the rifting of the Atlantic Ocean cause the Cretaceous thermal maximum? Geology 31, 115–118.

Reolid, M., Sánchez-Quiñónez, C. A., Alegret, L., Molina, E., 2015. Palaeoenvironmental turnover across the Cenomanian-Turonian transition in Oued Bahloul, Tunisia: foraminifera and geochemical proxies. Palaeogeography, Palaeoclimatology, Palaeoecology 417, 491–510.

Sabatino, N., Coccioni, R., Manta, D.S., Baudin, F., Vallefuoco, M., Traina, A., Sprovieri, M., 2015. High-resolution chemostratigraphy of the late Aptian–early Albian oceanic anoxic event (OAE 1b) from the Poggio le Guaine section (Umbria–Marche Basin, central Italy) . Palaeogeography, Palaeoclimatology, Palaeoecology 426, 319–333.

Sageman, B.B., Murphy, A.E., Werne, J.P., Ver Straeten, C.A., Hollander, D.J., Lyons, T.W., 2003. A tale of shales: the relative roles of production, decomposition, and dilution in the accumulation of organic-rich strata, Middle-Upper Devonian, Appalachian basin. Chemical Geology 195, 229–273.

Sepkoski, J.J., 1989. Periodicity in extinction and the problem of catastrophism in the history of life. Journal of the Geological Society 146, 7–19.

Snow, L.J., Duncan, R.A., 2005. Trace element abundances in the Rock Canyon Anticline, Pueblo, Colorado, marine sedimentary section and their relationship to Caribbean plateau constuction and oxygen anoxic event 2. Paleoceanography 20, PA305.

Schlanger, S.O., Jenkyns, H.C., 1976. Cretaceous oceanic anoxic events: causes and consequences. Geologie en Mijnbouw 55, 179–184.

Skelton, P.W., 2003. The Cretaceous world. The Open University, Cambridge University Press, Cambridge (360 pp.) .

Sinninghe Damsté, J.S., van Bentum, E.C., Reichart, G.-J., Pross, J., Schouten, S., 2010. A CO_2 decrease-driven cooling and increased latitudinal temperature gradient during the mid-Cretaceous Oceanic Anoxic Event 2: Earth and Planetary Science Letters 293, 97–103.

Steuber, T., Rauch, M., Masse J.P., Malkoc, M., 2005. Low-latitude seasonality of Cretaceous temperatures in warm and cold episodes. Nature 437, 1341–1344.

Suess, E., 1980. Particulate organic carbon flux in the oceans: surface productivity and oxygen utilization. Nature 288, 260–263.

Takashima, R., Nishi, H., Huber B.T., Leckie, R.M., 2006. Greenhouse world and the Mesozoic ocean. Oceanography 19, 64–74.

Thunell, R.C., Williams, D.F., Belyea, P.R., 1984. Anoxic events in the Mediterranean in relation to the evolution of Late Neogene climates. Marine Geology 59, 105–134.

Trabucho Alexandre, J., Tuenter, E., Henstra, G.A., van der Zwan, K.J., van de Wal, R.S.W., Dijkstra, H.A, de Boer, P.L., 2010. The mid-Cretaceous North Atlantic nutrient trap: Black shales and OAEs, Paleoceanography, 25, PA4201.

van Helmond, N.A.G.M., Sluijs, A., Reichart, G.-J., Sinninghe Damsté, J.S., Slomp, C.P., 2013. A perturbed hydrological cycle during Oceanic Anoxic Event 2. Geology 42, 123–126.

Wagner, T., Wallmann, K., Herrle, J.O., Hofmann, P., Stuesser, I., 2007. Consequences of moderate ~25,000 yr lasting emission of light CO_2 into the mid-Cretaceous ocean. Earth and Planetary Science Letters 259, 200–211.

Wang, Q.J., Xu, X.H., Jin, P.H., Li, R.Y., Li, X.Q., Sun, B.N., 2013. Quantitative reconstruction of Mesozoic paleoatmospheric CO_2 based on stomatal parameters of fossil Baiera furcata of Ginkgophytes. Geological review 59, 1035–1045.

Weissert, H., Erba, E., 2004. Volcanism, CO_2 and palaeoclimate: a Late Jurassic–Early Cretaceous carbon and oxygen isotope record. Journal of the Geological Society 161, 695–702.

Weissert, H., Lini, A., 1991. Ice age interludes during the time of Cretaceous greenhouse climate? En: Muller, W., McKenzie, J.A., Weissert, H. (Eds.) , Controversies in Modern Geology. Academic Press, New York, 173–191.

Westermann, S., Stein, M., Matera, V., Fiet, N., Fleitmann, D., Adatte, T., Föllmi, K.B., 2013. Rapid changes in the redox conditions of the western Tethys Ocean during the OAE 1a interval (early Aptian) . Geochimica et Cosmochimica Acta 121, 467–486.

Wilson, P.A., Norris, R.D., 2001. Warm tropical ocean surface and global anoxia during the mid-Cretaceous period. Nature 412, 425–429.

Wortmann, U.G., Chernyavsky, B., 2007. Effect of evaporite deposition on Early Cretaceous carbon and sulphur cycling. Nature 446, 654–656.

Zimmerman, H. B., Boersma, A., McCoy, F.W., 1987. Carbonaceous sediments and paleoenvironment of the Cretaceous South Atlantic Ocean, En: Brooks, J., Fleet, A.J. (Eds.) , Mesozoic and Cenozoic Sequence Stratigraphy of European Basins. Society of economic paleontologists and mineralogists Special Publication 60, 3–13.

"Los Eventos Anóxicos Oceánicos han coloreado no solo el camino de la historia geológica sino también el de la humanidad"
Jenkyns (1980)

CAPÍTULO 2

LOS EVENTOS ANÓXICOS OCEÁNICOS DEL CRETÁCICO EN MÉXICO

Artículo: **Núñez-Useche, F.**, Barragán, R., Moreno-Bedmar, J.A., Canet, C., 2015. Mexican archives for the major Cretaceous Oceanic Anoxic Events. Boletín de la Sociedad Geológica Mexicana 66(3), 491-505.

Boletín de la Sociedad Geológica Mexicana
Volumen 66, núm. 3, 2014, p. 491-505

Mexican archives for the major Cretaceous Oceanic Anoxic Events

Fernando Núñez-Useche[1,2,*], Ricardo Barragán[2], Josep A. Moreno-Bedmar[2], Carles Canet[3]

[1] Posgrado en Ciencias de la Tierra, Universidad Nacional Autónoma de México, Delegación Coyoacán, 04510, Distrito Federal, México.
[2] Instituto de Geología, Universidad Nacional Autónoma de México, Delegación Coyoacán, 04510, Distrito Federal, México.
[3] Instituto de Geofísica, Universidad Nacional Autónoma de México, Delegación Coyoacán, 04510, Distrito Federal, México.

[*] fernandonunezu@comunidad.unam.mx

Abstract

Oceanic Anoxic Events (OAEs) are interpreted as brief episodes of oxygen-depleted conditions in the global ocean that resulted from profound perturbations in the carbon cycle. These events favored widespread deposition of organic carbon-rich sediments and the subsequent formation of hydrocarbon source rocks. The most important of these events for the Cretaceous period are the globally recognized OAE 1a (early Aptian, Selli event), the OAE 2 (Cenomanian/Turonian boundary, Bonarelli event), and the Atlantic-restricted OAE 3 (Coniacian/Santonian boundary). In Mexico, several sedimentary successions of these ages are proved hydrocarbon source rocks and potential targets for oil and gas shale exploration; however, in most cases, it is unknown how these global events influenced redox conditions under which they were deposited. In general, there is little research to document and characterize properly these events. This work exposes and analyzes the current state of the study of these events in Mexico, and proposes new stratigraphic units to prospect and methodologies for further studies. The OAE 1a has been isotopically constrained in the northeastern part of the country within sediments with high organic carbon content in the lowermost part of the La Peña Formation. However, recent research suggests that the base of the La Peña Formation seems isochronous and younger than the OAE 1a. Accordingly, this event must be recorded in the underlying sediments of the Cupido/Lower Tamaulipas formations. Because of its age and lithostratigraphic features, the Agua Salada Formation of the Lampazos Platform also seems to be linked to this event. The OAE 2 has been documented in northeastern Mexico in the Agua Nueva and Indidura formations, and in southern Mexico in the uppermost part of the Morelos Formation. Trace metal enrichment in these rocks indicates that the emplacement of the Caribbean plateau probably played an important role in the record of this anoxic event across Mexico. Poorly oxygenated conditions during the Cenomanian/Turonian in northeastern México lasted until the early Coniacian. Other stratigraphic units that probably record this event are the Agua Nueva, Eagle Ford, Soyatal, and Maltrata formations. The record of the OAE 3 remains unknown. We hypothesize that Coniacian/Santonian Mexican paleogeography and sedimentary pattern could trigger at least intermittent anoxic/dysoxic conditions favorable for organic carbon burial, and suggest searching for these conditions in the San Felipe, Indidura or Austin formations.

Keywords: Cretaceous organic-carbon-rich sediments, Oceanic Anoxic Events (OAEs), Mexico, hydrocarbon source rocks, stable carbon isotopes.

Resumen

Los Eventos Anóxicos Oceánicos (OAEs, por sus siglas en inglés) corresponden a breves periodos en los que predominan condiciones empobrecidas en oxígeno disuelto en el océano global como resultado de profundas transformaciones en el ciclo del carbono. Estos eventos favorecieron el depósito de sedimentos ricos en carbono orgánico y la subsiguiente formación de rocas generadoras de hidrocarburos. Los eventos más importantes que tuvieron lugar durante el Cretácico son los globalmente reconocidos: OAE 1a (Aptiano temprano, evento Selli), OAE 2 (límite Cenomaniano/Turoniano, evento Bonarelli), y el OAE 3 (límite Coniaciano/Santoniano) restringido a la cuenca del océano Atlántico. En México, numerosas unidades estratigráficas depositadas durante el tiempo de ocurrencia de estos

eventos son rocas generadoras de hidrocarburos y potenciales objetivos de exploración para petróleo y gas. Sin embargo, en la mayoría de los casos no es clara la forma en que estos eventos influyeron en las condiciones redox bajo las cuales tuvo lugar su depósito. En general, son pocas las investigaciones que documentan y caracterizan apropiadamente estos eventos. Este trabajo expone y analiza el estado actual de estudio de estos eventos en México y propone nuevas localidades y unidades estratigráficas a prospectar, así como metodologías a aplicar en futuros estudios. El OAE 1a se ha definido isotópicamente en el noreste de México en los sedimentos con alto contenido de carbono orgánico de la parte inferior de la Formación La Peña. Sin embargo, estudios recientes indican que la base de esta unidad parece ser isocrónica y asignable a una edad más joven que la definida para el OAE 1a. En consecuencia, esta investigación propone que es probable que el registro de dicho evento se encuentre en las formaciones subyacentes Cupido/Tamaulipas Inferior. Por su edad y características litológicas, la Formación Agua Salada de la Plataforma de Lampazos también parece estar ligado a este evento. El OAE 2 ha sido documentado en el noreste de México en las formaciones Agua Nueva e Indidura, y en el sur de México en la parte superior de la Formación Morelos. El enriquecimiento en metales traza de estas unidades indican que el emplazamiento de la plateau del Caribe desempeñó un papel clave en el registro de este OAE a lo largo del país. Las condiciones empobrecidas en oxígeno durante el Cenomaniano/Turoniano persistieron en el noreste de México hasta el Coniaciano temprano. Otras unidades estratigráficas cuyo estudio parece prometedor para encontrar el OAE 2 son las formaciones Agua Nueva, Eagle Ford, Soyatal y Maltrata. Aunque el registro del OAE 3 es aún desconocido, es posible considerar que la paleogeografía y el patrón sedimentario durante el Coniaciano/Santoniano pudieron al menos originar condiciones anóxicas/disóxicas intermitentes, favorables para el enterramiento de materia orgánica. Se sugiere la búsqueda de este evento en las formaciones San Felipe, Indidura o Austin.

Palabras clave: Sedimentos cretácicos enriquecidos en carbono orgánico, eventos anóxicos oceánicos (OAEs), México, rocas generadoras de hidrocarburos, isótopos estables de carbono.

1. Introduction

The Cretaceous period represents a time of profound transformations in the history of the planet with significant implications in the course towards current conditions. Some of the major episodes of environmental change in the ocean-atmosphere system occurred during the so-called Oceanic Anoxic Events (OAEs). They were short-lived episodes (<1 My) of global marine anoxia that in some cases resuted in widespread organic carbon burial (Schlanger and Jenkyns, 1976; Arthur and Schlanger, 1979; Jenkyns, 1980; Arthur *et al*., 1990). Such events were the result of important chemical changes in the Cretaceous ocean related to perturbations in the carbon cycle. The study of the sedimentary, geochemical and biological records of these goes back over 30 years (Schlanger and Jenkyns, 1976; Arthur and Schlanger, 1979), with the Deep Sea Drilling Project (DSDP) and the Ocean Drilling Program (ODP). These research programs provided geological data for investigations related to the evolution of the Mesozoic oceans. Numerous subsequent investigations focused on pelagic and hemipelagic sediments of the Paleo-Tethys Ocean improved high resolution definition of age and duration of these events, explored the environmental changes under which they took place, and detected regional and local variations that affected their occurrence (Menegatti *et al*., 1998; Erba *et al*., 1999; Leckie *et al*., 2002; Hofmann *et al*., 2003; Weissert and Erba, 2004; Lamolda and Paul, 2007; Mort *et al*., 2007; Millán *et al.*, 2009; Moreno-Bedmar *et al*., 2009, 2012a; Bover-Arnal *et al*., 2010; Westermann *et al*., 2010; Keller *et al*., 2011; Föllmi, 2012; Eldrett *et al*., 2014, and others referenced in this paper).

The importance of recognizing and studying such Cretaceous events resides in the fact that, along with the Jurassic OAEs, they are responsible for the generation of more than 50 % of the global hydrocarbons (Klemme and Ulmishek, 1991).

In Mexico, important hydrocarbon source rocks were deposited during the Cretaceous OAEs; however, research documenting and characterizing such events is scarce. In part, this situation is due to a shortage of biostratigraphic and/or geochronologic studies, which prevents the construction of a proper time framework and the identification of distinctive stratigraphic levels coeval with these events. In some cases a later diagenetic overprint related to tectonic deformation further complicates identification by disturbing the primary geochemical signatures of these events.

In this paper, we discuss the current state of study of the major Cretaceous OAEs in Mexico based on available literature. The examination of this information highlights inconsistencies and agreements between the existing records and allows identifying critical unresolved questions. We also propose a way to tackle the problematic issues and listed stratigraphic units with minor reports of high organic carbon content and/or poorly oxygenated conditions potentially linked to these OAEs. This contribution summarizes and integrates this knowledge, so that it provides a comprehensive view of the major Cretaceous OAEs in Mexico. It aims to be a starting point to search for new records of such events. This study seeks to contribute to a better understanding of the development of poorly oxygenated conditions associated with the deposition of hydrocarbon source rocks, and thus it can assist in evaluating potential exploration opportunities.

2. A brief look at the major Cretaceous OAEs

The Mesozoic DSDP and ODP record mostly comprises Cretaceous sedimentary rocks, which is why OAEs were originally described from deposits of this age (Schlanger and Jenkyns, 1976; Arthur and Schlanger, 1979; Jenkyns, 1980). From their conception, the OAEs were linked to the deposition of organic carbon-rich sediments (mostly referred to as black shales) acting as hydrocarbon source rocks and commonly related to giant oil-field reservoirs (Arthur and Schlanger, 1979). The causes of enhanced synchronous organic matter sequestration by sediments during OAEs are thought to be the result of complex feedback mechanisms such as sea level rise, increase in oceanic crust production and CO_2 outgassing, emplacement of large igneous provinces, high surface ocean temperature, acceleration of the hydrological cycle, changes in ocean circulation patterns and, enhanced marine productivity (Sinton and Duncan, 1997; Leckie *et al*., 2002; Mort *et al*., 2007; Méhay *et al*., 2009; Keller *et al*., 2011; Föllmi, 2012). These components controlled production and preservation of organic matter in sedimentary environments and resulted in characteristic sedimentary features, carbon isotope patterns and trace element enrichment; signatures that can be traced in the sedimentary record. Its is noteworthy that regional or local conditions have the potential to modify these records.

Several OAEs occurred during the Cretaceous, particularly during the Barremian-Santonian interval; Figure 1A (Leckie *et al*., 2002; Jenkyns, 2010; Föllmi, 2012). However, the most studied OAEs due to the distribution of their record, duration, global impact on the ocean-atmosphere system, and importance for hydrocarbons production, are (a) the early Aptian OAE 1a (Selli event), (b) the Cenomanian/Turonian boundary OAE 2 (Bonarelli event), and (c) the Coniacian/Santonian boundary OAE 3. They are classically recognized by the presence of a long-term positive $\delta^{13}C$ excursion that can be predated by a short-lived negative spike. The positive carbon isotope excursions are related with a heightened ^{12}C removal from seawater resulting from the enhanced burial of organic carbon in marine sediments during episodes of high productivity (Ingall *et al*., 1993; Leckie *et al*., 2002; Jarvis *et al*., 2006; Mort *et al*., 2007). The negative carbon isotope excursions are commonly linked to a rapid release of isotopically light carbon into the ocean-atmosphere system either to organic matter decomposition or CO_2 degassing associated with volcanism and/or massive methane release from clathrates (Beerling *et al*., 2002; Jahren, 2002; Méhay *et al*., 2009).

The OAE 1a was included in the initially described OAE 1 occurring from late Barremian through middle Albian (Schlanger and Jenkyns, 1976; Arthur and Schlanger, 1979; Jenkyns, 1980). It was not until Arthur *et al*. (1990) that the OAE 1a was recognized as an isolated event in the early Aptian. This event is associated with increased marine productivity, a sea-level rise, a major episode of drowning of carbonate platforms, and a widespread nannoconid crisis (Erbacher *et al*., 1996; Menegatti *et al*., 1998; Weissert and Erba, 2004; Millán *et al*., 2009; Föllmi, 2012). It has a temporal relationship with (a) the onset of the long-term mid-Cretaceous greenhouse, which prompted high rates of continental runoff and nutrient supply (Jones and Jenkyns, 2001; Leckie *et al*., 2002; Weissert and Erba, 2004), and (b) the initiation of an interval of increased submarine volcanism in the Pacific ocean related to the emplacement of the Ontong Java-Manihiki plateau, which stimulated marine productivity through the hydrothermal input of biolimiting metals (*e.g*. Fe, Co, Mn, Cu, Zn, Se) (Larson, 1991; Jones and Jenkyns, 2001; Jahren, 2002). Currently, the proper way to record this event is by identifying the distinctive segments of Menegatti *et al*. (1998), which are characteristic long-term carbon isotope trends linked to different disturbances in the global carbon cycle during the late Barremian/Aptian. According to this global standard pattern, the onset of OAE 1a is marked by a sharp negative $\delta^{13}C$ excursion (segment C3) followed by an abrupt and prolonged positive $\delta^{13}C$ excursion (segments C4 to C6) (Erba *et al*., 1999; Leckie *et al*., 2002; Millán *et al*., 2009; Bover-Arnal *et al*., 2010; Najarro *et al*., 2011; Moreno-Bedmar *et al*., 2012a).

The OAE 2 is the most widespread and best defined OAE of the Cretaceous OAE. The anoxic conditions developed during this event are interpreted as the consequence of enhanced marine productivity due to iron fertilization prompted by the emplacement of the Caribbean large igneous province (Sinton and Duncan, 1997; Snow *et al*., 2005). According to Mort *et al*. (2007), an active mechanism that sustained marine productivity during the OAE 2 was the recycling of P and other nutrients from sediments overlain by anoxic waters. The Bonarelli event is traditionally associated with a broad positive carbon isotope excursion (Schlanger and Jenkyns, 1976; Jenkyns, 1980; Snow *et al*., 2005; Jarvis *et al*., 2006; Westermann *et al*., 2010). Other investigations report the occurrence of a small abrupt negative carbon isotope excursion predating the positive shift in $\delta^{13}C$ (Hasegawa and Saito, 1993; Erbacher *et al*., 2004; Kuroda *et al*., 2007).

The less studied among the Cretaceous OAEs is the OAE 3 (Jenkyns, 1980; Arthur *et al*., 1990; Hofmann *et al*., 2003). It is the longest of the OAEs and, unlike OAE 1a and OAE 2, its record is regionally limited and characterized by a moderate positive $\delta^{13}C$ excursion. Organic carbon-rich sediments related to this OAE have been documented on both sides of the Atlantic Basin (Wagner *et al*., 2004). This distribution was likely influenced by the deepening and widening of the connection between the Central and South Atlantic, and the free exchange between deep and surface water masses during the Coniacian/Santonian (Wagner and Pletsch, 1999; Pletsch *et al*., 2001; Wagner *et al*., 2004). As result, restricted epicontinental basins developed along the upper continental margins of the Atlantic Basin, together with an oxygen minimum zone favoring the preservation of

rich organic sediment (Dean *et al*., 1984; Erlich *et al*., 1999).

3. Major Cretaceous OAEs in Mexico: current state and discussion

3.1. The OAE 1a (Selli event)

Research regarding the OAE 1a has focused on the pelagic Barremian/Aptian succession of northeastern Mexico. Although the $\delta^{13}C$ signal of this event was identified, little effort has been done in order to study its effects on the Mexican Sea. Critical questions that remain unanswered are those related to (a) the redox regime, (b) changes on the water chemistry, and (c) impact on the carbonate platform development. A multi-proxy investigation based on sedimentary, paleontological and geochemical proxies could provide answers to these questions. Given that the Aptian-Albian is a time interval containing hydrocarbons source rocks in some wells across northern Mexico (Monreal and Longoria, 2000), answering these questions is also important in order to increase the knowledge of the hydrocarbon system.

Early studies related to the known (at that time) OAE 1 were conducted by Scholle and Arthur (1980) at cretaceous organic carbon-rich pelagic limestones of the Sierra Madre Oriental exposed at Peregrina Canyon and rancho Jacalitos (Tamaulipas and Nuevo León states, respectively; Figures 1B and 2). These authors identified a positive carbon isotope excursion ($\delta^{13}C_{carb}$ = ~1.5 – 2.0 ‰) near the Aptian/

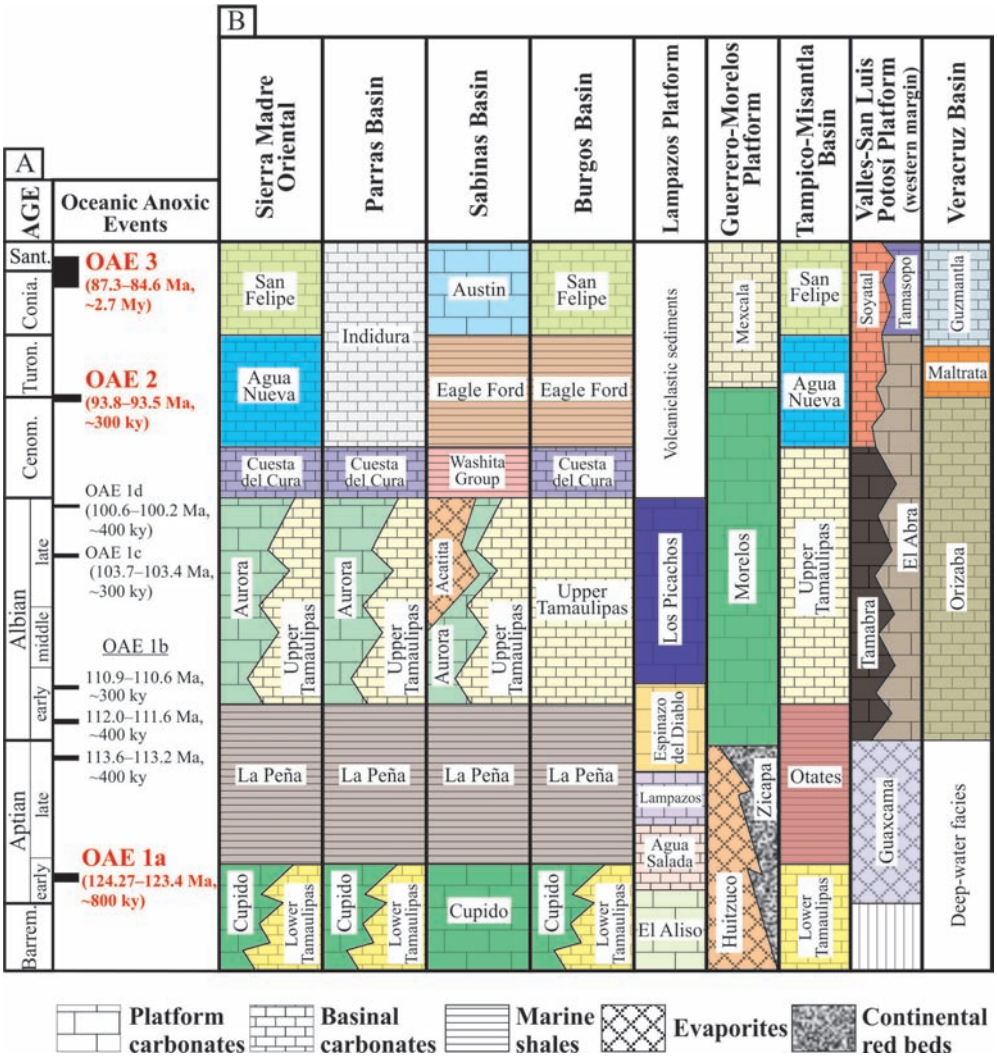

Figure 1. A. Cretaceous Oceanic Anoxic Events (OAEs) of the Barremian-Santonian interval. Approximate absolute-age durations are from Ogg *et al*. (2004) and Wagner *et al*. (2004). Three major events are in bold and red. B. Stratigraphic correlation chart of the areas mentioned in this investigation. Sources: Sierra Madre Oriental : Goldhammer (1999); Parras Basin: Lehmann *et al*., (1999); Sabinas Basin: Eguiluz-de Antuñano and Amezcua (2003); Burgos Basin: Salvador and Quezada-Muñetón (1989); Lampazos Platform: Monreal and Longoria (2000), Santa María-Díaz and Monreal (2008); Guerrero-Morelos Platform: Hernández-Romano *et al*. (1997), Aguilera-Franco (2003), Elrick *et al*. (2009); Tampico-Misantla Basin: López-Doncel (2003); Valles San Luis Potosí Platform: López-Doncel (2003), Omaña (2011); Veracruz Basin: Ortuño-Arzate *et al*. (2003).

Albian boundary that assigned to this event. At Peregrina Canyon, the $\delta^{13}C$ anomaly is predated by an interval with high total organic carbon (TOC) content (up to ~0.8 %; ~3 – 4 × background) (Figure 3A). Unfortunately, they failed to mention about the exact lithostratigraphic position of such anomaly. It was not until the study of Bralower *et al*. (1999) that the first report of the OAE 1a occurred. They studied the carbon isotope record of four Barremian/Aptian localities in northeastern Mexico. The most complete record of the OAE 1a was found in the Santa Rosa Canyon section, in the leading edge of the Sierra Madre Oriental thrust and fold belt (Nuevo León State; Figures 1B and 2). The Barremian/Aptian exposed succession of such section corresponds to the lime mudstones with chert nodules of the Lower Tamaulipas Formation and the overlying intercalation of marls and mudstones of the La Peña Formation. The former is the basinal equivalent of the shallow-water skeletal limestones of the Cupido Formation, which represents a carbonate platform with the same name that developed around the Coahuila block. Bralower *et al*. (1999) constructed an organic carbon isotope ($\delta^{13}C_{org}$) curve for Santa Rosa and compared it to the curve of Peregrina Canyon developed by Scholle and Arthur (1980). Based on this comparison, these authors reinterpreted the chronostratigraphic position of the latter, defined the segments of Menegatti *et al*. (1998), and identified the OAE 1a at Peregrina Canyon (Figure 3B). At Santa Rosa, the OAE 1a consists of a positive $\delta^{13}C$ shift about 2.0 ‰ predated by a ~1.5 ‰ negative spike toward the base of the La Peña Formation (Figure 3C). This stratigraphic interval is also characterized by a two-fold increase in TOC (2 – 3 %). Later, Li *et al*. (2008) resampled in greater detail the Santa Rosa Canyon section, and developed a new $\delta^{13}C_{org}$ curve with a new position of the OAE 1a. According to their results, this event is located between the uppermost part of the Lower Tamaulipas Formation and the base of the La Peña Formation (Figure 3D). Besides the isotope data, Bralower *et al*. (1999) and Li *et al*. (2008) constrained their $\delta^{13}C_{org}$ curves through the determination of planktonic foraminifera and calcareous nannofossil biozones. Based on the magnetostratigraphic data of Clement *et al*. (2000), Li *et al*. (2008) also suggested that OAE 1a lasted ~1.28 My, being its record at Santa Rosa a relatively expanded OAE 1a succession.

The investigations of Bralower *et al*. (1999) and Li *et al*. (2008) might be questionable considering that

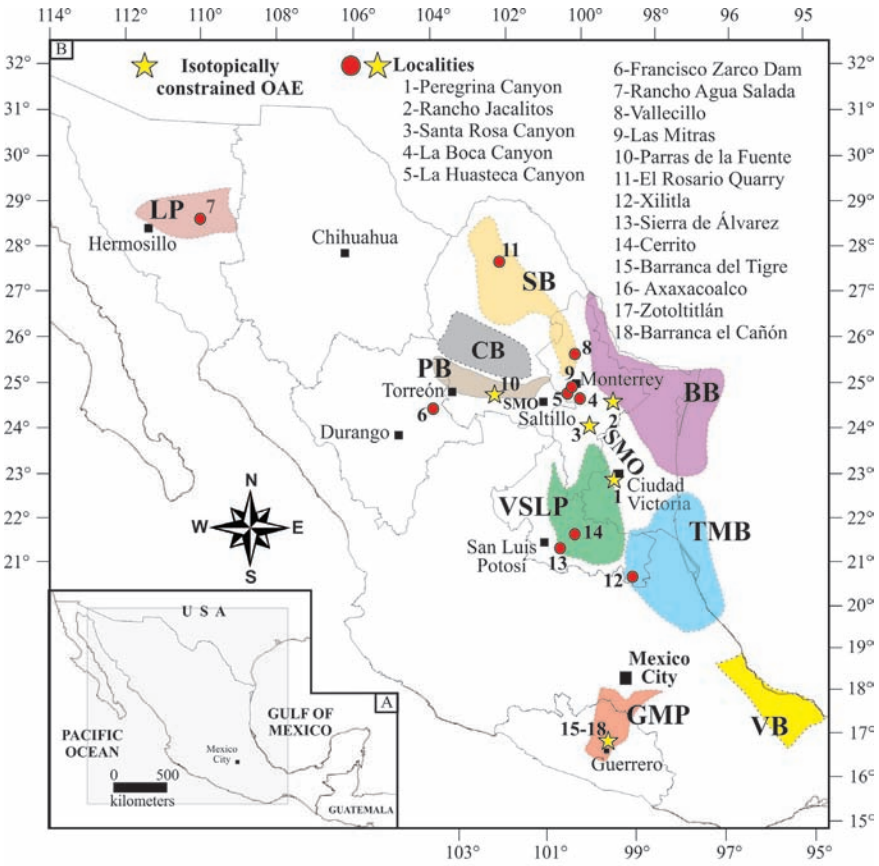

Figure 2. A. Sketch map of México. Boxed area is shown in detail in B. B. Location of paleogeographic elements and localities related to the record of the major Cretaceous OAEs. BB = Burgos Basin, CB = Coahuila Block, GMP = Guerrero-Morelos Platform, LP = Lampazos Platform, PB = Parras Basin, SB = Sabinas Basin, TMB = Tampico-Misantla Basin, VSLP = Valles-San Luis Potosí Platform, VB = Veracruz Basin. Sources: Goldhammer (1999); Lehmann *et al*. (1999); Lawton *et al*. (2001); López-Doncel (2003); Ortuño-Arzate *et al*. (2003).

they sampled separate segments instead of a continuous stratigraphic section, with a lack of data for ~7 m at the Lower Tamaulipas/La Peña contact, immediately above the negative $\delta^{13}C$ spike of Li *et al*. (2008) (Figure 3D). Considering the ammonite biostratigraphy (the most accurate for the Aptian to date), a misidentification of the OAE 1a at Santa Rosa Canyon section is indeed highly possible. Although there is no ammonite database for the La Peña Formation of Santa Rosa, if we consider that the base of this formation is isochronous and assignable to the *Dufrenoyia justinae* Zone (Barragán-Manzo and Méndez-Franco, 2005; Barragán and Maurrasse, 2008; Moreno-Bedmar *et al*., 2011; 2012b; Moreno-Bedmar and Delanoy, 2013), we can infer that the lowermost part this unit at Santa Rosa Canyon section also belongs to this ammonite zone. At La Boca and the Huasteca Canyon sections (Nuevo León State; Figure 2), close to Santa Rosa Canyon, the ammonite record of the lowermost part of the La Peña Formation also starts in the *Dufrenoyia justinae* Zone (Cantú-Chapa, 1976; Barragán-Manzo and Méndez-Franco, 2005; Barragán and Maurrasse, 2008). In the ammonite Mediterranean biostratigraphic scheme of Reboulet *et al*. (2014), this Mexican ammonite zone is representative of the uppermost part of the late early Aptian *Dufrenoyia furcata* Zone. Therefore, it is likely that the base of the La Peña Formation at Santa Rosa section has a younger age than the OAE 1a event, commonly restricted to the early Aptian *Deshayesites forbesi* Zone (Moreno-Bedmar *et al*., 2009; 2012a; Najarro *et al*., 2011; Bover-Arnal *et al*., 2010; Gaona-Narvaez *et al*., 2013). Hence, the OAE 1a should be located within the Lower Tamaulipas Formation (or the Cupido Formation) instead of the La Peña Formation (or the time-equivalent Otates Formation consisting of shaly and organic-rich limestones) (Figure 4). This situation would imply that the deposition of the Cupido Formation lasted beyond the early Aptian and probably the Cupido Platform survived the OAE 1a.

If the previous scenario is correct, what is the significance of the organic carbon-rich sediments at the base of the La Peña Formation? Such levels with high TOC have been reported at the Francisco Zarco dam section (Durango State; Figure 2) (Barragán, 2001) and La Huasteca section (Nuevo León State; Figure 2) (Barragán and Maurrasse, 2008). In both places, the La Peña Formation also starts within the *Dufrenoyia justinae* Zone. This interval has been correlated by Millán *et al*. (2009) and Skelton and Gili (2012) with TOC-enriched sediments of the base of the Lareo Formation (*Dufrenoyia furcata* Zone) from the Basque-Cantabrian basin in Spain, and corresponding to the so-called Aparein level. It is a new OAE occurring in the upper part of the early Aptian, associated with a carbonte platform termination. As suggested for the Aparein level by Millán *et al*. (2009), the TOC-enriched levels at the base of the La Peña Formation may represent the last period of dysoxia/anoxia at the top of the early Aptian (Bralower *et al*., 1994; Föllmi, 2012).

On the other hand, it is noteworthy that magneto-

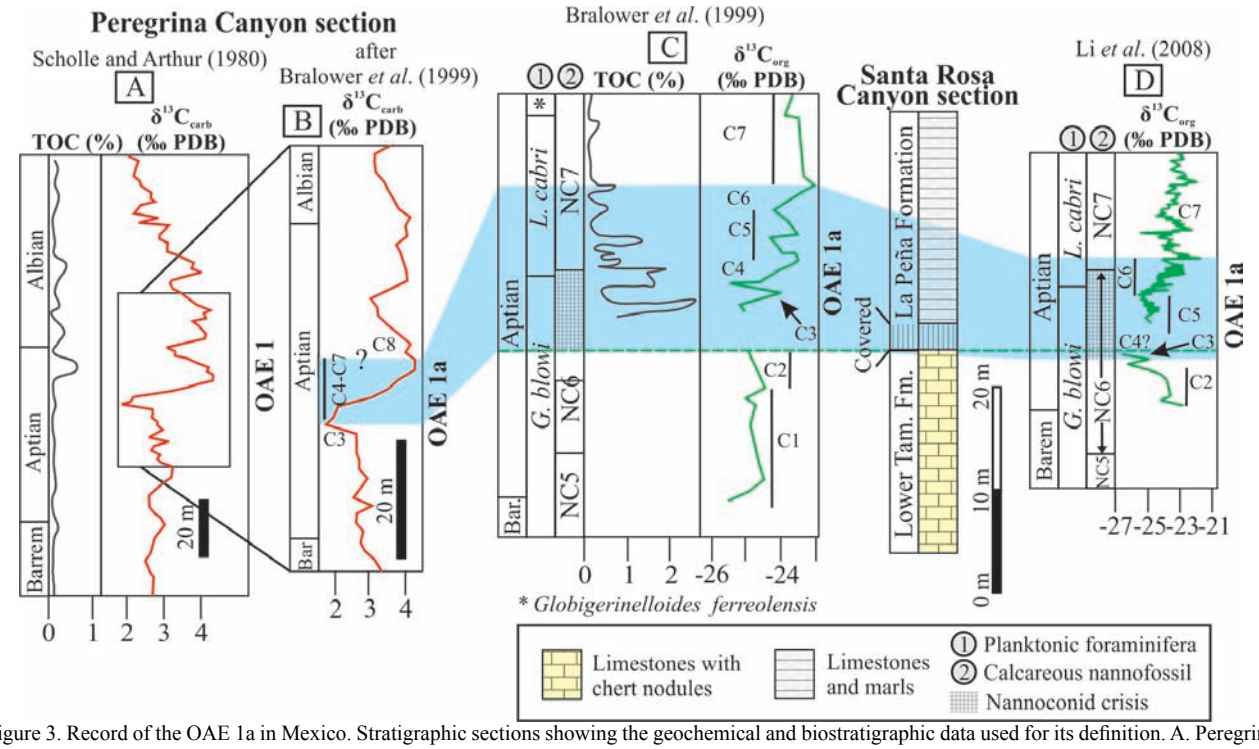

Figure 3. Record of the OAE 1a in Mexico. Stratigraphic sections showing the geochemical and biostratigraphic data used for its definition. A. Peregrina Canyon section (Scholle and Arthur, 1980). B. Peregrina Canyon section (Bralower *et al*., 1990). In the interpretation of Bralower *et al*. (1999) of the curve by Scholle and Arthur (1980), the segments C4 to C6 were not individually identified; therefore the isotope end of the OAE 1a was not determined. C, D. Santa Rosa Canyon section (Bralower *et al*., 1999 and Li *et al*., 2008, respectively).

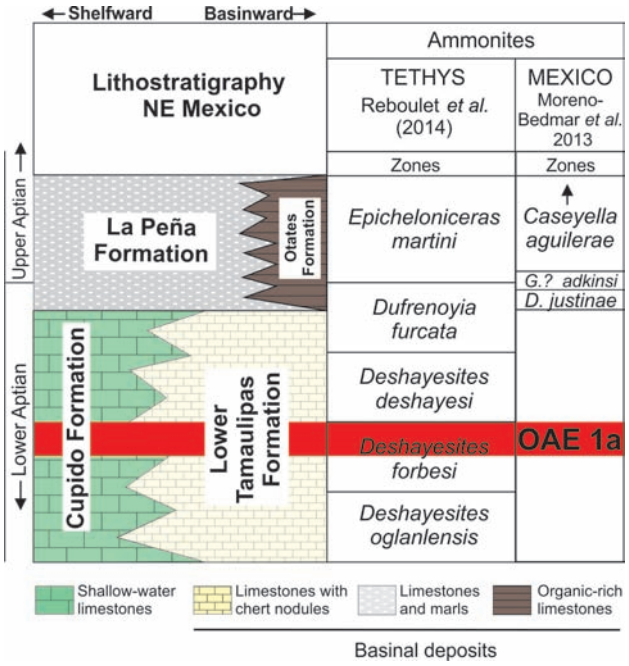

Figure 4. Aptian lithostratigraphy of northeastern México correlated with the standard Mediterranean ammonite zonation (*pro parte*) and the Mexican ammonite zonation. The red rectangle marks the current age calibration of the OAE 1a. Note that based on ammonite biostratigraphy, the base of the La Peña formation is younger than the OAE 1a.

stratigraphic and micropaleontological data support the presence of the OAE 1a at the base of the La Peña Formation. In this regard, a characteristic interval link to the record of the OAE 1a that both Bralower *et al*. (1999) and Li *et al*. (2008) documented at the base of the La Peña Formation is the nannoconid crisis interval. In this case, our supposition might be wrong and key topics such as the isochronism/diachronism of the La Peña Formation and the correspondence between planktonic foraminifera, calcareous nannofossil and ammonite biozones have to be strongly addressed.

In order to answer these questions, further carbon isotope and biostratigraphic/magnetostratigraphic studies must be conducted in the Lower Tamaulipas(Cupido)/La Peña formations. The age of the demise of the Cupido Platform (the Cupidito facies) should be determined along with a precise identification of the segments of Menegatti *et al*. (1998). For instance, these tasks could be undertaken in the lowermost 7 m of the La Peña Formation at the Santa Rosa Canyon section. A properly constrained C-isotope curve is key to identify the signal of global and regional/local events. Given the nature of nearshore deposits of the Cupido Formation along with diagenetic processes that could mask the primary geochemical signal (*e.g.* fresh-water input, elevated evaporation rates), the Lower Tamaulipas Formation seems to be a suitable candidate for carbon isotope studies. In the search for the record of anoxic/dysoxic conditions, an interesting new approach could be the study of oxygen levels from the fossil assemblage and trace element data. Thus, these redox regimes would not only be recorded but could also be deciphered in terms of their global and/or local effects. On the other hand, if the Aparein level was precisely located, it will be its first record outside Europe, implying a wider paleogeographic extension for this event, and supporting its probable use as a chemostratigraphic marker.

3.1.1. Other reports and prospects for further studies

Lampazos Platform: Monreal and Longoria (2000) correlated the OAE 1a (as defined by Bralower *et al*., 1999 at Santa Rosa Canyon) with the base of the Agua Salada Formation of the Lampazos Platform (Figures 1B and 2). This unit is characterized mainly by calcareous shale and limestone beds consisting of pelagic skeletal wackestones and floatstones. It is important to mention that the re-assignment of the middle part of the Agua Salada Formation to the early Aptian, as well as the presence of black shales in its lower part (which may be the lithologic expression of the anoxic episode), support the hypothesis of the base of this unit recording the OEA la (González-León, 1988; Monreal and Longoria, 2000; Santa María-Díaz and Monreal, 2008). The occurrence of the ammonite *Dufrenoyia justinae* in the upper part of the unit at Rancho Agua Salada section (Sonora State; Figure 2) (González-León, 1988) does not exclude this possibility.

3.2. The OAE 2 (Bonarelli event)

This OAE is the most documented and studied in Mexico and elsewhere. The record of the OAE 2 has been reported in southern, central and northern Mexico (Scholle and Arthur, 1980; Duque-Botero and Maurrasse, 2004; Ifrim, 2006; Blanco-Piñón *et al*., 2008, 2014; Rojas-León *et al*., 2008; Duque-Botero *et al*., 2009; Elrick *et al*., 2009; Blanco *et al*., 2010, 2011; Ifrim *et al*., 2011). The interest in studying this event lies in the fact that several Cenomanian/Turonian rocks are proved or potential prolific hydrocarbon source rocks. Despite this, the genetic link of the OAE 2 with these rocks in several basins is still poorly understood.

3.2.1. Northeastern Mexico

At Peregrina Canyon (Figure 2), within the hemipelagic limestones and shaly limestones (mudstones and wackestones) of the Agua Nueva Formation, Scholle and Arthur (1980) found a positive shift in $\delta^{13}C$ values of cabonates of ~1.5 ‰ spanning almost the entire Turonian, which was interpreted as the geochemical signature of the OAE 2 (Figure 5A). This positive $\delta^{13}C$ excursion overlaps partly with an organic carbon-rich interval (up to 2.5 %, about 10 – 12 × background values).

Recent studies focused on the Agua Nueva Formation have linked its informal Vallecillo Member (Blanco-Piñón, 2003), a Konservat-Lagerstätten deposit, to the OAE 2 occurrence (Blanco-Piñón, 2003; Ifrim, 2006; Ifrim *et al*., 2011). At Vallecillo section (Nuevo Léon State; Figure

2), this member is characterized by laminated marly limestones to plattenkalk with abundant and very well preserved fish fossils. At Las Mitras section (Nuevo León State; Figure 2), the base of this member is a black shale level. Ifrim (2006) constrained the age of the Vallecillo Member to the latest Cenomanian/early Turonian time interval through ammonite, inoceramid and planktonic foraminifera biostratigraphy. This author unsuccessfully searched for the carbon isotope signal of the OAE 2 in both the Vallecillo and Las Mitras sections. According to him, such task was not possible due to the existence of a diagenetic overprint evidenced by a clear negative correlation between $\delta^{13}C$ and $\delta^{18}O$ values. In this regard, we recommend further efforts to find the carbon isotope signature of this event, including a characterization of the TOC content. It is possible that the characteristic inflection point in the $\delta^{13}C$ curve at the Vallecillo section that marks the onset of the OAE 2 is recorded in a lower stratigraphic position, considering that such point occurs in an older planktonic foraminifera biozone (*Rotalipora cushmani*) than that recorded at the base of the Vallecillo section (*Whiteinella archaeocretacea*). Ifrim (2006) interpreted the presence of pyrite framboids with the same morphology and uniform size of around 2 µm in the Vallecillo Member as a sign of anoxic pore-water conditions with high H_2S content. Strong depletion in Mn and remarkable peaks of Cu, Ni and Zn also portray poorly oxygenated settings. Based on the fossil assemblage distribution, this author proposed that the onset of the oxygen depletion above the seafloor began in the late Cenomanian and reached the seafloor in the latest Cenomanian as result of the vertical expansion of the oxygen minimum zone.

Duque-Botero and Maurrasse (2004) and Duque-Botero *et al*. (2009) examined the Cenomanian/Turonian stratigraphic interval of the Indidura Formation in several stratigraphic sections from the Parras Basin at the Coahuila State (Figure 1B). This unit consists mainly of pelagic mudstones to wackestones and intercalated shales. At the base of the Parras de la Fuente section (Figure 2), within the identified CC10 (containing the Cenomanian/Turonian boundary) and the lower part of the CC11 calcareous nannoplankton biozones, these investigations documented a positive $\delta^{13}C$ anomaly up to ~2 ‰ in organic carbon that related to the OAE 2 (Figure 5B). This interval comprises ~15 – 16 m and does not exhibit high TOC (0 – 1.5 %); however, it records redox indices [(V/(V+Ni), V/Cr and Mo content)] that reveal oxygen-depleted conditions at the time of its deposition.

According to Duque-Botero *et al*. (2009), poorly oxygenated conditions favoring the deposition of organic carbon-rich sediments in northeastern Mexico prevailed during the Cenomanian/Turonian and lasted for about 4 million years (that is, until the Coniacian). Therefore, such conditions also influenced the deposition of the Indidura Formation. As it is attested by the cyclic laminations of bacterial microspheres, interpreted as blooms of cyanobacteria, these conditions resulted from intense primary productivity associated with periodic incursions of riverine Fe-rich waters. Accordingly, Ifrim (2006) suggest that although the uppermost water layers became

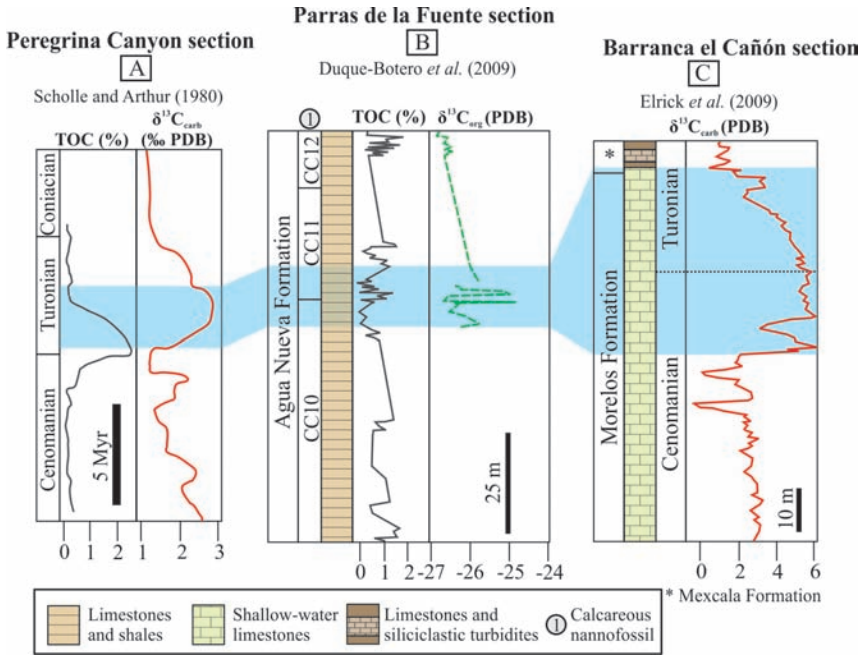

Figure 5. Record of the OAE 2 in Mexico. Stratigraphic sections showing the geochemical and biostratigraphic data used for its definition. A. Peregrina Canyon section (Scholle and Arthur, 1980). B. Parras de la Fuente section (Duque-Botero *et al*., 2009). C. Barranca el Cañón section (Elrick *et al*., 2009). Among the sections studied by Elrick *et al*. (2009) containing the carbon isotope expression of the OAE 2, only the Barranca el Cañón section is shown due to its completeness.

oxygenated during the early Turonian, the bottom remained anoxic. Stinnesbeck *et al*. (2005) also pointed to the prevalence of poorly oxygenated conditions until the early Coniacian, based on the excellent preservation showed by a Turonian/lower Coniacian fossil assemblage (including vertebrate fossils with soft tissues) at El Rosario quarry (Coahuila State; Figure 2), in strata assigned to the Austin Formation of the Sabinas Basin (Figures 1B and 2). This unit consists of intercalated marl and limestone (chalk) deposited under open marine conditions.

3.2.2. Guerrero-Morelos Platform

The OAE 2 in southern Mexico was mentioned for the first time by Hernández-Romano *et al*. (1997) in a study of the Guerrero-Morelos Platform (Figures 1B and 2). These authors studied the Morelos and Mezcala formations at the Barranca del Tigre, Axaxacoalco and Zotoltitlán sections (Guerrero State; Figure 2). The Morelos Formation is composed of shallow-marine limestones that was part of an Albian/Cenomanian carbonate platform in southern Mexico. It is characterized by bioclastic and intraclastic limestones. On the other hand, the Mezcala Formation corresponds to interbedded hemipelagic limestones and siliciclastic turbidites. Based on the vertical distribution of microfossils (benthonic and planktonic foraminifera, calcareous algae and calcisphaerulids), the three sections were constrained to the middle Cenomanian/early Turonian time interval. These authors suggested that the OAE 2 caused, in part, the drowning of the platform, which occurred first in the western zone. According to their model, the expansion of an oxygen minimum zone related to an upwelling system along the Pacific side of the platform and the sea level rise during the latest Cenomanian/earliest Turonian, resulted in the invasion of oxygen-poor waters over the platform, disappearance of benthos, and shut down of the carbonate production. This is reflected by a drastic diminishing of benthic flora and fauna, and the appearance of an organism assemblage resistant to low oxygen levels from the Morelos Formation to the Mezcala Formation. This transition is also characterized by black, organic-rich, laminated sediments lacking bioturbation. A greater subsidence rate of the western portion of the platform also stimulated its demise. On the other hand, the platform termination in the eastern part occurred in the middle Turonian as result of the interplay of terrigenous-clastic supply and a new impingement of anoxic waters.

Elrick *et al*. (2009) also studied the Barranca del Tigre and Axaxacoalco sections and added them to their investigation of the Barranca el Cañón section (Guerrero State; Figure 2). Over a ~40 m-thick interval of the Morelos Formation containing the Cenomanian/Turonian boundary (in the three sections), they found an abrupt $\delta^{13}C$ positive shift (3 – 4 ‰) in carbonates that related to the isotopic signature of the OAE 2 (Figure 5C). However, the sediments of this interval lack the typical features of oxygen-depleted conditions, such as TOC enrichment or laminated fabrics; instead, these rocks exhibit a bioturbated fabric reflecting a well oxygenated setting. Such redox regime was associated with the abundant supply of oxygen from the ocean surface-atmosphere interface to the shallow-water sediments. The study of Elrick *et al*. (2009) not only resulted in the first isotopically constrained expression of the Bonarelli event in southern Mexico, but is also an important contribution to the poor database of this event in both the proto-Pacific area and carbonate platform settings. So far, the Mexican record of the OAE 2 at the Guerrero-Morelos Platform is one of the most stratigraphically expanded and contains one of the largest reported positive $\delta^{13}C$ excursions to date.

Across the Mexican territory, the $\delta^{13}C$ anomaly related to the OAE 2 has been interpreted as the response of seawater to the increase of iron caused by the emplacement of the Caribbean plateau. Such scenario is feasible since the area of volcanic eruptions (over the Galapagos hot spot) took place at a relatively short distance from Mexico (~2000 to 4000 km according to the tectonic plate reconstruction of Wignall, 1994). Considering the model of surface circulation during Late Cretaceous (Barron and Peterson, 1990), and the Cenomanian/Turonian Mexican paleogeography (Goldhammer, 1999; Padilla y Sánchez, 2007), water masses carrying metals may have been transported to the Mexican Sea, thereby intensifying primary production and producing $\delta^{13}C$ positive values. For the Mezcala Formation, Snow (2003) measured the abundance of trace elements with short and long residence time in seawater and found concentrations consistent with the increase of magmatic and hydrothermal activities. According to Elrick *et al*. (2009), this hypothesis is also supported by the coincidence of strong peaks of trace elements at the onset of the $\delta^{13}C$ excursion and at the end of the maximum positive excursion at the Barranca el Cañón. Duque-Botero *et al*. (2009) also suggest the influence of the Caribbean plateau volcanism on the Indidura Formation deposition; however, this relation is still poorly studied. Arguments supporting this scenario are: (1) the record of the effects of this activity on the positive $\delta^{13}C$ excursion at the Rock Canyon section in the Western Interior Seaway (around 5000 km from the source) (Snow, 2003; Snow *et al*., 2005), indicating that the Mexican Sea must have acted as a bridge and was also affected; and (2) the trace element abundances measured by Duque-Botero *et al*. (2009) coinciding with the end of the maximum $\delta^{13}C$ positive excursion. In order to corroborate the link between the OAE 2 and the Caribbean plateau volcanic and hydrothermal activity, it is necessary to examine trace metal enrichment patterns of elements in other sections deposited at the Cenomanian/Turonian sections.

Unlike the studies that have addressed the OAE 1a, those focused on the OAE 2 have looked into the causes of the drawdown in seawater oxygen concentrations and/or the occurrence of the positive carbon isotope excursion; however, additional studies are still needed. Some of the promising stratigraphic units that could constitute the basis for further research are listed below. It is significantly

important to search for signs of submarine volcanic activity by measuring trace metal abundances. It allows to clarify the effects of this activity on sewater chemistry and Mexican carbonate platforms. In this task, useful proxies that could be included are the strontium ($^{87}Sr/^{86}Sr$) and osmium ($^{197}Os/^{186}Os$) isotope ratios. These isotope measurements will allow an accurate differentiation between the signatures of local weathering and global ocean crust production (Jones and Jenkyns, 2001; Leckie *et al*., 2002). Furthermore, $^{87}Sr/^{86}Sr$ ratios will help increasing the age control, especially in stratigraphic sections lacking a proper biostratigraphic age control.

3.2.3. Other references and prospects for further studies

Burgos and Sabinas basins: The Eagle Ford Formation of the Burgos and Sabinas basins (Figures 1B and 2) is a proved oil and gas source rock. This unit was deposited on a shallow-marine shelf at the southern end of the Western Interior Seaway (WIS) of North America, and is characterized by mixed siliciclastic-carbonate mudstones and shales. It has a TOC content of about 1 – 4 % with mainly marine-derived organic matter (type II) (Escalera-Alcocer, 2012). Within the frame of the current interest for non-conventional hydrocarbons, the Eagle Ford Formation is one of the top-ranked prospects in Mexico (EIA/ARI, 2013). The OAE 2 recorded in the organic carbon-rich deposits of this unit has been recognized and characterized in Texas, USA (Kearns, 2011; Eldrett *et al*., 2014).

Tampico-Misantla Basin: Several studies report that the Agua Nueva Formation of the Tampico-Misantla Basin (Figure 1B) at the Xilitla section contains the record of the OAE 2 (Blanco *et al*., 2010, 2011; Blanco-Piñón *et al*., 2008, 2014; Rojas-León *et al*., 2008). The Xilitla section (San Luis Potosí State; Figure 2) consists mainly of intercalated hemipelagic mudstones and wackestones, shales and bentonites. Calcareous beds contain common fishes and inoceramids. The evidences of poorly oxygenated conditions near the seafloor during its deposition are: (a) total lack of bioturbation, (b) fine lamination of the sediments, (c) TOC up to 9.9 %, and (d) presence of framboidal pyrite. These investigations also found structures of algal/bacterial origin in both micritic matrix and pyrite laminae. Recently, Castañeda-Posadas *et al*. (2014) reported also the presence of brackish and fresh-water stomatocysts in laminated pyrite from Xilitla beds preserved under oxygen-deficiency conditions in a low energy environment. They proposed that the riverine input could be responsible for the delivery of this type of continental material to the marine realm.

Valles-San Luis Potosí Platform: The base of the Soyatal Fomation in the western margin of the Valles-San Luis Potosí Platform (Figures 1B and 2) has been assigned by Omaña (2011) and Omaña *et al*. (2013) to the latest Cenomanian/early Turonian through planktonic foraminifera. It is composed of dark calcareous limestones, marly limestones and shales, commonly interpreted as turbidite deposits. The analysis of several stratigraphic sections, mainly the Sierra de Álvarez section (Figure 2), allowed these authors to determinate that changes in nutrient gradient across the El Abra/Soyatal formations was a determinant factor for the drowning of the Valles-San Luis Potosí Platform. This event was triggered by changes in the global sea-level and eutrophic conditions during the OAE 2. At the Cerritos section (Figure 2), these changes are evidenced by a pithonellid bloom associated with a microfossil assemblage indicative of low oxic–dysoxic bottom conditions (Omaña *et al*., 2014).

Veracruz Basin: The deep-water facies of the Turonian Maltrata Formation of the Veracruz Basin (Figures 1B and 2), and the tectonic front of the Córdoba Platform, are well-known source rocks of hydrocarbons (González-García and Holguín-Quiñones, 1992; Ortuño-Arzate *et al*., 2003). This unit consists of dark limestones and shaly limestones with an average TOC content of 3 – 4 % and marine-derived organic matter (type II) (Ortuño-Arzate *et al*., 2003).

3.3. The OAE 3

The OAE 3 has not yet been recognized in Mexico; however sediments linked to this OAE in America have been documented in Venezuela (Davis *et al*., 1999; Erlich *et al*., 1999; Crespo de Cabrera *et al*., 1999), Colombia (Vergara, 1997; Rangel *et al*., 2000), Surinam (Shipboard Scientific Party, 2002), Ecuador (Brookfield *et al*., 2009), and in areas rather close to Mexico such as Costa Rica and Panama (Erlich *et al*., 1996; 2003), and the Western Interior Seaway, USA (Bottjer and Stein, 1994; Dean and Arthur, 1998). In most of these areas, the temporal distribution of black shales related to the OAE 3 indicates that it was not a single and distinct event, but several discrete episodes that occurred over a long time interval, from the Coniacian to the Santonian (Wagreich, 2012). Considering the basin conditions favorable for the development of the OAE 3 in the aforementioned areas and the Coniacian/Santonian Mexican paleogeography and sedimentary pattern, we explore the possibilities of Mexican basins and stratigraphic units for recording this OAE.

Unlike the areas where the OAE 3 is documented, in Mexico there was not a restricted epicontinental sea during the Late Cretaceous. Although the Mexican Sea was separated from the Pacific Ocean by a large Cenomanian volcanic arc (Grajales-Nishimura *et al*., 1992; Goldhammer, 1999; Centeno-García *et al*., 2008) as result of a major eustatic sea level rise, it had a real connection with both the Atlantic (through the proto-Caribbean) and the Western Interior Seaway (McFarlan and Menes, 1991; Goldhammer, 1999). Such scenario may have allowed for the mixing of intermediate waters, reducing the possible occurrence of oxygen-depleted at the seafloor. However, a closer assessment of the Coniacian/Santonian Mexican Sea shows that it was not a broad unbroken depositional realm. This sea consisted of marine basins separated by relatively prominent topographic submerged/emerged

highs. In eastern Mexico, most of the basement high blocks that resulted from the opening of the Gulf of Mexico had been flooded and only persisted as shrunken islands that on top gave rise to isolated shelf carbonates. The karstic platforms of the Upper Guzmantla and the Upper Tamasopo formations were developed on the drowned and backstepped Córdoba and Valles San Luis Potosí platforms, respectively (Horbury *et al*., 2003). Further south, the Artesa-Nuevo Mundo and Chiapas platforms also remained high (Cros *et al*., 1998; Williams-Rojas and Hurley, 2001). On the other hand, in central Mexico the Laramide phase of deformation occurred between 90 and 65 Ma (Hernández-Jáuregui, 1997; López-Oliva *et al*., 1998), and resulted in a foreland basin system to the east of the tectonic front, encompassing syntectonic sub-basins confined by positive topography (folds and overthrust faults). Together, these topographic highs (submerged or emerged) constituted paleobathymetric barriers that could have controlled (partially restricted) the exchange of bottom waters between basins and the open sea, thus favoring bottom dysoxic/anoxic conditions.

Widespread volcanic ash fall is characteristic of the Coniacian/Santonian time interval in the eastern and southern Gulf of Mexico, as evidenced by abundant bentonite beds interlayered with limestones and shales (Salvador, 1991; Padilla y Sánchez, 2007). This volcanic activity might increase nutrient availability in the ocean surface. Different investigations have determined that ash particles can supply large amounts of bio-available elements to the ocean such as Fe and other important nutrients (PO_3^{-4}, Si, Zn, Mn, Ni, Co and Cu) (Frogner *et al*., 2001; Langmann *et al*., 2010). On the other hand, an increase of terrigenous input prompted by the presence of mountain blocks built by the Laramide orogeny could also enhance primary productivity. The magnified export of organic matter coupled with soil-derived nutrients can stimulate primary production and increase mid-water oxygen consumption (Erbacher *et al*., 1996; Leckie *et al*., 2002). Furthermore, an enhanced continental runoff caused salinity stratification, which is another factor favorable for oxygen-drawdown (Arthur and Natland, 1979); however, associated processes such as massive fluvial outflow and turbidite sedimentation can cause mixing of intermediate-deep waters with oxygenated surface waters (Erlich *et al*., 2003), reducing the preservation potential of organic matter in the water column and on the seafloor.

The foregoing scenario allows the assumption that Coniacian/Santonian Mexican Sea likely developed oxygen-depleted conditions related to the OAE 3; however, they must have been intermittent, disturbed by mixing with oxygenated waters (anoxic/dysoxic variations). One of the main hurdles to overcome in the search for these conditions is the volcanic and detrital supply that may have diluted carbonate and organic material, complicating the detection of the OAE 3. This is the case in the study of (a) the San Felipe Formation, deposited in almost the entire eastern and southern Gulf of Mexico Basin (Figure 1B) and consisting of shaly limestones, calcareous shales and abundant bentonite; (b) the Soyatal Formation (Valles-San Luis Potosí Platform; Figures 1B and 2); and (c) the Mezcala Formation (Guerrero-Morelos Platform; Figures 1B and 2). These stratigraphic units do not seem to be the most suitable for studying redox conditions. In the Formation, TOC content above 1 % is a promising feature likely related to the OAE 3. (González García and Holguín Quiñones, 1992). Given that this unit is a target for shale gas exploration (EIA/ARI, 2013), an appropriate paleoredox study searching for possible links with OAE 3 is key to assisting the exploration. Furthermore, the presence of bentonite beds in this stratigraphic unit allow its radiometric dating (*e.g.* U/Pb, K/Ar, $^{40}Ar/^{39}Ar$). For the Soyatal Formation is noteworthy that Omaña (2011) did not report foraminiferal evidence suggesting stressed poorly oxygenated conditions during the Coniacian/Santonian. According to this author, after the crisis suffered by planktonic foraminifera during the OAE 2, the fossil assemblage from Turonian to late Santonian reflects normal conditions. Since in northeastern Mexico orogenic deformation and subsequent shift from carbonate to clastic deposition started in the early Campanian (Gray *et al*., 2001), the Indidura (Parras Basin; Figures 1B and 2) and Austin formations (Sabinas Basin; Figures 1B and 2) were less prone to detrital contamination.

As previously mentioned, poorly oxygenated conditions during deposition of both units has already been proposed for the early Coniacian (Stinnesbeck *et al*., 2005; Duque-Botero *et al*., 2009); however, similar redox conditions across the Coniacian/Santonian time interval (related to the OAE 3) have not been documented.

4. Conclusions

The $\delta^{13}C$ signal of the OAE 1a has been found in northeastern Mexico in the lower part of the La Peña Formation. Considering the ammonite data, it is probable that the OAE 1a has been misidentified and its record is present within the Cupido/Lower Tamaulipas formations. Sediments with high TOC content at the base of the La Peña Formation could correspond to the European Aparein level or represent the last pulse of dysoxia/anoxia that occurred at the top of the early Aptian. To clarify this situation are necessary new studies that calibrate the age of the Cupido (Lower Tamuilipas)/La Peña formational contact, and construct high-resolution carbon isotope curves throughout such interval. The Agua Salada Formation of the Lampazos platform is another promising unit to be examined searching for the record of this event.

The most documented and studied Cretaceous OAE in Mexico is the OAE 2. It is documented in the organic carbon-rich sediments of the Agua Nueva and Indidura formations in northeastern Mexico, and in the nearshore sediments of the Morelos Formation in southern Mexico. Although trace element concentrations of these records

suggest that the emplacement of the Caribbean plateau stimulated surface water productivity, thereby decreasing O_2 availability and causing the positive $\delta^{13}C$ excursion, it is important to search for new evidence of this activity. The Eagle Ford Formation (Burgos and Sabinas basins), the Agua Nueva Formation (Tampico-Misantla Basin), the Soyatal Formation (Tampico-Misantla Basin), and the Maltrata Formation (Veracruz Basin) are excellent prospects in which to document this event.

Although the OAE 3 has been reported in areas relatively close to Mexico, its record in this country is unknown. Even though the Coniacian/Santonian Mexican Sea was not a truly favorable setting for the record of this event, the paleogeography and the sedimentary pattern may have contributed at least to the development of intermittent anoxic/dysoxic conditions. The San Felipe (several basins), Indidura (Parras Basin) and Austin (Sabinas Basin) formations are candidates to study the record of such conditions.

Acknowledgements

We are most grateful to Miguel Company and Hugh Jenkyns for their insightful comments that helped to improve the final version of the manuscript. We also thank the member of the editorial advisory board Hermann Darío Bermúdez for his valuable suggestions.

References

Aguilera-Franco, N., 2003, Cenomanian–Coniacian zonation (foraminifers and calcareous algae) in the Guerrero–Morelos basin, southern México: Revista Mexicana de Ciencias Geológicas, 20 (3), 202-222.

Arthur, M.A., Natland, J.H., 1979, Carbonaceous sediments in the North and South Atlantic: The role of salinity in stable stratification of Early Cretaceous basins: Maurice Ewing Series, 3, 375-401.

Arthur, M.A., Schlanger, S.O., 1979, Cretaceous "oceanic anoxic events" as causal factors in development of reef-reservoired giant oil fields: American Association of Petroleum Geologists Bulletin, 63 (6), 870-885.

Arthur, M.A., Brumsack, H.-J., Jenkyns, H.C., Schlanger, S.O., 1990, Stratigraphy, geochemistry, and paleoceanography of organic carbon-rich Cretaceous sequences, *in* Ginsburg, R.N., Beaudoin, B. (eds.), Cretaceous Resources, Events, and Rhythms: Norwell, Massachusetts, Kluwer Academic, 75-119.

Barragán, R., 2001, Sedimentological and paleoecological aspects of the Aptian transgressive event of Sierra del Rosario, Durango, northeast México: Journal of South American Earth Sciences, 14 (2), 189-202.

Barragán, R., Maurrasse, F.J-M.R., 2008, Lower Aptian (Lower Cretaceous) ammonites from the basal strata of the La Peña Formation of Nuevo León State, northeast México: biochronostratigraphic implications: Revista Mexicana de Ciencias Geológicas, 25 (1), 145-157.

Barragán-Manzo, R., Méndez-Franco, A.L., 2005, Towards a standard ammonite zonation for the Aptian (Lower Cretaceous) of northern México: Revista Mexicana de Ciencias Geológicas, 22 (1), 39-47.

Barron, E.J., Peterson, W.H., 1990, Mid-Cretaceous ocean circulation: Results from model sensitivity studies: Paleoceanography, 5, 319-337.

Beerling, D.J., Lomas, M.R., Gröcke, D.R., 2002, On the nature of methane gas-hydrate dissociation during the Toarcian and Aptian oceanic anoxic events: American Journal of Science, 302, 28-49.

Blanco-Piñón, A., 2003, Peces fósiles de la Formación Agua Nueva (Turoniano) en el Municipio de Vallecillo, Nuevo León, NE-México: Linares, Nuevo León, México, Universidad Autónoma de Nuevo León, tesis doctoral, 330 p.

Blanco-Piñón, A., Maurrasse, F.J-M.R., Rojas-León, A., Duque-Botero, F., 2008, Cyanobacteria/Foraminifera Association from Anoxic/Dysoxic Beds of the Agua Nueva Formation (Upper Cretaceous - Cenomanian/Turonian) at Xilitla, San Luis Potosí, Central México, *in* American Geophysical Union, Spring Meeting 2008, Eos Transactions AGU 89 (23), 24A-04.

Blanco-Piñón, A., Maurrasse, F.J.-M.R., Zavala Díaz-de la Serna, F.J., López-Doncel, R.A., Ángeles-Trigueros, S.A., Hernández-Avila, J., Juárez-Arriaga, E., 2014, Evidencias petrográficas de estructuras de origen algal/bacteriano en carbonatos de la Formación Agua Nueva (Cenomaniano/Turoniano: Cretácico Superior) en Xilitla, S.L.P., México Central: Boletín de la Sociedad Geológica Mexicana, 66 (2), 397-412.

Blanco, A., Zavala, F.J., Hernández-Ávila, J., Maurrasse, F., Duque-Botero, F., Ramírez-Cardona M., 2010, Microbial preservation in sedimentary pyrite from Cretaceous organic matter-rich carbonate mudstone: a preliminary report (Resume): Lunar and Planetary Science Conference, The Woodlands, Tx, EUA, Lunar and Planetary Institute 2487.

Blanco, A., Maurrasse, F.J., Duque, F., Delgado, A., 2011, Anoxic–dysoxic–oxic conditions in the Cenomanian Agua Nueva Formation (Upper Cretaceous) in central México, and their relation to Oceanic Anoxic Event 2 (OAE 2), in Geological Society of America Annual Meeting, Minneapolis, USA, Abstracts with Programs, 43 (5), 421.

Bottjer, R.J., Stein, J.A., 1994, Relationship of stratigraphic traps to submarine unconformities: Examples from the Tocito Sandstone, San Juan Basin, New México and Colorado, *in* Dolson, C., Hendricks, M.L., Wescott, W.A. (eds.), Unconformity-Related Hydrocarbons in Sedimentary Sequence: Rocky Mountain Association of Geologists, Denver, Colorado, 181-208.

Bover-Arnal, T., Moreno-Bedmar, J.A., Salas, R., Skelton, P.W., Bitzer, K., Gili, E., 2010, Sedimentary evolution of an Aptian syn-rifting carbonate system (Maestrat Basin, E Spain): effects of accommodation and environmental change: Geologica Acta, 8 (3), 249-280.

Bralower, T.J., Arthur, M.A., Leckie, R.M., Sliter, W.V., Allard, D.J., Schlanger, S.O., 1994, Timing and paleoceanography of oceanic dysoxia/anoxia in the Late Barremian to Early Aptian (Early Cretaceous): Palaios, 9(4), 335-369.

Bralower, T.J, CoBabe, E., Clement, B., Sliter,W.V., Osburn, C.L., Longoria, J., 1999, The record of global change in mid-Cretaceous (Barremian-Albian) sections from the Sierra Madre, northeastern México: Journal of Foraminiferal Research, 29 (4), 418-437.

Brookfield, M.E., Hemmings, D.P., Van Straaten, P., 2009, Paleoenvironments and origin of the sedimentary phosphorites of the Napo Formation (Late Cretaceous, Oriente Basin, Ecuador): Journal of South American Earth Sciences, 28 (2), 180-192.

Cantú-Chapa, C.M., 1976, Estratigrafía de la Formación La Peña (Aptiano Sup.) en el área de Monterrey, N. L.: Revista del Instituto Mexicano del Petróleo, 8 (4), 7-16.

Castañeda-Posadas, C., Blanco-Piñón, A., Hernández-Ávila, J., Ambrocio-Cruz, S.P., Lizárraga-Mendiola, L., Ángeles-Trigueros, S.A., 2014, Fossil stomatocysts in Upper Cretaceous sedimentary pyrite from central México: International Journal of Geosciences, 5, 214-221.

Centeno-García, E., Guerrero-Suástegui, M., Talavera-Mendoza, O., 2008, The Guerrero Composite Terrane of western México: Collision and subsequent rifting in a supra-subduction zone, *in* Draut, A.E., Clift, P.D., Scholl, D.W. (eds.), Formation and Application of the Sedimentary record in Arc Collisions Zones: Boulder, Colorado, Geological Society of America Special Paper, 436, 279-308.

Clement, B.M, Poetisi, E., Bralower, T.J., CoBabe, E., Longoria, J., 2000, Magnetostratigraphy of mid-Cretaceous limestones from the Sierra Madre of northeastern México: Geophysical Journal International, 143 (1), 219-229.

Crespo de Cabrera, S., Sliter, W.V., Jarvis, I., 1999, Integrated foraminiferal biostratigraphy and chemostratigraphy of the Querecual Formation (Cretaceous), eastern Venezuela: Journal of Foraminiferal Research, 29 (4), 487-499.

Cros, P., Michaud, F., Fourcade, E., Fleury, J.J., 1998, Sedimentological evolution of the Cretaceous carbonate platform of Chiapas (México): Journal of South American Earth Sciences, 11 (4), 311-332.

Davis, C., Pratt, L., Sliter, W., Mompart, L., Murat, B., 1999, Factors influencing organic carbon and trace metal accumulation in the upper Cretaceous La Luna Formation of the western Maracaibo Basin, Venezuela, *in* Barrera, E., Johnson, C. (eds.), The Evolution of Cretaceous Ocean/Climate Systems: Boulder, Colorado, Geological Society of America Special Paper, 332, 203-230.

Dean, W.E., Arthur, M.A., 1998, Geochemical expressions of cyclicity in Cretaceous pelagic limestone sequences: Niobrara Formation, Western Interior Seaway, *in* Dean, W.E., Arthur, M.A. (eds.), Stratigraphy and Paleoenvironments of the Cretaceous Western Interior Seaway, USA: Society for Sedimentary Geology (SEPM), Concepts in Sedimentology and Paleontology, 6, 227-255.

Dean, W.E., Arthur, M.A., Stow, D.A.V., 1984, Origin and geochemistry of Cretaceous deep-sea black shales and multicolored claystones, with emphasis on Deep Sea Drilling Project Site 530, southern Angola Basin: Initial Reports of the Deep Sea Drilling Project, 75, 819-844.

Duque-Botero, F., Maurrasse, F.J-M.R., 2004, Cyanobacterial productivity, variations of the organic carbon and facies of the Indidura Formation (Cenomanian-Turonian), Northeastern México: Journal of Iberian Geology: an international publication of Earth Sciences, 31, 85-98.

Duque-Botero, F., Maurrasse, F.J-M.R., Hickey-Vargas, R., Melinte, M. C., Jaffe, R., López-Oliva, J.G., 2009, Microspheroid accumulations and geochemical characteristics of a Cenomanian–Turonian anoxic basin: the record of the Indidura Formation, NE México: Geologic Problem Solving with Microfossils: A Volume in Honor of Garry D. Jones, Society of Economic Paleontologists and Mineralogists, Special Publications, 93, 171-186.

Eguiluz-de Antuñano S., Amezcua, N.T., 2003, Coalbed methane resources of the Sabinas Basin, Coahuila, México, *in* Bartolini, C., Buffler, R.T., Blickwede, J. (eds.), The Circum-Gulf of México and the Caribbean: Hydrocarbon habitats, basin formation, and plate tectonics: American Association of Petroleum Geologists Memoir, 79, 395–402.

Eldrett, J.S., Minisini, D., Bergman, S.C., 2014, Decoupling of the carbon cycle during Ocean Anoxic Event 2: Geology, doi 10.1130/G35520-1.

Elrick, M., Molina-Garza, R., Duncan, R., Snow, L., 2009, C-isotope stratigraphy and paleoenvironmental changes across OAE2 (mid-Cretaceous) from shallow-water platform carbonates of southern México: Earth and Planetary Science Letters, 277 (3), 295-306.

Energy Information Administration (EIA)/ Advanced Resources International (ARI), 2013, World Shale Gas and Shale Oil Resource Assessment Technically Recoverable Shale Gas and Shale Oil Resources: An Assessment of 137 Shale Formations in 41 Countries Outside the United States, United States Department of Energy, 707 p.

Erba, E., Channell, J.E.T., Claps, M., Jones, C., Larson, R., Opdyke, B., Premoli Silva, I., Riva, A., Salvini, G., Torricelli, S., 1999, Integrated stratigraphy of the Cismon APTICORE (Southern Alps, Italy): a "reference section" for the Barremian–Aptian interval at low latitudes: Journal of Foraminiferal Research, 29, 371-392.

Erbacher, J., Thurow, J., Littke, R., 1996, Evolution patterns of radiolaria and organic matter variations: A new approach to identify sea level changes in mid-Cretaceous pelagic environments: Geology, 24 (6), 499-502.

Erbacher, J., Friedrich, O., Wilson, P.A., Birch, H., Mutterlose, J., 2004, Stable organic carbon isotope stratigraphy across Oceanic Anoxic Event 2 of Demerara Rise, western tropical Atlantic: Geochemistry Geophysics Geosystems, 6 (6), 1-9.

Erlich, R.N., Astorga, A., Sofer, Z., Pratt, L.M., Palmer, S.E., 1996, Palaeoceanography of organic -rich rocks of the Loma Chumico Formation of Costa Rica, Late Cretaceous, eastern Pacific: Sedimentology, 43 (4), 691-718.

Erlich, R.N., Palmer-Koleman, S.E., Lorente, M.A., 1999, Geochemical characterization of oceanographic and climatic changes recorded in upper Albian to lower Maastrichtian strata, western Venezuela: Cretaceous Research, 20 (5), 547-581.

Erlich, R.N., Villamil, T., Keens-Dumas, J., 2003, Controls on the deposition of Upper Cretaceous organic carbon–rich rocks from Costa Rica to Suriname, *in* Bartolini, C., Buffler, R.T., Blickwede, J. (eds.), The Circum-Gulf of México and the Caribbean: Hydrocarbon habitats, basin formation, and plate tectonics: American Association of Petroleum Geologists Memoir, 79, 1-45.

Escalera-Alcocer, J., 2012, Producción Potencial de recursos no convencionales asociado a plays de aceite y gas de lutitas en México, en ExpoForo PEMEX, Ciudad de México, México, 37 p.

Föllmi, K.B., 2012, Early Cretaceous life, climate and anoxia: Cretaceous Research, 35, 230-257.

Frogner, P., Gíslason, S.R., Óskarsson, N., 2001, Fertilizing potential of volcanic ash in ocean surface water: Geology, 29 (6), 487-490.

Gaona-Narvaez, T., Maurrasse, J-M.R., Moreno-Bedmar, J.A., 2013, Stable carbon-isotope stratigraphy and ammonite biochronology at Madotz, Navarra, northern Spain: implications for the timing and duration of oxygen depletion during OAE-1a: Cretaceous Research, 40, 143-157.

Goldhammer, R.K.,1999, Mesozoic sequence stratigraphy and paleogeographic evolution of northeast México, *in* Bartolini, C., Wilson, J.L., Lawton, T.F. (eds.), Mesozoic Sedimentary and Tectonic History of North-Central México: Boulder, Colorado, Geological Society of America Special Paper, 340, 1-58.

González-García, R., Holguín-Quiñones, N., 1992, Las rocas generadoras de México: Boletín de la Asociación Mexicana de Geólogos Petroleros, 42 (1), 16-30.

González-León, C., 1988, Estratigrafía y geología estructural de las rocas sedimentarias cretácicas del área de Lampazos, Sonora: Revista de la Universidad Nacional Autónoma de México, Instituto de Geología, 7 (2), 148-162.

Grajales-Nishimura, J.M., Terrell, D.J., Damon, P.E., 1992, Evidencias de la prolongación del arco magmático cordillerano del Triásico Tardío-Jurásico en Chihuahua, Durango y Coahuila: Boletín de la Asociación Mexicana de Geólogos Petroleros, 42 (2), 1-18.

Gray, G.G., Pottorf, R.J., Yurewicz, D.A., Mahon, K.I., Pevear, D.R., Chuchla, R.J., 2001, Thermal and chronological record of syn- to post-Laramide burial and exhumation, Sierra Madre Oriental, México, *in* Bartolini, C., Buffler, R.T., Cantú-Chapa, A. (eds.), The western Gulf of México Basin: Tectonics, sedimentary basins, and petroleum systems: American Association of Petroleum Geologists Memoir, 75, 159-181.

Hasegawa, T., Saito, T., 1993, Global synchroneity of a positive carbon isotope excursion at the Cenomanian/Turonian boundary: validation by calcareous microfossil biostratigraphy of the Yezo Group, Hokkaido, Japan: The Island Arc, 2, 181-191.

Hernández-Jáuregui, R., 1997, Sedimentación sintectónica de la Formación Soyatal (Turoniano Medio-Campaniano) y modelado cinemático de la cuenca de flexura de Maconí, Querétaro: México D.F., México, Instituto Politécnico Nacional, tesis de maestría, 94 p.

Hernández-Romano, U., Aguilera-Franco, N., Martínez-Medrano, M., Barceló-Duarte, J., 1997, Guerrero-Morelos Platform drowning at the Cenomanian–Turonian boundary, Huitziltepec area, Guerrero State, southern México: Cretaceous Research, 18 (5), 661-686.

Hofmann, P., Wagner, T., Beckmann, B., 2003, Millennial- to centennial-scale record of African climate variability and organic carbon accumulation in the Coniacian–Santonian eastern tropical Atlantic (Ocean Drilling Program Site 959, off Ivory Coast and Ghana): Geology, 31 (2), 135-138.

Horbury, A.D., Hall, S., González, P.F., Rodríguez, F.D., Reyes, F.A., Ortiz, G.P. Martínez, M.M, Quintanilla, R.G., 2003, Tectonic sequence stratigraphy of the western margin of the Gulf of México in the late Mesozoic and Cenozoic: Less passive than previously imagined, *in* Bartolini, C., Buffler, R.T., Blickwede, J. (eds.), The Circum-Gulf of México and the Caribbean: Hydrocarbon habitats, basin formation, and plate tectonics: American Association of Petroleum Geologists Memoir, 79, 184-245.

Ifrim, C., 2006, The fossil lagerstätte at Vallecillo, north-eastern México: Pelagic plattenkalks related to Cenomanian-Turonian boundary anoxia: Karlsruhe, Germany, Universität Fridericiana, tesis doctoral, 151 p.

Ifrim, C., Götz, S., Stinnesbeck, W., 2011, Fluctuations of the oxygen minimum zone at the end of Oceanic Anoxic Event 2 reflected by benthic and planktic fossils: Geology, 39 (11), 1043-1046.

Ingall, E.D., Bustin, R.M., Van Cappellen, P., 1993, Influence of water column anoxia on the burial and preservation of carbon and phosphorus in marine shales: Geochimica et Cosmochimica Acta, 57, 303-316.

Jahren, A.H., 2002, The biogeochemical consequences of the mid-Cretaceous superplume: Journal of Geodynamics, 34, 177-191.

Jarvis, I., Gale, A.S., Jenkyns, H.C., Pearce, M.A., 2006, Secular variation in Late Cretaceous carbon isotopes: a new $\delta^{13}C$ carbonate reference curve for the Cenomanian–Campanian (99.6–70.6 Ma): Geological Magazine, 143 (5), 561-608.

Jenkyns, H.C., 1980, Cretaceous anoxic events: from continents to oceans: Journal of the Geological Society, 137 (2), 171-188.

Jenkyns, H.C., 2010, Geochemistry of oceanic anoxic events: Geochemistry, Geophysics, Geosystems, 11 (3), 1-30.

Jones, C.E., Jenkyns, H.C., 2001, Seawater strontium isotopes, oceanic anoxic events, and seafloor hydrothermal activity in the Jurassic and Cretaceous: American Journal of Science, 301 (2), 112-149.

Kearns, T.J., 2011, Chemostratigraphy of the Eagle Ford Formation: Texas, USA, University of Texas at Arlington, USA, master degree thesis, 254 p.

Keller, C.E., Hochuli, P.A., Weissert, H., Bernasconi, S.M., Giorgioni, M., Garcia, T.I., 2011, A volcanically induced climate warming and floral change preceded the onset of OAE1a (Early Cretaceous): Palaeogeography, Palaeoclimatology, Palaeoecology, 305 (1), 43-49.

Klemme, H.D., Ulmishek, G.F., 1991, Effective Petroleum Source Rocks of the World: Stratigraphic Distribution and Controlling Depositional Factors: American Association of Petroleum Geologists Bulletin, 75 (12), 1809-1851.

Kuroda, J., Ogawa, N.O., Tanimizu, M., Coffin, M. F., Tokuyama, H., Kitazato, H., Ohkouchi, N., 2007, Contemporaneous massive subaerial volcanism and late cretaceous Oceanic Anoxic Event 2: Earth and Planetary Science Letters, 256 (1), 211-223.

Lawton, T.F., Vega, F.J., Giles, K.A., Rosales-Domnguez, C., 2001, Stratigraphy and Origin of the La Popa Basin, Nuevo Len and Coahuila, México, *in* Bartolini, C., Buffler, R.T., Cantú-Chapa, A., (eds.), The Western Gulf of México Basin: Tectonics, sedimentary basins, and petroleum systems: American Association of Petroleum Geologists Memoir, 75, 219-240.

Lamolda, M.A., Paul, C.R.C., 2007, Carbon and oxygen stable isotopes across the Coniacian/Santonian boundary at Olazagutia, northern Spain: Cretaceous Research, 28 (1), 37-45.

Langmann, B., Zakšek, K., Hort, M., Duggen, S., 2010, Volcanic ash as fertilizer for the surface ocean: Atmospheric Chemistry and Physics Discussions, 10 (8), 711-734.

Larson, R.L., 1991, Latest pulse of the Earth: evidence for a mid-Cretaceous super plume: Geology, 19, 547-550.

Leckie, R.M., Bralower, T.J., Cashman, R., 2002, Oceanic anoxic events and plankton evolution: Biotic response to tectonic forcing during the mid-Cretaceous: Paleoceanography, 17 (3), 13.1-13.29 doi 10.1029/2001PA000623.

Lehmann, C., Osleger, D.A., Montañez, I.P., Sliter, W., Vanneau, A.A., Banner, J., 1999, Evolution of Cupido and Coahuila carbonate platforms, early Cretaceous, northeastern México: Geological Society of America Bulletin, 111(7), 1010-1029.

Li, Y.-X., Bralower, T.J., Montañez, I.P., Osleger, D.A., Arthur, M.A., Bice, D.M., Herbert, T.D., Erba, E., Premoli Silva, I., 2008, Toward an orbital chronology for the early Aptian Oceanic Anoxic Event (OAE1a, ~120 Ma): Earth and Planetary Science Letters, 271 (1), 88–100.

López-Doncel, 2003, La Formación Tamabra del Cretácico medio en la porción central del margen occidental de la Plataforma Valles-San Luis Potosí, centro-noreste de México: Revista Mexicana de Ciencias Geológicas, 20 (1), 1-19.

López-Oliva, J.G., Keller, G., Stinnesbeck, W., 1998, El límite Cretácico/Terciario (K/T) en el noreste de México; extinción de foraminíferos planctónicos: Revista Mexicana de Ciencias Geológicas, 15 (1), 109-113.

McFarlan Jr, E., Menes, L.S., 1991, Lower Cretaceous. The Gulf of México Basin: Boulder, Colorado, Geological Society of America, The Geology of North America, J, 181-204.

Méhay, S., Keller, C.E., Bernasconi, S.M., Weissert, H., Erba, E., Bottini, C., Hochuli, P.A., 2009, A volcanic CO_2 pulse triggered the Cretaceous Oceanic Anoxic Event 1a and a biocalcification crisis: Geology, 37, 819-822.

Menegatti, A.P., Weissert, H., Brown, R.S., Tyson, R.V., Farrimond, P., Strasser, A., Caron M., 1998, High resolution $\delta^{13}C$ stratigraphy through the early Aptian "Livello Selli" of the Alpine Tethys: Paleoceanography, 13 (5), 530-545.

Millán, M.I., Weissert, H.J., Fernández-Mendiola, P.A., García-Mondéjar, J., 2009, Impact of Early Aptian carbon cycle perturbations on evolution of a marine shelf system in the Basque-Cantabrian Basin (Aralar, N Spain): Earth and Planetary Science Letters, 287 (3), 392-401.

Monreal, R., Longoria, F., 2000, Stratigraphy and structure of the Lower Cretaceous of Lampazos, Sonora, (northwest México) and its relationship to the Gulf Coast succession: American Association of Petroleum Geologists Bulletin, 84 (11), 1811-1831.

Moreno-Bedmar, J.A., Delanoy, G., 2013, About the generic attribution of *Megatyloceras casei* Humphrey, 1949 (Ammonoidea, Ancyloceratina), from the Aptian of México: Carnets de Géologie [Notebooks on Geology], Brest, Letter 2013/06 (CG2013_L06), 315-323.

Moreno-Bedmar, J.A., Company, M., Bover-Arnal, T., Salas, R., Delanoy, G., Martínez, R., Grauges, A., 2009, Biostratigraphic characterization by means of ammonoids of the lower Aptian Oceanic Anoxic Event (OAE 1a) in the eastern Iberian Chain (Maestrat Basin, eastern Spain): Cretaceous Research, 30, 864-872.

Moreno-Bedmar, J.A., Bover-Arnal, T., Barragán, R., Salas, R., 2011, La transgresión tetisiana del Aptiense inferior terminal: comparación entre su registro en México y España y relación con el ciclo global de tercer orden Ap4: Paleontologia i Evolució, Memòria especial, Sabadell, 5, 259-262.

Moreno-Bedmar, J.A., Company, M., Sandoval, J., Tavera, J.M., Bover-Arnal, T., Salas, R., Delanoy, G., Maurrasse F.J.-M.R., Martínez, R., 2012a, Lower Aptian ammonite and carbon isotope stratigraphy in the eastern Prebetic Domain (Betic Cordillera, southeastern Spain): Geologica Acta, 10 (4), 333-350.

Moreno-Bedmar, J.A., Bover-Arnal, T., Barragán, R., Salas, R., 2012b, Uppermost Lower Aptian transgressive records in México and Spain: chronostratigraphic implications for the Tethyan sequences: Terra Nova, 24 (4), 333-338.

Mort, M., Adatte, T., Föllmi, K.B., Keller, G., Steinmann, P., Matera, V., Berner, Z., Stüben, D., 2007, Phosphorous and the roles of productivity and nutrient recycling during oceanic event 2: Geology, 35, 483-486.

Najarro, M., Rosales, I., Moreno-Bedmar, J.A., de Gea, G.A., Barrón, E., Company, M., Delanoy, G., 2011, High-resolution chemo- and biostratigraphic records of the Early Aptian oceanic anoxic event in Cantabria (N Spain): Palaeoceanographic and palaeoclimatic implications: Palaeogeography, Palaeoclimatology, Palaeoecology, 299, 137-158.

Ogg, J., Agterberg, F.P., Gradstein, F.M., 2004, The Cretaceous Period, *in* Gradstein, F., Ogg, J., Smith, A. (eds.), A Geologic Time Scale: Cambridge, Cambridge University Press, 344-383.

Omaña, L., 2011, Bioestratigrafía, Paleoecología y paleogeografía del Cretácico Superior con base en Foraminíferos de la parte occidental de la Plataforma de Valles-San Luis Potosí, México: México D.F., México, Universidad Nacional Autónoma de México, tesis doctoral, 198 p.

Omaña, L., López-Doncel, R., Torres J.R., Alencáster G., 2013, Biostratigraphy and paleoenvironment of the Cenomanian/Turonian boundary interval based on foraminifera from W Valles-San Luis Potosí Platform, México: Micropaleontology, 58 (6), 457-485.

Omaña, L., Torres, J.R., López-Doncel, R., Alencáster, G., López-Caballero, I., 2014, A pithonellid bloom in the Cenomanian-Turonian boundary interval from Cerritos in the western Valles–San Luis Potosí platform, México: Paleoenviromental significance: Revista Mexicana de Ciencias Geológicas, 31 (1), 28-44.

Ortuño-Arzate, S., Ferket, H., Cacas, M.C., Swennen, R., Roure, F., 2003, Late Cretaceous carbonate reservoirs in the Córdoba Platform and Veracruz Basin (Eastern México), *in* Bartolini, C., Buffler, R.T., Blickwede, J.F. (eds.), The circum-Gulf of México and Caribbean region: Plate tectonics, basin formation and hydrocarbon habitats: American Association of Petroleum Geologists Memoir, 79, 476-514.

Padilla y Sánchez, R.J., 2007, Evolución geológica del sureste mexicano desde el Mesozoico al presente en el contexto regional del Golfo de México: Boletín de la Sociedad Geológica Mexicana, 59 (1), 19-42.

Pletsch, T., Erbacher, J., Holbourn, A. E. J., Kuhnt, W., Moullade, M., Oboh-Ikuenobe, F.E., Söding, E., Wagner, T., 2001, Cretaceous separation of Africa and South America: the view from the West African margin (ODP Leg 159): Journal of South American Earth Sciences, 14 (2), 147-174.

Rangel, A., Parra, P., Niño, C., 2000, The La Luna formation: Chemostratigraphy and organic facies in the Middle Magdalena Basin: Organic Geochemistry, 31 (12), 1267-1284.

Reboulet, S., Szives, O., Aguirre-Urreta, B., Barragán, R., Company, M., Idakieva, V., Ivanov, M., Kakabadze, M.V., Moreno-Bedmar, J.A., Sandoval, J., Baraboshkin, E.J., Çaglar, M.K., Főzy, I., González-Arreola, C., Kenjo, S., Lukeneder, A., Raisossadat, S.N., Rawson, P.F., Tavera, J.M., 2014, Report on the 5th International Meeting of the IUGS Lower Cretaceous Ammonite Working Group, the Kilian Group (Ankara, Turkey, 31st August 2013), Cretaceous Research, 50, 126-137.

Rojas-León, A., Blanco-Piñón, A., Maurrasse F., J.-M.R., Hernández-Ávila, J., 2008, Contenido de material orgánico en los sedimentos de la Formación Agua Nueva (Cenomaniano/Turoniano) en Xilitla, San Luis Potosí y su relación con el OAE 2, *in* XVIII Congreso Nacional de Geoquímica, Hermosillo, Sonora, Actas INAGEQ, 18 (1), 55-57.

Salvador, A., 1991, Triassic-Jurassic, *in* Salvador, A. (ed.), The Gulf of México Basin: Boulder, Colorado, The Geological Society of North America, Geology of North America, J, 131-180.

Salvador, A., Quezada-Muñetón, J.M., 1989, Stratigraphic Correlation Chart, Gulf of México Basin, in The Geology of North America, The Gulf of México Basin: The Geological Society of America, J, 131-180.

Santa María-Díaz, A., Monreal, R., 2008, La Formación Los Picachos en la Sierra de Los Chinos, Sonora, México: Boletín de la Sociedad Geológica Mexicana, 60 (1), 111-120.

Schlanger, S.O., Jenkyns, H.C., 1976, Cretaceous oceanic anoxic events – causes and consequences: Geologie en Mijnbouw, 55 (3-4), 179-184.

Scholle, P.A., Arthur, M.A., 1980, Carbon isotope fluctuations in Cretaceous pelagic limestones: potential stratigraphic and petroleum exploration tool: American Association of Petroleum Geologists Bulletin, 64 (1), 67-87.

Shipboard Scientific Party, Leg 207, 2002, preliminary report: Ocean Drilling Project Preliminary Report, 63 p.

Sinton, C.W., Duncan, R.A., 1997, Potential links between ocean plateau volcanism and global ocean anoxia at the Cenomanian-Turonian boundary: Economic Geology, 92 (7-8), 836-842.

Skelton, P.W., Gili, E., 2012, Rudists and carbonate platforms in the Aptian: a case study on biotic interactions with ocean chemistry and climate: Sedimentology, 59 (1), 81-117.

Snow, L.J, 2003, Hydrothermal links between ocean plateau formation and global anoxia at the Cenomanian-Turonian Boundary: Oregon, USA, Oregon State University, Master degree thesis, 213 p.

Snow, L.J., Duncan R.A., Bralower T.J., 2005, Trace element abundances in the Rock Canyon Anticline, Pueblo, Colorado, marine sedimentary section and their relationship to Caribbean plateau construction and oxygen anoxic event 2: Paleoceanography, 20, PA3005.

Stinnesbeck, W., Ifrim, C., Schmidt, H., Rindfleisch, A., Buchy, M. C., Frey, E., González-González, A.H., Vega, F.J., Cavin, L., Keller, G., Smith, K.T., 2005, A new lithographic limestone deposit in the Upper Cretaceous Austin Group at El Rosario, county of Múzquiz, Coahuila, northeastern México: Revista Mexicana de Ciencias Geológicas, 22 (3), 401-418.

Vergara, L.S., 1997, Cretaceous black shales in the Upper Magdalena Valley, Colombia. New organic geochemical results (Part II): Journal of South American Earth Sciences, 10 (2), 133-145.

Wagner, T., Pletsch, T., 1999, Tectono-sedimentary controls on Cretaceous black shale deposition along the opening equatorial Atlantic gateway (ODP Leg 159), *in* Cameron, N., Bate, R., Clure, V. (eds.), The Oil and Gas Habitat of the South Atlantic: London, Geological Society Special Publication, 153, 241-265.

Wagner, T., Sinninghe Damsté, J.S., Hofmann, P., Beckmann, B., 2004, Euxinia and primary production in Late Cretaceous eastern equatorial Atlantic surface waters fostered orbitally driven formation of marine black shales: Paleoceanography, 19, PA3009.

Wagreich, M., 2012, OAE 3-regional Atlantic organic carbon burial during the Coniacian-Santonian: Climate of the Past, 8 (5), 1447-1455.

Weissert, H., Erba, E., 2004, Volcanism, CO_2 and palaeoclimate: a Late Jurasic–Early Cretaceous carbon oxygen isotope record: Journal of the Geological Society, 161, 1-8.

Westermann, S., Caron, M., Fiet, N., Fleitmann, D., Matera, V., Adatte, T., Föllmi, K.B., 2010, Evidence for oxic conditions during oceanic anoxic event 2 in the northern Tethyan pelagic realm: Cretaceous Research, 31 (5), 500-514.

Wignall, P.B., 1994, Black Shales: Oxford, Oxford University Press, 127 p.

Williams-Rojas, C.T, Hurley, N.F., 2001, Geologic controls on reservoir performance in Muspac and Catedral gas fields, southeastern México, *in* Bartolini, C., Buffler, R.T., Cantú-Chapa, A. (eds.), The western Gulf of México Basin: Tectonics, sedimentary basins, and petroleum systems: Boulder, Colorado, American Association of Petroleum Geologist Memoir, 75, 443-472.

Manuscript received: May 5, 2014.
Corrected manuscript received: August 20, 2014.
Manuscript accepted: September 8, 2014.

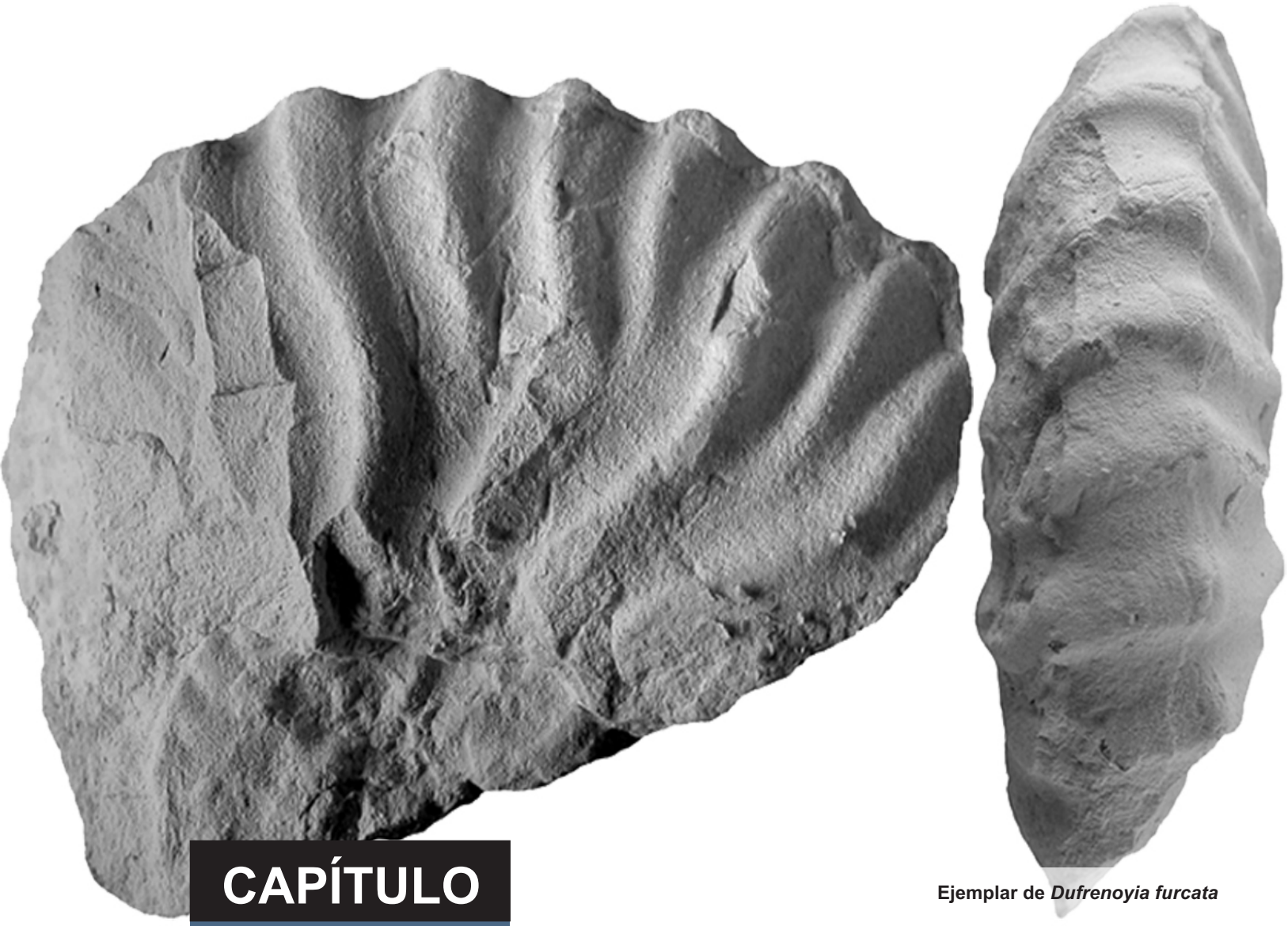

Ejemplar de *Dufrenoyia furcata*

CAPÍTULO

3

LA EXCURSIÓN ISOTÓPICA NEGATIVA DE CARBONO EN LA ZONA DE FURCATA

Artículo: **Núñez-Useche, F.**, Moreno-Bedmar, J.A., Company, M., Barragán, R., 2014. A negative carbon isotope excursion within the Dufrenoyia furcata Zone: proposal for a new episode for chemostratigraphic correlation in the Aptian. Carnets de Géologie [Notebooks on Geology] 14(6).

A negative carbon isotope excursion within the *Dufrenoyia furcata* Zone: proposal for a new episode for chemostratigraphic correlation in the Aptian

Fernando NUÑEZ-USECHE [1]

Josep Anton MORENO-BEDMAR [2]

Miguel COMPANY [3]

Ricardo BARRAGÁN [4]

Abstract: In this work we discuss a proposed updated division of the C7 isotope segment of MENEGATTI *et al.* (1998). The new standard division of the segment C7 is based on a revision of published Barremian-Aptian carbon isotope curves from stratigraphic sections of the Prebetic Domain in Spain. It includes four distinct isotopic subunits labeled C7a to C7d, with a characteristic negative carbon isotope excursion at the base of the segment and which correlates with the *Dufrenoyia furcata* ammonite Zone. The negative excursion is recognized on a regional extent, and the term Intra-Furcata Negative Excursion (IFNE) is proposed to identify it. We provide possible sites correlatable with the IFNE in both the Old and New worlds, which suggest its potential use as an even global chemostratigraphic marker for the Aptian record.

Key Words: Aptian; C7 segment; negative carbon isotope excursion; *Dufrenoyia furcata* Zone.

Citation : NÚÑEZ-USECHE F., MORENO-BEDMAR J.A., COMPANY M. & BARRAGÁN R. (2014).- A negative carbon isotope excursion within the *Dufrenoyia furcata* Zone: proposal for a new episode for chemostratigraphic correlation in the Aptian.- *Carnets de Géologie* [*Notebooks on Geology*], Brest, vol. 14, nº 6, p. 129-137.

Résumé : ***Une excursion négative de la courbe isotopique du carbone au sein de la Zone à Dufrenoyia furcata : proposition pour un nouvel épisode permettant la corrélation chimiostratigraphique dans l'Aptien.-*** Dans ce travail nous proposons une mise à jour de la subdivision du segment isotopique C7 de MENEGATTI *et al.* (1998). Ce nouveau standard est fondé sur une révision des courbes isotopiques du carbone publiées pour le Barrémo-Aptien à partir de coupes stratigraphiques du domaine prébétique en Espagne. Le segment C7 inclut quatre sous-unités isotopiques distinctes répertoriées C7a à C7d et est caractérisé à sa base par une excursion isotopique négative qui est corrélée avec la Zone d'ammonites à *Dufrenoyia furcata*. Cette excursion négative est reconnue à l'échelon régional, et le terme Excursion Négative Intra-Furcata (ENIF) est proposé pour sa dénomination. Nous proposons d'autres sites, à la fois dans l'Ancien et le Nouveau Monde, qui paraissent révéler cette ENIF, ce qui suggère ses potentialités comme marqueur chimiostratigraphique global pour l'Aptien.

Mots-clefs : Aptien ; segment C7 ; excursion négative des isotopes du carbone ; Zone à *Dufrenoyia furcata*.

---

[1] *Posgrado en Ciencias de la Tierra, Departamento de Paleontología, Instituto de Geología, Universidad Nacional Autónoma de México, Ciudad Universitaria, Delegación Coyoacán, 04510 México, D.F. (Mexico)*
fernandonunezu@comunidad.unam.mx

[2] *Departamento de Paleontología, Instituto de Geología, Universidad Nacional Autónoma de México, Ciudad Universitaria, Delegación Coyoacán, 04510 México, D.F. (Mexico)*
josepamb@geologia.unam.mx

[3] *Departamento de Estratigrafía y Paleontología, Facultad de Ciencias, Universidad de Granada Avenida Fuentenueva s/n, 18002 Granada (Spain)*
mcompany@ugr.es

[4] *Departamento de Paleontología, Instituto de Geología, Universidad Nacional Autónoma de México, Ciudad Universitaria, Delegación Coyoacán, 04510 México, D.F. (Mexico)*
ricardor@geologia.unam.mx

Manuscript online since May 8, 2014
[Editor: Michel MOULLADE; copy editor: Bruno GRANIER; language editor: Phil SALVADOR]

Introduction

The carbon isotope segments of MENEGATTI *et al.* (1998) describe long-term trends linked to different disturbances in the global carbon cycle during the Late Barremian-Aptian interval. They derived from high-resolution studies of carbon isotope stratigraphy from sections at the western and eastern margins of the Alpine Tethys. From C1 to C8, each segment is characterized by a distinctive pattern of variation in the inorganic ($\delta^{13}C_{carb}$) and organic carbon ($\delta^{13}C_{org}$) isotope curve. Their recognition in several paleogeographic domains worldwide has provided evidence of their reliability as a well-established standard pattern for the carbon isotope curve and attests to their use as a valuable tool for correlations between different stratigraphic sections (BRALOWER *et al.,* 1999; GEA *et al.*, 2003; RENARD *et al.*, 2005; LI *et al.*, 2008; MÉHAY *et al.*, 2009; MILLÁN *et al.*, 2009; BOVER-ARNAL *et al.*, 2010; NAJARRO *et al.*, 2011; MORENO-BEDMAR *et al.*, 2012). Among the different isotope segments, greatest emphasis has been given to segments C3 to C6 because they characterized the most prominent shift in the C-isotope curve during the early Aptian, the Oceanic Anoxic Event 1a (OAE 1a, Selli event, ~120 Ma) (SCHLANGER & JENKYNS, 1976; JENKYNS, 1980, 1999; ARTHUR *et al.*, 1990). So far the other segments have received less attention, but conspicuous fluctuations within their temporal pattern also have the potential to be used as chemostratigraphic markers. Characterizing in detail these minor but significant episodes allow us to improve the chemostratigraphic and chronologic resolution of the original segments (MENEGATTI *et al.*, 1998).

In this paper we focus on segment C7 (MENEGATTI *et al.*, 1998), and we attempt to identify particular characteristics of useful minor isotopic trends that can be recognized in different stratigraphic sections. We propose a new division of segment C7 into discrete sub-units based on similar isochronous behavior of $\delta^{13}C$ values within this segment, as provided in different published European sections. We also provide evidence to demonstrate that the most significant sub-unit within C7 is characterized by a negative $\delta^{13}C$ shift that we propose should be considered as a new and important element of correlation for the lower Aptian record. We also aim to motivate future research that may further reveal the minor isotopic shift discussed in this study in order to increase its known record and verify its potential as a tool for spatio-temporal correlations.

The isotope C7 segment

The C7 isotope segment (MENEGATTI *et al.*, 1998) the longest of all segments, corresponds to the maximum positive $\delta^{13}C$ excursion of the lower Aptian record, and is known as the Cismon event (WEISSERT & LINI, 1991; WEISSERT *et al.*, 1998). Based on the planktonic foraminifera biozones used by MENEGATTI *et al.* (1998) from Cismon core reference section in Italy

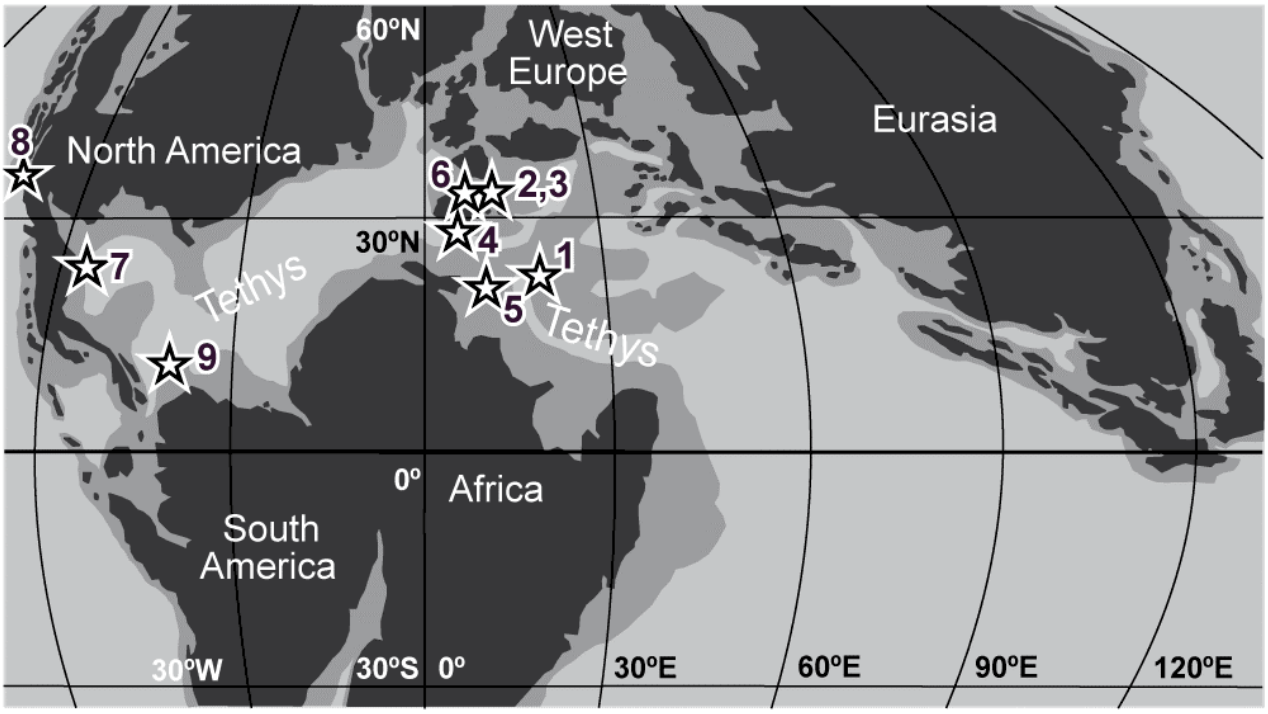

Figure 1: Map showing location of stratigraphic sections mentioned in this contribution in a paleogeografical reconstruction at 120 Ma (BLAKEY, 2010; © Ron BLAKEY, Colorado Plateau Geosystems). 1- Cismon core section, Italy (MENEGATTI *et al.*, 1998; ERBA *et al.*, 1999); 2- Serre Chaitieu section, Vocontian Basin, France (HERRLE *et al.*, 2004), 3- Cassis-La Bédoule section, France (MOULLADE *et al.*, 1998), 4- Prebetic Domain sections, Spain (MORENO-BEDMAR *et al.*, 2012, this study); 5- Djebel Serdj section, Tunisia (HELD *et al.*, 2008), 6- Igaratza section, Basque-Cantabrian Basin, Spain (MILLÁN *et al.*, 2009), 7- Santa Rosa section, Mexico (LI *et al.*, 2008), 8- Permanente Quarry section, USA (ROBINSON *et al.*, 2008), 9- Curití section, Colombia (GAONA-NARVAEZ *et al.*, 2013).

(Fig. 1), C7 spans from the upper part of the *Globigerinelloides blowi* through the entire *Leupoldina cabri* Zone (Fig. 2.A). However, at the same section, ERBA *et al.* (1999) constrained this segment mostly to the *Leupoldina cabri* Zone and stated that its uppermost part falls within the *Globigerinelloides ferreolensis* Zone (Fig. 2.B). Despite the overall high $\delta^{13}C$ values that originally defined segment C7 (MENEGATTI *et al.*, 1998), the actual pattern includes minor, relatively abrupt negative to positive excursions. Numerous investigations have addressed the issue of these minor carbon isotopic variations and divided segment C7 into discrete subsegments or zones that emphasize the value of these isotopic trends as suitable correlation patterns. In this respect, a detailed $\delta^{13}C_{carb}$ analysis in sections from the Vocontian Basin, Southeast France (HERRLE *et al.,* 2004) allowed the splitting of segment C7 into three units labeled Ap7, Ap8 and Ap9 at Serre Chaitieu section (Fig. 1). Furthermore, since Ap7 consisted of a prominent positive $\delta^{13}C_{carb}$ excursion that included distinct lower magnitude variations, HERRLE *et al.* (2004) also subdivided unit Ap7 into four sub-units (Fig. 2.D). According to this scheme, sub-unit Ap7b is located within the uppermost part of the planktonic foraminifera *L. cabri* Zone and encloses the lowest $\delta^{13}C$ values in the lower part of segment C7.

Subsequently, DEBOND *et al.* (2012) studied the Aptian $\delta^{13}C$ signal at Ocean Drilling Program Site 765C, Leg 123, off the northwestern margin of Australia. They found differences with the scheme proposed by MENEGATTI *et al.* (1998), especially with respect to the values in the segment C7. They divided the segment C7 of site 765C into two zones which also found on a composite section with better sampling resolution and conformed with $\delta^{13}C_{carb}$ data from the Cismon core section (ERBA *et al.*, 1999) and the Vocontian Basin (HERRLE *et al.*, 2004) (Fig. 2.C). In this section, Zone C7a represents increasing values and correlates with the lower Aptian highest positive $\delta^{13}C$ excursion of MENEGATTI *et al.* (1998). This zone is equivalent to the lower and middle part of the C7 segment of ERBA *et al.* (1999), which is the upper part of the C6 segment of HERRLE *et al.* (2004). Zone C7b of the composite section is equivalent to a period of high $\delta^{13}C$ variation not clearly distinct in the Cismon core section, and corresponds to the uppermost part of the C7 segment of ERBA *et al.* (1999) and to the unit Ap7 of HERRLE *et al.* (2004). The latter correlation reduced the upper extent of HERRLE's segment C7 and made it more coherent with the original age-calibration of the segments defined by MENEGATTI *et al.* (1998) (see in Fig. 2). Based on the pattern of $\delta^{13}C$ values of HERRLE *et al.* (2004) and ammonite biostratigraphy data analysis, MORENO-BEDMAR *et al.* (2012) even proposed that only sub-units Ap7a to Ap7c defined by HERRLE *et al.* (2004) correspond to segment C7.

The main issue with these proposed subdivisions for segment C7 (HERRLE *et al.*, 2004; DEBOND *et al.*, 2012) is that they are based in each case only on the carbon isotopic record of a single section, and the sub-units cannot be clearly recognized in other stratigraphic sections; therefore, their potential as chemostratigraphic tools remains unproven and may only have a local value.

Division of the segment C7 in the Prebetic Domain, Spain

The present study uses $\delta^{13}C_{carb}$ values within segment C7 from different published stratigraphic sections of the Prebetic Domain in Spain, including the L'Alcoraia, Racó Ample and Cau sections (MORENO-BEDMAR *et al.*, 2012) (Figs. 1 and 3). Carbon isotope determinations were carried out with reproducibility better than 0.03 ‰ . All these sections have been calibrated by means of ammonite biostratigraphy (MORENO-BEDMAR *et al.*, 2012), and the Cau section has also been correlated with planktonic foraminifera zonation (GEA *et al.*, 2003).

Since segment C7 shows a similar pattern in all these sections, we divided it into four distinct isotopic trends labeled C7a to C7d, from bottom to top (Fig. 3). While sub-unit C7a is represented by somewhat variable but overall constant values, the sub-unit C7b consists of a conspicuous negative excursion followed by a positive shift (sub-unit C7c). Finally, uniform to slightly increasing values characterize sub-unit C7d. These sub-units are identified in sections from the Prebetic Domain but are not clearly correlatable with the sub-units defined by HERRLE *et al.* (2004) or DEBOND *et al.* (2012).

All the sections shown in MORENO-BEDMAR *et al.* (2012) include the well-defined negative excursion of sub-unit C7b, which corresponds to the lowest carbon isotope data within segment C7. This negative shift has an amplitude of about 0.7 ‰ in the L'Alcoraia section, 1.2 ‰ in the Racó Ample section and close to 1 ‰ in the Cau section (Fig. 3). This sub-unit occurs within the middle to upper part of the *Leupoldina cabri* Zone. A more consistent biostratigraphic position for this $\delta^{13}C$ sub-unit is achieved if it is correlated with established Mediterranean ammonite zones. As shown in Figure 3, the negative inflection equivalent to subunit C7b consistently occurs in the *Dufrenoyia furcata* Zone. Taking into account the subzones of the *Dufrenoyia furcata* Zone showed in MORENO-BEDMAR *et al.* (2012) for the Cau and Racó Ample sections, it seems that the lower part of the zone is condensed and consequently this sub-unit is located about the middle part of the zone. The fact that this negative carbon isotope excursion is defined by a single point is significant. This may be a result low sedimentation rate in an outer-ramp environment where these sections were deposited (CASTRO, 1998; GEA, 2004; CASTRO *et*

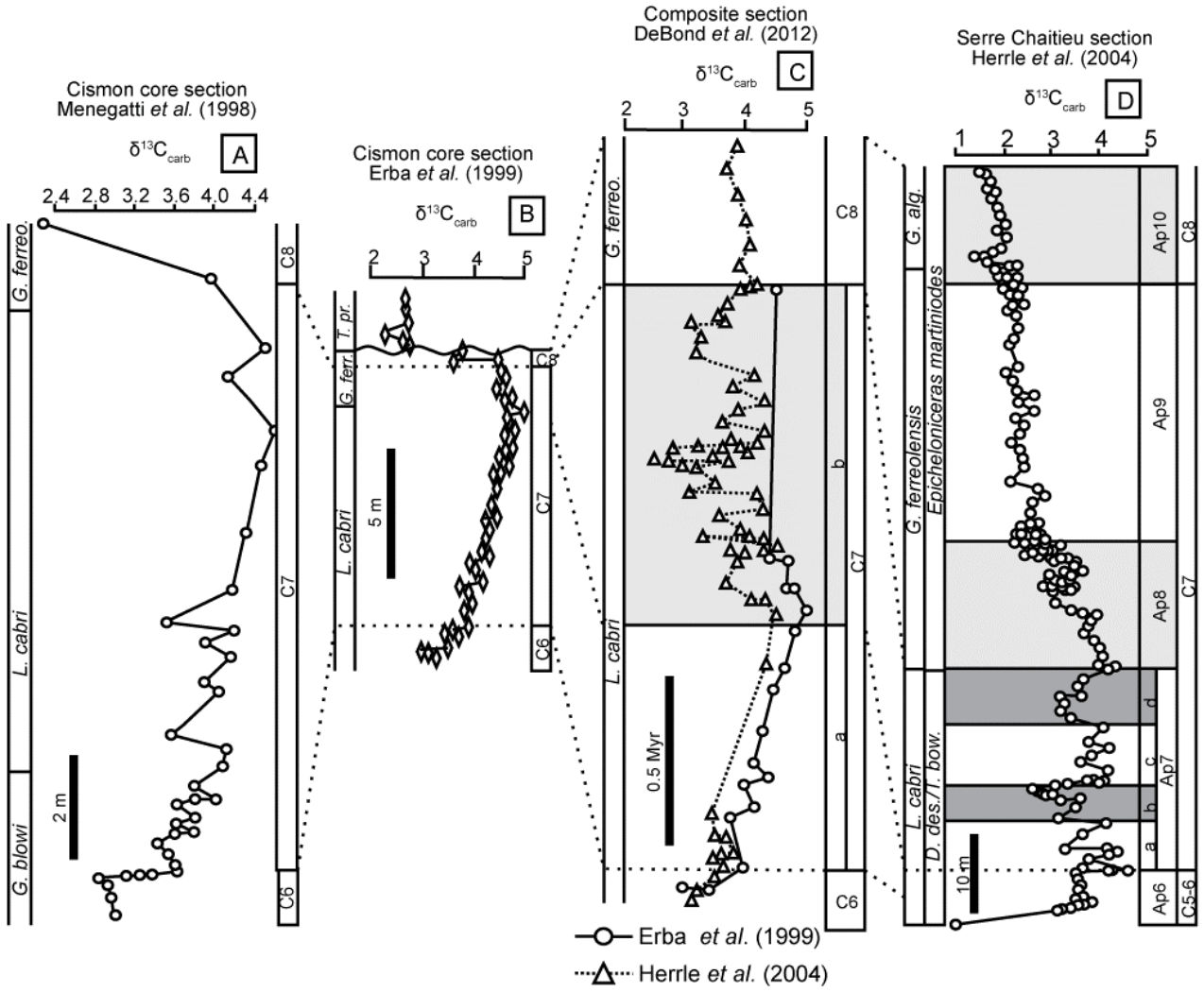

Figure 2: The C7 isotope segment of MENEGATTI *et al.* (1998) and ERBA *et al.* (1999) and the subsequent divisions of HERRLE *et al.* (2004) and DEBOND *et al.* (2012). Dashed lines are used for correlation. Scale bar in A, B and D indicates distance interval in meters (m), whereas in C represents time interval in million years (Myr).

al., 2008). Since this negative inflection is not linked to a significant lithologic change nor is it coeval with an oxygen isotope shift (see Appendix 1), it can be considered as a primary carbon isotope signal. Diagenetic overprinting can be also excluded, given the presence of this negative carbon isotope excursion, with a similar value and biostratigraphic position, in geographically distant stratigraphic sections.

Intra-Furcata Negative Excursion (IFNE): Definition

The $\delta^{13}C_{carb}$ values of segment C7 of the three sections from the Prebetic Domain (Fig. 3) reveal that the negative carbon isotope excursion represented by sub-unit C7b appears in the same chemo- and bio-stratigraphic position and displays a similar drop in carbon isotope values at each location. Hence, this excursion appears to represent a constant chemostratigraphic marker with regional significance. This characteristic carbon isotope trend is here named the Intra-Furcata Negative Excursion (IFNE), which is defined as a negative carbon isotope excursion with the lowest values within segment C7, and can be correlated with the middle part of the *Dufrenoyia furcata* ammonite Zone (Fig. 3). Regarding planktonic foraminifera biozones, the IFNE can be recognized within the middle to the upper part of the *Leupoldina cabri* Zone. However, considering inconsistency regarding the definition of the base of this planktonic foraminifera biozone (BOLLI, 1959; PREMOLI SILVA & VERGA, 2004), such correlation for the IFNE is less accurate.

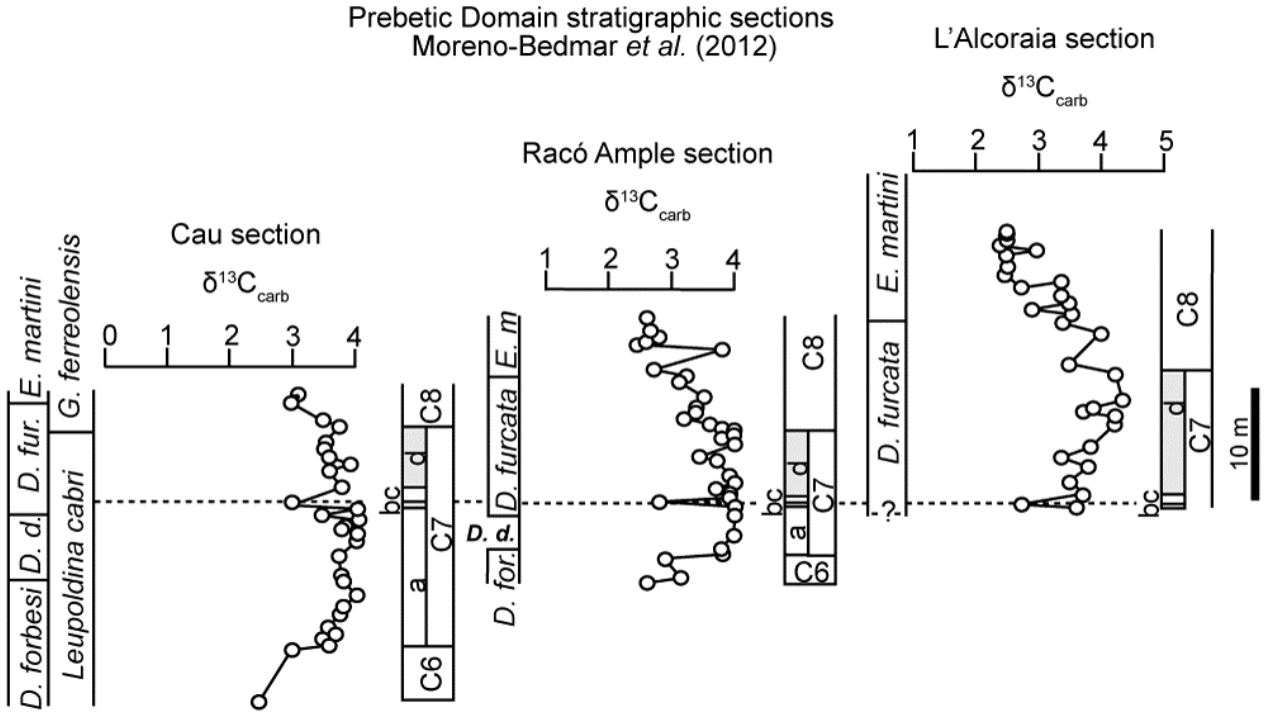

Figure 3: Carbon-isotope stratigraphy of sections in the Prebetic Domain: Cau, Racó Ample and L'Alcoraia sections. Proposed sub-units for dividing the segment C7 are shown. Sections are correlated (dashed line) using the negative carbon isotope excursion represented by the sub-unit C7b (IFNE). For all sections scale bar is 10 m.

Probable expressions of the "IFNE" in the Old World

Although more studies are needed, it is likely that the IFNE appears elsewhere beyond the Prebetic Domain (Fig. 4.A) because a comparable negative variation also occurs in other stratigraphic sections in Old World. The Cassis-La Bédoule Stratotype section in southeast France (MOULLADE *et al.*, 1998) is such an example, as a negative shift in the $\delta^{13}C_{carb}$ curve (~1.2 ‰) is recorded within the planktonic foraminifera *L. cabri* Zone, and is correlatable with the *Dufrenoyia furcata* Zone (*e.g.*, ROPOLO *et al.*, 2006; MORENO-BEDMAR *et al.*, 2012) (Fig. 4.B). In the Vocontian Basin, a negative carbon isotope excursion similar to IFNE has been documented by HERRLE *et al.* (2004) (Ap7b=~1.5 ‰). This correlation is very reliable because Ap7b has been related to the Niveau Blanc (HERRLE *et al.*, 2004), which is a significant reference level observed in most sections of the Vocontian Basin, and its upper part has been associated with the lower part of the *Dufrenoyia furcata* Zone (DUTOUR, 2005). This biochronologic correlation is also in agreement with the reconstructed carbon isotope segments of MENEGATTI *et al.* (1998) in the Vocontian Basin, as shown in Figure IX of MORENO-BEDMAR *et al.* (2012) (Fig. 4.C). Another comparable negative carbon isotope shift that may be equivalent to the IFNE is reported in the Aptian outcrops of the Djebel Serdj area, north-central Tunisia (HELD *et al.*, 2008). It consists of a $\delta^{13}C_{carb}$ negative variation of ~2.5 ‰ within the *L. cabri* Zone (Fig. 4.D).

In the Basque-Cantabrian Basin (Spain), at Igaratza section, MILLÁN *et al.* (2009) documented a pronounced negative $\delta^{13}C_{carb}$ spike predating the Aparein level and within the *Dufrenoyia furcata* Zone. Since according to MILLÁN *et al.* (2009) this negative carbon isotope excursion overlies the segment C8 and records a variation of about ~4.1 ‰, we consider that this does not correspond to the IFNE. Instead, it is more likely that the carbon isotope drop of ~1 ‰ to the middle part of the segment C7 correlates with the IFNE (Fig. 4.E). A firm correlation is not possible due to the fact that this drop is included in the *Deshayesites deshayesi* - *Dufrenoyia furcata* transition Zone. All mentioned sections in this chapter are located in Figure 1.

Probable expressions of the "IFNE" in the New World

A cursory review of the literature reveals that fewer published data are available for the New World regarding the Aptian interval; however, carbon isotope data from some sites show isotopic trends that could correspond to the IFNE. The $\delta^{13}C_{org}$ curve of the Santa Rosa section in northeastern Mexico displays a negative carbon isotope excursion of ~2.0 ‰ toward the base of segment C7 in the La Peña Formation, within the *L. cabri* planktonic foraminifera Zone (LI *et al.*, 2008). Since ammonite data are not available for the Santa Rosa section, we cannot determine whether or not this carbon isotopic drop is related to the Mexican ammonite zone

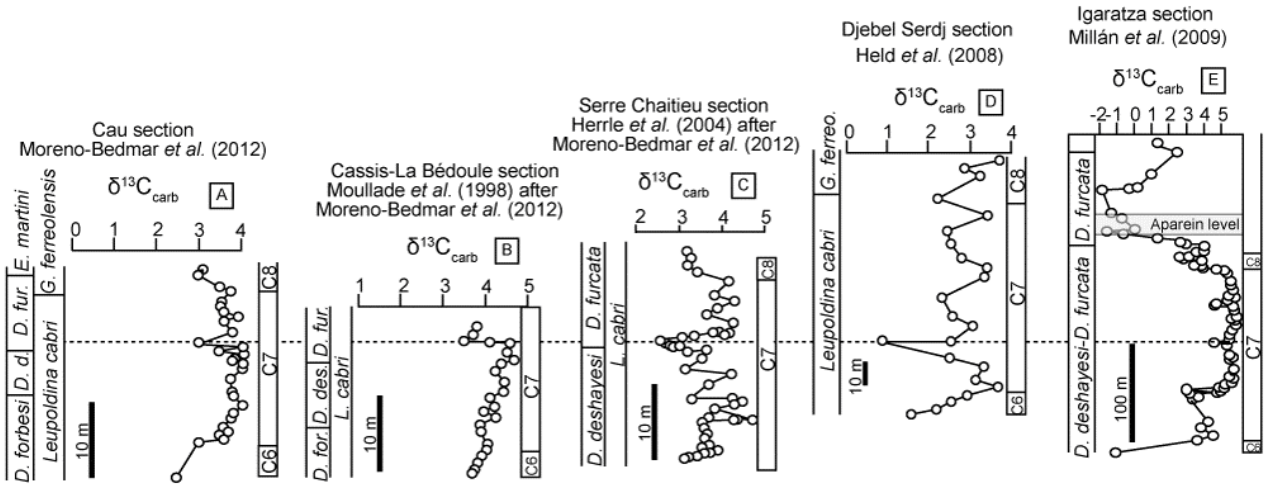

Figure 4: Different stratigraphic sections in the Old World which exhibit a negative carbon isotope excursion similar to the IFNE. Cau section of the Prebetic Domain is shown for comparison. Dashed line correlates the stratigraphic sections using IFNE as a characteristic chemostratigraphic marker. Ammonite biozones plotted for the Cassis-La Bédoule (MOULLADE *et al.,* 1998) and the Serre Chaitieu (Vocontian Basin) sections (HERRLE *et al.*, 2004) correspond to the interpretation of MORENO-BEDMAR *et al.* (2012). Planktonic foraminifera zones of the Djebel Serdj section are also depicted (HELD *et al.*, 2008). The segment C7 of the Vocontian Basin is also in agreement with MORENO-BEDMAR *et al.* (2012). The Igaratza section [reference section of the Aparein level of MILLÁN *et al.* (2009)] is shown for comparison with the IFNE.

equivalent to the European *Dufrenoyia furcata* Zone. In the USA, a decrease of 0.4 ‰ in carbon isotope composition of organic matter is reported at the base of the segment C7 of the La Calera limestone exposed at the Permanente Quarry in California (ROBINSON *et al.*, 2008). A lack of biostratigraphic data along with the carbon isotope data prevents us from further constraining the age of this negative excursion. In Colombia, the $\delta^{13}C_{org}$ curve of the Curití section shows a pronounced negative inflection in the lowermost part of the segment C7 that reaches ~2.0 ‰ (GAONA-NARVAEZ *et al.*, 2013) and is also compatible with the IFNE**.** All mentioned sections in this chapter are located in Figure 1.

Conclusions

A review of the $\delta^{13}C_{carb}$ curve in three different stratigraphic sections of the Prebetic Domain in Spain reveals a consistent pattern that allows us to propose a quadripartite division of the segment C7 of MENEGATTI *et al.* (1998). We divided segment C7 into distinct isotopic trends labeled, from bottom to top, C7a, C7b, C7c and C7d. The most conspicuous of these subdivisions corresponds to sub-unit 7b and consists of a negative carbon isotope excursion, with the lowest values within the lower middle part of segment C7. Since its record is chronologically linked to the *Dufrenoyia furcata* Zone, this isotope trend is here named the Intra-Furcata Negative Excursion (IFNE).

The chemostratigraphic record of the IFNE does not seem to be limited to the Prebetic Domain in Spain. We provide several plausible sites in both the Old and New worlds where a comparable negative carbon isotope excursion may be equivalent to the IFNE. Although additional research is needed, we wish to highlight the possible use of the IFNE as a new chemostratigraphic marker that has the potential to provide a more robust chronologic framework for the lower Aptian record.

Acknowledgments

The authors are grateful to Drs Karl FÖLLMI, Florentin MAURRASSE and Peter SKELTON for the careful review and the helpful comments and suggestions that significantly improved the original manuscript. Special thanks also are due to Michel MOULLADE and Bruno GRANIER for their constructive editing. We are very grateful to the Language Editor, Phil SALVADOR, for his corrections which allowed significant improvements to the manuscript.

Bibliographic references

ARTHUR M.A., BRUMSACK H.J., JENKYNS H.C. & SCHLANGER S.O. (1990).- Stratigraphy, geochemistry and paleoceanography of organic carbon-rich Cretaceous sequences. *In*: GINSBURG R.N. & BEAUDOIN B. (eds.), Cretaceous resources, events and rhythms-background and plans for research.- Kluwer Academic Publications, Dordrecht, p. 75-119.

BLAKEY R.C. (2010).- Paleogeographic maps.- Colorado Plateau Geosystems, Phoenix, AZ. URL: http://cpgeosystems.com/

BOVER-ARNAL T., MORENO-BEDMAR J.A., SALAS R., SKELTON P.W., BITZER K. & GILI E. (2010).- Sedimentary evolution of an Aptian syn-rift carbonate system (Maestrat Basin, E Spain): effects of accommodation and environmental change.- *Geologica Acta*, Barcelona, vol. 8, p. 249-280.

BOLLI H.B. (1959).- Planktonic foraminifera from the Cretaceous of Trinidad, B.W.I.- *Bulletin of American Paleontology*, New York, vol. 39, 257-277.

BRALOWER T.J., COBABE E., CLEMENT B., SLITER W.V., OSBURN C.L. & LONGORIA J. (1999).- The

record of global change in mid-Cretaceous (Barremian-Albian) sections from the Sierra Madre, northeastern Mexico.- *Journal of Foraminiferal Research*, Washington, vol. 29, nº 4, p. 418-308.

CASTRO J.M. (1998).- Las plataformas del Valanginiense superior-Albiense superior en el Prebético de Alicante.- Ph.D. thesis, Universidad de Granada, 464 p.

CASTRO J.M., GEA G.A. de, RUÍZ-ORTÍZ P.A. & NIETO J.M. (2008).- Development of carbonate platforms on an extensional (rifted) margin: the Valanginian-Albian record of the Prebetic of Alicante (SE Spain).- *Cretaceous Research*, London, vol. 29, p. 848-860.

DEBOND N., OAKES R.L., PAYTAN A. & WORTMANN U.G. (2012).- Early Aptian carbon and sulphur isotope signatures at ODP Site 765.- *Isotopes in Environmental and Health Studies*, Leipzig-Halle, vol. 48, nº 1, p. 180-194.

DUTOUR Y. (2005).- Biostratigraphie, évolution et renouvellements des ammonites de l'Aptien supérieur (Gargasien) du bassin vocontien (Sud-Est de la France).- Ph.D. thesis, Université Claude Bernard, Lyon, 302 p.

ERBA E., CHANNELL J.E.T., CLAPS M., JONES C., LARSON R., OPDYKE B., PREMOLI SILVA I., RIVA A., SALVINI G. & TORRICELLI S. (1999).- Integrated stratigraphy of the Cismon Apticore (southern Alps, Italy); a "reference section" for the Barremian-Aptian interval at low latitudes.- *The Journal of Foraminiferal Research*, Lawrence, vol. 29, nº 4, p. 371-391.

GAONA-NARVAEZ T., MAURRASSE F.J-M.R. & ETAYO-SERNA F. (2013).- Geochemistry, palaeoenvironments and timing of Aptian organic-rich beds of the Paja Formation (Curití, Eastern Cordillera, Colombia). *In*: BOJAR A.-V., MELINTE-DOBRINESCU M.C. & SMIT J. (eds.), Isotopic studies in Cretaceous research.- *Geological Society*, London, *Special Publication*, vol. 382, p. 31-48.

GARCÍA-MONDÉJAR J., OWEN H.J., RAISOSSADAT N., MILLÁN M.I. & FERNÁNDEZ-MENDIOLA P.A. (2009).- The early Aptian of Aralar (northern Spain): stratigraphy, sedimentology, ammonite biozonation, and OAE1.- *Cretaceous Research*, London, vol. 30, nº 2, p. 434-464.

GEA G.A. de (2004).- Bioestratigrafía y eventos del Cretácico Inferior en las Zonas Externas de la Cordillera Bética.- Universidad de Jaén, 658 p.

GEA G.A. de, CASTRO J.M., AGUADO R., RUIZ-ORTIZ P.A. & COMPANY M. (2003).- Lower Aptian carbon isotope stratigraphy from a distal carbonate shelf setting: the Cau section, Prebetic zone, SE Spain.- *Palæogeography, Palæoclimatology, Palæoecology*, Amsterdam, vol. 200, p. 207-219.

HELD M., BACHMANN M. & LEHMANN J. (2008).- Microfacies, biostratigraphy, and geochemistry of the hemipelagic Barremian-Aptian in north-central Tunisia: Influence of the OAE 1a on the southern Tethys margin.- *Palæogeography, Palæoclimatology, Palæoecology,* Amsterdam, vol. 261, p. 246-260.

HERRLE J.O., KÖßLER P., FRIEDRICH O., ERLENKEUSER H. & HEMLEBEN C. (2004).- High-resolution carbon isotope records of the Aptian to lower Albian from SE France and the Mazagan Plateau (DSDP Site 545): a stratigraphic tool for paleoceanographic and paleobiologic reconstruction.- *Earth and Planetary Science Letters*, Amsterdam, vol. 218, p. 149-161.

JENKYNS H.C. (1980).- Cretaceous anoxic events: From continents to oceans.- *Journal of the Geological Society*, London, vol. 137, nº 2, p. 171-188.

JENKYNS H.C. (1999).- Mesozoic anoxic events and palaeoclimate.- *Zentralblatt für Geologie und Paläontologie*, Stuttgart, Teil 1 (1997), Heft 7-9, p. 943-949.

LI Y.-X., BRALOWER T.J., MONTAÑEZ I.P., OSLEGER D.A., ARTHUR M.A., BICE D.M., HERBERT T.D., ERBA E. & PREMOLI SILVA I. (2008).- Toward an orbital chronology for the early Aptian Oceanic Anoxic Event (OAE1a, ~120 Ma).- *Earth and Planetary Science Letters*, Amsterdam, vol. 271, p. 88-100.

MÉHAY S., KELLER C.E., BERNASCONI S.M., WEISSERT H., ERBA E., BOTTINI C. & HOCHULI P.A. (2009).- A volcanic CO_2 pulse triggered the Cretaceous Oceanic Anoxic Event 1a and a biocalcification crisis.- *Geology*, Boulder, vol. 37, p. 819-822.

MENEGATTI A.P., WEISSERT H., BROWN R.S., TYSON R.V., FARRIMOND P., STRASSER A. & CARON M. (1998).- High-resolution $\delta^{13}C$ stratigraphy through the early Aptian "Livello Selli" of the Alpine Tethys.- *Paleoceanography*, Washington, vol. 13, nº 5, p. 530-545.

MILLÁN M.I., WEISSERT H.J., FERNÁNDEZ-MENDIOLA P.A. & GARCÍA-MONDÉJAR J. (2009).- Impact of early Aptian carbon cycle perturbations on evolution of a marine shelf system in the Basque-Cantabrian Basin (Aralar, N Spain).- *Earth and Planetary Science Letters*, Amsterdam, vol. 287, p. 392-401.

MORENO-BEDMAR J.A., COMPANY M., SANDOVAL J., TAVERA J.M., BOVER-ARNAL T., SALAS R., DELANOY G., MAURRASSE F.J.-M.R. & MARTÍNEZ R. (2012).- Lower Aptian ammonite and carbon isotope stratigraphy in the eastern Prebetic domain (Betic Cordillera, southeastern Spain).- *Geologica Acta*, Barcelona, vol. 10, nº 4, p. 333-350.

MOULLADE M., KUHNT W., BERGEN J.A., MASSE J.-P. & TRONCHETTI G. (1998).- Correlation of biostratigraphic and stable isotope events in the Aptian historical stratotype of La Bédoule (southeast France).- *Comptes Rendus de l'Académie des Sciences*, Paris, (Série IIa, Sciences de la Terre et des Planètes), n° 327, p. 693-698.

NAJARRO M., ROSALES I., MORENO-BEDMAR J.A., GEA G.A. de, BARRÓN E., COMPANY M. & DELANOY G. (2011).- High-resolution chemo- and biostratigraphic records of the early Aptian oceanic anoxic event in Cantabria (N Spain):

Palaeoceanographic and palaeoclimatic implications.- *Palæogeography, Palæoclimatology, Palæoecology*, Amsterdam, vol. 299, p. 137-158.

PREMOLI SILVA I. & VERGA D. (2004).- Practical manual of Cretaceous planktonic foraminifera.- International School on Planktonic Foraminifera, Course: Cretaceous, Perugia, 283 p.

RENARD M., RAFÉLIS M. de, EMMANUEL L., MOULLADE M., MASSE J.-P., KUHNT W., BERGEN J.A. & TRONCHETTI G. (2005).- Early Aptian $\delta^{13}C$ and manganese anomalies from the historical Cassis-La Bédoule stratotype sections (S.E. France): relationship with a methane hydrate dissociation event and stratigraphic implications.- *Carnets de Géologie* [*Notebooks on Geology*], Brest, Article 2005/04 (**CG2005_A04**), 18 p.

ROBINSON S.A., CLARKE L.J., NEDERBRAGT A. & WOOD I.G. (2008).- Mid-Cretaceous oceanic anoxic events in the Pacific Ocean revealed by carbon-isotope stratigraphy of the Calera Limestone.- *Geological Society of America*, *Bulletin*, Tulsa, vol. 120, nº 11-12, p. 1416-1426.

ROPOLO P., MOULLADE M., GONNET R., CONTE G. & TRONCHETTI G. (2006).- The Deshayesitidae STOYANOV, 1949 (Ammonoidea) of the Aptian historical stratotype region at Cassis-La Bédoule (SE France).- *Carnets de Géologie* [*Notebooks on Geology*], Brest, Memoir 2006/01 (**CG2006_M01**), 46 p. (14 Pls.).

SCHLANGER S.O. & JENKYNS H.C. (1976).- Cretaceous oceanic anoxic events: causes and consequences.- *Geologie en Mijnbouw*, Utrecht, vol. 55, p. 179-184.

WEISSERT H. & LINI A. (1991).- Ice Age interludes during the time of Cretaceous greenhouse climate? *In*: MULLER D.W., MCKENZIE J.A. & WEISSERT H. (eds.), Controversies in modern geology: Evolution of geologic theories in sedimentology, earth history and tectonics.- Academic Press, London, p. 173-191.

WEISSERT H., LINI A. & FÖLLMI K.B. & KUHN O. (1998).- Correlation of Early Cretaceous carbon isotope stratigraphy and platform drowning events: A possible link?- *Palæogeography, Palæoclimatology, Palæoecology*, Amsterdam, vol. 137, p. 189-203.

Appendix:
Carbon and Oxygen isotope data from stratigraphic sections in the Prebetic Domain

Cau section			Raco Ample section			L'Alcoraia section		
Sample	$\delta^{13}C_{carb}$ (‰ PDB)	$\delta^{18}O_{carb}$ (‰ PDB)	Sample	$\delta^{13}C_{carb}$ (‰ PDB)	$\delta^{18}O_{carb}$ (‰ PDB)	Sample	$\delta^{13}C_{carb}$ (‰ PDB)	$\delta^{18}O_{carb}$ (‰ PDB)
54	3.10	-1.78	46	2.63	-2.29	212	3.01	-1.50
53	3.05	-2.16	45	2.66	-2.14	210	2.99	-2.03
51	3.41	-2.07	44	2.78	-2.35	209	2.92	-1.77
50	3.70	-1.67	43	2.64	-1.99	208	3.38	-2.24
49	3.57	-1.92	42	2.46	-2.06	207	2.98	-1.74
48	3.55	-2.04	41	3.82	-2.32	206	3.08	-1.55
47	3.61	-2.15	40	2.70	-2.50	205	3.01	-1.65
46b	3.88	-1.66	39	3.17	-2.27	204	3.68	-1.10
46a	3.58	-1.72	38	3.13	-2.02	203	3.38	-1.52
46	3.78	-2.02	37	3.47	-2.32	202	3.17	-1.69
44*	**3.04**	**-1.97**	36	3.43	-2.45	201	3.74	-1.44
43	4.04	-1.67	35	3.39	-2.52	200	3.78	-1.47
42	3.54	-2.52	34	3.24	-2.41	199	3.30	-2.12
41	4.07	-1.22	33	3.57	-2.46	198	3.85	-1.29
39	3.88	-2.02	32	3.100	-2.36	197	3.76	-1.92
38	3.78	-2.08	31	3.96	-2.35	196	4.23	-1.42
37	3.96	-1.95	30	4.03	-2.27	195	3.76	-1.92
35	4.04	-1.49	29	3.81	-2.47	194	4.36	-1.41
33	3.71	-2.09	28	3.97	-2.25	193	4.44	-1.57
32	3.77	-1.96	27	3.44	-2.61	191	4.13	-2.07
31	3.84	-1.96	26	3.74	-2.56	190	4.02	-2.34
30	3.99	-1.85	24	3.93	-2.41	189	4.43	-1.85
29a	3.100	-2.01	23	4.02	-2.39	188	4.36	-1.65
29	3.59	-1.97	22	3.64	-2.46	187	4.11	-1.75
28	3.69	-1.69	21	3.93	-2.08	186	3.71	-2.50
27	3.52	-1.85	20	3.89	-2.25	185	4.08	-2.06
26	3.61	-1.92	**19a***	**2.82**	**-2.76**	184	3.77	-2.31
25	2.97	-1.98	19	4.00	-2.06	183	3.97	-2.32
23	2.48	-2.05	18	3.96	-2.24	**182***	**3.07**	**-1.44**
			16	4.00	-2.43	181	3.84	-2.09
Reproducibility	± 0.03	±0.03	15	3.83	-2.56			
			14	3.75	-2.32	Reproducibility	± 0.01	± 0.06
***IFNE**			13	2.91	-2.73			
			11a	3.10	-2.27			
			11	2.62	-2.25			
			Reproducibility	± 0.02	± 0.05			

Rocas sedimentarias del Barremiano-Aptiano en Sierra del Rosario, Durango

CAPÍTULO 4

EPISODIOS DE CAMBIO GLOBAL ACELERADO DURANTE EL APTIANO DEL NORESTE DE MÉXICO

Artículo: **Núñez-Useche, F.**, Barragán, R., Moreno-Bedmar, J.A., Canet, C., 2014. Geochemical and paleoenvironmental record of the early to early late Aptian major episodes of accelerated change: Evidence from Sierra del Rosario, Northeast Mexico. Sedimentary Geology 324 (2015) 47–66, http://dx.doi.org/10.1016/j.sedgeo.2015.04.006.

Sedimentary Geology 324 (2015) 47–66

Contents lists available at ScienceDirect

Sedimentary Geology

journal homepage: www.elsevier.com/locate/sedgeo

Geochemical and paleoenvironmental record of the early to early late Aptian major episodes of accelerated change: Evidence from Sierra del Rosario, Northeast Mexico

Fernando Núñez-Useche [a,b,*], Ricardo Barragán [b], Josep Anton Moreno-Bedmar [b], Carles Canet [c]

[a] Posgrado en Ciencias de la Tierra, Universidad Nacional Autónoma de México, Del. Coyoacán, 04510 México D.F., Mexico
[b] Instituto de Geología, Universidad Nacional Autónoma de México, Del. Coyoacán, 04510 México D.F., Mexico
[c] Instituto de Geofísica, Universidad Nacional Autónoma de México, Del. Coyoacán, 04510 México D.F., Mexico

ARTICLE INFO

Article history:
Received 4 February 2015
Received in revised form 14 April 2015
Accepted 15 April 2015
Available online 24 April 2015

Editor: B. Jones

Keywords:
Cretaceous
Organic-carbon rich sediments
OAE 1a
IFNE
Noire level
Redox conditions

ABSTRACT

The lower to lower-upper Aptian succession of northern Mexico documents the drowning of the shallow-water Cupido/Cupidito carbonate platform system followed by deposition of the deep-water sediments of the La Peña Formation. Using $\delta^{13}C$ stratigraphy, geochemical and mineralogical information coupled with previous microfacies, paleontological and total organic carbon (TOC) data from a stratigraphic section, which includes such lithological change, this study identifies distinctive episodes of accelerated global environmental change, and determines the paleoenvironmental conditions conducive to the deposition of TOC-rich intervals. Within the Cupidito unit, the Oceanic Anoxic Event 1a (OAE 1a) is recorded near the base of the section and the Intra-Furcata Negative Excursion in the topmost beds of the unit. The upper part of the section, within the La Peña Formation, is correlatable with the Noire level. Organic-carbon rich intervals occur in the lower and middle part of the OAE 1a, upper part of the Cupidito unit, base of the La Peña Formation, and in the Noire level equivalent. Reducing conditions within the sediment and oxic–dysoxic at the seafloor, locally controlled, persisted both before and during OAE 1a interval in the Cupidito lagoon. Oxygen-depleted conditions (dysoxic–anoxic) were more permanent and stronger during the deposition of the base of the la Peña Formation and the Noire equivalent level. It is proposed here that deposition of the lower-middle part of the OAE 1a and the base of the La Peña Formation was influenced by climate-controlled increases in detrital and accompanying nutrient influx that supplied especially biolimiting nutrients (Fe, P), fostering marine productivity and TOC burial. Upwelling of nutrient-rich deeper waters and minor arrival of nutrients from runoff, both account for the domination of radiolaria and organic-carbon burial during the Noire level equivalent. Record of the OAE 1a time-equivalent facies in the Cupidito lagoonal sediments confirms the diachronism of the Cupidito–La Peña flooding. Heterozoan carbonate production in the Cupidito ramp was uninterrupted during and after OAE 1a. Periodic arrival of detrital components and nutrients during warmer/humid periods accelerated platform drowning, which peaked during the diachronic deposition of the La Peña Formation.

1. Introduction

The Aptian represents a time of accelerated global change in the lithosphere–ocean–atmosphere system with profound imprint on climatic, paleogeographic, sedimentary and biotic evolutionary patterns. These changes were brought by a battery of interrelated events with positive and negative feedbacks. Increase in ocean crust production and midplate and plate margin volcanism raised the level of atmospheric CO_2 and induced episodes of extreme greenhouse conditions (Menegatti et al., 1998; Larson, 1991; Leckie et al., 2002; Jenkyns, 2003; Weissert and Erba, 2004; García-Mondéjar et al., 2009; Tejada et al., 2009; Keller et al., 2011). These climate conditions accelerated the hydrologic cycle and increased continental weathering and runoff (Erba, 1994; Föllmi et al., 1994; Leckie et al., 2002; Föllmi, 2012). They also resulted in various episodes of global rise in sea-level (Haq et al., 1988); several crises and demises of carbonate platforms in the peri-Tethyan region (Föllmi et al., 1994; Wissler et al., 2003; Barragán and Maurrasse, 2008; Millán et al., 2009); a biocalcification crisis, which affected most of the pelagic biota (Larson and Erba, 1999; Weissert and Erba, 2004); and major global perturbations in carbon cycling (Menegatti et al., 1998; Weissert and Erba, 2004).

* Corresponding author at: Instituto de Geología, Universidad Nacional Autónoma de México, Del. Coyoacán, 04510 México D.F., Mexico.
E-mail addresses: fernandonunezu@comunidad.unam.mx, fernandonunezu@gmail.com (F. Núñez-Useche).

http://dx.doi.org/10.1016/j.sedgeo.2015.04.006
0037-0738/

The combination of these events produced stressful conditions triggering conspicuous global episodes of environmental change that can be indentified in the stratigraphic record by their specific carbon-isotope signature and/or by the presence of organic-carbon rich sediments (Föllmi, 2012). For the late Barremian–early late Aptian age, such events include: (a) several perturbations during the Barremian–Aptian transition marking the switch from an interval with normal conditions, to an episode of intensified greenhouse conditions and accelerated paleoceanographic change associated with several organic-carbon rich levels (Menegatti et al., 1998; Föllmi, 2012; Sanchez-Hernandez and Maurrasse, 2014); (b) the early Aptian OAE 1a (Livello Selli event) considered as one of the most important global perturbations in the carbon cycle in the Cretaceous, defined by a negative spike in the carbon-isotope curve followed by a shift toward positive values, and usually concomitant organic-carbon rich sediments deposited under poorly-oxygenated conditions (Schlanger and Jenkyns, 1976; Jenkyns, 1980, 1999; Menegatti et al., 1998; Erba et al., 1999); and (c) a set of early late Aptian episodes associated with the Noire and Fallot levels in the Vocontian Basin, France (Bréhéret, 1997; Herrle et al., 2004); and with an organic-carbon rich level reported in Italy (Cobianchi et al., 1997; Luciani et al., 2006), which is equivalent to the Aparein level in the Basque–Cantabrian Basin, Spain (García-Mondéjar et al., 2009; Millán et al., 2009). Recently, Núñez-Useche et al. (2014) proposed a new chemostratigraphic event, termed Intra-Furcata Negative Excursion (IFNE) for the Prebetic Domain in Spain. It is characterized by a negative excursion in $\delta^{13}C$ record within the *Dufrenoyia furcata* ammonite Zone.

The Francisco Zarco Dam section of the south-facing paleomargin of the Cupido carbonate platform, northeastern Mexico (Durango State) contains a transgressive Barremian–Aptian succession that records several organic-carbon rich intervals and the gradual drowning of the carbonate platform (Araujo and Martínez, 1981; Barragan, 2001; Barragán-Manzo and Díaz-Otero, 2004; Barragán-Manzo and Méndez-Franco, 2005; Núñez-Useche and Barragán, 2012; Moreno-Bedmar et al., 2012a, 2013). The section exhibits a completely outcropping succession composed of the transgressive shallow-water Cupidito unit (upper part of the Cupido Formation; Wilson and Pialli, 1977), and the overlying deep-water facies of the La Peña Formation. In the present study we integrate previous biostratigraphic and total organic carbon (TOC) information with new geochemical ($\delta^{13}C$ of the carbonate fraction and whole-rock major and trace elements) and mineralogical (mineral composition and pyrite framboid size) data to unravel the evolution of paleoenvironmental conditions in response to global and local changes. The specific objectives are: (a) to describe $\delta^{13}C$ major trends and correlate them with global and local episodes of environmental changes that took place during the early–early late Aptian interval; and (b) to understand the paleoenvironmental conditions that resulted in organic-carbon sequestration in sediments and its possible causes and forcing mechanisms. We further address the apparent inconsistency regarding the lithostratigraphic position of the OAE 1a in northeastern Mexico, previously identified in the base of the La Peña Formation (Bralower et al., 1999; Li et al., 2008) but recorded in this study within the Cupidito unit. Altogether, the data presented herein provide an excellent case to investigate the local response to episodes of global accelerated change and its link with detrital flux and nutrient input coupled with marine productivity, oxygen consumption in the water column and organic-carbon burial.

2. Geological setting

The development of extensive shallow-water carbonate platforms around the Gulf of Mexico reached its maximum extent during the early Aptian (Scott, 1990; Wilson and Ward, 1993; Lehmann et al., 1999) (Fig. 1). This paleogeographic configuration was favored by post-Berriasian tectonic subsidence related to the crustal cooling and opening of the Gulf of Mexico (Goldhammer et al., 1991). In northeastern Mexico, the Cupido and Coahuila carbonate platforms developed around the Coahuila basement block during Barremian through Albian time (Fig. 1). This block controlled the geometry and stacking pattern of carbonate facies and also acted as a source area for detrital sediments (Wilson and Selvius, 1984; Goldhammer et al., 1991).

The late Barremian Cupido platform was a flat-topped, rimmed shelf with a broad interior shallow lagoon isolated by a variable margin (Fig. 1). The southern part of this margin is a high-energy shoal that changes along strike to a discontinuous coral-rudist reef in the east margin facing the ancestral Gulf of Mexico (Lehmann et al., 1999). These settings are recorded by massive, shallow-water limestone of the Cupido Formation (Imlay, 1937; Humphrey, 1949; Conklin and Moore, 1977; Wilson and Pialli, 1977; Goldhammer et al., 1991; Lehmann et al., 1999). The hemipelagic mudstone of the Lower Tamaulipas Formation (Stephenson, 1922; Muir, 1936) represent the down-dip, low energy deposits accumulated on the surrounding deeper water shelf (Fig. 1).

During the latest Barremian–earliest Aptian (Fig. 1), deposition of transgressive facies of the Cupidito unit across a homoclinal ramp profile (Wilson and Pialli, 1977) marked the retrogradational backstep and beginning of the drowning of the Cupido platform, in response to a major second-order marine transgression (Goldhammer et al., 1991; Lehmann et al., 1999). According to Conklin and Moore (1977), the Cupidito unit contains isolated rudist pinnacle reefs, which are interpreted by Lehmann et al. (1999) as the fossil record of the response of the platform system to the drowning event. The flooding event continued through the deposition of the deep-water carbonates of the La Peña Formation throughout the early Aptian-earliest Albian (Fig. 1).

The Cupidito–La Peña flooding event has been widely accepted as diachronic, usually interpreted as a time-transgressive facies boundary above which the base of the La Peña Formation rise biostratigraphically toward shelfal sections (Goldhammer et al., 1991; Goldhammer, 1999; Lehmann et al., 1999). However, the results of recent investigations focused on ammonite data suggest that the base of the La Peña Formation is rather isochronous and assignable everywhere to the upper part of the late early Aptian *Dufrenoyia furcata* Zone (Barragán-Manzo and Méndez-Franco, 2005; Barragán and Maurrasse, 2008; Moreno-Bedmar et al., 2011, 2012a; Moreno-Bedmar and Delanoy, 2013). Since the transition from the Cupidito to the La Peña facies occurred simply by landward migration of the shallow-water marine depositional sites toward the Coahuila block, Goldhammer et al. (1991) and Lehmann et al. (2000) consider that the Cupidito–La Peña contact cannot be interpreted either a drowning unconformity or a standard sequence boundary. This lithostratigraphic boundary is not a prominent unconformity, but rather is a transitional flooding surface. The termination of this platform has been correlated with the early to early late Aptian episode of shallow carbonate platform demise throughout the peri-Tethyan region (Föllmi et al., 1994).

The La Peña Formation records a sudden moderate increase in detrital components evidenced by the appearance of fine-grained siliciclastic components in limestone and calcareous shale. Siliciclastic components were derived from distal highlands to the north and west (Goldhammer et al., 1991). The shale beds of this unit contain frequent ammonites and small rounded clasts of phosphorite. With a highly variable thickness controlled by both the accommodation space and the paleorelief, this unit blankets large extensions of the southwest Gulf of Mexico (Goldhammer et al., 1991; Lehmann et al., 1999; Barragan, 2001).

Once the deposition of the La Peña Formation ended, the significantly backstepped Coahuila carbonate platform was established during the early Albian (Fig. 1). It consisted of a restricted evaporitic lagoon (interbedded massive carbonates and evaporites of the Acatita Formation) isolated by a shallow shoal margin (massive shallow-water limestone of the Aurora Formation). On the surrounding areas of this platform took place the deposition of the deep-water carbonates of the Upper Tamaulipas Formation characterized by hemipelagic mudstone (Goldhammer et al., 1991; Lehmann et al., 1999).

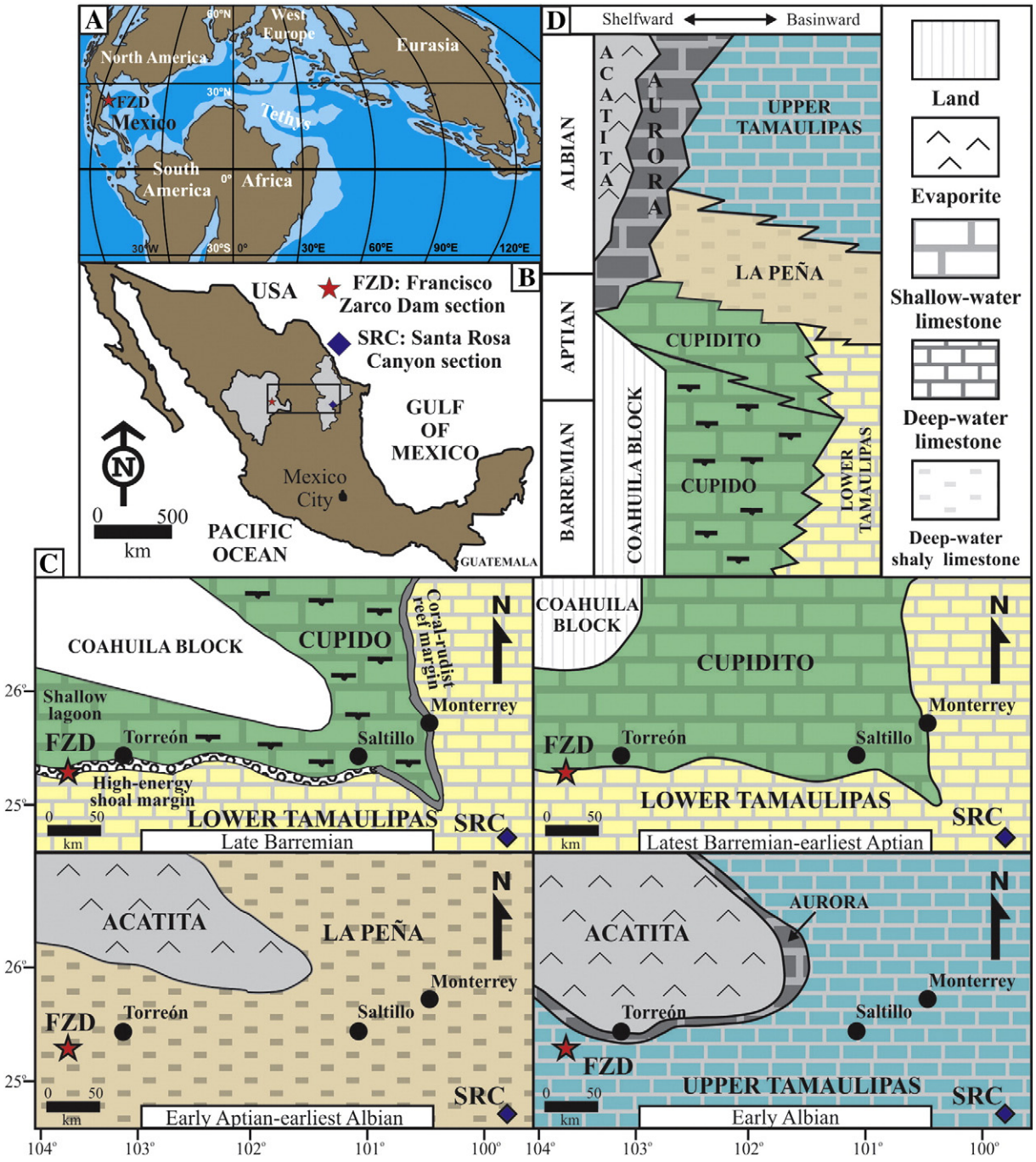

Fig. 1. A — Paleoceanographic reconstruction of the Aptian (http://jan.ucc.nau.edu/~rcb7/) showing the location of Mexico; B — Map of Mexico displaying the location of the Francisco Zarco Dam (FZD) and the Santa Rosa Canyon (SRC) sections, and the area enlarged in (C); C — Paleogeographic maps of northeastern Mexico for selected times from late Barremian to early Albian (modified from Lehmann et al., 1999); D — Synthetic lithostratigraphic scheme and age distribution (modified from Lehmann et al., 1999 and Goldhammer, 1999).

3. The Francisco Zarco Dam stratigraphic section: lithostratigraphic character and previous investigations

The Francisco Zarco Dam section (FZD section; 25° 16′ N/103° 46′ W) is located along the western exposed limb of an open anticline situated at the southern part of the Sierra del Rosario in eastern Durango State, about 40 km southwest of the city of Torreón (Fig. 1). Excellently exposed alongside the road leading to the Francisco Zarco Dam, this section shows the Cupidito unit and the overlying La Peña and Upper Tamaulipas formations (Fig. 2A). In this paper we focus on a 102.2 m interval that comprises the uppermost 73.1 m of the Cupidito unit and the lowermost 29.1 m of the La Peña Formation. Relevant available information concerning age, stratigraphy and sedimentology of the stratigraphic units is summarized as follows.

3.1.1. Cupido Formation/Cupidito unit

Based on the occurrence of the benthic foraminifera *Palorbitolina lenticularis* at ~30 and ~70 m below the base of the section studied herein, Araujo and Martínez (1981) suggest that the Cupidito unit encompasses the late Barremian–early Aptian transition. However, the exact stratigraphic position of the boundary between these ages is not yet defined. Since the upper part of the Cupidito unit is neither a condensed interval nor a hiatus, it must be stratigraphically coeval with the lower-middle part of the late early Aptian *D. furcata*

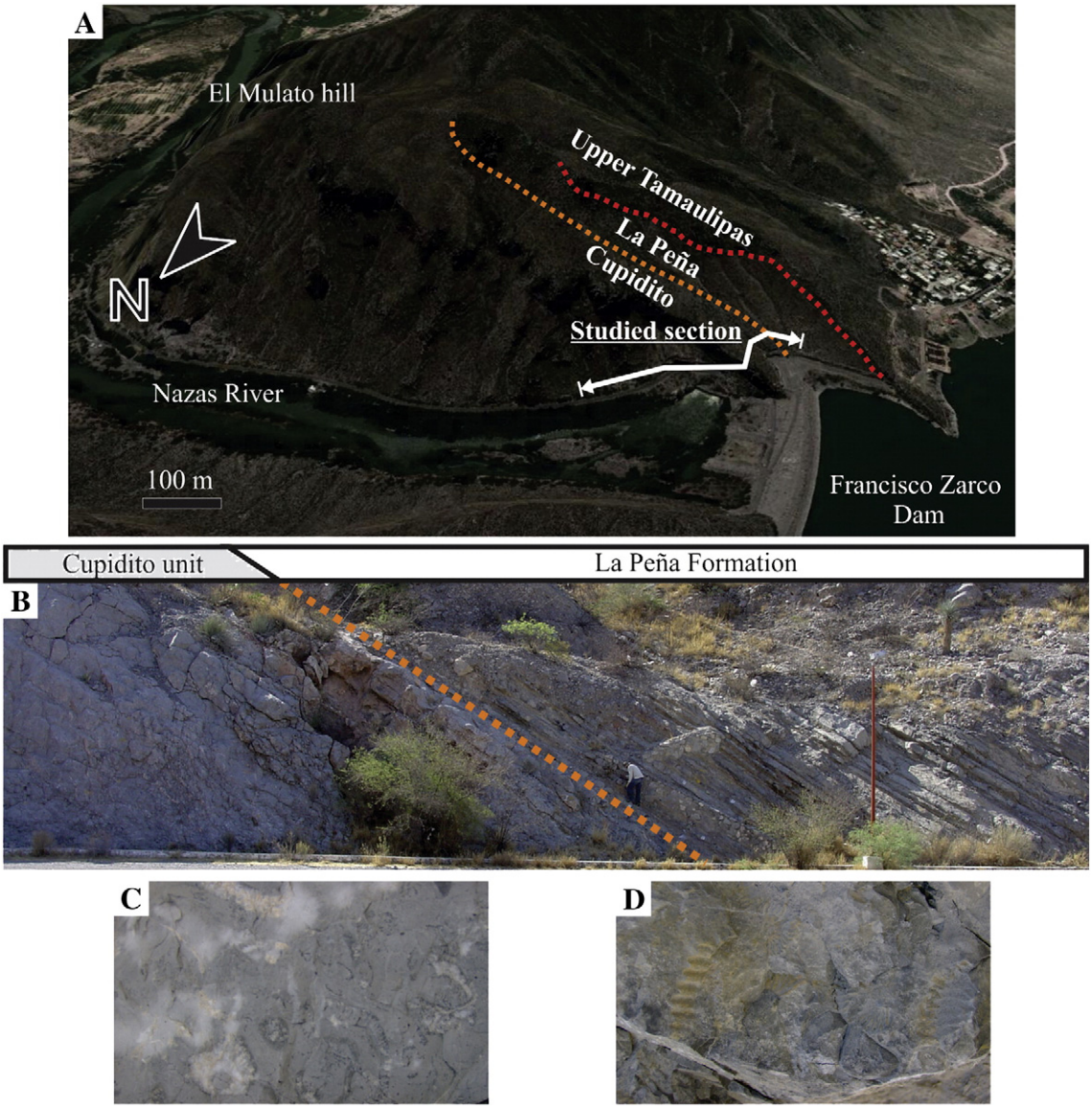

Fig. 2. General characteristics of the Francisco Zarco Dam (FZD) section. A — Panoramic view in Google Earth of the area showing the studied stratigraphic profile; B — Outcrop photograph of the Cupidito–La Peña contact; C — Rudist-shells fragments in the uppermost part of the Cupidito unit; D — Casts of ammonite shells in the base of the La Peña Formation.

Zone. This is by considering the ammonite zonation of the overlying La Peña Formation (Barragan, 2001; Moreno-Bedmar et al., 2013) (Fig. 3A).

The Cupidito unit consists of thickly- and very thickly-bedded, gray to dark-gray limestone that occasionally are partially or completely dolomitized. Chert nodules are scattered as irregular shaped and elongate lenses parallel to bedding, mainly within the lowest 40 m. The sediments are somewhat bioturbated. Núñez-Useche and Barragán (2012) characterize and illustrate in detail the facies of the Cupidito unit. From such study, four distinct associations of microfacies can be described and interpreted as follows (Fig. 3A):

(I) Wackestone and packstone containing miliolids, orbitolinids, worm tubes, dasycladacean algae and mollusk fragments (peritidal and subtidal facies deposited in a shallow lagoon with different levels of restriction);
(II) Grainstone and rudstone with superficial and well-sorted ooids (mainly with radial micro-fabric), crinoids, miliolids, filamentous algae and intraclasts, and incipient vadose pendant cement in the uppermost beds (shallow-water shoal facies);
(III) Grainstone and packstone containing abundant crinoids, and common peloids, intraclasts, miliolids and mollusk fragments (high-energy, shelf margin facies); and
(IV) Wackestone and floatstone containing randomly orientated rudists with algal incrustations, common crinoids, peloids, miliolids and brachiopod fragments, as well as rare coral fragments (fore-reef facies).

No subaerial exposure surface reflecting a clear emersion phase is observed. At the outcrop scale, the Cupidito–La Peña contact is concordant (Fig. 2B) but very distinctive due to the sharp contrast between the underlying massive, rudist-bearing limestone (Fig. 2C) and the overlying shale and shaly limestone beds with ammonites (Fig. 2D).

Barragan (2001) reports an overall low TOC content (below <1%) in the sediments of Cupidito and describes two stratigraphic TOC-rich intervals (Fig. 3B); one spans from 13 to 30 m and shows an upward decreasing trend in TOC (values between 5.15% and 1.13%), and the other encompasses the uppermost 10 m of the unit (from 62 to 72 m) and shows TOC values of up to 6.23%. These intervals are hereinafter

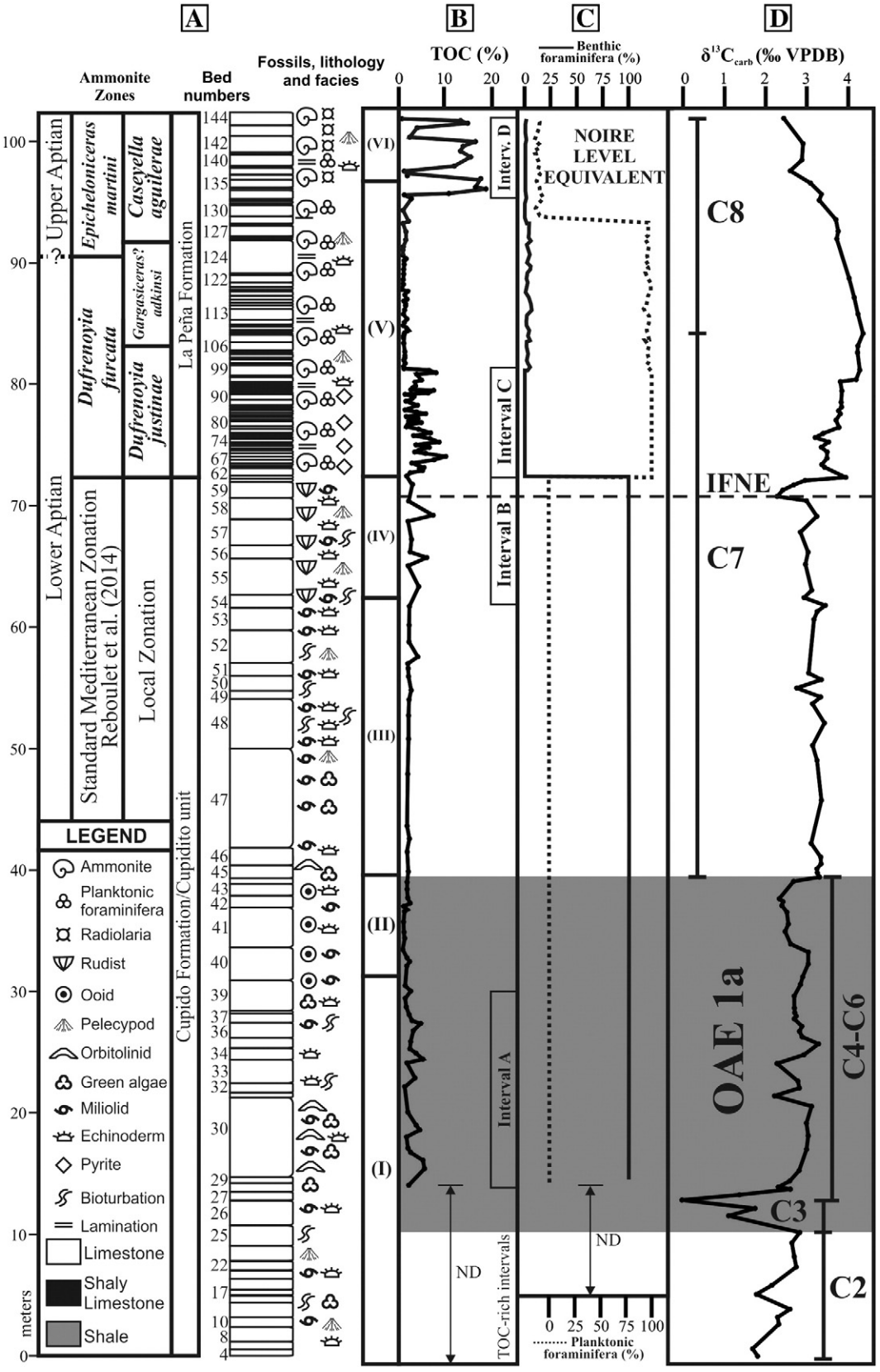

Fig. 3. Summary of the lithostratigraphy, biostratigraphy and carbon chemostratigraphy of the Francisco Zarco Dam section. A—Stratigraphic column showing fossils, lithology and facies. Age distribution and ammonite zonation for the La Peña Formation are from Moreno-Bedmar et al. (2013) (considering the standard Mediterranean zonation of Reboulet et al., 2014). Microfacies associations (I)–(VI) are based on Núñez-Useche and Barragán (2012) and described in Section 3; B — Vertical variation in TOC (Barragan, 2001) and TOC-rich intervals named in this study; C — Relative abundances of benthic and planktonic foraminifera (Barragan, 2001); D — Carbon stratigraphy (this study): vertical variation in δ13C including the characteristic Aptian carbon-isotope C2–C8 segments from Menegatti et al. (1998). The location of major chemostratigraphic events (OAE 1a, Intra-Furcata Negative Excursion = IFNE, Noire level equivalent) is also showed. ND = No data available from this or other works.

named TOC-rich intervals A and B, respectively. This author also points out that foraminiferal assemblages observed in the Cupidito unit are dominated by benthic specimens (Fig. 3C).

3.1.2. La Peña Formation

The studied part of the La Peña Formation has been dated in several works as latest early–early late Aptian based on ammonite biostratigraphy (upper part of the *D. furcata* Zone–*Epicheloniceras martini* Zone) (Barragan, 2001; Barragán-Manzo and Méndez-Franco, 2005; Moreno-Bedmar et al., 2013) (Fig. 3A). The base of the unit does not show any features of condensation (hardgrounds or horizons enriched with authigenic minerals such as glauconite or phosphorite). It comprises medium- and thick-bedded, dark-gray micritic shaly limestone intercalated with thin- and medium-bedded gray shale, both containing abundant ammonites without signs of reworking or condensation. Overall, the abundance of ammonites decreases upward in the section. The sediments are finely laminated and contain disseminated pyrite. According to Núñez-Useche and Barragán (2012), the La Peña Formation consists of two associations of microfacies (Fig. 3A):

(V) Mudstone and wackestone with abundant planktonic foraminifera, and common echinoderms, pelecypod fragments and ostracods; and
(VI) Wackestone and packstone with extremely abundant radiolaria, common planktonic foraminifera and ostracods, and rare pelecypods (including inoceramids) and ammonite fragments.
Both facies are interpreted as deposited in the distal parts of the outer neritic area.

Barragan (2001) describes two important TOC enriched intervals throughout this unit (Fig. 3B). The first one corresponds to the lowest 9 m (TOC between 1.94 and 8.72%), and coincides with the total disappearance of benthic foraminifera and the appearance of planktonic foraminifera (across the shift of facies from the Cupidito unit to the La Peña Formation) (Fig. 3C). The second interval corresponds to the uppermost 6 m (TOC values of up to 18.39%) and concurs with a radiolarian-dominated zone (Fig. 3B). These intervals are hereinafter named TOC-rich intervals C and D, respectively.

4. Material and methods

We used standard analytical techniques to examine bulk rock samples from limestone beds of the Cupidito unit (without petrographic evidence of dolomitization) and shaly limestone beds of the La Peña Formation. The samples were broken into small fragments to remove surface contamination and to have better access to the unaltered rock.

The carbonate fraction for stable isotope analysis ($\delta^{13}C_{carb}$) of 113 samples throughout the section was extracted with a dental drill from micritic matrix in order to avoid calcite veins, macrofossils or areas altered by circulation of meteoric water. Approximately 50–60 μg of sample were treated with H_3PO_4 (100%) at 70 °C and the produced CO_2 was analyzed with a Thermo Finnigan MAT-252 stable isotope ratio mass spectrometer at the *Unitat de Medi Ambient-Serveis Cientificotècnics* of the *Universitat de Barcelona*. The isotope results are expressed in ‰ relative to the VPDB standard and have a precision of ±0.02‰.

Mineralogical composition was determined in ten samples of limestone from both the Cupidito unit and the La Peña Formation. The samples were ground with an agate pestle and mortar to <75 μm and mounted in aluminum holders for X-ray powder diffraction analysis. A Shimadzu XRD-6000 X-ray diffractometer equipped with a Cu tube and graphite monochromator was used at the XRD laboratory of the *Instituto de Geología*, *Universidad Nacional Autónoma de México* (UNAM). The analyses were carried out on randomly oriented samples using the measurement range (2θ) of 4 to 70° at a speed of 1°/min. Four samples were also analyzed by the step scan method with integration time of 2 s and step size of 0.02. Phase identification was made with a PDF-2 database using Shimadzu software. Rietveld refinement of the data was done with TOPAS Academic v.4.1 software (http://www.topas-academic.net/).

Major and trace element concentrations were measured on 59 rock samples from the Cupidito unit and the lower part of the La Peña Formation. This analysis was not performed on samples from the uppermost 8.5 m of the section. Fresh chips of rock samples (free of veinlets, stylolites and hydrocarbons) were washed with distilled water and dried prior to being pulverized with an agate pestle and mortar to <75 μm. These analyses were done at the Activation Laboratories Ltd. (Actlabs) in Canada, by inductively coupled plasma mass spectrometry (ICP-MS; Perkin Elmer Sciex ELAN 9000) after the digestion of 1.0 g of sample using four different acids (HF, $HClO_4$, HNO_3 and HCl) (Package code Ultratrace 6). Percentages of the relative standard deviation were consistently below 10% as checked by standards and analysis of replicate samples.

The size of at least 150 pyrite framboids per sample in seven thin sections from the TOC-rich intervals C and D of the La Peña Formation (Fig. 3B) was measured by eyepiece micrometer under reflected light mode of an Olympus BX60 optical microscope using maximum magnification (×100). Despite this microscope has a low resolution in comparison to the backscattered electron microscope normally used in this type of research, it ensures the requirement for size distribution analysis of pyrite framboids (down to 0.1 to 1 μm level).

5. Results

5.1. Carbon-isotope stratigraphy

The stratigraphic distribution of carbon-isotope values for the FZD section is illustrated in Fig. 3D (Appendix A). In general, the measured $\delta^{13}C_{carb}$ values vary between −0.04 and +4.35‰. The Cupidito unit is characterized by a general upward increase in $\delta^{13}C$, with values between +1.67 and +2.82‰ within the lowest 9.4 m and between +2.20 and 3.44‰ from 11.7 m to the top of the unit. This pattern of variation is interrupted by two distinctive negative excursions in the carbon-isotope record. Of these, the most prominent occurs between 9.4 and 11.7 m and has an amplitude of 2.86‰ (down to +0.04‰). It is followed by a positive excursion of 3.25‰ that finishes at 39.9 m. The second corresponds to a discrete isotope drop of 0.7‰ (from +2.98 to +2.27‰) between 70.7 and 71 m, and is followed by a positive shift of 1.6‰ that finishes at the first sample from the base of the La Peña Formation. The general trend in the $\delta^{13}C$ record of the La Peña Formation shows an increase in values from +3.41 to +4.35‰ within the lowest 11.0 m. From 86.0 m upward in the succession there is a decline in the trend from +4.35 to +2.43‰.

5.2. Bulk mineralogy

The analyzed rocks are composed of both detrital and non-detrital minerals (Table 1). The Cupidito unit consists mainly of calcite (76.53–99.06%) and moderate to minor concentrations of potassium feldspar (2.56–6.81%), phyllosilicates (0.18–4.94%), quartz (0.52–3.09%), gypsum (0.11–5.5%), and dolomite (found only in sample FZD-09; 6.86%). The content of detrital components is highly variable throughout this unit; however, the highest occur in their lowest ~22 m. Otherwise, the La Peña Formation is mainly composed of calcite (86.41–93.72), moderate concentrations of potassium feldspar (1.67–5.55%), phyllosilicates (2.5–5.4%), quartz (0.94–3.15%) and low presence of gypsum (0.15–1.04%). Dolomite was not detected in samples of this unit. In all cases, phyllosilicates have a distinctive diffraction line at 10 Å suggesting that they belong to the illite group.

Table 1
Mineral composition obtained by XRD analysis.

Bed/sample	Distance base (m)	Phyllosilicates (%)	Gypsum (%)	Quartz (%)	Potassium Feldspar (%)	Calcite (%)	Dolomite (%)
FZD-143 [a]	101.1	4.89	0	3.15	5.55	86.41	0
FZD-135	96.5	5.4	0.15	2.01	1.89	90.54	0
FZD-99	81.5	3.37	0	2.55	4.56	89.52	0
FZD-84[a]	77.9	4.6	1.04	1.59	1.67	91.1	0
FZD-62 [a]	72.6	2.5	0.32	0.94	2.52	93.72	0
FZD-48t	53.9	0.13	0.23	0.62	0	99.06	0
FZD-47 m	45.9	0.18	0.28	0.52	0	99.02	0
FZD-32	22.2	4.56	0	1.25	2.56	91.63	0
FZD-27b	12.9	4.94	0.11	3.09	2.58	89.22	0
FZD-09[a]	2.1	3.54	5.5	0.76	6.81	76.53	6.86

[a] Samples analyzed by step scan

5.3. Major and trace elements

Several studies show that major and trace elements in marine sediments have either a detrital source and/or a marine source (Calvert and Pedersen, 1993; Canet et al., 2004; Algeo and Maynard, 2004; Rimmer et al., 2004; Brumsack, 2006; Tribovillard et al., 2006; Piper and Calvert, 2009; Sanchez-Hernandez and Maurrasse, 2014). According to these studies, elements such as Al (mainly incorporated into detrital silicates), Zr and Ti (bound to the heavy mineral fraction), and K (although also present in seawater, it is a typical element of light silicates) represent mainly the influence of detrital input on the sedimentary geochemical signal. The marine fraction involves several trace elements that in seawater have a redox-sensitive behavior, the RSTEs. They participate actively in several geochemical reactions under different redox regimes, and thus, they may become authigenically enriched or depleted in sediments. Major and trace element concentrations are reported here as parts per million (ppm) and percentage (%) (Appendix B) and their variations are discussed in this section.

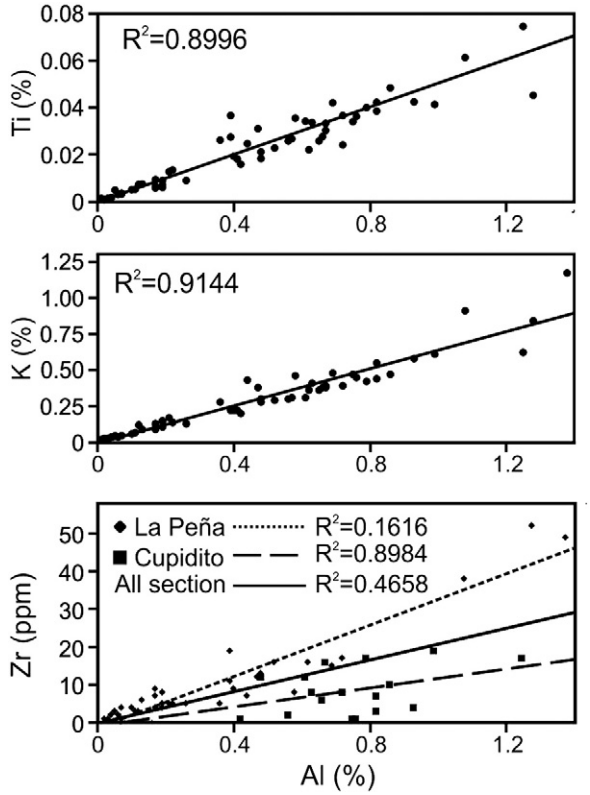

Fig. 4. Correlation of Ti, K and Zr with Al.

5.3.1. Detrital proxy elements

For the entire section studied herein, a high positive correlation of Al with Ti and with K was found ($R^2 = 0.89$ and 0.91, respectively) (Fig. 4). Al and Zr have a strong positive correlation for the Cupidito unit samples ($R^2 = 0.89$) but weak for the La Peña Formation samples ($R^2 = 0.16$) (Fig. 4). Raw trends of these elements are very similar (Fig. 5). All these elements exhibit synchronous and comparable increases in the lower part of the studied section at 1.7 m (values of up to 1.38% for Al, 49 ppm for Zr, 0.0873% for Ti and 1.17% for K); 5.8 m (values of up to 0.69% for Al, 15 ppm for Zr, 0.0421% for Ti and 0.48% for K); 12.2 m (values of up to 1.28% for Al, 52 ppm for Zr, 0.0454% for Ti and 0.84% for K); and from 19.5 to 27 m (values of up to 1.08% for Al, 38 ppm for Zr, 0.0614% for Ti and 0.91% for K), within the Cupidito unit. A uniform decrease can be observed from de middle part of the Cupidito unit at 27.0 m and it is followed by a stable phase of low values (down to 0.01% for Al, <1 ppm for Zr, 0.0006 for Ti and 0.02% for K) that lasts until the upper part of the unit, being interrupted by a punctual slight increase at 62.5 m (values of up to 0.22% for Al, 5 ppm for Zr, 0.0137% for Ti and 0.14% for K). Concentrations of these elements have a rising trend in the uppermost 3 m of the Cupidito unit and reach high values in the base of the La Peña Formation, from 73.1 to 80 m (values of up to 1.25% for Al, 19 ppm for Zr, 0.0747% for Ti and 0.62% for K).

5.3.2. Indices of chemical weathering

Two indices were calculated using major element concentrations to assess the degree of chemical weathering undergone by the source rock: the Chemical Index of Alteration (CIA; Nesbitt and Young, 1982); and the Chemical Index of Weathering (CIW′; Cullers, 2000; Chemical Proxy of Alteration-CPA of Buggle et al., 2011). Concentrations of elements involved in these indices are listed in Appendix B.

The CIA gives a quantitative measure of the removal of labile cations (e.g. Ca^{2+}, Na^{+}, K^{+}) relative to stable residual constituents (Al^{3+}, Ti^{4+}). Using molecular proportions, CIA is normally calculated as:

$$CIA = [Al_2O_3/(Al_2O_3 + CaO^* + Na_2O + K_2O)] \times 100$$

where CaO* represents only the calcium that is incorporated in silicate minerals. Therefore, if the measured CaO corresponds to bulk concentration, it is necessary to make a correction by subtracting Ca from carbonates and phosphates. Given that bulk-rock analyses do not show a significant fraction of detrital minerals containing calcium (except gypsum), we presumed that most of Ca is of marine origin (proxy for skeletal $CaCO_3$) and calculate this index excluding the CaO* from the equation.

Alternatively, and for comparison, we also calculate the CIW′ (Cullers, 2000; Buggle et al., 2011). The classical CIW was introduced by Harnois (1988) as a K-free index that account for feldspar weathering. This author considers that K shows no consistent behavior during weathering and eliminates it from the CIA calculation. The CIW′ used in this study is a modified version of the CIW for carbonate-rich sediments proposed by Cullers (2000). This index excludes Ca to

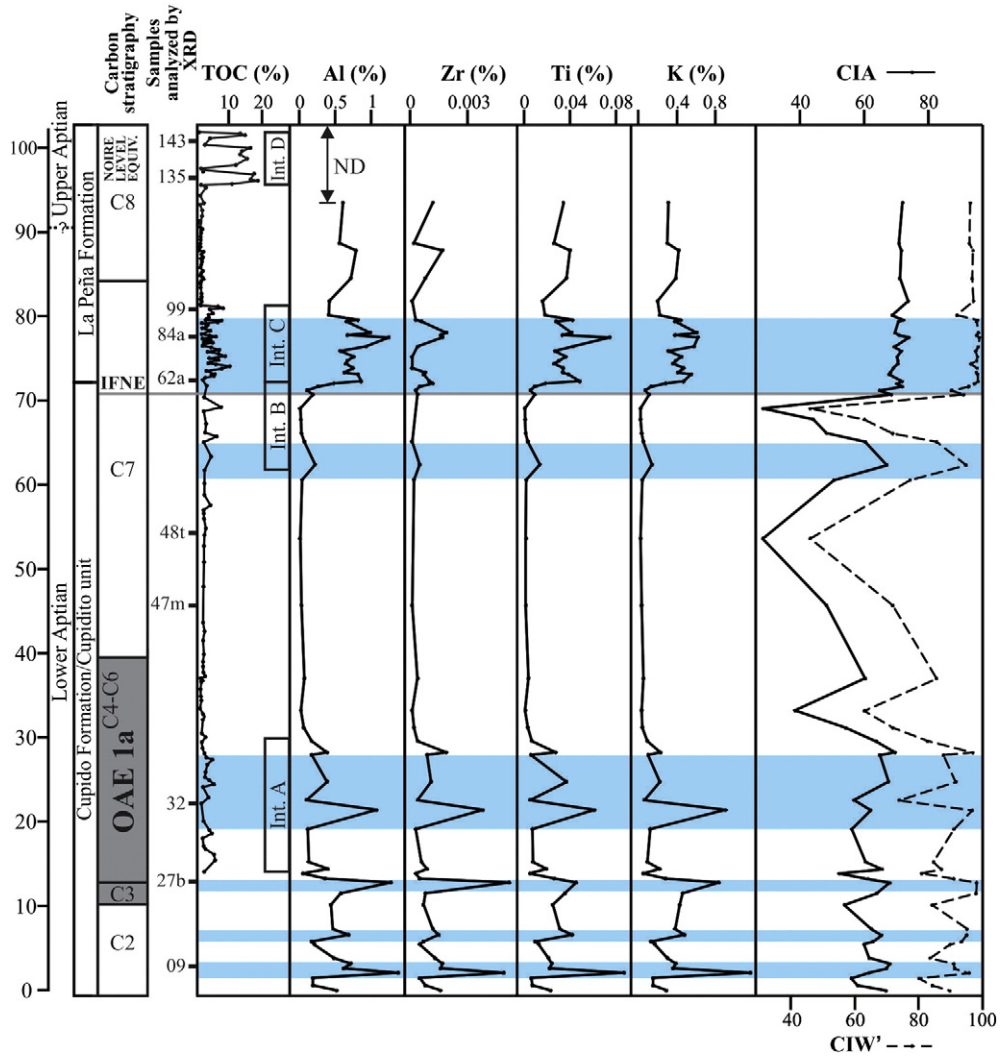

Fig. 5. Vertical variations in content of typically detrital elements (% in weight) compared with CIA and CIW′ profiles. Blue shaded intervals correspond to significant peaks in detritism associated with warmer/humid periods. Unshaded intervals correspond to low detritism associated with colder/drier periods. Age distribution, carbon stratigraphy, vertical variation in TOC and TOC-rich intervals are shown for reference. ND = No data available from this or other works.

overcome the CIW uncertainty related to the estimation of silicate Ca in calcareous sediments, which may lead to biased weathering profiles. Given the presence of dolomite and gypsum in some samples studied herein, this index may be more reliable for studying variations in chemical weathering in the FZD section. Using molecular proportions, CIW′ was calculated as:

$$CIW' = [Al_2O_3/(Al_2O_3 + Na_2O] \times 100.$$

For both CIA and CIW′ calculations, in those samples with Na below the detection limit (<0.01%) the number of moles of Na_2O was estimated using this maximum value. Fig. 5 shows the distribution of calculated indices of chemical weathering. The obtained values for the CIA and CIW′ indices differ significantly. CIA fluctuates between ~28 and 74 and averages ~62, whereas CIW′ fluctuates between ~46 and 99 and averages ~89. Because values of CIA and CIW′ may be overestimated because of elimination of CaO and K_2O in their calculation (Fedo et al., 1995), in the present work, weathering intensity is mainly interpreted from the vertical variations of these indices instead of their absolute values. Distinct peaks of CIA and CIW' in the lower and upper part of the studied interval of the Cupidito unit coincide with increases in detrital-source elements (Al, Zr, Ti and K). Highest and almost invariant values can be observed for the La Peña Formation.

5.3.3. Redox-sensitive trace elements (RSTEs)

In order to interpret the sources of trace elements (detrital vs. marine origin) in the FZD section, we calculated their correlation coefficient (R^2) with Al, which is an element entirely attributed to the detrital fraction. Normalization to Al (TE/Al ratio) was also perfomed. This normalization was not conducted in samples with low Al content (samples with very low detrital fraction; down to 1% according to XRD analysis), to avoid exaggerated and unrealistic RSTE/Al peaks (Brumsack, 2006).

From R^2 values (Table 2), it clearly appears that Fe is significantly correlated with Al ($R^2 = 0.80$), and V and U are moderately correlated with Al ($R^2 = 0.67$ and 0.60, respectively). Consequently, a significant amount of these elements may have a detrital origin and their fluctuations can be influenced by variation in the detrital influx.

The stratigraphic variation of Al-normalized RSTEs is illustrated in Fig. 6. Highly variable ratios regularly above the average shale are present in the Cupidito unit. Except for the Cr/Al and Mn/Al that show the highest peak within the lower 2 m (82.6×10^{-4} and 600.0×10^{-4}, respectively), trace elements display only minor to moderate increases in the lower 10 m of the section. In general, high concentrations occur between 10 and 25 m with values of 29.0×10^{-4} for U/Al, 86.1×10^{-4} for V/Al, 144.2×10^{-4} for Ni/Al, 7.0×10^{-4} for Co/Al, 16.2×10^{-4} for Cu/Al, 133.8×10^{-4} for Zn/Al, 32.8×10^{-4} for Mo/Al,

Table 2
Values of coefficient of correlation (R^2) between RSTEs and Al.

Trace element	R^2
U	0.6001
V	0.6701
Cr	0.4401
Ni	0.4155
Co	0.2959
Pb	0.4658
Cu	0.0049
Zn	0.2419
Mo	0.1219
Mn	0.3845
Fe	0.8023
P	0.4328

and 2.7 for Fe/Al. In the Cupidito unit, P/Al ratio presents relatively constant average shale-like values and only shows a minor peak of 0.06 at 23 m; and Pb/Al is commonly below the average shale value and display a peak of 5.4×10^{-4} at 13 m. The uppermost 1.5 m of the Cupidito unit contain the highest peaks of Co/Al (7.3×10^{-4}) and Cu/Al (24.5×10^{-4}), a significant peak of Mn/Al (490.9×10^{-4}), and minor to moderate peaks for the other elements.

Otherwise, the La Peña Formation displays a slight to moderate enrichment (above the average shale) in most of the RSTEs and less variable profiles with respect to those observed in the Cupidito unit. Major increases can be observed in the lower 8 m of the unit with values of 9.3×10^{-4} for U/Al, 76.2×10^{-4} for V/Al, 66.5×10^{-4} for Cr/Al, 2.6×10^{-4} for Pb/Al, 16.0×10^{-4} for Cu, 90.0×10^{-4} for Zn/Al. Ni/Al, Mo/Al and Fe/Al present low, rather constant values through the La Peña Formation. Co/Al, Pb/Al and Mn/Al are regularly below the average shale.

5.4. Pyrite framboid size distribution

Different investigations have proved that the size distribution of pyrite framboids is a successful proxy for interpreting the paleoredox conditions at the time of pyrite formation (Wilkin et al., 1996, 1997; Wignall and Newton, 1998; Bond and Wignall, 2010; Rajabi et al., 2014).

In the studied thin sections of the La Peña Formation, pyrite framboids occur randomly distributed and, occasionally, they form mm-thick lenses. They rarely as clusters (Fig. 7). The statistic parameters of pyrite framboid size distribution are presented in Table 3 and illustrated in Fig. 7. Framboids range in size from 2.2 μm to 26.3 μm. Meanwhile in beds 63, 77, 134 and 142 they are usually smaller than 6.0–8.0 μm in diameter, framboids with diameters larger than 10–15 μm are more common in beds 65 and 73.

6. Discussion

6.1. Analysis and correlation of the $\delta^{13}C$ curve

Vertical fluctuations in $\delta^{13}C$ of sedimentary successions encode important information about paleoenvironmental changes associated with global perturbations in the global carbon pool, and can be used as a high resolution tool for precise correlations between different

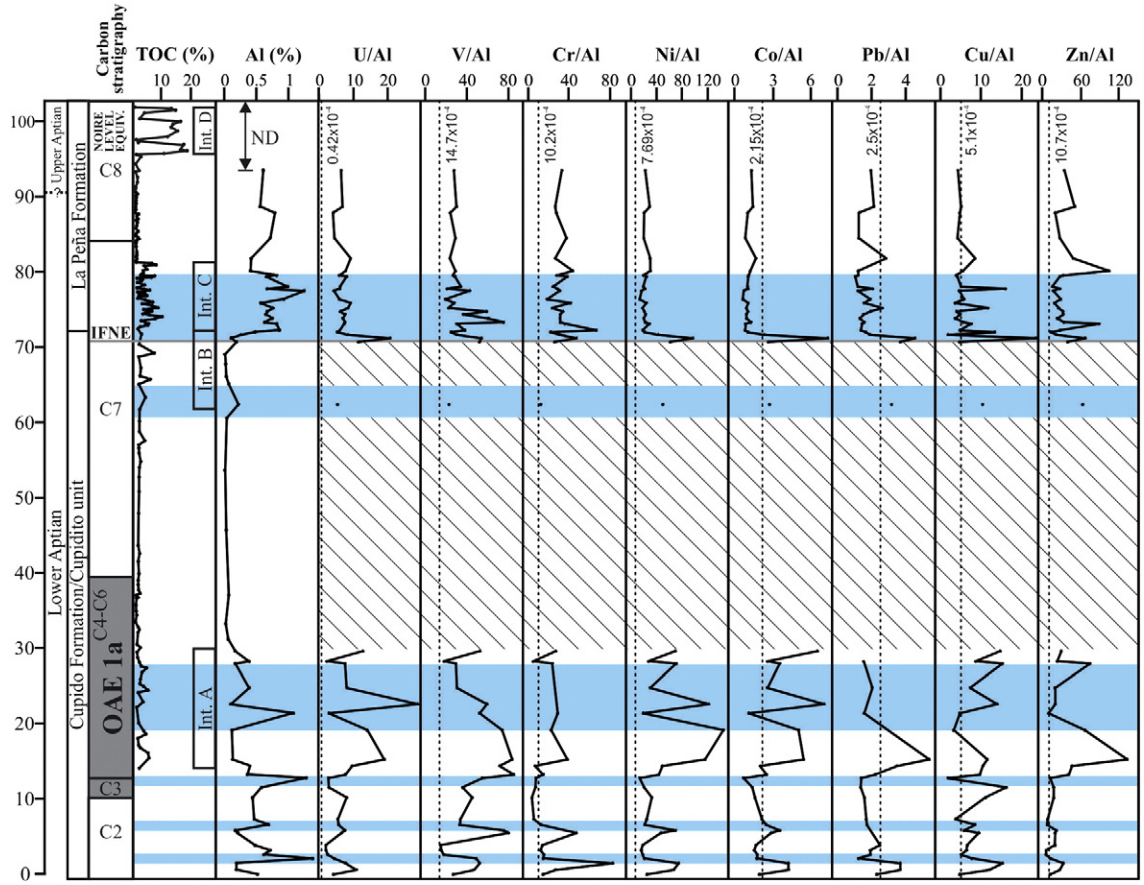

Fig. 6. Vertical variations in RSTEs. Al-normalized concentrations of RSTEs throughout the studied section. Except Fe/Al and P/Al ratios, all represent values $\times 10^{-4}$. The hatched area represents unnormalized values due to very low Al content. Dashed lines represent the Al-normalized concentrations of each corresponding element in the average shale from Wedepohl (1991) and Brumsack (2006). Age distribution, carbon stratigraphy, vertical variation in TOC and Al, and TOC-rich and detritism intervals are shown for reference. ND = No data available from this or other works.

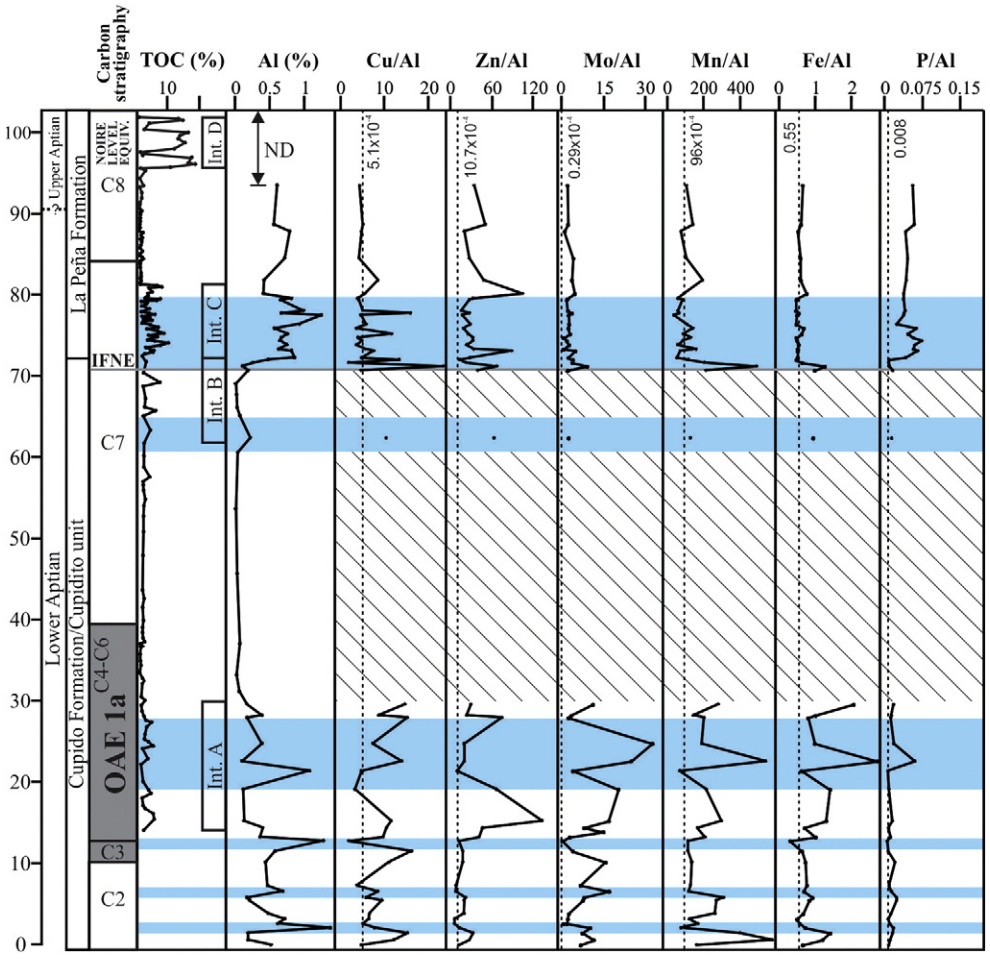

Fig. 6 (*continued*).

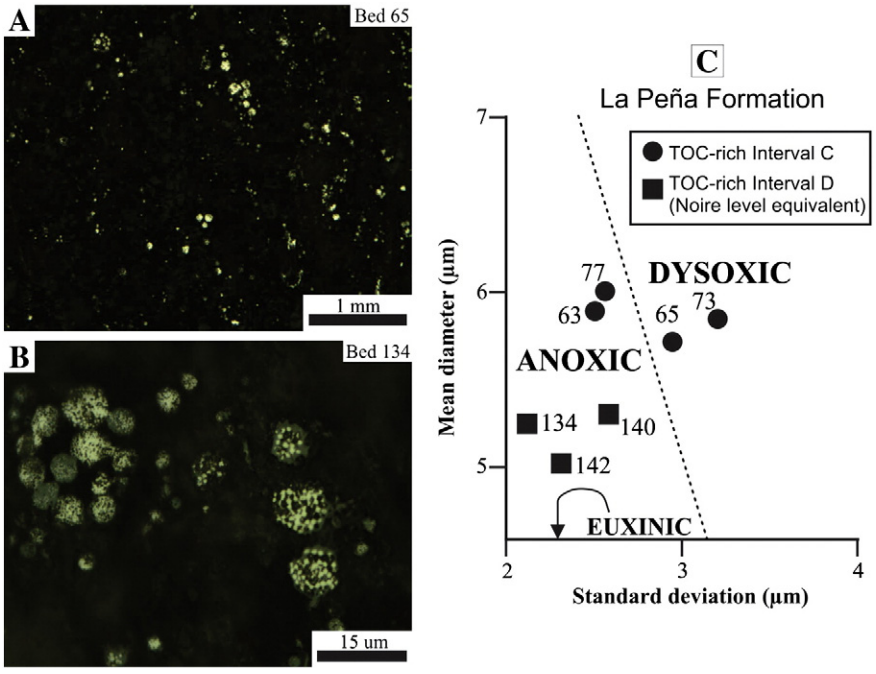

Fig. 7. Pyrite framboids in the La Peña Formation. A and B — microphotographs taken under reflected light that show microscopic features of the pyrite framboids; C — Mean versus standard deviation plot of pyrite framboid size. The boundary between zones for euxinic, anoxic and dysoxic environments is that seen in modern depositional settings (Wilkin et al., 1996).

Table 3
Pyrite framboid size statistic parameters.

Bed	Distance base (m)	N[a]	Mean[b] (μm)	S.D.[c]	Min F.D.[d] (μm)	Max F.D.[e] (μm)
142	100.2	165	5	2.3	2.4	9.2
140	98.8	150	5.3	2.6	1.9	10.1
134	96.0	350	5.2	2.1	2.2	10.6
77	76.2	268	6	2.5	2.7	15.5
73	75.9	150	5.9	3.2	5	14.3
65	73.7	165	5.7	2.9	3.2	18.8
63	72.8	328	5.8	2.5	2.8	15.2

[a] Number of measured framboids.
[b] Mean framboid diameter.
[c] Standard deviation of framboid diameter.
[d] Minimum framboid diameter in sample.
[e] Maximum framboid diameter in sample.

stratigraphic sections (Erba et al., 1999; García-Mondéjar et al., 2009; Millán et al., 2009; Moreno-Bedmar et al., 2009, 2012b; Najarro et al., 2011; Elkhazri et al., 2013; Núñez-Useche et al., 2014). However, it is known that besides post-depositional diagenetic alteration, regional/local paleoceanographic conditions, mainly in carbonate platforms systems, may cause the carbon-isotope signal to deviate from the open ocean global signal (Immenhauser et al., 2008; Di Lucia et al., 2012). Therefore, before attempting a correlation with other Barremian-Aptian curves, we tried to assess the reliability of the $\delta^{13}C$ record of the studied section.

6.1.1. Reliability of the $\delta^{13}C$ record

In the FZD section there is a low covariance between $\delta^{13}C$ and $\delta^{18}O$ (Appendix A) ($R^2 = 0.017$ for the entire section; $R^2 = 0.034$ for the Cupidito unit; and $R^2 = 0.0005$ for the La Peña Formation). The $\delta^{13}C$ mean values for the FZD section fall within the range of Barremian–Aptian seawater (~0.5–5‰) determined by Prokoph et al. (2008) from low latitude biotic calcite. Moreover, there are not particular C-isotope trends associated with a specific type of facies (Fig. 3). For instance, the two negative excursions in the carbon-isotope record of the Cupidito unit (between 9.4–11.7 m and 70.7–71 m) fall in the middle of the microfacies association I (peritidal and subtidal facies) and the upper part of microfacies association IV (fore-reef facies), respectively. None of these narrow stratigraphic intervals relate to an emersion phase or to an interval rich in ooids or crinoids which may shift the carbon-isotope record to lower values (Föllmi et al., 2006). In fact, the stratigraphic intervals related to this type of facies (microfacies associations II and III) do not show any significant decrease in $\delta^{13}C$ values. The positive carbon-isotope excursion between 11.7 and 39.9 m is defined by many data points and extends across different types of facies (mostly microfacies associations I and II). Likewise, despite the drastic shift of facies from the Cupidito unit to the La Peña Formation, the general carbon-isotope trend across this lithological boundary shows little variation. Summing up, this suggests that variations in $\delta^{13}C$ are not significantly biased by diagenesis and cannot be related solely to facies changes.

6.1.2. Identification of isotopic segments of Menegatti et al. (1998)

According to the foregoing discussion, the carbon-isotope record of the FZD section can be considered as a pristine marine signal. It closely correlates with the long-term global segments C2 to C8 of Menegatti et al. (1998).

The conspicuous negative excursion in the carbon-isotope record of the lower part of the studied section (beds 25–27), with a value of 2.86‰, can be assignable to segment C3. Together, the following two points support this correlation.

1- The two levels with *Palorbitolina lenticularis* reported by Araujo and Martínez (1981) (see Section 3) occur at ~40 and ~80 m below the onset of the negative peak. The present study confirms the occurrence of this benthic foraminifer 40 m below the segment C3. It is included in a 2.3 m thick bed of wackestone/floatstone with abundant miliolids, orbitolinids, and worm tubes. Since the first occurrence of *Palorbitolina lenticularis* occurs in the late Barremian (Ogg and Ogg, 2006), the negative excursion in the FZD section is therefore included in the latest Barremian–early Aptian interval.
2- Besides the early Aptian negative carbon-isotope excursion (segment C3), another negative spike is associated with the Barremian-Aptian boundary in many localities (Moullade et al., 1998, 2000; Erba et al., 1999; Godet et al., 2006). However, the amplitude of this negative excursion varies considerably from one section to another. In the Cassis-La Bédoule section SE France the amplitude of the shift is ~2‰ (Moullade et al., 1998, 2000; Renard et al., 2005), which is higher than for the basinal Tethyan sections (0.4‰ at Cismon outcrop NE Italy, Menegatti et al., 1998; 0.22‰ at Gorgo a Cerbara section Central Italy, Stein et al., 2011; and 0.2‰ at Angles outcrop SE France, Godet et al., 2006). However, it is lower than for the shallow-water outcrop of Lopper (4‰; Stein et al., 2012). In deep-water sediments of northern Mexico (Scholle and Arhur, 1980) and shallow-water sediments of the coeval Sligo platform in Texas (Phelps et al., 2015), the Barremian–Aptian negative excursion is not over 1‰. Thus, it is not a prominent regional carbon-isotope signal. In both cases, segment C3 (with a value of about 2 and 3‰, respectively) is the only negative excursion comparable in scale to that reported in this study.

Building upon previous correlation, the underlying trend should correspond to segment C2. Following the $\delta^{13}C$ negative excursion, the return to ^{13}C enriched values (positive excursion of 3.25‰) can be traced until bed 45. This interval can be correlated with undifferentiated C4–C6 segments. It is not possible to recognize each segment independently. The slow increase of the $\delta^{13}C$ values that begins at bed 45 and finishes at bed 108 is analogous to segment C7. The uppermost part of the segment within the Cupidito unit is stratigraphically coeval with the lower-middle part of the late early Aptian *D. furcata* Zone, as previously discussed in Section 3. The upper part of this segment lies within the La Peña Formation and contains the highest values of $\delta^{13}C$ (from +4.19 to +4.35‰). According to the ammonite zonation of Moreno-Bedmar et al. (2013) (Fig. 3A), this part of segment C7 can be dated as latest early Aptian (upper part of the *D. furcata* Zone). Following the segment C7 there is a negative trend that can be correlated with segment C8. Based on the investigation of Moreno-Bedmar et al. (2013) (Fig. 3A), it can be dated as latest early-early late Aptian (*D. furcata*–*E. martini* transition).

6.1.3. Correlation of the $\delta^{13}C$ curve with other sections

The here proposed correlation of the carbon-isotope record of the FZD section with those published by Menegatti et al. (1998) allows chemostratigraphic correlations with other sections, and discussion about four significant global/regional events as follows from oldest to youngest (Fig. 8):

1- Constrained by the time-equivalent segments C3 to C6 of Menegatti et al. (1998) (Fig. 7), OAE 1a is located in the lagoonal facies of the Cupidito unit and has a thickness of about 30.6 m. Taking into account that this event has an estimated duration of 1.0–1.3 My (Li et al., 2008), the average sedimentation rate for the Cupidito facies lies between 2.3 and 3.0 cm/ky, which is well within the lower range of sedimentation rates reported by Enos (1991) for lagoonal settings.
2- In the uppermost part of the Cupidito unit, bed 59 yields a clear negative excursion followed by a rapid positive excursion. This negative peak of 0.7‰ is located in the middle part of segment C7 and, as discussed before, included in the coeval lapse of the *D. furcata* Zone. It can be correlated with the Intra-Furcata Negative Excursion (IFNE) (0.7–1.2‰) defined by Núñez-Useche et al. (2014) from the Prebetic domain in Spain (Fig. 8F), which is equivalent to the isotope

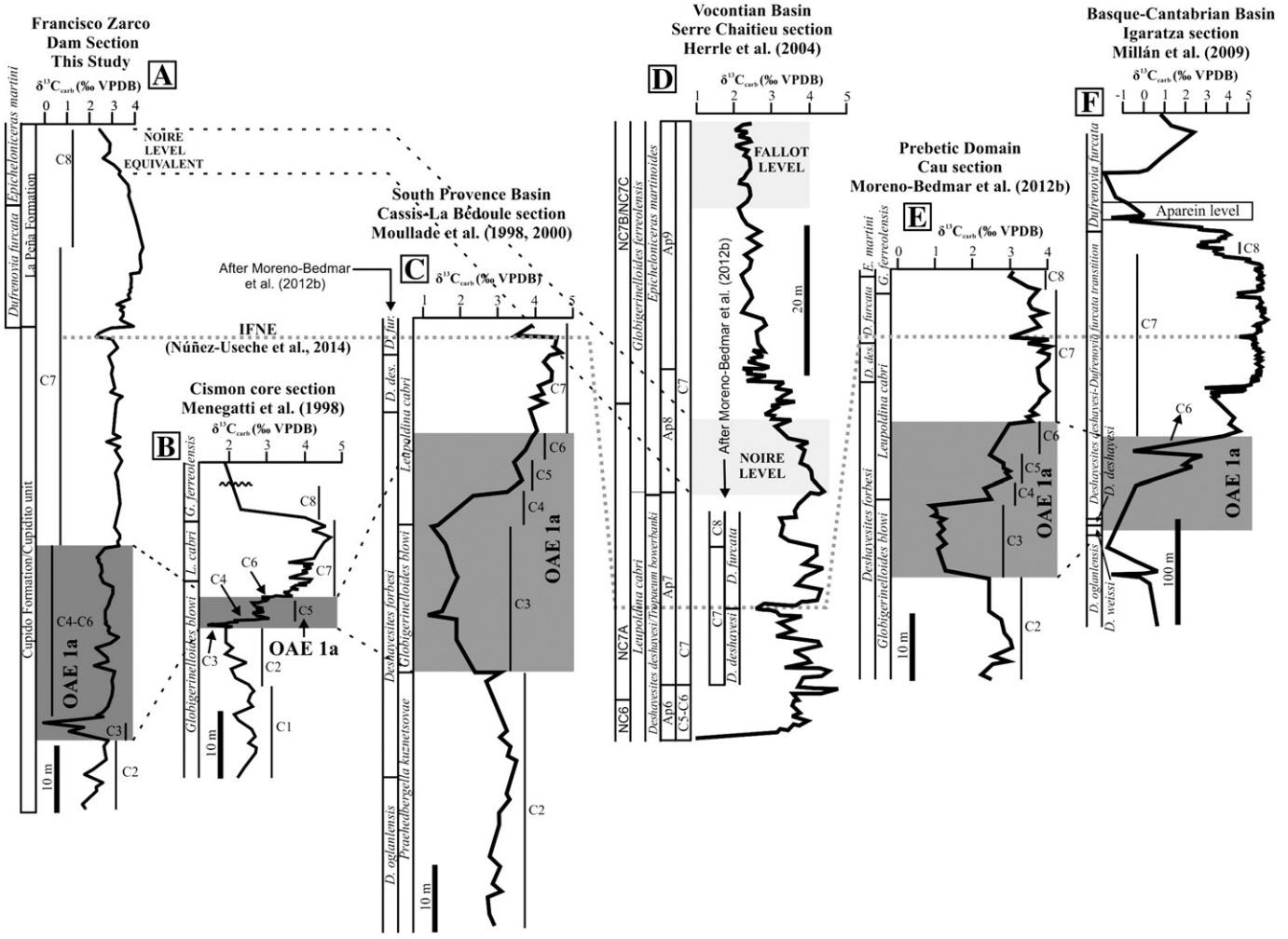

Fig. 8. Correlation of stable carbon-isotope curves of different stratigraphic sections. A — Francisco Zarco Dam section (this study); B — Cismon core (Menegatti et al., 1998); C — Cassis-La Bédoule (Moullade et al., 1998; Moreno-Bedmar et al., 2012b); D — Serre Chaitieu (Vocontian Basin; Herrle et al., 2004; Moreno-Bedmar et al., 2012b); E — Cau (Moreno-Bedmar et al., 2012b); F — Igaratza (Millán et al., 2009). C1 to C8 refer to the stable carbon-isotope segments defined by Menegatti et al. (1998). Dashed lines correlate the OAE 1a, IFNE and Noire level.

drop (1.2‰) reported within segment C7 in the $\delta^{13}C$ curve from the Cassis-La Bédoule section of Moullade et al. (1998) (Fig. 8C), the subunit Ap7b of the Vocontian Basin, France (Herrle et al., 2004) (both included in the *D. furcata* Zone by Moreno-Bedmar et al., 2012b) (Fig. 8D), and the negative shift of about 1‰ described in the middle part of segment C7 at the Basque–Cantabrian Basin (Millán et al., 2009) (Fig. 8E). The record of a new possible IFNE strengthens the potential of this carbon-isotope drop as a new chemostratigtaphic marker for the lower Aptian.

3- The base of the La Peña Formation is an organic-carbon rich interval (TOC-rich interval C) in the upper part of the *D. furcata* Zone. TOC reaches values of up to 8.72% in the FZD section (Barragan, 2001) (Fig. 3B), and up to 3.2% in the La Huasteca section (Barragán and Maurrasse, 2008). Otherwise, the lower part of the Lareo Formation from the Basque–Cantabrian Basin is a TOC-enriched (values of up to 2.11%) interval which also dates from the *D. furcata* Zone and is known as the Aparein level (García-Mondéjar et al., 2009; Millán et al., 2009) (Fig. 8E). It is equivalent to an organic-carbon rich level reported in Italy (Cobianchi et al., 1997; Luciani et al., 2006). Both the Mexican and the Spanish intervals have been correlated in light of their similar biostratigraphic position (Millán et al., 2009; Skelton and Gili, 2012; Moreno-Bedmar et al., 2012a); however, this study shows that apparently they do not fit chemostratigraphically. Whereas the base of the La Peña Formation is time-equivalent with the transition of the segments C7 to C8, the Aparein level postdates a pronounced negative $\delta^{13}C_{carb}$ spike (with amplitude of 4–5‰) overlying the segment C8 (Fig. 8E). Such a discrepancy can be explained by considering the lack of a worldwide well-established C-isotope profile in the *D. furcata* ammonite Zone. Further studies are needed to check whether these intervals are correlatable or they link to different events associated with a major phase of oxygen-poor or anoxic conditions recognized on a global scale during the late early Aptian (Föllmi, 2012).

4- The uppermost 6 m of the section correspond to the TOC-rich interval D (TOC values of up to 18%) within the base of the early late Aptian *E. martini* Zone (Moreno-Bedmar et al., 2013) (Fig. 3). This interval is probably time-equivalent to the Noire level black-shale horizon defined in the Vocontian Basin (Bréhéret, 1997; Herrle et al., 2004), which is also included in the lower part of the *Epicheloniceras martinoides* ammonite Zone (Herrle et al., 2004) (Fig. 8D). Both intervals coincide with a negative carbon-isotope trend (Herrle et al., 2004; Föllmi, 2012) (Fig. 8D).

6.2. Weathering, detrital input and climate

The variation in the detrital influx is reconstructed from the profiles of Al, Zr, Ti and K (Fig. 5). Increases in the detrital influx occurred episodically before and during the lower part of the OAE 1a interval (segment C3) and the TOC-rich interval A. From this interval onward, a decrease took place and persisted until the uppermost part of the

Cupidito unit. It is followed by a slight to moderate punctual increase. Toward the end of the deposition of the Cupidito unit (close to the interval in which the IFNE occurred and partially coincident with the TOC-rich interval B) continental influence raised and detrital input remained high. This trend persisted during sedimentation of the TOC-rich interval C in the lower part of the La Peña Formation. Thereafter, detrital input decreased and varied erratically, rising and falling irregularly. The most significant peaks in detritism correspond to the blue shaded intervals in Fig. 5.

The above described changes in detrital influx are irregular and do not fit with a steady and long-term sea-level rise, as is recorded in the lower Aptian succession of northern Mexico (Goldhammer et al., 1991; Goldhammer, 1999; Lehmann et al., 1999, 2000), including those exposed in the FZD section (Barragan, 2001; Núñez-Useche and Barragán, 2012). Periods of sea-level rise normally result in the decrease of the input of detrital material to marine environments, since the depocenter shift landward. According to Weissert (1990) and Wortmann et al. (2004), the increase in detrital influx on the shallow-marine Tethyan and Atlantic shelves during the Aptian was triggered predominantly by climate. A warm and/or humid climate link to intensified greenhouse conditions accelerated water cycling and chemical continental weathering of parent rocks. It was accompanied by the input of fine clay particles into sediments. In this study, the calculated indices (CIA and CIW′) are used to infer weathering profiles and pinpoint climate fluctuations (Nesbitt and Young, 1982; Fedo et al., 1995, 1997; Cullers, 2000) (Fig. 5). CIA and CIW′ increases mostly coincides with peaks in detritism (blue shaded intervals), which indicates that a relative intensification in both weathering in the source area and detrital output took place during deposition of these intervals. They represent periods with warmer/more humid prevailing conditions. Conversely, intervals with lower detritism and low CIA and CIW′ values denote a decrease in the intensity of chemical weathering (unshaded intervals in Fig. 5). They represent periods with colder/drier climatic conditions that substantially reduced the chemical continental weathering and runoff of fine particles. According to the above analysis, detrital influx in the FZD section was indeed climate controlled. A link between TOC concentrations and climate controlled detrital influxes is obvious, as the TOC-rich intervals A and C (and B in a minor extent) coincide with peaks in detritism.

The interpretation proposed here is in agreement with two characteristic global warming trends that occurred during (a) the late Barremian–early Aptian (Larson, 1991; Jenkyns, 2003; Weissert and Erba, 2004; Zakharov et al., 2013; Bottini et al., 2014) linked with methane release from gas hydrate melting (Jahren et al., 2001; Jenkyns, 2003) and intensive volcanic activity eventually related to the Ontong-Java plateau (Tejada et al., 2009; Keller et al., 2011); and (b) the late early Aptian *D. furcata* Zone (García-Mondéjar et al., 2009; Zakharov et al., 2013), both almost coinciding with the time of occurrence of the warmer/humid periods defined in the FZD section. Likewise, colder/drier periods (unshaded intervals in Fig. 5) could be triggered by global cooling episodes in the early Aptian (during and after the onset of the OAE 1a), attributed to a drawdown of carbon dioxide due to enhanced marine organic-carbon burial and continental weathering (Menegatti et al., 1998; Erba et al., 2010; Jenkyns, 2010; Jenkyns et al., 2012).

6.3. Evaluating paleo-redox conditions

Several studies of RSTEs in marine sediments demonstrated their use to distinguish oxygen levels. Sediments deposited under oxygen-depleted marine environments have higher concentrations of certain RSTEs (Huerta-Diaz and Morse, 1992; Algeo and Maynard, 2004; Brumsack, 2006; Sanchez-Hernandez and Maurrasse, 2014). Such conditions favor that trace elements associate mainly with the organic matter fraction and/or authigenic Fe-sulfides or precipitate directly from the water column as mineral phases including discrete sulfide particles. Conversely, under reduced bottom-water conditions Mn diffuses and oxidizes and reprecipitates as Mn oxides or $MnCO_3$ when find oxic conditions either in the water column or in the pore water (Calvert and Pedersen, 1993; Algeo and Maynard, 2004; Tribovillard et al., 2006). Since RSTEs are prone to secondary mobilization, especially under variable bottom-water redox conditions (Algeo and Maynard, 2004; Rimmer et al., 2004; Tribovillard et al., 2006), they must be carefully interpreted.

In the FZD section, the RSTEs enrichment is higher and more variable in the Cupidito unit than in the La Peña Formation (Fig. 6). Since different mechanisms account for this distribution, we discuss separately each stratigraphic unit.

6.3.1. Redox conditions during deposition of the Cupidito unit

In the Cupidito unit most of RSTEs show similar profiles (Fig. 6). Minor peaks recorded in the segment C2 and build up more strongly within the segment C3–TOC-rich interval. A similar behavior is observed even for the Pb/Al (regularly below the average shale) and Mo/Al (frequently above the average shale) ratios. At first glance, the RSTEs pattern indicates deposition under low oxygen bottom-waters conditions, episodic during segment C2 and progressively more permanent upward. This scenario fits with high concentrations of organic matter in the TOC-rich interval A. It also agrees with documented episodic anoxic–dysoxic conditions during earliest Aptian which become more severe toward the OAE 1a in the Tethys Basin (Föllmi, 2012; Föllmi et al., 2012; Stein et al., 2011; Sanchez-Hernandez and Maurrasse, 2014). However, the occurrence of a high and constant benthic foraminiferal abundance and punctuated bioturbated levels within the same intervals (Fig. 3) indicate that oxygen-depleted conditions inferred from geochemical proxies was not permanent. Contrasting results for the same intervals may therefore hint to markedly variable bottom-water redox conditions.

Weakly reducing conditions at the seafloor are also suggested by the enrichment in Mn. The positive correlation between Mn/Al and Ca/Al for the Cupidito unit samples ($R^2 = 0.6$) indicates fixation of dissolved Mn as mixed Mn–Ca-carbonates under oxygen-depleted conditions where Mn was enriched in pore water (Brumsack, 2006). Otherwise, the coincidence of peaks of Mn/Al with peaks of U/Al, V/Al, Ni/Al, Co/Al, Cu/Al and Zn/Al (Fig. 6) implies that the oxic–anoxic interface must have resided within the sediments or at most at the sediment–water interface. This interface could not have risen durably into the water column, because no such Mn enrichment could have been recorded. Hence, reducing conditions prevailed within the sediments whereas more oxic–dysoxic conditions favorable for benthic life dominated the sediment–water interface.

It is widely accepted that during the OAE 1a interval several organic-rich deposits with higher concentrations of certain RSTEs were deposited in pelagic and hemipelagic marine environments under oxygen-poor or anoxic conditions almost on a global scale (Heldt et al., 2008; Huck et al., 2010; Millán et al., 2009; Najarro et al., 2011; Stein et al., 2012; Sanchez-Hernandez and Maurrasse, 2014). In contrast, organic-rich levels are often scarce or absent in shallow-water carbonate sediments across the OAE 1a interval. Although many Tethyan carbonate platforms were drowned before OAE 1a, redox conditions in those which underwent uninterrupted carbonate production during this event seem to have been more influenced by regional/local paleoceanographic conditions (Immenhauser et al., 2005; Föllmi et al., 2006; Huck et al., 2010; Di Lucia et al., 2012). In a similar fashion, the subtle balance between reducing conditions in the sediments and favorable oxygen conditions for benthic life in the Cupidito lagoon might reflect the interaction of local factors occurring in shallow-water environments such as:

1- Strong to moderate degree of surface-water–atmospheric O_2 mixing: This process prevents the development of permanent oxygen-depleted conditions at the seafloor. However, it may

be affected by increased continental runoff and freshwater influx creating a low-salinity surface which diminish the interchange.

2- Seasonal productivity: In addition to control the benthic foraminiferal abundance, the organic-matter flux also influence the oxygen content in bottom water masses. The burial of organic matter can lead to organic-carbon rich sediments in oxygen-containing conditions; however, beyond a certain quantity, it results in oxygen consumption at the seafloor (Calvert and Pederson, 1993; Jorissen et al., 1995; Friedrich et al., 2010).

3- Wastermass restriction: The degree of restriction, especially in shallow regions of the ocean, determines the mixing rate with more open ocean water masses and the rate of oxygen renewal to bottom waters. In turn, oxygen replenishment regulates organic-matter oxidation (Wilkin et al., 1996; Algeo and Rowe, 2012).

It is noteworthy that Al-normalized RSTEs concentrations associate with a moderate TOC enrichment in the Cupidito unit. The heights of the peaks in RSTEs contents observed in Fig. 6 for this part of the section seem exaggerated considering the proposed weak reducing bottom conditions. They are even too large compared with the peaks measured in the TOC-rich interval C, which, as is discussed below, deposited under more uniform oxygen-depleted conditions. Hence, these concentrations are difficult to explain by considering only local redox conditions in the Cupidito lagoon.

We hypothesize that besides local conditions, the RSTEs distribution in the Cupidito unit probably also reflects a major global availability of trace metals in seawater associated with magmatic degassing and hydrothermal activity produced during the formation of the Ontong-Java plateau during the late Barremian–early Aptian (Duncan et al., 2007; Tejada et al., 2009; Keller et al., 2011). Although some links between the emplacement of this plateau and trace metal anomalies in coeval marine sediments have been suggested in some studies (Sinton and Duncan, 1997; Larson and Erba, 1999; Leckie et al., 2002; Walczak, 2006; Duncan et al., 2007; Tejada et al., 2009), this relationship is quite recently strengthened by Erba et al. (2015). According to these authors, local redox conditions exerted a secondary effect on abundance anomalies of trace elements, which were mainly controlled by the volcanism related to the greater Ontong-Java event (including the emplacement of the Ontong-Java, Manihiki, and Hikurangi Plateaus) with a paroxysmal phase coincident with OAE 1a. Further work is necessary to determine the influence of this event in the trace element abundance peaks observed in OAE1a time-equivalent facies of the Cupidito unit.

6.3.2. Redox conditions during deposition of the La Peña Formation

In the case of the La Peña Formation, the TOC-rich interval C features (disappearance of benthic foraminifera and domination of planktonic foraminifera, fine lamination, and presence of disseminated pyrite) (Fig. 3 and 7) clearly reflect deposition under reduced bottom-water conditions. Barragan (2001) related this redox regime to the invasion of dysoxic/anoxic waters onto the Cupido platform, likely as consequence of the global expansion of the oxygen minimum zone and high sea-level during the Aptian. Indeed, this interval displays an enrichment in RSTEs that suggests depletion in O_2 content during its deposition. The minor variability that these elements record with respect to that shown in the Cupidito unit also suggests that redox conditions were less fluctuating. This matches with the low Mn/Al values (frequently below the average shale; especially at the TOC-rich interval C), reflecting long-term oxygen-depleted conditions that favored Mn diffusion out of the sediments.

Consistent with Mn/Al, Co/Al is also depleted in the La Peña Formation. This occurs in sediments deposited underneath zones of high marine productivity of the Gulf of California (Brumsack, 1989) or the Peruvian margin (Böning et al., 2004), where Mn-and Fe-oxyhydroxides enriched in Co are transported away under oxygen-depleted conditions. In the present case, Co likely mobilized from particles which settled through a poorly-oxygenated water column before reaching the sediment. The existence of anoxic instead of euxinic conditions may also account for the above mentioned Co depletion. This element may be enriched in sediments deposited under euxinic conditions given that it forms stable sulfides only when H_2S is present; however, it may have a limited incorporation into authigenic sulfides under anoxic conditions (Luther, 1991; Huerta-Diaz and Morse, 1992; Algeo and Maynard, 2004). A similar process may be invoked in order to explain the low values of Pb/Al.

Information concerning O_2 levels from the La Peña Formation is also deduced from the size distribution of pyrite framboids. Sediments deposited underneath oxic/dysoxic waters have higher mean framboid diameter than those deposited from euxinic environments in which the framboids formed in the water column and do not have enough time to grow before they sink below the iron reduction zone (Wilkin et al., 1996, 1997; Suits and Wilkin, 1998; Wignall and Newton, 1998; Bond and Wignall, 2010). According to this proxy, bottom waters were poorly-oxygenated during deposition of the TOC-rich intervals C and D. In the mean vs. standard deviation plot of pyrite framboid size data, samples of the TOC-rich interval C plot in the anoxic and dysoxic zones (as is suggested by the RSTEs enrichment) and samples of the TOC-rich interval D plot in the anoxic zone (Fig. 7C). These latter contain a population characterized by minimal and not very variable sizes, which suggests that deposition of these sediments occurred underneath a stronger anoxic regime, as proposed by Barragan (2001).

6.4. Detrital and nutrient input, marine productivity and redox conditions

TOC-rich intervals A and C (and B in a minor extent) coincide partially with climate controlled increases in detrital influx, thus indicating a direct relationship between detrital influx and organic-matter burial (Fig. 6). Whilst continental runoff may have supplied terrestrial organic matter, it also could enhance nutrient delivery to the basin, stimulating marine productivity and thus causing direct marine organic-carbon sequestration and depleted O_2 concentration at the seafloor. This mechanism has been proposed as responsible of enhanced burial of several black shales during the Cretaceous (Erba, 1994; Larson and Erba, 1999; Leckie et al., 2002; Jenkyns, 2010; Sanchez-Hernandez and Maurrasse, 2014), and can be also applied to explain the formation of Pliocene Mediterranean sapropels (Wehausen and Brumsack, 1998; Meyers, 2006). In the FZD section, this scenario is in agreement with the positive correlation of Fe and P with Al.

Iron and phosphorus are important biolimiting elements in the ocean. Delivery of both elements to surface waters stimulates widespread marine productivity (Larson and Erba, 1999; Leckie et al., 2002; Brumsack, 2006; Bodin et al., 2007; Stein et al., 2012; Sanchez-Hernandez and Maurrasse, 2014). The fluxes of these elements into the seawater/sediment system are mainly controlled by continental runoff.

Iron concentration in the FZD sediments is frequently above the average shale in the Cupidito unit (raw concentration ranges from 0.08 to 1.03%, average 0.26%; Appendix B) and close to that in the La Peña Formation (raw concentration ranges from 0.26 to 0.65%, average 0.41%; Appendix B) (Fig. 6). Fe concentrations in this height in a calcareous dominated setting like the represented by the FZD section should have been sufficient to support enhanced marine productivity. Positive correlation of this element with Al (Table 2) supports that it was supplied by detrital fluxes.

For the lower part of the Cupidito unit, P shows concentration close to that of average shale (raw P concentration ranges from 0.001 to 0.024%, average 0.004%; Appendix B). Moderate correlation of P with Al ($R^2 = 0.6$) and Fe ($R^2 = 0.76$; Fe/Al and P/Al profiles have roughly consistent trends in Fig. 6) suggest that P was delivered mainly by detrital input. In this case, P must have been carried to the sediments mainly adsorbed onto particulate inorganic phosphorus or detrital iron-oxyhydroxides derived from weathering (Jarvis et al., 1994; Piper and Perkins, 2004). Because the deposition of this interval of the Cupidito

unit coincides with pronounced oceanic magmatic episodes of the Greater Ontong-Java event, marine productivity in the Cupidito ramp might also have been stimulated by the associated introduction of Fe and other biolimiting metals into the ocean (Sinton and Duncan, 1997; Larson and Erba, 1999; Leckie et al., 2002; Tejada et al., 2009; Erba et al., 2015).

For the La Peña Formation, P is consistently enriched with respect to average shale (raw P concentration ranges from 0.018 to 0.077%, average 0.037%; Appendix B) and lacks a positive correlation with Al ($R^2 = 0.25$). Furthermore, P/Al is decoupled of Fe/Al and shows covariation with TOC in the TOC-rich interval C (Fig. 6). These P relationships indicate that a considerable portion of the total P is probably present as organic P (its presence as an authigenic phase was not detected neither by petrographic nor XRD analyses), and its enrichment at TOC-rich interval C can be interpreted as the result of high nutrient levels in seawater (Bodin et al., 2007; Stein et al., 2012). Under oxygen-depleted bottom waters, P from the uppermost sediments is prone to be remobilized and returned to the water column to sustain marine productivity (Böning et al., 2004; Bodin et al., 2006; Stein et al., 2011; Tribovillard et al., 2006). Given that dysoxic–anoxic bottom waters are inferred for TOC-rich interval C but high P values persist in sediments, P recycling processes must have been limited by some mechanism such as water column stratification. Another possibility is that P may have been transferred into an authigenic phase rather than transferred back into the bottom waters. Although in the FZD section P is not present as an authigenic phase, Lehmann et al. (1999) reported phosphorite clasts in the shale beds of this unit in coeval stratigraphic sections.

In summary, our results indicate that delivery of Fe and P by continental runoff was a local factor that triggered eutrophication of the surface waters, stimulating marine productivity and triggering organic-matter burial. The fluxes of these elements increased due to warm/humid conditions that intensified chemical continental weathering and detrital and nutrient input. Likewise, positive excursions in $\delta^{13}C$ occurring in the TOC-rich intervals A and C are in agreement with enhanced ^{12}C removal due to marine productivity. Spatial variations in $\delta^{13}C$ and TOC are also consistent with changes observed in the trace metal data, thus indicating that marine productivity and the production and export of organic matter contributed to decrease oxygen concentrations and enrich sediments in a selection of RSTEs. As we discussed before, variable bottom-water redox conditions occurred within the Cupidito lagoon as consequence of the interaction of local processes.

The TOC-rich interval D has been previously interpreted as deposited under anoxic bottom conditions related to eutrophication of surface waters that resulted from a local upwelling system in a basinal environment (Barragan, 2001; Núñez-Useche and Barragán, 2012). Certainly, the sudden increase in radiolarian and marked decline in benthic foraminiferal abundance associated with this interval (Fig. 3) have been also observed in modern sediments deposited under regions of intense upwelling systems (Diester-Haass, 1977). Data from this study show that the TOC-rich interval D coincides with a decrease in $\delta^{13}C$ values (Fig. 3), which indeed may have resulted from the strong mixing of surface waters with cold nutrient-rich deeper waters depleted in ^{13}C (Wefer et al., 1999; Peeters et al., 2002). Considering the model applied to explain the origin of the underlying TOC-rich intervals, we hypothesize that eutrophic conditions could also be induced by nutrient supply to the surface waters related to increased rates of continental runoff during warmer/humid periods (Fig. 5). The transfer of continental-derived-freshwater may also account for the decrease in carbon-isotope values in the TOC-rich interval D; however, this shift must have required large amounts of freshwater and accompanied detrital components, which are no reflected in sedimentary facies. The results of XRD analysis show that samples from this interval (see Table 1, samples FZD-135 and FZD-143a) have an abundance of detrital components quite similar to that found in the other samples. Therefore, the arrival of nutrients from runoff probably was secondary with respect to nutrient advection due to upwelling. The scarce of planktonic foraminifera in the TOC-rich interval D is probably related to the shoaling of the carbonate compensation depth as consequence of high productivity and/or unfavorable conditions for calcareous plankton in surface waters.

6.5. Time-equivalent facies of the OAE 1a and diachronism of the Cupidito–La Peña flooding

Deposits of the OAE 1a in the section investigated are included in the Cupidito unit. By contrast, Li et al. (2008) associate this event with the organic-carbon rich facies of the uppermost part of the Lower Tamaulipas Formation–lower part of the La Peña Formation at the Santa Rosa Canyon section (SRC section; see location in Fig. 1) (Fig. 9). This inconsistency regarding the lithostratigraphic position of the OAE 1a as well as unpublished nannoplankton data of the lowermost part of the La Peña Formation confirms the diachronism of the Cupidito–La Peña flooding event, as previously proposed by some studies (Goldhammer, 1999; Lehmann et al., 1999, 2000), and rules out the isochronous hypothesis (Barragán-Manzo and Méndez-Franco, 2005; Barragán and Maurrasse, 2008; Moreno-Bedmar et al., 2011, 2012a; Moreno-Bedmar and Delanoy, 2013) (see Section 2). According to the diachronous model, this flooding event took place by onlap and shifted gradually landward, which implies that the Cupidito–La Peña lithostratigraphic contact in coeval basinal sections like the SRC section is older than the same contact in shelfal sections like the FZD (Fig. 9A). This scenario explains that OAE 1a time-equivalent facies occur in a lower lithostratigraphic position in the SRC section and appear higher in the FZD section (Fig. 9). It also allows the correlation of the negative excursion in the $\delta^{13}C$ record of 2.0‰ toward the base of segment C7 in the SRC section (within the *Leupoldina cabri* planktonic foraminifera Zone) with the IFNE recorded in the FZD section (see Núñez-Useche et al., 2014) (Fig. 9).

The diachronism of the base of the La Peña Formation can be also deduced from biostratigraphic age data. Deposition of this unit in the SRC section onsets in the middle early Aptian (upper part of the *Globigerinelloides blowi* foraminifera Zone; Li et al., 2008) (Fig. 9), and much later, in the latest early Aptian in the FZD section (upper part of the *D. furcata* Zone; Moreno-Bedmar et al., 2013) (Fig. 9). If we roughly assume that the base of the La Peña Formation coincides with the onset of the OAE 1a at the SRC section (Li et al., 2008, Fig. 9), and with the base of the *D. furcata* Zone in the FZD section (Moreno-Bedmar et al., 2013, Fig. 3A), and consider the published numerical ages of these events of ~124 Ma (Meyers et al., 2006) and ~122 Ma (Scott, 2014), respectively, it is possible to approximately estimate that the onset of the La Peña Formation deposition occurred diachronously, with a difference in age of about 2 My between the two sections.

6.6. Carbonate platform response to the drowning and OAE 1a

Initial flooding of the Cupido platform started in the latest Barremian–earliest Aptian with the stepwise transformation of the rimmed shelf with marginal reefs and barrier shoals to the Cupidito ramp (Goldhammer et al., 1991; Lehmann et al., 1999) (Fig. 1). This change of the platform architecture marked an important turning point from photozoan towards heterozoan-dominated carbonate production along with the transition from Cupido to transgressive Cupidito facies. This early platform drowning coincides with the installation of an heterozoan mode platform over the photozoan rudist-rich ecosystem (Urgonian Platform) in the northern Tethyan, which started at the very end of the Barremian and peaked immediately before the OAE 1a (Wissler et al., 2003; Föllmi et al., 2006, 2007; Huck et al., 2011, 2013; Stein et al., 2012). The data show the onset of such drowning phase in Mexico at the Cupido–Cupidito boundary also predating the OAE 1a.

Several shoal-water carbonate systems along the northern Tethyan margin underwent demise and subsequent drowning before the onset of the OAE 1a (Wissler et al., 2003; Weissert and Erba, 2004;

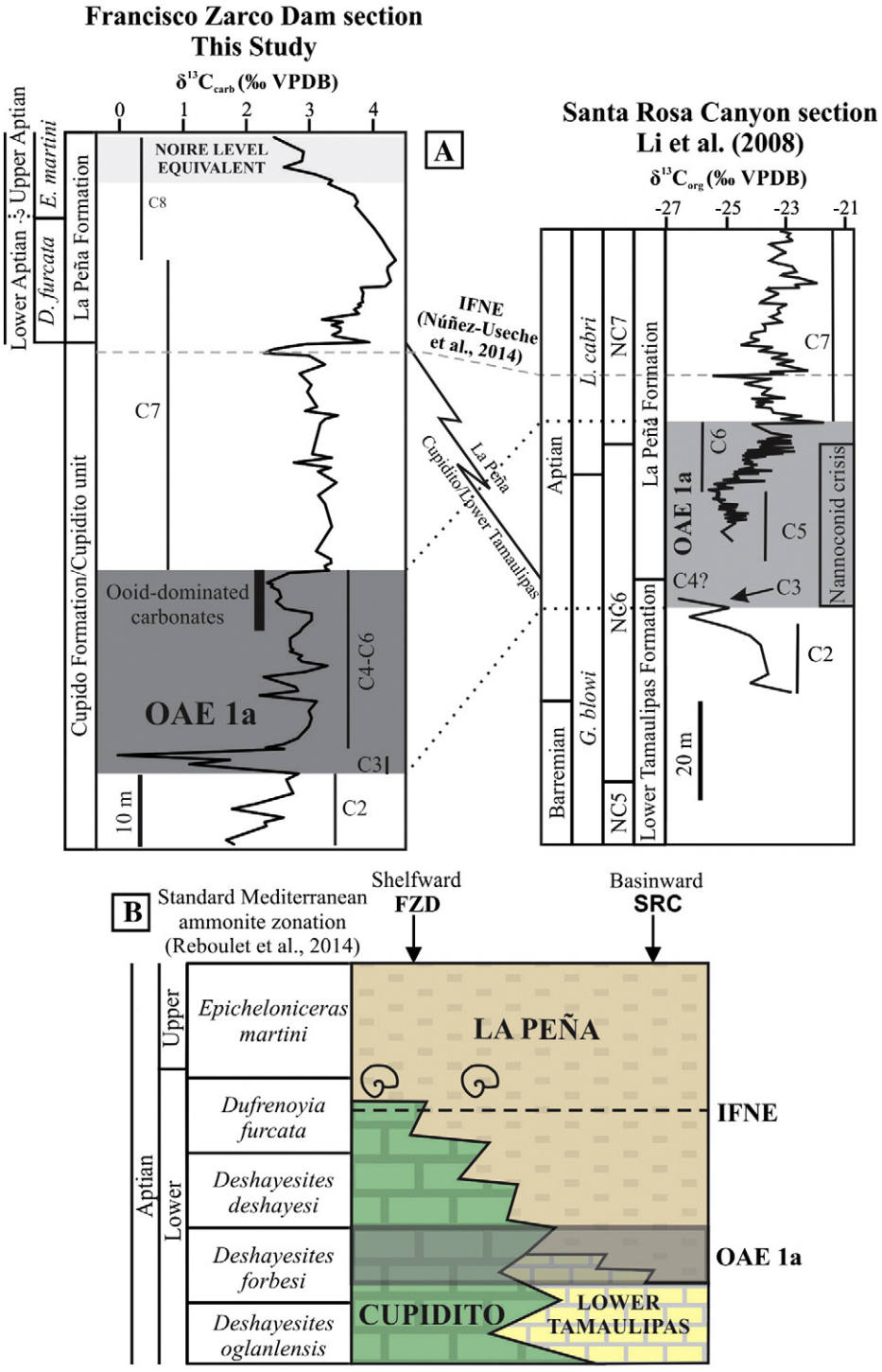

Fig. 9. Mexican record of the OAE 1a. A—Geochemical correlation of δ13C curves between the Francisco Zarco Dam (FZD) section (this study) and the Santa Rosa Canyon (SRC) section (Li et al., 2008); B—Lithostratigraphic position of the OAE 1a and IFNE confirms the diachronism of the Cupidito-La Peña flooding event. The base of the la Peña Formation in the FZD section correlates with the upper part of the Mediterranean Dufrenoyia furcata Zone of Reboulet et al. (2014) (Barragan, 2001; Moreno-Bedmar et al., 2013). The OAE is included in the Deshayesites forbesi Zone (Moreno-Bedmar et al., 2009, 2012b; Najarro et al., 2009; Föllmi, 2012).

Immenhauser et al., 2005; Föllmi et al., 2006; Huck et al., 2011, 2013; Skelton and Gilli, 2012). However, in the Cupidito ramp in northern Mexico carbonate production continued during this event. Indeed, the beginning of the OAE 1a is not characterized by a noticeable variation in the Cupidito facies. In the FZD section there is not evident change in the lagoonal facies in the C2–C3 transition (Fig. 3A). However, basinal sediments of the Santa Rosa Canyon section record the onset of the "nannoconid crisis" (Erba, 1994; Erba et al., 1999, 2010; Weissert and Erba, 2004) at this time (Fig. 9). This biotic turnover is the result of a worldwide biocalcification carbonate crisis occurring shortly before and during the early Aptian negative carbon-isotope excursion (segment C3) (Erba et al., 1999, 2010; Weissert and Erba, 2004; Millán et al., 2009), and also affected platform environments stressing rudist bivalves and corals and favoring *Lithocodium*/*Bacinella* or similar microbial blooms (Immenhauser et al., 2005; Huck et al., 2010; Skelton and Gilli, 2012). The biocalcification crisis is the response to a period of ocean acidification caused by a major injection of volcanogenic CO_2 derived from the emplacement of the Ontong-Java (Leckie et al.,

2002; Méhay et al., 2009; Erba et al., 2010). Remarkable in the FZD section is the presence of radial ooid-dominated carbonates (microfacies association II; Figs. 3 and 9) in the uppermost 9 m of succession which represents the OAE 1a interval. Similar oolitic successions have been documented in southern Italy during the early Toarcian oceanic anoxic event and in carbonate platforms of the northern Tethyan margin also associated with the early Aptian OAE 1a (; Trecalli et al., 2012; Föllmi and Godet, 2013). This facies can be a consequence of excessive carbonate production during a phase of alkalinity in the oceans following a phase of ocean acidification (Kump et al., 2009; Föllmi and Godet, 2013). In the FZD section, a major acceleration of weathering and organic-matter burial during deposition of the TOC-rich interval A (Fig. 5) may have induced drawdown of CO_2 and caused the alkalinity recovery. Núñez-Useche and Barragán (2012) proposed that ooid accumulation toward the upper part of the microfacies association II occurred close to the vadose zone, as is indicated by the presence of pendant cement. This suggests gradual carbonate aggradation probably as an attempt of the Cupidito ramp to keep up with drowning.

The phase of heterozoan carbonate growth of the Cupidito ramp continued after the global crisis associated with OAE 1a, as is indicated by the crinoids-rich carbonate succession in the post-OAE 1a interval in the FZD section. In a similar fashion, shallow-water carbonate platforms in Oman underwent uninterrupted carbonate production during this event (Immenhauser et al., 2005). We suggest that the perturbation of carbonate production and export during OAE 1a which affected various shelves and open marine environments did not significantly disturb the Cupidito ramp.

In the post-OAE 1a succession, the presence of rudist-debris in the uppermost part of the Cupidito unit (Figs. 2C and 3A) indicates that photozoan ecosystems also persisted in inner areas of the ramp, probably as isolated rudist pinnacle reefs (Conklin and Moore, 1977). Reduced rates of chemical weathering and continental runoff during colder/drier periods after OAE 1a (Fig. 5) might have caused low nutrient conditions, which induced favorable growth conditions for these carbonate ecosystems.

Definitive drowning of the Cupidito ramp during latest early Aptian occurred in response to a long-term global sea-level rise. Diachronic flooding, which peaked during the deposition of the La Peña Formation, is the result of the regional paleogeographic configuration (Fig. 1). In the FZD section, this transgressive episode is correlated with the transgressive part of the Tethyan sequence Ap4 of Hardenbol et al. (1998) (Moreno-Bedmar et al., 2012a). The termination of platform growth is coeval with a drowning event in the Basque–Cantabrian Basin, Spain (Najarro et al., 2011; García-Mondéjar et al., 2009; Millán et al., 2009), and a protracted platform drowning and demise phase in the Helvetic platforms which lasted until the late Aptian (Föllmi et al., 1994, 2006). This study reveals that the Cupidito ramp underwent periodic arrival of detrital components and nutrients link to an increased rate of continental runoff during warmer/humid periods. Such conditions may have increasingly stressed the carbonate factory, thus accelerating platform demise.

7. Conclusions

The recognized $\delta^{13}C$ trends within the FZD section match C2 to C8 segments observed from other global Aptian sections. Coupled with available biostratigraphic data, these segments permit correlation of some intervals with the OAE 1a (in the shallow lagoonal deposits of the Cupidito unit, encompassing the TOC-rich interval A), the IFNE (uppermost portion of the Cupidito unit), and the Noire level (uppermost part of the section, TOC-rich interval D). It is also possible to raise a doubt on the previously proposed correlation between the Spanish Aparein level and the TOC-rich interval C at the base of the La Peña Formation.

Various increases in detrital influx occurred episodically in the lower part of the section, within the segment C2 and the lower-middle part of OAE 1a. A slight increase can be also observed in the upper part of the Cupidito unit. Meanwhile, the base of the La Peña Formation is coeval with a sustained increase. Concurrent high values of CIA and CIW′ with these peaks in detritism indicate weathering intensification, presumably during periods with warmer/humid conditions. This observation fits with global warming conditions occurring at these time intervals.

Reducing conditions within the sediment and more oxic–dysoxic at the seafloor occurred during the deposition of the lower part of the Cupidito unit. This subtle balance was controlled by the interaction of local processes rather than by paleoceanographic changes related to the OAE 1a perturbation. It is probable that the apparent excess of RSTEs in the Cupidito unit also reflects the higher availability of these elements in seawater associated with the greater Ontong-Java plateau event. Oxygen depletion was more persistent within the lower part of the La Peña Formation (TOC-rich interval C), as is corroborated by sustained low Mn/Al ratios. Anoxic/dysoxic bottom waters for this interval are indicated by the size distribution of pyrite framboids. This proxy also suggests anoxic conditions during the deposition of the TOC-rich interval D.

Coincidence of TOC-rich intervals with significant peaks in detritism suggests a direct relationship between continental runoff and organic-matter burial. Correlations among Fe, P and Al confirm that detrital influx delivered these biolimiting nutrients, fostered local marine productivity, organic-matter burial and, subsequently, oxygen depletion in bottom waters. This model is supported by the concomitant occurrence of positive excursions in $\delta^{13}C$ and RSTEs enrichment at TOC-rich intervals A and C. High TOC values in the TOC-rich interval D together with the domination of radiolaria and low $\delta^{13}C$ values are indicative of mixing of surface waters with cold nutrient-rich deeper waters and minor arrival of nutrients from runoff.

The inconsistency regarding the lithostratigraphic position of the OAE 1a (appearing in a higher lithostratigraphic position in shelfal sections) confirms the diachronism of the Cupidito–La Peña flooding event. It is possible to roughly estimate that the onset of the La Peña Formation deposition occurred diachronously, with a difference in age of about 2 My between basin and platform environments.

The shift from the photozoan Cupido platform to the heterozoan Cupidito ramp during the latest Barremian–earliest Aptian marks the beginning of the drowning of the carbonate platform in response to a long-term global sea-level rise. The perturbation of carbonate production and export during OAE 1a which affected various shelves and open marine environments did not significantly disturb the Cupidito lagoon, which continued its growth in heterozoan mode during this event. Remarkably is the presence of ooid-dominated facies in the uppermost part of the OAE1a succession probably associated to a phase of alkalinity recovery. After OAE 1a, local photozoan ecosystems flourished in response to low nutrient conditions associated with low continental runoff during colder/drier periods. Definitive drowning of the Cupido/Cupidito platform system peaked during diachronous deposition of the La Peña Formation in response to a global transgressive event. Periodic arrival of detrital components and nutrients to the Cupidito ramp during warmer/humid periods accelerated platform demise by stressing the carbonate factory.

Supplementary data to this article can be found online at http://dx.doi.org/10.1016/j.sedgeo.2015.04.006.

Acknowledgements

This research was supported by grants PAPIIT IN109912, DGAPA, UNAM; CONACyT-SEP 177510, and the Dana Russell Memorial Grant from the American Association of Petroleum Geologists Grant-in-aid program provided to the first author. Teresa Pi is acknowledged for the XRD analyses. Sedimentary Geology reviewers J.M. Castro and K. Föllmi are thanked for very constructive contributions.

References

Algeo, T.J., Maynard, J.B., 2004. Trace-element behavior and redox facies in core shales of Upper Pennsylvanian Kansas-type cyclothems. Chemical Geology 206 (3), 289–318.

Algeo, T.J., Rowe, H., 2012. Paleoceanographic applications of trace-metal concentration data. Chemical Geology 324, 6–18.

Araujo, M.J., Martínez, C.A., 1981. Estudio estratigráfico sedimentario del Neocomiano, Prospecto Tlahualillo-La Zarca, Durango y Chihuahua: México. Unpublished report Instituto Mexicano del Petróleo, Subdirección. Técnica de Exploración. Proyecto C-1101.

Barragan, R., 2001. Sedimentological and paleocological aspects of the Aptian transgressive event of Sierra del Rosario, Durango, northeast Mexico. Journal of South America Earth Sciences 14, 189–202.

Barragán, R., Maurrasse, F.J.-M.R., 2008. Lower Aptian (Lower Cretaceous) ammonites from the basal strata of the La Peña Formation of Nuevo León State, northeast Mexico: biochronostratigraphic implications. Revista Mexicana de Ciencias Geológicas 25, 145–157.

Barragán-Manzo, R., Díaz-Otero, C., 2004. Análisis de microfacies y datos micropaleontológicos de la transición Barremiano–Aptiano en la Sierra del Rosario, Durango, México. Revista Mexicana de Ciencias Geológicas 21 (2), 247–259.

Barragán-Manzo, R., Méndez-Franco, A.L., 2005. Towards a standard ammonite zonation for the Aptian (Lower Cretaceous) of northern Mexico. Revista Mexicana de Ciencias Geológicas 22, 39–47.

Bodin, S., Godet, A., Föllmi, K.B., Vermeulen, J., Arnaud, H., Strasser, A., Fiet, N., Adatte, T., 2006. The late Hauterivian Faraoni oceanic anoxic event in the western Tethys: evidence from phosphorus burial rates. Palaeogeography, Palaeoclimatology, Palaeoecology 235, 245–264.

Bodin, S., Godet, A., Matera, V., Steinmann, P., Vermeulen, J., Gardin, S., Adatte, T., Coccioni, R., Föllmi, K.B., 2007. Enrichment of redox-sensitive trace metals (U, V, Mo, As) associated with the late Hauterivian Faraoni oceanic anoxic event. International Journal of Earth Sciences 96, 327–341.

Bond, D., Wignall, P.B., 2010. Pyrite framboid study of marine Permian–Triassic boundary sections: a complex anoxic event and its relationship to contemporaneous mass extinction. Geological Society of America Bulletin 122 (7/8), 1265–1279.

Böning, P., Brumsack, H.J., Böttcher, M.E., Schnetger, B., Kriete, C., Kallmeyer, J., Borchers, S.L., 2004. Geochemistry of Peruvian near-surface sediments. Geochimica et Cosmochimica Acta 68 (21), 4429–4451.

Bottini, C., Erba, E., Tiraboschi, D., Jenkyns, H.C., Schouten, S. Sinninghe, Damsté, J.S., 2014. Climate variability and relationship with ocean fertility during the Aptian Stage. Climate of the Past Discussion 10 (1), 689–738.

Bralower, T.J., CoBabe, E., Clement, B., Sliter, W.V., Osburn, C.L., Longoria, J., 1999. The record of global change in mid-Cretaceous (Barremian–Albian) sections from the Sierra Madre, northeastern Mexico. Journal of Foraminiferal Research 29 (4), 418–437.

Bréhéret, J.G., 1997. L'Aptien et l'Albien de la fosse Vocontienne (des bordures au bassin). Évolution de la sédimentation et enseignements sur les évènements anoxiques. Université de Tours, Tours (Ph. D. Thesis, 614 p.).

Brumsack, H.J., 1989. Geochemisty of recent TOC-rich sediments from the Gulf of California and the Black Sea. Geologische Rundschau 78 (3), 851–882.

Brumsack, H.J., 2006. The trace metal content of recent organic carbon-rich sediments: implications for Cretaceous black shale formation. Palaeogeography, Palaeoclimatology, Palaeoecology 232 (2), 344–361.

Buggle, B., Glaser, B., Hambach, U., Gerasimenko, N., Marković, S., 2011. An evaluation of geochemical weathering indices in loess–paleosol studies. Quaternary International 240 (1), 12–21.

Calvert, S.E., Pedersen, T.F., 1993. Geochemistry of recent oxic and anoxic sediments: implications for the geological record. Marine Geology 113, 67–88.

Canet, C., Alfonso, P., Melgarejo, J.C., Belyatsky, B.V., 2004. Geochemical evidences of sedimentary-exhalative origin of the shale-hosted PGE–Ag–Au–Zn–Cu occurrences of the Prades Mountains (Catalonia, Spain): trace-element abundances and Sm–Nd isotopes. Journal of Geochemical Exploration 82 (1), 17–33.

Cobianchi, M., Luciani, V., Bosellini, A., 1997. Early Cretaceous nannofossils and planktonic foraminifera from northern Gargano (Apulia, southern Italy). Cretaceous Research 18, 249–293.

Conklin, J., Moore, C., 1977. Paleoenvironmental analysis of the Lower Cretaceous Cupido Formation, northeast Mexico. In: Bebout, D.G., Loucks, R.G. (Eds.), Cretaceous carbonates of Texas and Mexico. University of Texas Bureau of Economic Geology Report of Investigations 89, pp. 302–323.

Cullers, R.L., 2000. The geochemistry of shales, siltstones and sandstones of Pennsylvaniane Permian age, Colorado, USA: implications for provenance and metamorphic studies. Lithos 51, 181–203.

Di Lucia, M., Trecalli, A., Mutti, M., Parente, M., 2012. Bio-chemostratigraphy of the Barremian–Aptian shallow-water carbonates of the southern Apennines (Italy): pinpointing the OAE1a in a Tethyan carbonate platform. Solid Earth 3, 1–28.

Diester-Haass, L., 1977. Radiolarian/planktonic foraminiferal ratios in a coastal upwelling region. Journal of Foraminiferal Research 7, 26–33.

Duncan, R.A., Tiraboschi, D., Erba, E., Walczak, P.S., Clarke, L.J., 2007. The Cretaceous OAE 1a-submarine plateau link: additional geochemical evidence from marine sedimentary sections. Eos, Transactions, American Geophysical Union vol. 88 (Abstract T13A–1125).

Elkhazri, A., Abdallah, H., Razgallah, S., Moullade, M., Kuhnt, W., 2013. Carbon-isotope and microfaunal stratigraphy bounding the Lower Aptian Oceanic Anoxic Event 1a in northeastern Tunisia. Cretaceous Research 39, 133–148.

Enos, P., 1991. Sedimentary parameters for computer modeling. In: Franseen, E.K., Watney, W.L., Kendall, C.G.St.C., Ross, W. (Eds.), Sedimentary modeling: Computer Simulations and Methods for Improved Parameter Definition. Kansas Geological Survey Bulletin vol. 233, pp. 63–100.

Erba, E., 1994. Nannofossils and superplumes: the early Aptian "nannoconid crisis". Paleoceanography 9, 483–501.

Erba, E., Channell, J.E.T., Claps, M., Jones, C., Larson, R., Opdyke, B., Premoli Silva, I., Riva, A., Salvini, G., Torricelli, S., 1999. Integrated stratigraphy of the Cismon APTICORE (Southern Alps, Italy): a "reference section" for the Barremian–Aptian interval at low latitudes. Journal of Foraminiferal Research 29, 371–392.

Erba, E., Bottini, C., Weissert, H.J., Keller, C.E., 2010. Calcareous nannoplankton response to surface-water acidification around Oceanic Anoxic Event 1a. Science 329 (5990), 428–432.

Erba, E., Duncan, R.A., Bottini, C., Tiraboschi, D., Weissert, H., Jenkyns, H.C., Malinverno, A., 2015. Environmental consequences of Ontong Java Plateau and Kerguelen Plateau volcanism. In: Neal, C.R., Sager, W.W., Sano, T., Erba, E. (Eds.), The Origin, Evolution, and Environmental Impact of Oceanic Large Igneous Provinces. Geological Society of America Special Paper 511.

Fedo, C.M., Nesbitt, H.W., Young, G.M., 1995. Unraveling the effects of potassium metasomatism in sedimentary rocks and paleosols, with implications for paleoweathering conditions and provenance. Geology 23, 921–924.

Fedo, C.M., Young, G.M., Nesbitt, G.M., 1997. Paleoclimatic control on the composition of the Paleoproterozoic Serpent Formation, Huronian Supergroup, Canada: a greenhouse to icehouse transition. Precambrian Research 86, 201–223.

Friedrich, O., 2010. Benthic foraminifera and their role to decipher paleoenvironment during mid-Cretaceous Oceanic Anoxic Events–the "anoxic benthic foraminifera" paradox. Revue de micropaléontologie 53 (3), 175–192.

Föllmi, K.B., 2012. Early Cretaceous life, climate and anoxia. Cretaceous Research 35, 230–257.

Föllmi, K.B., Godet, A., 2013. Palaeoceanography of Lower Cretaceous Alpine platform carbonates. Sedimentology 60 (1), 131–151.

Föllmi, K.B., Weissert, H., Bisping, M., Funk, H., 1994. Phosphogenesis, carbon-isotope stratigraphy, and carbonate-platform evolution along the Lower Cretaceous northern Tethyan margin. Geological Society of America Bulletin 106, 729–746.

Föllmi, K.B., Godet, A., Bodin, S., Linder, P., 2006. Interactions between environmental change and shallow water carbonate buildup along the northern Tethyan margin and their impact on the Early Cretaceous carbon isotope record. Paleoceanography 21 (PA4211), 4211–4216.

Föllmi, K.B., Bodin, S., Godet, A., Linder, P., Van De Schootbrugge, B., 2007. Unlocking paleo-environmental information from Early Cretaceous shelf sediments in the Helvetic Alps: stratigraphy is the key! Swiss Journal of Geosciences 100 (3), 349–369.

Föllmi, K.B., Bôle, M., Jammet, N., Froidevaux, P., Godet, A., Bodin, S., Adatte, T., Matera, V., Fleitmann, D., Spangenberg, J.E., 2012. Bridging the Faraoni and Selli oceanic anoxic events: short and repetitive dys- and anaerobic episodes during the late Hauterivian to early Aptian in the central Tethys. Climates of the Past 8, pp. 171–189.

García-Mondéjar, J., Owen, H.G., Raisossadat, N., Millán, M.I., Fernández-Mendiola, P.A., 2009. The Early Aptian of Aralar (northern Spain): stratigraphy, sedimentology, ammonite biozonation, and OAE1. Cretaceous Research 30, 434–464.

Godet, A., Bodin, S., Föllmi, K.B., Vermeulen, J., Gardin, S., Fiet, N., Addate, T., Berner, Z., Stüben, D., Van de Schootbrugge, B., 2006. Evolution of the marine stable carbon-isotope record during the early Cretaceous: a focus on the late Hauterivian and Barremian in the Tethyan realm. Earth and Planetary Science Letters 242 (3), 254–271.

Goldhammer, R.K., 1999. Mesozoic sequence stratigraphy and paleogeographic evolution of northeast Mexico. In: Bartolini, C., Wilson, J.L., Lawton, T.F. (Eds.), Mesozoic sedimentary and Tectonic History of North-Central Mexico. Boulder, Colorado, Geological Society of America, Special Paper 340, pp. 1–59.

Goldhammer, R.K., Lehmann, P.J., Todd, R.G., Wilson, J.L., Ward, W.C., Johnson, C.R., 1991. Sequence stratigraphy and cyclostratigraphy of the Mesozoic of the Sierra Madre Oriental, Northeast Mexico, A field guidebook: Society of Economic Paleontologists and Mineralogists, Gulf Coast Section. pp. 1–84.

Haq, B.U., Hardenbol, J., Vail, P.R., 1988. Mesozoic and Cenozoic chronostratigraphy and cycles of sea-level change. In: Wilgus, C., Hastings, B., Ross, C., Posamentier, H., Van Wagoner, J., Kendal, C.G.S.C. (Eds.), Sea-level Change: An Integrated Approach. 9 Society of Economic Paleontologists and Mineralogists, Special Publication 42, pp. 71–108.

Hardenbol, J., Thierry, J., Farley, M.B., Jacquin, T., de Graciansky, P.C., Vail, P.R., 1998. Mesozoic and Cenozoic sequence chronostratigraphic framework of European basins. In: De Graciansky, P.C., Hardenbol, J., Jacquin, T., Vail, P.R. (Eds.), Mesozoic and Cenozoic Sequence Stratigraphy of European Basins. Society of Economic Paleontologists and Mineralogists, Special Publications 60, pp. 3–14.

Harnois, L., 1988. The CIW index: a new chemical index of weathering. Sedimentary Geology 55, 319–322.

Heldt, M., Bachmann, M., Lehmann, J., 2008. Microfacies, biostratigraphy, and geochemistry of the hemipelagic Barremian–Aptian in north-central Tunisia: influence of the OAE 1a on the southern Tethys margin. Palaeogeography, Palaeoclimatology, Palaeoecology 261 (3), 246–260.

Herrle, J.O., Kößler, P., Friedrich, O., Erlenkeuser, H., Hemleben, C., 2004. High-resolution carbon isotope records of the Aptian to Lower Albian from SE France and the Mazagan Plateau (DSDP Site 545): a stratigraphic tool for paleoceanographic and paleobiologic reconstruction. Earth and Planetary Science Letters 218, 149–161.

Huck, S., Rameil, N., Korbar, T., Heimhofer, U., Wieczorek, T.D., Immenhauser, A., 2010. Latitudinally different responses of Tethyan shoal-water carbonate systems to the Early Aptian oceanic anoxic event (OAE 1a). Sedimentology 57 (7), 1585–1614.

Huck, S., Heimhofer, U., Rameil, N., Bodin, S., Immenhauser, A., 2011. Strontium and carbon-isotope chronostratigraphy of Barremian–Aptian shoal-water carbonates: northern Tethyan platform drowning predates OAE 1a. Earth and Planetary Science Letters 304 (3–4), 547–558.

Huck, S., Heimhofer, U., Immenhauser, A., Weissert, H., 2013. Carbon-isotope stratigraphy of Early Cretaceous (Urgonian) shoal-water deposits: diachronous changes in

carbonate-platform production in the north-western Tethys. Sedimentary Geology 290, 157–174.
Huerta-Diaz, M.A., Morse, J.W., 1992. Pyritization of trace metals in anoxic marine sediments. Geochimica et Cosmochimica Acta 56 (7), 2681–2702.
Humphrey, W.E., 1949. Geology of Sierra de los Muertos area, Mexico (with descriptions of Aptian cephalopods from the La Peña Formation). Geological Society of America Bulletin 60, 89–176.
Imlay, R.W., 1937. Geology of the middle part of the Sierra de Parras, Coahuila, Mexico. Geological Society of America Bulletin 48, 567–630.
Immenhauser, A., Hillgärtner, H., van Bentum, E., 2005. Microbial-foraminiferal episodes in the Early Aptian of the southern Tethyan margin: ecological significance and possible relation to oceanic anoxic event 1a. Sedimentology 52, 77–99.
Immenhauser, A., Holmden, C., Patterson, W.P., 2008. Interpreting the carbon-isotope record of ancient shallow epeiric seas: lessons from the recent. In: Pratt, B.R., Holmden, C. (Eds.), Dynamics of Epeiric Seas. Geological Association of Canada Special Publication 48, pp. 135–174.
Jahren, A.H., Arens, N.C., Sarmiento, G., Guerrero, J., Amundson, R., 2001. Terrestrial Record of methane hydrate dissociation in the Early Cretaceous. Geology 29, 159–162.
Jarvis, I., Burnett, W.C., Nathan, Y., Almbaydin, F.S.M., Attia, A.K.M., Castro, L.N., Flicoteaux, R., Hilmy, M.E., Husain, V., Qutawnnah, A.A., Serjani, A., Zanin, Y.N., 1994. Phosphorite geochemistry: state of the art and environmental concerns. Eclogae Geologicae Helveticae 87, 643–700.
Jenkyns, H.C., 1980. Cretaceous anoxic events: from continents to oceans. Journal of the Geological Society of London 137, 171–188.
Jenkyns, H.C., 1999. Mesozoic anoxic events and palaeoclimate. Zentralblatt für Geologie und Paläontologie 1997, 943–949.
Jenkyns, H.C., 2003. Evidence for rapid climate change in the Mesozoic–Palaeogene greenhouse world. Philosophical Transactions of the Royal Society of London. Series A: Mathematical. Physical and Engineering Sciences 361, 1885–1916.
Jenkyns, H.C., 2010. Geochemistry of oceanic anoxic events. Geochemistry, Geophysics, Geosystems 11 (3), 1525–2027.
Jenkyns, H.C., Schouten-Huibers, L., Schouten, S., Sinninghe Damsté, J.S., 2012. Warm Middle Jurassic–Early Cretaceous high-latitude sea-surface temperatures from the Southern Ocean. Climate of the Past 8 (1), 215–226.
Jorissen, F.J., de Stigter, H.C., Widmark, J.G.V., 1995. A conceptual model explaining benthic foraminiferal microhabitats. Marine Micropaleontology 26, 3–15.
Keller, C.E., Hochuli, P.A., Weissert, H., Bernasconi, S.M., Giorgioni, M., Garcia, T.I., 2011. A volcanically induced climate warming and floral change preceded the onset of OAE1a (Early Cretaceous). Palaeogeography, Palaeoclimatology, Palaeoecology 305, 43–49.
Kump, L.R., Bralower, T.J., Ridgwell, A., 2009. Ocean acidification in deep time. Oceanography 22, 94–107.
Larson, R.L., 1991. Latest pulse of earth: evidence for a mid-Cretaceous superplume. Geology 19, 547–550.
Larson, R.L., Erba, E., 1999. Onset of the mid-Cretaceous greenhouse in the Barremian–Aptian: igneous events and the biological, sedimentary, and geochemical responses. Paleoceanography 14, 663–678.
Leckie, R.M., Bralower, T.J., Cashman, R., 2002. Oceanic anoxic events and plankton evolution: biotic response to tectonic forcing during the mid-Cretaceous. Paleoceanography 17 (3), 1–29.
Lehmann, C., Osleger, D.A., Montañez, I.P., Sliter, W., Arnaud-Vanneau, A., Banner, J., 1999. Evolution of Cupido and Coahuila carbonate platforms, Early Cretaceous, northeastern Mexico. Geological Society of America Bulletin 111 (7), 1010–1029.
Lehmann, C., Osleger, D.A., Montañez, I.P., 2000. Sequence stratigraphy of Lower Cretaceous (Barremian–Albian) carbonate platforms of northeastern Mexico: regional and global correlations. Journal of Sedimentary Research 70 (2), 373–391.
Li, Y.-X., Bralower, T.J., Montañez, I.P., Osleger, D.A., Arthur, M.A., Bice, D.M., Herbert, T.D., Erba, E., Premoli Silva, I., 2008. Toward an orbital chronology for the early Aptian Oceanic Anoxic Event (OAE1a, ~120 Ma). Earth and Planetary Science Letters 271, 88–100.
Luciani, V., Cobianchi, M., Lupi, C., 2006. Regional record of a global oceanic anoxic event: OAE1a on the Apulia platform margin, Gargano Promontory, southern Italy. Cretaceous Research 27, 754–772.
Luther III, G.W., 1991. Pyrite synthesis via polysulfide compounds. Geochimica et Cosmochimica Acta 55, 2839–2849.
Méhay, S., Keller, C.E., Bernasconi, S.M., Weissert, H., Erba, E., Bottini, C., Hochuli, P.A., 2009. A volcanic CO_2 pulse triggered the Cretaceous oceanic anoxic event 1a and a biocalcification crisis. Geology 37, 819–822.
Menegatti, A.P., Weissert, H., Brown, R.S., Tyson, R.V., Farrimond, P., Strasser, A., Caron, M., 1998. High-resolution $\delta^{13}C$ stratigraphy through the early Aptian "Livello Selli" of the Alpine Tethys. Paleoceanography 13 (5), 530–545.
Meyers, P.A., 2006. Paleoceanographic and paleoclimatic similarities between Mediterranean sapropels and Cretaceous black shales. Palaeogeography, Palaeoclimatology, Palaeoecology 235 (1), 305–320.
Meyers, P.A., Bernasconi, S.M., Forster, A., 2006. Origins and accumulation of organic matter in expanded Albian to Santonian black shale sequences on the Demerara Rise, South American margin. Organic Geochemistry 37 (12), 1816–1830.
Millán, M.I., Weissert, H.J., Fernández-Mendiola, P.A., García-Mondéjar, J., 2009. Impact of Early Aptian carbon cycle perturbations on evolution of a marine shelf system in the Basque-Cantabrian Basin (Aralar, N Spain). Earth and Planetary Science Letters 287, 392–401.
Moreno-Bedmar, J.A., Delanoy, G., 2013. About the generic attribution of Megatyloceras casei HUMPHREY, 1949 (Ammonoidea, Ancyloceratina), from the Aptian of Mexico. Carnets de Geologie-Notebooks on Geology, Letter 2013/06 (CG2013_L06), pp. 315–323.
Moreno-Bedmar, J.A., Company, M., Bover-Arnal, T., Salas, R., Delanoy, G., Martínez, R., Grauges, A., 2009. Biostratigraphic characterization by means of ammonoids of the lower Aptian Oceanic Anoxic Event (OAE 1a) in the eastern Iberian Chain (Maestrat Basin, eastern Spain). Cretaceous Research 30, 864–872.
Moreno-Bedmar, J.A., Bover-Arnal, T., Barragán, R., Salas, R., 2011. La transgresión tetisiana del Aptiense inferior terminal: comparación entre su registro en México y España y relación con el ciclo global de tercer orden Ap4. Paleontologia i Evolució Memòria especial 5 pp. 259–262.
Moreno-Bedmar, J.A., Bover-Arnal, T., Barragán, R., Salas, R., 2012a. Uppermost Lower Aptian transgressive records in Mexico and Spain: chronostratigraphic implications for the Tethyan sequences. Terra Nova 24, 333–338.
Moreno-Bedmar, J.A., Company, M., Sandoval, J., Tavera, J.M., Bover-Arnal, T., Salas, J.A., Delanoy, R., Maurrasse, G., F.J.-M.R., Martínez, R., 2012b. Lower Aptian ammonite and carbon isotope stratigraphy in the eastern Prebetic Domain (Betic Cordillera, southeastern Spain). Geologica Acta 10, 1–2.
Moreno-Bedmar, J.A., Barragán, R., Company, M., Bulot, L.G., 2013. Aptian (Lower Cretaceous) ammonite biostratigraphy of the Francisco Zarco Dam stratigraphic section (Durango State, Northeast Mexico). Journal of South America Earth Sciences 42, 150–158.
Moullade, M., Kuhnt, W., Bergen, J.A., Masse, J.-P., Tronchetti, G., 1998. Correlation of biostratigraphic and stable isotope events in the Aptian historical stratotype of La Bédoule (southeast France). Comptes Rendus de l'Académie des Sciences, Paris, (Série IIa, Sciences de la Terre et des Planètes) 327, pp. 693–698.
Moullade, M., Tronchetti, G., Kuhnt, W., Masse, J.-P., 2000. Les foraminifères de la série du stratotype historique de l'Aptien inférieur dans la région de Cassis-la Bédoule (SE France). In: Moullade, M., Tronchetti, G., Masse, J.-P. (Eds.), Le stratotype historique de l'Aptien inférieur (Bédoulien) dans la région de Cassis-la Bédoule (SE France). Géologie Méditerranéenne 25, pp. 187–225.
Muir, J.M., 1936. Geology of the Tampico Region, Mexico. American Association of Petroleum Geologists Bulletin 19, 1–280.
Najarro, M., Rosales, I., Moreno-Bedmar, J.A., de Gea, G.A., Barrón, E., Company, M., Delanoy, G., 2011. High-resolution chemo- and biostratigraphic records of the Early Aptian oceanic anoxic event in Cantabria (N Spain): palaeoceanographic and palaeoclimatic implications. Palaeogeography, Palaeoclimatology, Palaeoecology 299, 137–158.
Nesbitt, H.W., Young, G.M., 1982. Early Proterozoic climates and plate motions inferred from major elemental chemistry of lutites. Nature 199, 715–717.
Núñez-Useche, F., Barragán, R., 2012. Microfacies analysis and paleoenvironmental dynamic of the Barremian–Albian interval in Sierra del Rosario, eastern Durango state, Mexico. Revista Mexicana de Ciencias Geológicas 29 (1), 204–218.
Núñez-Useche, F., Moreno-Bedmar, J.A., Company, M., Barragán, R., 2014. A negative carbon isotope excursion within the *Dufrenoyia furcata* Zone: proposal for a new episode for chemostratigraphic correlation in the Aptian. Carnets de Géologie [Notebooks on Geology]. Brest 14 (6), 129–137.
Ogg, J.G., Ogg, G., 2004. Early Cretaceous (103–138 Ma time slice). In: Ogg, F.M., J.G., Smith, A.G. (Eds.), A Geologic Time Scale. Cambridge University Press, p. 589.
Peeters, F.J.C., Brummer, G.-J.A., Ganssen, G., 2002. The effect of upwelling on the distribution and stable isotope composition of Globigerina bulloides and Globigerina ruber (planktic foraminifers) in modern surface waters of the NW Arabian Sea. Global and Planetary Change 34, 269–291.
Phelps, R.M., Kerans, C., Da-Gama, R.O., Jeremiah, J., Hull, D., Loucks, R.G., 2015. Response and recovery of the Comanche carbonate platform surrounding multiple Cretaceous oceanic anoxic events, northern Gulf of Mexico. Cretaceous Research 54, 117–144.
Piper, D.Z., Calvert, S.E., 2009. A marine biogeochemical perspective on black shale deposition. Earth-Science Reviews 95 (1), 63–96.
Piper, D.Z., Perkins, R.B., 2004. A modern vs. Permian black shale—the hydrography, primary productivity, and water-column chemistry of deposition. Chemical Geology 206 (3), 177–197.
Prokoph, A., Shields, G.A., Veizer, J., 2008. Compilation and time-series analysis of a marine carbonate n18O, bonate87Sr/86Sr and t34S database through Earth history. Earth-Science Reviews 87, 113–133.
Rajabi, A., Rastad, E., Canet, C., Alfonso, P., 2014. The early Cambrian Chahmir shale-hosted Zn–Pb deposit, Central Iran: an example of vent-proximal SEDEX mineralization. Mineralium Deposita 1–20.
Reboulet, S., Szives, O., Aguirre-Urreta, B., Barragán, R., Company, M., Idakieva, V., Ivanov, M., Kakabadze, M.V., Moreno-Bedmar, J.A., Sandoval, J., Baraboshkin, E.J., Çaglar, M.K., Főzy, I., GonzálezArreola, C., Kenjo, S., Lukeneder, A., Raisossadat, S.N., Rawson, P.F., Tavera, J.M., 2014. Report on the 5th International Meeting of the IUGS Lower Cretaceous Ammonite Working Group, the Kilian Group (Ankara, Turkey, 31st August 2013). Cretaceous Research 50, pp. 126–137.
Renard, M., De Rafélis, M., Emmanuel, L., Moullade, M., Masse, J.-P., Kuhnt, W., Bergen, J.A., Tronchetti, G., 2005. Early Aptian δ13C and manganese anomalies from thehistorical Cassis-La Bédoule stratotype sections (S.E.France): relationship with a methane hydrate dissociation event and stratigraphic implications. Notebooks on Geology Article2005/04(CG2005_A04), pp. 1–18.
Rimmer, S.M., Thompson, J.A., Goodnight, S.A., Robl, T.L., 2004. Multiple controls on the preservation of organic matter in Devoian–Mississippian marine black shales: geochemical and petrographic evidence. Palaeogeography, Palaeoclimatology, Palaeoecology 215, 125–154.
Sanchez-Hernandez, Y., Maurrasse, F.J.M., 2014. Geochemical characterization and redox signals from the latest Barremian to the earliest Aptian in a restricted marine basin: El Pui section, Organyà Basin, south-central Pyrenees. Chemical Geology 372, 12–31.
Schlanger, S.O., Jenkyns, H.C., 1976. Cretaceous oceanic anoxic events: causes and consequences. Geologie en Mijnbouw 55, 179–184.
Scholle, P.A., Arthur, M.A., 1980. Carbon isotope fluctuations in Cretaceous pelagic limestones: potential stratigraphic and petroleum exploration tool. AAPG Bulletin 64 (1), 67–87.
Scott, R.W., 1990. Models and stratigraphy of mid-Cretaceous reef communities, Gulf of Mexico: SEPM (Society for Sedimentary Geology) Concepts in Sedimentology and Paleontology 2 p. 102.

Scott, R.W., 2014. A Cretaceous chronostratigraphic database: construction and applications. Carnets de Géologie[Notebooks on Geology]. Brest 14 (2), 15–37.
Sinton, C.W., Duncan, R.A., 1997. Potential links between ocean plateau volcanism and global ocean anoxia at the Cenomanian–Turonian boundary. Economic Geology 92, 836–842.
Skelton, P.W., Gili, E., 2012. Rudists and carbonate platforms in the Aptian: a case study on biotic interactions with ocean chemistry and climate. Sedimentology 59 (1), 81–117.
Stein, M., Föllmi, K.B., Westermann, S., Godet, A., Adatte, T., Matera, V., Fleitmann, D., Berner, Z., 2011. Progressive palaeoenvironmental change during the Late Barremian Early Aptian as prelude to Oceanic Anoxic Event 1a: evidence from the Gorgo a Cerbara section (Umbria-Marche basin, central Italy). Palaeogeography, Palaeoclimatology, Palaeoecology 302 (3), 396–406.
Stein, M., Arnaud-Vanneau, A., Adatte, T., Fleitmann, D., Spangenberg, J.E., Föllmi, K.B., 2012. Palaeoenvironmental and palaeoecological change on the northern Tethyan carbonate platform during the Late Barremian to earliest Aptian. Sedimentology 59 (3), 939–963.
Stephenson, L.W., 1922. Some Upper Cretaceous shells of the rudistid group from Tamaulipas Mexico. Proceedings of the United States, Natural History Museum 61 (Art. 1, no. 2422).
Suits, N.S., Wilkin, R.T., 1998. Pyrite formation in the water column and sediments of a meromictic lake. Geology 26 (12), 1099–1102.
Tejada, M.L.G., Suzuki, K., Kuroda, J., Coccioni, R., Mahoney, J.J., Ohkouchi, N., Sakamoto, T., Tatsumi, Y., 2009. Ontong Java Plateau eruption as a trigger for the early Aptian oceanic anoxic event. Geology 37, 855–858.
Trecalli, A., Spangenberg, J., Adatte, T., Föllmi, K.B., Parente, M., 2012. Carbonate platform evidence of ocean acidification at the onset of the early Toarcian oceanic anoxic event. Earth and Planetary Science Letters 357, 214–225.
Tribovillard, N., Algeo, T.J., Lyons, T., Riboulleau, A., 2006. Trace metals as paleoredox and paleoproductivity proxies: an update. Chemical Geology 232 (1), 12–32.
Walczak, P.S., 2006. Submarine plateau volcanism and Cretaceous Ocean Anoxic Event 1a: geochemical evidence from Aptian sedimentary sections. (M. Sc. Thesis), Oregon State university (171 pp.).
Wedepohl, K.H., 1991. The composition of the upper earth's crust and the natural cycles of selected metals. Metals in natural raw materials. Natural Resources. In: Merian, E. (Ed.), Metals and Their Compounds in the Environment. Weinheim, John Wiley, Hoboken, N.J., pp. 3–17.
Wefer, G., Berger, W.H., Bijma, J., Fischer, G., 1999. Clues to ocean history: a brief overview of proxies. In: Fischer, G., Wefer, G. (Eds.), Use of proxies in paleoceanography: examples from the South Atlantic. Springer, Berlin-Heidelberg, pp. 1–68.
Wehausen, R., Brumsack, H.J., 1998. The formation of Pliocene Mediterranean sapropels: constraints from high-resolution major and minor element studies. Proceedings ocean drilling program scientific results. National Science Foundation, pp. 207–218.
Weissert, H., 1990. Siliciclastics in the early Cretaceous Tethys and north Atlantic oceans — documents of periodic greenhouse climate conditions. Memorie della Societa Geologica Italiana 44, 59–69.
Weissert, H., Erba, E., 2004. Volcanism, CO_2 and palaeoclimate: a Late Jurassic–Early Cretaceous carbon and oxygen isotope record. Journal of the Geological Society 161 (4), 695–702.
Wignall, P.B., Newton, R., 1998. Pyrite framboid diameter as a measure of oxygen-deficiency in ancient mudrocks. American Journal of Science 298, 537–552.
Wilkin, R.T., Barnes, H.L., Brantley, S.L., 1996. The size distribution of framboidal pyrite in modern sediments: an indicator of redox conditions. Geochimica et Cosmochimica Acta 60 (20), 3897–3912.
Wilkin, R.T., Arthur, M.A., Dean, W.E., 1997. History of water-column anoxia in the Black Sea indicated by pyrite framboid size distributions. Earth and Planetary Science Letters 148 (3), 517–525.
Wilson, J.L., Pialli, G., 1977. A Lower Cretaceous shelf margin in northern Mexico. In: Bebout, D.G., Loucks, R.G. (Eds.), Cretaceous carbonates of Texas and Mexico: University of Texas Bureau of Economic Geology Report of Investigations 89, pp. 286–294.
Wilson, J.L., Selvius, D.B., 1984. Early Cretaceous in the Monterry-Saltillo area of northern Mexico. In: Wilson, J.L., Ward, W.C., Finneran, J. (Eds.), A field Guide to Upper Jurassic and Lower Cretaceous carbonate platforms and basin systems, Monterrey-Saltillo area, northeast Mexico: Society of Economic Paleontologists and Mineralogists, Gulf Coast Section, p. 76.
Wilson, J.L., Ward, W.C., 1993. Early Cretaceous carbonate platforms of northeastern and east-central Mexico. In: Simo, J.A., Scott, R.W., Masse, J.-P. (Eds.), Cretaceous carbonate platforms. American Association of Petroleum Geologists Memoir 56, pp. 35–50.
Wissler, L., Funk, H., Weissert, H., 2003. Response of Early Cretaceous carbonate platforms to changes in atmospheric carbon dioxide levels. Palaeogeography, Palaeoclimatology, Palaeoecology 200, 187–205.
Wortmann, U.G., Herrle, J.O., Weissert, H., 2004. Altered carbon cycling and coupled changes in Early Cretaceous weathering patterns: evidence from integrated carbon isotope and sandstone records of the western Tethys. Earth and Planetary Science Letters 220, 69–82.
Zakharov, Y.D., Baraboshkin, E.Y., Weissert, H., Michailova, I.A., Smyshlyaeva, O.P., Safronov, P.P., 2013. Late Barremiane early Aptian climate of the northern middle latitudes: stable isotope evidence from bivalve and cephalopod molluscs of the Russian Platform. Cretaceous Research 44, 183–201.

Appendix A. $\delta^{13}C_{carb}$ and $\delta^{18}O$ from analyzed samples of the Francisco Zarco Dam section.

Bed/ Sample	Distance base (m)	$\delta^{13}C$ (‰ VPDB)	$\delta^{18}O$ (‰ VPDB)	Bed/ Sample	Distance base (m)	$\delta^{13}C$ (‰ VPDB)	$\delta^{18}O$ (‰ VPDB)
FZD-144	102.3	2.43	-4.51	FZD-47b	42.4	3.09	-6.27
FZD-142	100.2	2.90	-4.64	FZD-46m	41.2	3.32	-5.91
FZD-140	98.8	2.87	-4.41	FZD-46b	40.7	3.33	-5.78
FZD-138	97.9	2.59	-5.07	FZD-45t	40.3	3.23	-5.60
FZD-136	96.9	3.08	-4.35	FZD-45m	39.9	3.24	-5.52
FZD-134	96.0	3.34	-4.38	FZD-45b	39.6	3.29	-5.49
FZD-132	95.5	3.29	-4.33	FZD-44	39.2	2.67	-5.49
FZD-129	93.9	3.69	-4.35	FZD-42t	37.8	2.32	-5.52
FZD-127	92.9	3.75	-4.29	FZD-42m	37.5	2.41	-5.50
FZD-125	92.3	3.71	-4.68	FZD-42b	37.2	2.38	-5.23
FZD-122	89.1	4.01	-4.39	FZD-41d	36.7	2.50	-5.54
FZD-117	87.5	4.14	-4.71	FZD-41c	35.7	2.54	-5.37
FZD-113	86.1	4.23	-4.63	FZD-41b	35.1	2.46	-5.41
FZD-108	84.5	4.35	-4.53	FZD-41a	34.0	2.60	-5.44
FZD-106	83.5	4.23	-4.67	FZD-40t	33.4	3.02	-5.15
FZD-104	82.9	4.22	-4.75	FZD-40m	32.4	3.02	-5.16
FZD-99	81.5	4.27	-4.68	FZD-40b	31.3	2.89	-5.49
FZD-97	80.7	4.19	-4.63	FZD-39t	30.7	2.83	-5.31
FZD-96	80.5	3.80	-4.58	FZD-39m	29.7	2.68	-4.87
FZD-92	79.7	3.84	-4.70	FZD-39b	28.8	2.69	-5.41
FZD-89	78.8	3.82	-4.71	FZD-38	28.4	2.70	-5.05
FZD-87	78.4	3.83	-4.79	FZD-37t	28.1	2.73	-5.16
FZD-85	78.1	3.76	-4.67	FZD-37m	27.9	2.68	-5.29
FZD-84	77.9	3.80	-4.85	FZD-36t	27.2	2.87	-5.35
FZD-81	77.3	3.70	-4.81	FZD-36m	26.8	2.81	-5.19
FZD-79	76.7	3.77	-4.75	FZD-36b	26.4	2.87	-5.52
FZD-77	76.2	3.38	-4.82	FZD-35	25.8	3.27	-4.19
FZD-75	75.9	3.19	-5.04	FZD-34	24.9	2.92	-4.49
FDZ-73	75.5	3.51	-4.75	FZD-33t	24.2	2.26	-5.07
FZD-71	75.1	3.34	-5.10	FZD-33b	22.7	2.77	-4.28
FZD-69	74.7	3.48	-4.80	FZD-32	22.2	2.81	-4.55
FZD-67	74.2	3.48	-4.76	FZD-31	21.5	2.20	-5.21
FZD-65	73.7	3.35	-4.51	FZD-30e	20.6	3.10	-5.23
FZD-64	73.4	3.41	-4.81	FZD-30d	19.2	2.98	-5.21
FZD-62	72.6	3.93	-4.88	FZD-30d	18.2	3.02	-5.13
FZD-60	72.3	2.94	-4.59	FZD-30b	17.1	2.98	-5.27
FZD-59t	72.0	2.67	-4.69	FZD-30a	15.3	2.80	-5.24
FZD-59m	71.5	2.40	-5.18	FZD-29	14.5	2.57	-4.93
FZD-59b	71.0	2.27	-5.47	FZD-28t	14.0	2.29	-4.93
FZD-58t	70.7	2.98	-5.75	FZD-28m	13.8	2.59	-5.24
FZD-58b	69.4	3.23	-5.53	FZD-27t	13.3	1.35	-5.78
FZD-57	68.1	2.83	-5.54	FZD-27b	12.9	-0.04	-6.25
FZD-56	66.4	3.02	-5.64	FZD-26t	12.2	1.73	-5.00
FZD-55b	65.4	2.96	-5.93	FZD-26b	11.6	1.09	-5.19
FZD-55a	63.3	3.11	-5.78	FZD-25t	10.2	2.82	-5.41
FZD-54b	62.7	2.92	-5.73	FZD-25b	9.4	2.63	-5.60
FZD-54a	62.0	3.44	-5.39	FZD-23	8.2	2.68	-4.74
FZD-53t	61.5	3.24	-5.78	FZD-22	7.4	2.73	-4.55
FZD-53m	60.9	3.16	-6.02	FZD-19	5.9	2.14	-4.50
FZD-51a	56.4	3.03	-5.71	FZD-17	5.1	1.76	-4.26
FZD-50c	55.9	3.34	-5.85	FZD-14	3.9	2.58	-1.42
FZD-50b	55.2	2.74	-5.93	FZD-12	3.2	2.28	-2.69
FZD-49	54.5	3.32	-5.48	FZD-10	2.6	2.31	-4.27
FZD-48t	53.9	3.13	-5.59	FZD-6	0.6	1.67	-4.61
FZD-48m	52.3	3.42	-5.81	FZD-4b	0.0	1.79	-4.56
FZD-48b	50.5	3.13	-5.73				
FZD-47t	49.2	3.23	-5.92				
FZD-47m	45.9	3.34	-5.90				

Appendix B. Concentrations of major and trace elements measured in selected samples of the Francisco Zarco Dam section.

Bed/ Sample	Distance base (m)	Al (%)	Zr (ppm)	Ti (%)	K (%)	Na (%)	Ca (%)	U (ppm)	V (ppm)	Cr (ppm)	Ni (ppm)	Co (ppm)	Pb (ppm)	Cu (ppm)	Zn (ppm)	Mo (ppm)	Mn (ppm)	Fe (%)	P (%)
FZD-129	93.8	0.61	12	0.0344	0.31	0.02	32.5	4	17	20.1	13.6	0.8	1.2	2.7	21.6	1.2	67	0.41	0.034
FZD-122	89.0	0.56	2	0.026	0.3	0.02	33.7	3.9	17	14.9	16.1	0.8	1.2	2.9	29	1.2	81	0.35	0.033
FZD-120	88.2	0.79	17	0.0401	0.42	0.02	33.3	3.3	19	21.7	15.8	0.8	1	3.8	16.6	0.7	63	0.43	0.033
FZD-110	84.8	0.72	8	0.0368	0.39	0.02	33.9	3.3	21	26.9	14.1	0.6	0.9	3.1	20.5	3	78	0.44	0.033
FZD-101	82.1	0.42	1	0.0161	0.2	0.01	34.8	3.9	10	11.1	12.4	0.7	1.2	3.6	20.7	1.5	83	0.26	0.018
FZD-96	80.5	0.41	< 1	0.0183	0.22	0.03	34	3.2	12	17.9	12.3	0.5	0.5	2.3	43.2	1.9	184	0.32	0.077
FZD-93	79.9	0.82	3	0.0423	0.44	0.01	33.5	4.9	22	22.9	15.4	0.9	1	3.2	27.4	1.7	51	0.43	0.031
FZD-92	79.7	0.66	6	0.0278	0.38	0.01	34.6	5.4	19	25.2	15.8	0.7	0.7	2.8	18.9	1.1	59	0.33	0.025
FZD-87	78.4	0.99	19	0.0415	0.61	0.01	31.5	6.2	34	24	18.9	1	1.2	5.1	16.5	2.1	63	0.49	0.04
FZD-85	78.0	0.67	16	0.0334	0.38	0.01	32.2	4.1	14	19	14.4	0.7	1.4	10.7	19.1	2.4	46	0.38	0.026
FZD-84	77.8	1.25	17	0.0747	0.62	0.01	31.7	5.5	54	38.7	20.6	0.9	1.5	5.9	22.7	3	51	0.65	0.047
FZD-79	76.7	0.93	4	0.0425	0.58	0.01	32.3	5.6	18	17.1	12.5	0.6	1.8	5.5	27.7	2.4	104	0.47	0.022
FZD-77	76.2	0.57	< 1	0.0268	0.31	0.01	34.7	5.3	16	23.6	13.5	0.6	0.9	2.1	11.5	1.3	83	0.4	0.036
FZD-73	75.5	0.76	1	0.0363	0.45	0.01	33.5	6.5	17	17.8	13.6	0.7	2	8.9	20.1	2.2	71	0.49	0.035
FZD-71	75.0	0.67	< 1	0.0304	0.39	0.01	34.2	4.2	40	22.8	13.8	0.7	1.3	2.7	22.3	0.5	89	0.34	0.038
FZD-69	74.7	0.65	< 1	0.026	0.36	0.02	34.5	5	24	20.4	14.8	0.6	1	3.2	21.8	1.1	59	0.34	0.048
FZD-67	74.1	0.75	1	0.0342	0.47	0.01	34.3	5.3	46	23.5	14.7	0.7	1	2.8	18.3	1.9	47	0.42	0.045
FZD-65	73.6	0.63	8	0.0337	0.41	0.01	34.1	4.8	48	19.8	13.8	0.8	1	3.6	22	0.5	102	0.34	0.036
FZD-64	73.4	0.82	7	0.0387	0.55	0.01	33.4	6.1	25	29.6	23.4	0.7	1.2	6.3	73.8	4	63	0.44	0.054
FZD-62	72.5	0.86	10	0.0486	0.47	0.01	32.8	5.3	33	57.2	15.5	0.7	1.2	4.2	25	2	50	0.46	0.036
FZD-60	72.3	0.48	12	0.0185	0.28	0.01	32.8	2.6	12	10.5	10	0.5	0.8	6.4	7	1.9	57	0.24	0.004
FZD-59t	71.9	0.26	5	0.0092	0.13	0.01	35.1	2.2	8	8	10.9	0.6	0.5	0.5	6	1	54	0.17	0.002
FZD-59m	71.5	0.11	3	0.0055	0.07	0.01	34.9	2.3	6	5.2	10.6	0.8	0.5	2.7	7.5	1	54	0.14	0.001
FZD-59b	71.0	0.19	4	0.0091	0.11	0.01	35.9	2.2	10	4.9	11.6	0.5	0.7	0.9	7.7	0.4	41	0.19	0.003
FZD-58b	69.3	0.01	< 1	0.0006	0.02	< 0.01	35.9	1	5	18.9	10.4	0.5	< 0.5	0.7	3.2	< 0.1	27	0.08	< 0.001
FZD-57	68.0	0.02	< 1	0.001	0.02	< 0.01	35.1	1	5	6.8	10	0.5	< 0.5	1.6	15.7	< 0.1	19	0.08	< 0.002
FZD-56	66.4	0.03	< 1	0.0015	0.03	< 0.01	35.5	1.1	5	6.3	10.4	0.5	1.6	9.6	2.7	< 0.1	27	0.09	0.001
FZD-55b	65.4	0.07	1	0.0033	0.05	0.01	31.1	0.7	4	7.2	8.2	0.4	< 0.5	2.1	3.9	0.2	41	0.09	0.001
FZD-54b	62.6	0.22	5	0.0137	0.14	0.01	36.7	1.2	5	2.7	10.8	0.6	0.7	2.3	14.1	0.52	29	0.21	0.003
FZD-53m	60.8	0.04	2	0.0019	0.04	< 0.01	37.4	0.8	3	0.7	10.3	0.5	0.8	2.4	6.7	0.33	21	0.1	0.001
FZD-48t	53.9	0.01	< 1	0.0016	0.02	< 0.01	36.8	1.2	8	4.6	10.4	0.5	< 0.5	2.3	2.5	0.78	6	0.1	0.004
FZD-47m	45.9	0.03	1	0.0015	0.03	< 0.01	36.6	0.8	4	1.5	10.2	0.5	< 0.5	1.3	4.2	0.14	10	0.1	0.002
FZD-42b	37.2	0.07	4	0.0037	0.05	0.01	38.1	1.8	11	1.4	18.5	0.6	0.6	41.5	5.9	1.03	27	0.17	0.002
FZD-40t	33.4	0.02	1	0.0011	0.03	< 0.01	37.8	0.8	6	2.4	10.5	0.5	< 0.5	< 0.2	1.1	0.63	24	0.1	0.001

Bed/ Sample	Distance base (m)	Al (%)	Zr (ppm)	Ti (%)	K (%)	Na (%)	Ca (%)	U (ppm)	V (ppm)	Cr (ppm)	Ni (ppm)	Co (ppm)	Pb (ppm)	Cu (ppm)	Zn (ppm)	Mo (ppm)	Mn (ppm)	Fe (%)	P (%)
FZD-40b	31.3	0.06	2	0.0031	0.04	0.02	28.1	0.7	4	< 0.5	14.4	0.9	0.6	5.8	7.4	0.6	46	0.25	0.002
FZD-39m	29.7	0.17	4	0.0068	0.09	0.03	40.9	2.2	9	4.6	11.7	1.1	< 0.5	2.5	5.2	1.9	48	0.35	0.003
FZD-38	28.4	0.39	19	0.0276	0.23	0.01	35.8	0.9	7	1.9	10.5	1	0.6	3.4	9.5	1.3	57	0.4	0.005
FZD-37t	28.1	0.17	9	0.0059	0.1	0.02	37.4	1.3	5	4	12	0.6	< 0.5	2.6	12.9	0.39	35	0.14	0.002
FZD-34	24.9	0.39	11	0.0367	0.22	0.03	24.4	3.2	12	< 0.5	11.6	1	0.8	2.9	8.1	12.8	75	0.39	0.007
FZD-33b	22.7	0.1	4	0.0053	0.06	0.03	30.2	2.9	6	< 0.5	12.1	0.7	< 0.5	1.4	2.1	2.5	54	0.27	0.006
FZD-31	21.5	1.08	38	0.0614	0.91	0.03	27.4	3.2	57	31.1	20.2	1.2	1.7	5.2	11.7	4.3	79	0.69	0.007
FZD-30d	19.2	0.12	3	0.0074	0.12	0.01	36.1	1.7	9	2.7	17.3	0.6	< 0.5	0.4	8.1	2.45	26	0.17	0.001
FZD-30a	15.3	0.13	6	0.0077	0.09	0.02	32.8	2.5	11	5	15	0.7	0.7	1.5	17.4	2.2	39	0.17	0.002
FZD-29	14.5	0.4	9	0.0195	0.22	0.05	29.7	3.9	29	2.7	19.5	0.8	1.4	4.2	18.9	3.2	68	0.29	0.003
FZD-28t	14.0	0.05	3	0.005	0.05	0.01	34.2	2.6	16	< 0.5	13.6	0.8	< 0.5	2.1	8.8	0.75	49	0.12	0.002
FZD-27t	13.3	0.36	5	0.0264	0.28	0.03	34.4	2.8	31	5.3	15.6	0.9	0.8	3.5	15.3	1	76	0.37	0.004
FZD-27b	12.9	1.28	52	0.0454	0.84	0.02	31.2	3.6	71	9.9	17.1	0.9	1.8	2.5	16.5	0.4	151	0.43	0.006
FZD-26b	11.6	0.58	8	0.0357	0.46	0.01	32.7	1.7	21	4.2	11.7	0.8	0.8	9.4	10.9	2.34	68	0.38	0.004
FZD-25t	10.2	0.44	7	0.0249	0.43	0.07	33.2	3.6	20	1.6	14.2	0.7	0.7	4.9	8.3	6.93	61	0.33	0.009
FZD-22	7.4	0.47	12	0.0311	0.38	0.02	27.5	2.6	16	2.6	11.4	1	0.8	1.8	4.4	3.14	62	0.37	0.004
FZD-21	6.6	0.69	15	0.0421	0.48	0.03	29.1	4	23	8.5	14.6	1.7	1.2	5.9	6	11.8	84	0.49	0.009
FZD-19	5.8	0.17	7	0.0095	0.13	0.01	29.8	1.3	13	< 0.5	11.8	0.6	< 0.5	1	3.9	1.35	53	0.16	0.004
FZD-18	5.5	0.21	5	0.0128	0.17	0.02	17.8	1.4	17	9.9	9.8	0.6	< 0.5	2	4.4	1.6	57	0.18	0.005
FZD-14	3.9	0.48	13	0.0213	0.3	0.08	23.5	1	7	6.7	8.6	0.8	1.2	3.2	9.9	1.2	127	0.33	0.006
FZD-12	3.2	0.72	17	0.0243	0.39	0.06	29.8	1.5	11	8.7	11.3	1.1	1.4	4.7	5.1	1.5	90	0.37	0.005
FZD-10	2.6	0.62	16	0.0222	0.36	0.05	30.4	1.6	11	9.5	11.1	1.1	1.2	3.2	4.3	1.1	107	0.37	0.006
FZD-9	2.1	1.38	49	0.0873	1.17	0.05	30.1	6.2	68	20.4	28.6	2.4	1.7	10.8	18.7	14.1	111	1.03	0.024
FZD-8	1.5	0.19	5	0.0061	0.15	0.04	38	1.5	10	15.7	14.1	0.8	0.7	2.9	6.4	1.4	76	0.27	0.003
FZD-5	0.6	0.19	8	0.0073	0.15	0.03	39.1	2.1	9	5.1	12.7	0.8	0.7	2.3	5.4	2.2	114	0.23	0.002
FZD-4b	0.0	0.52	16	0.023	0.29	0.05	38.2	2.2	14	7.5	12.7	1	1.2	2.5	6.8	3.5	86	0.35	0.004

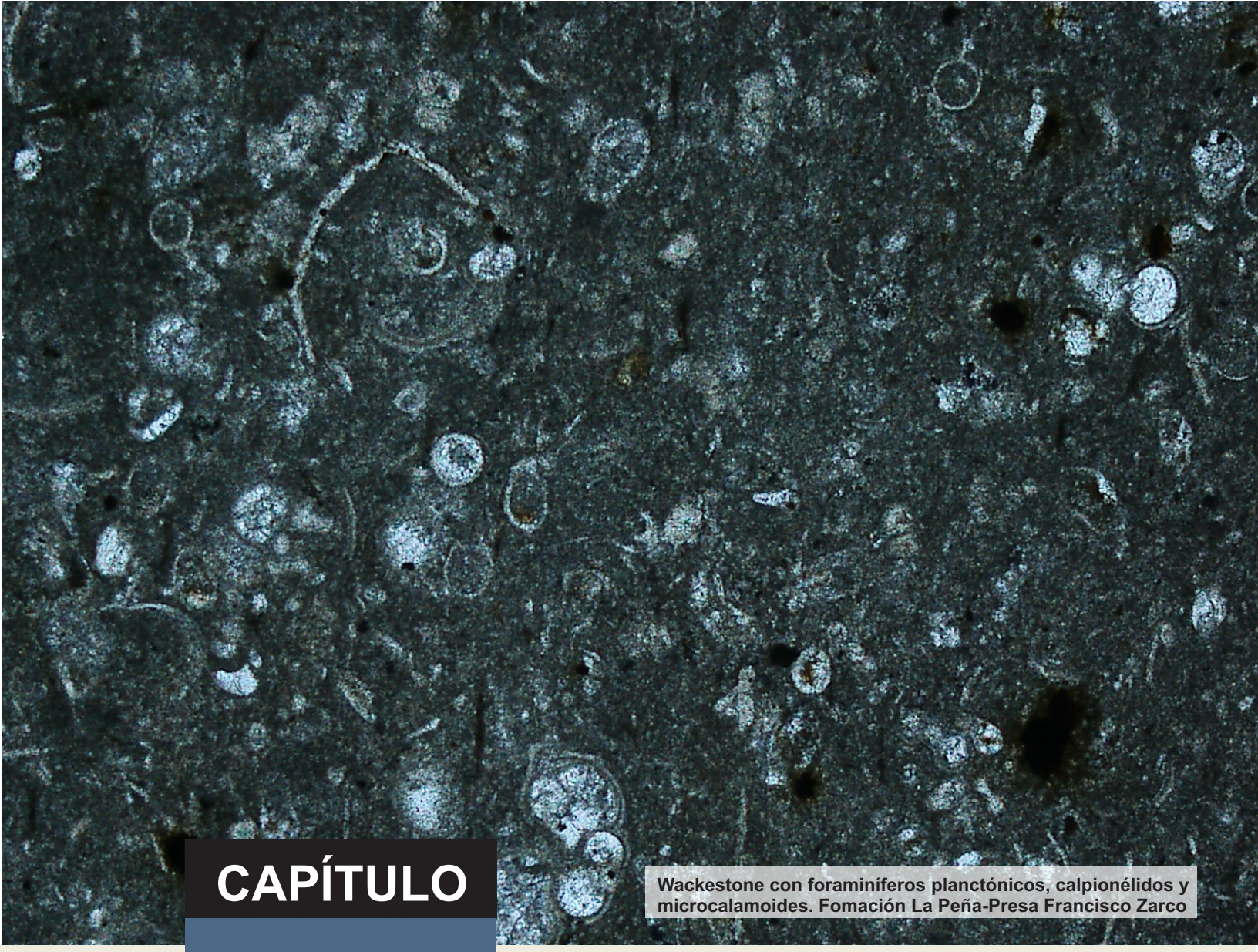

Wackestone con foraminíferos planctónicos, calpionélidos y microcalamoides. Fomación La Peña-Presa Francisco Zarco

CAPÍTULO

5

PERTURBACIÓN GLOBAL DURANTE EL APTIANO-ALBIANO EN EL NORESTE DE MÉXICO: OAE 1B

Artículo: **Núñez-Useche, F.**, Barragán, R., Canet, C., López-Martínez, R., Record of upper Aptian–lower Albian environmental perturbation in northeastern Mexico. Sometido a Journal of South American Earth Sciences.

Record of upper Aptian–lower Albian environmental perturbation in northeastern Mexico

Fernando Núñez-Useche[1], Riardo Barragán[2], Carles Canet[3], Rafael López-Martínez[2]

[1]*Posgrado en Ciencias de la Tierra, Universidad Nacional Autónoma de México, Del. Coyoacán, 04510 México D.F., Mexico*
[2]*Instituto de Geología, Universidad Nacional Autónoma de México, Del. Coyoacán, 04510 México D.F., Mexico*
[3]*Instituto de Geofísica, Universidad Nacional Autónoma de México, Del. Coyoacán, 04510 México D.F., Mexico*

Keywords:
Oceanic Anoxic Event 1b
Carbon- and strontium-isotope stratigraphy
Colomiellid biostratigraphy
Deep-water carbonates
Organic-rich sediments

ABSTRACT

Here we combine colomiellid biostratigraphy and strontium-isotope data of the upper Aptian–lower Albian, pelagic and organic-rich interval of the La Peña Formation in northeastern Mexico (western Gulf of Mexico basin). The studied sediments recorded a long-term negative carbon-isotope excursion during the Aptian–Albian transition recognizable worldwide and related to the Oceanic Anoxic Event (OAE) 1b set interval. Furthermore, punctuated and short-term negative spikes show values and positions similar to those associated with the Jacob, Kilian, Paquier and Leenhardt episodes. The highest total organic carbon (TOC) values and detrital mineral (quartz and phyllosilicate) contents occur during in the ^{13}C-depleted trend. An increase in the detrital index and the absence of feldspars suggest warm and humid conditions that may have led to intense biogeochemical weathering and runoff. An increased runoff may have been the cause of the $\delta^{13}C$ decrease, resulting in density stratification of the basin that favored the preservation of organic-matter under oxygen-depleted bottom water conditions.

1. Introduction

The Aptian–Turonian time interval witnessed the deposition of several discrete organic-rich horizons associated to isochronous, short-lived global perturbations of the carbon cycle (e.g., Leckie et al., 2002; Trabucho et al., 2011; Föllmi, 2012). These perturbations are the result of accelerated global/supra-regional episodes of environmental change commonly referred to as Oceanic Anoxic Events (OAEs) and are characterized by oxygen depletion in intermediate and bottom-water masses (e.g., Schlanger and Jenkyns, 1976; Jenkyns, 1980). Across the Aptian–Albian transition, such intervals are represented by a set of black shale horizons of which the most prominent are the uppermost Aptian Jacob and Kilian levels, and the lower Albian Paquier and Leenhardt levels, as defined in the Vocontian Basin, SE France (Herrle et al., 2004). The organic-rich levels that represent the Kilian (*ca* 112.5 Ma) and Paquier (*ca* 112 Ma) events are the most widespread of these horizons, being recorded in many sites of the Western Tethys and North Atlantic (Erbacher et al., 1999; Kuypers et al., 2002; Herrle, 2004; Tsikos et al., 2004; Wagner et al., 2007; Hofmann et al., 2008).

Among the Cretaceous OAEs, the OAE 1b is considered to result from a global perturbation of the global carbon cycle which was likely less significant than other OAEs, and consequently less studied. Unlike the early Aptian OAE 1a and the Cenomanian–Turonian OAE 2, which are both characterized by positive carbon-isotope excursions linked to high marine productivity (productivity-driven OAEs, according to Erbacher et al., 1996), the late Aptian–early Albian perturbations have more variable and less distinctive carbon-isotope signature and sedimentary expressions, determined by the effects of regional/local dissimilar paleoceanographic conditions (Wagner et al., 2007; Trabucho Alexandre et al., 2011; Sabatino et al., 2015). For instance, at some sites of the Western Tethys (e.g., Vocontian Basin) and North Atlantic (e.g., Mazagan Plateau, off Morocco, eastern North Atlantic), the Kilian and Paquier events are defined

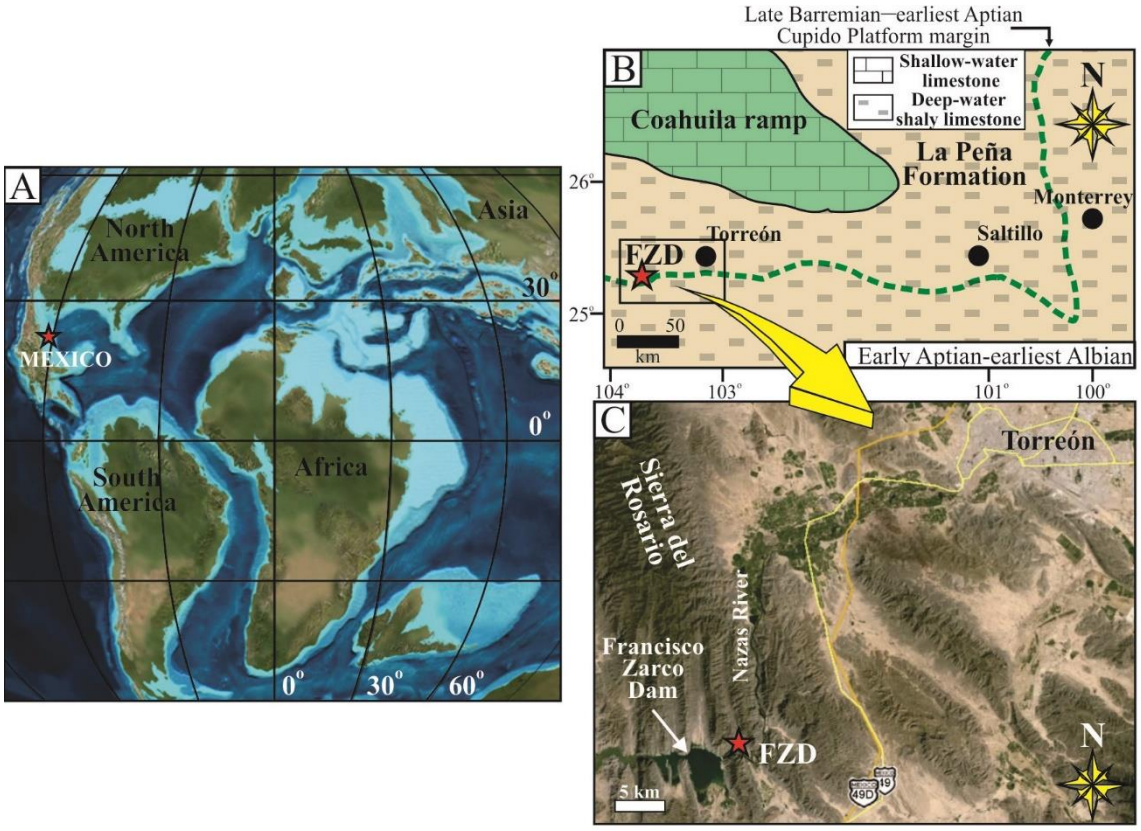

Fig. 1. Location of the section studied. A–Paleogeographic location of the Francisco Zarco Dam section (FZD) section, Mexico (early Albian paleogeographic map redrawn from Blakey website); B–Late Aptian–early Albian paleogeographic map of northeastern Mexico (modified from Lehmann et al., 1999); C–Location of the outctop in a Google Earth image of the boxed area in B.

by distinctive negative shifts in both marine carbonate ($\delta^{13}C_{carb}$) and organic matter ($\delta^{13}C_{org}$) carbon-isotope records with amplitudes of 1.5–2‰ and 2–4‰, respectively (Herrle et al., 2004; Wagner et al., 2007, 2008; Hofmann et al., 2008; Trabucho Alexandre et al., 2011). Nonetheless, in other sites (e.g., Umbria Marche Basin, central Italy, and Blake Nose Plateau, off Florida, western North Atlantic) they are represented by dissimilar and more complex shifts in $\delta^{13}C_{carb}$ and $\delta^{13}C_{org}$ records (Wagner et al., 2008; Trabucho Alexandre et al., 2011; Sabatino et al., 2015). Due to this variability, the feedback mechanism responsible for the perturbation in the climate/ocean dynamics during the late Aptian–early Albian remains still unclear. While some authors restrict the term OAE 1b to the lower Albian Paquier event (Erbacher et al., 2001; Hofmann et al., 2008), others consider the OAE 1b as a longer perturbation of the carbon-cycle embracing the four aforementioned short-lived episodes of accumulation of organic-rich sediments and peaking during the Paquier event (Leckie et al., 2002; Trabucho Alexandre et al., 2011; Föllmi, 2012; Coccioni et al., 2015; Sabatino et al., 2015).

In this paper, we present new chemostratigraphic and age data, along with mineralogical composition and total organic carbon content from an Aptian–Albian boundary section from northeastern Mexico, corresponding to the central North Atlantic Basin (western Gulf of Mexico basin). The aims of this study are to document the carbon-isotope variability, to explore its link to the global carbon cycle perturbation during OAE 1b, and to determine the processes that drove its occurrence. Our results expand the known records of OAE 1b to a site of the western margin of the North Atlantic and provide insights into the paleoceanographic evolution of this particular site during the event.

2. Geological setting and studied section

The Mesozoic tectonic and stratigraphic evolution of northeastern Mexico is the result of a complex superposition of events associated with two different provinces (Goldhammer, 1999): (*a*) the eastern Gulf of Mexico Province, related to the creation of a passive margin followed by the opening of the Atlantic Ocean, and (*b*) the western Pacific Mexico Province, governed by a convergent plate boundary. In such an intricate geological scenario, and during the Cretaceous crustal cooling stage, regional tectonic subsidence led to the flourishing of extensive carbonate platforms in the eastern Gulf of Mexico province during the Barremian–Albian interval, interrupted by punctuated episodes of clastic deposition (Wilson and Pialli, 1977; Conklin and Moore, 1977; Goldhammer et al., 1991; Wilson and Ward, 1993; Lehmann et al., 1998, 1999; Goldhammer, 1999).

The La Peña Formation is a mixed carbonate-argillaceous unit that crops out over an extensive area of northeastern Mexico. This unit was deposited during the peak of a major transgressive event in the eastern Gulf of Mexico Province and is a marker pelagic unit separating the development of the Barremian–early Aptian Cupido/Cupidito shelf (Cupido Formation/Cupidito unit) from the overlying late Aptian–Albian Coahuila ramp (Acatita/Aurora Formations) and coeval deep-water sediments (Upper Tamaulipas Formation) (Lehmann et al., 1999, 2000; Goldhammer, 1999; Barrargan, 2001; Humphrey and Diaz, 2003; Moreno-Bedmar et al., 2013). The base of this unit is diachronic as it has an early Aptian age (near coinciding with the onset of the OAE 1a) in basinal sections (Bralower et al., 1999; Li et al., 2008) and a late early Aptian age (upper part of the *Dufrenoyia furcata* ammonite Zone) in shelfal sections (Barragan, 2001; Barragán and Maurrasse, 2008; Moreno-Bedmar et al., 2013), almost just above the Intra-Furcata Negative Excursion (IFNE; Núñez-Useche et al., 2014) in the topmost part of the Cupido Formation (Núñez-Useche et al., 2015). Likewise, the top of the La Peña Formation is also a time-transgressive formation boundary (Goldhammer, 1999). The thickness of this unit is highly variable depending on the antecedent depositional paleorelief (Maldonado and Tello, 1976; Tinker, 1982; Cantú-Chapa, 1989). Goldhammer et al. (1991) considered differential compaction of subjacent lithologies as a probable factor controlling the width of this unit.

The Francizo Zarco Dam (FZD) section, studied in this research, is located in the southern portion of the Sierra del Rosario (25° 16′ N/103° 46′ W), Durango State, near the city of Torreón (Fig. 1), and is part of the southern shoal margin of the ancient Cupido platform (Fig. 1). It consists of massive limestone of the Cupido Formation (Cupidito unit), interbedded thin to medium-bedded shaly limestone and shale of the La Peña Formation, and medium to thick-bedded limestone of the Upper Tamaulipas Formation (Figs. 2 and 3). The La Peña Formation of the FZD section has a thickness of 110.9 m and is one of the most expanded and complete sections of the unit across the upper Aptian–Albian interval. In this paper we focus on a 58 m interval corresponding to the middle part of the unit and characterized by the progressive disappearance of ammonite and shale beds (typical of the underlying interval), and the presence of shaly limestone containing chert nodules and lenses parallel to bedding and diagenetic chert beds. Núñez-Useche and Barragán (2012) characterized and illustrated in detail the microfacies associations of this interval. They are as follows:

(A) Wackestone and packstone with extremely abundant radiolaria, common planktonic foraminifera and ostracods, and rare pelecypods (including inoceramids) and ammonite fragments; and

(B) Mudstone and wackestone with colomiellids, planktonic foraminifera and calcispheres.

These associations are interpreted as deposited in an open marine environment in a deep outer neritic to upper bathyal zone.

3. Material and methods

A total of 58 thin sections of shaly limestone beds previously prepared for microfacies analysis (Nuñez-Useche and Barragán, 2012) were observed under transmitted light microscopy (Olympus BX60) to study the vertical distribution of colomiellids according to the biozonation scheme of Trejo (1975) and Borza (1979).

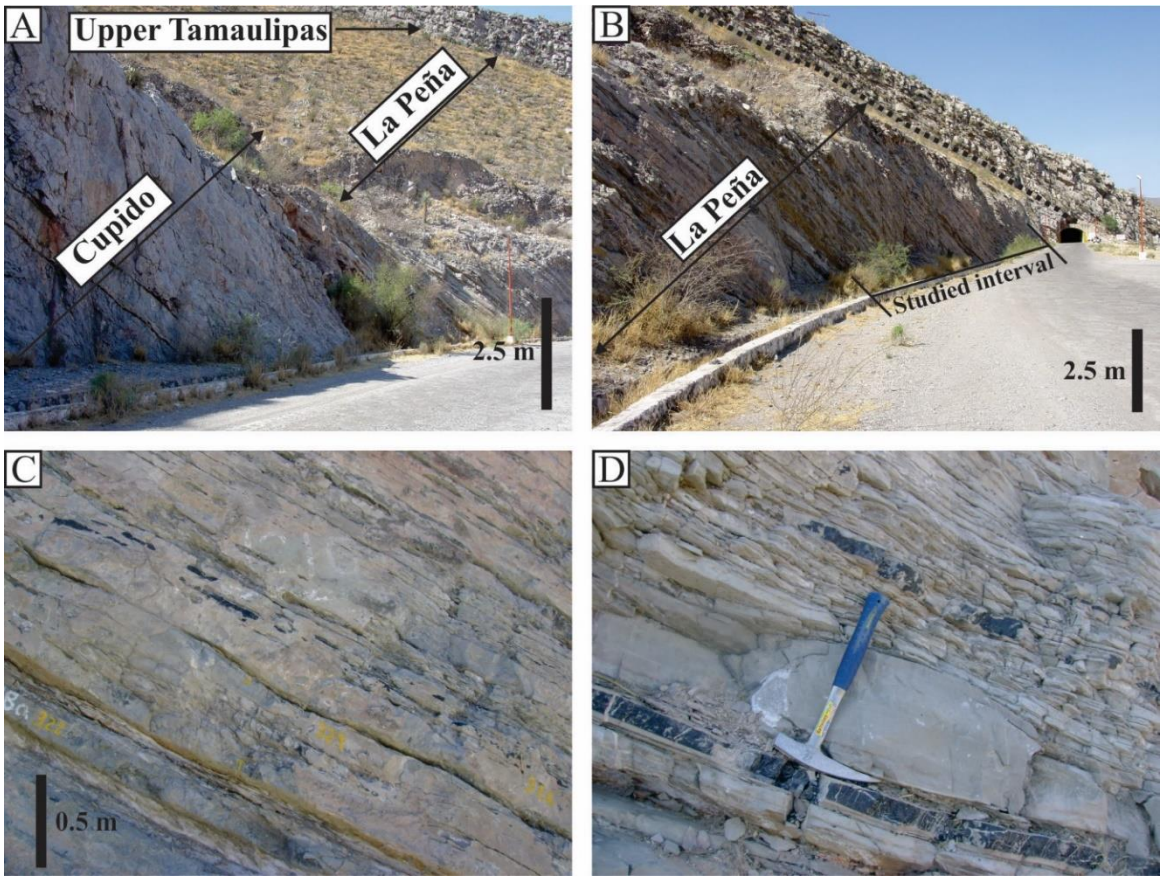

Fig. 2. Outcrop photographs. A–General view of the FZD section; B–Intercalation of thin-bedded shaly limestone and shale beds of the La Peña Formation and indication of the studied interval; C, D–Typical chert nodules and lenses.

Strontium-isotope ratios are usually measured in well-preserved fossils to obtain the $^{87}Sr/^{86}Sr$ signature of past seawater (Veizer, 1989; Bralower et al., 1997; Jones and Jenkyns, 2001); however, some studies (Prokoph et al., 2008; Madhavaraju et al., 2013a) have demonstrated that sometimes this signature can also be obtained successfully from bulk-rock samples. Considering the feasibility of this approach, in this research we analyzed 5 samples of carbonate matrix from shaly limestone beds (that lack signs of diagenetic alteration) for their strontium-isotope composition. These samples were oven dried (40 °C) and powdered using an agate mortar and pestle to <75 μm. They were analyzed at the *Laboratorio Universitario de Geoquímica Isotópica* (LUGIS), *Universidad Nacional Autónoma de México* (UNAM), using a Thermo Scientific Triton Plus mass spectrometer in static mode. Total blanks of strontium were 1.49 ng. The $^{87}Sr/^{86}Sr$ value of the internal standard (NBS987) was 0.710244 ± 12 (±1 SD, n= 33). All the analyses were normalized to an $^{86}Sr/^{88}Sr$ ratio value of 0.1194. Numerical ages were calculated using the look-up table (version 3:10 / 99; Howarth and McArthur, 1997). Sr, Fe and Mn concentrations in aliquots were analyzed at the Activation Laboratories Ltd. (Actlabs), Canada, to exclude diagenetic alteration and to evaluate the reliability of strontium-isotope data. These analyses were conducted by inductively coupled plasma mass spectrometry (ICP-MS; Perkin Elmer Sciex ELAN 9000) after the digestion of 1.0 g of sample using four different acids (HF, $HClO_4$, HNO_3 and HCl) (Package code Ultratrace 6). Percentages of the relative standard deviation were consistently below 10% as checked by standards and analysis of replicate samples.

Bulk-rock total carbon and total inorganic carbon were determined in 31 powdered samples with a HiperTOC solid analyzer (Thermo Scientific) at the *Laboratorio de Paleoambientes* of the *Instituto de Geología*, UNAM. The concentration of total carbon was measured by heating the sample to 980 °C, and total inorganic carbon was determined

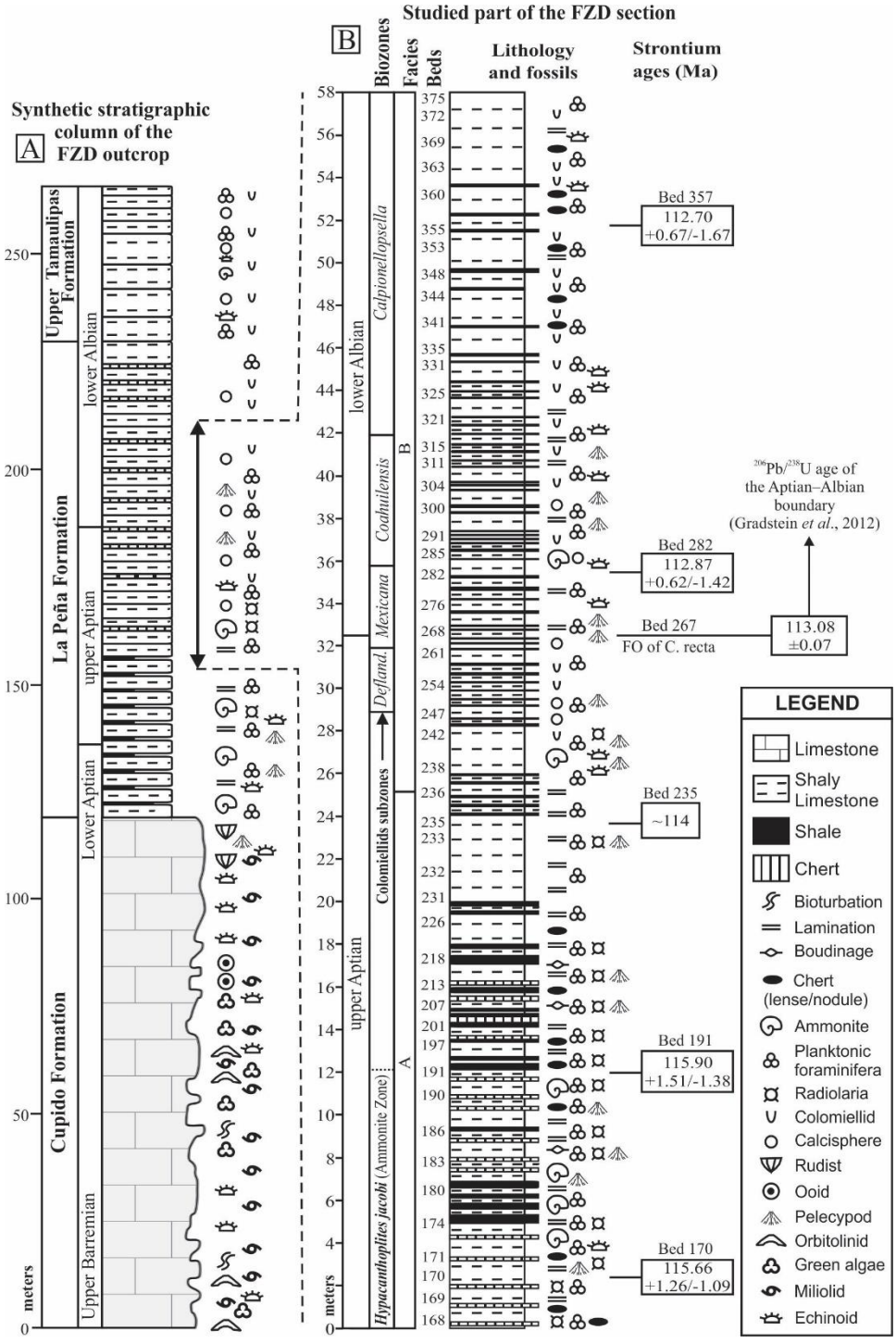

Fig. 3. A–Synthetic stratigraphic column and age distribution of the FZD section (modified from Núñez-Useche and Barragán, 2012 and Núñez-Useche et al., 2015); B–Studied interval with lithology, fossils and facies. Colomiellid and ammonite biostratigraphy and strontium-isotope age assignments are also shown.

by acidifying the sediment with 10% H_3PO_4. The total organic carbon (TOC) content was calculated by subtracting the total inorganic carbon from total carbon.

Carbon-isotope analysis was carried out on 70 carbonate samples obtained with a dental drill with a tungsten bit from the micritic matrix of shaly limestone. While microdrilling the polished hand samples under a binocular microscope, cements, calcite veins, macrofossils or areas altered by circulation of meteoric water were avoided. The analysis was performed at the LUGIS, UNAM.

Approximately 0.9 mg of sample was reacted under vacuum with orthophosphoric acid at 25 °C for 54 hours following the guidelines of McCrea (1950). The released CO_2 was analyzed with a mass spectrometer Thermo Finnigan MAT 253 coupled with Gas Bench II. Carbon-isotope values of carbonate fraction ($\delta^{13}C_{carb}$) are reported in permil relative to the VPDB (Vienna Pee Dee Belemnite) standard. Repeated analyses of samples and internal standards show a reproducibility better than 0.2‰

Mineralogical analyses were performed by X-ray diffraction (XRD) at the *Instituto de Geología*, UNAM, on 24 samples. For the XRD procedure, the samples were ground with an agate pestle and mortar to <75 μm and mounted in aluminum holders. The analyses were carried out on randomly oriented samples with a PANalytical Empyrean powder X-ray diffractometer equipped with a Ni Filter, a Pixel 3D detector and a Cu tube. Step-scanned data was collected from 5 to 70° (2θ) with an integration time of 40 s per 0.003° (2θ). The semi-quantitative results were based on the intensity of the corundum peak as a standard for a relative intensity ratio (RIR; Chung, 1974; Hillier, 2000). Detrital index (DI) was obtained by dividing the sum of quartz and phyllosilicates contents by calcite (in wt. %). This parameter is used to observe changes in detrital influx versus marine carbonate input.

All analytical data presented are available electronically in the Supplementary Appendix A.

4. Results

4.1. Biostratigraphy

Colomiellids are continuously present from 28.8 m (bed 248) above the base of the section upward. Their vertical succession in this interval allows us to identify five subzones as follows (bottom to top) (Fig. 3):

-Deflandronella Subzone (Trejo, 1975). This subzone is characterized by the First Occurrence (FO) of micro granular colomiellids at 28.8 m (bed 248). Two species are recorded: *Parachitinoidella cuvillieri* Trejo (Fig. 4A) and *Deflandronella veracruzana* Trejo (Fig. 4B).

-Mexicana Subzone (Trejo, 1975). The base of the subzone is characterized by the FO of *Colomiella mexicana* Bonet at 31.8 m (bed 263) (Fig. 4C). Mexicana subzone includes the Aptian–Albian boundary and can be detected by the FO of *Colomiella recta* Bonet at 33.8 m (bed 267) (Fig. 4D).

-Coahuilensis Subzone (Trejo, 1975). The base of this subzone is characterized by the FO of *Colomiella coahuilensis* Trejo at 35.7 m (bed 283) (Fig. 4E). It is noteworthy, however, that in studied samples *C. coahuilensis* is very scarce and specimens are smaller than those described by Trejo (1975) and Borza (1979).

-Calpionellopsella Subzone (Trejo, 1975). This subzone is defined by the FO of *Calpionellopsella maldonadoi* Trejo at 41.8 m (bed 318) (Fig. 4F) and extends up to the top of the section.

4.2. Strontium-isotope stratigraphy and trace element concentrations

The $^{87}Sr/^{86}Sr$ ratios from marine calcite are a powerful chemostratigraphic tool for dating and correlating sedimentary successions (Veizer, 1989; Bralower et al., 1997; Jones and Jenkyns, 2001; McArthur et al., 2004, 2012; Madhavaraju et al., 2013a). The strontium-isotope composition of the herein analyzed samples is given in Table 1. $^{87}Sr/^{86}Sr$ ratios vary from $0.707295 \pm 29\times10^{-6}$ (bed 170) towards the base of the section to $0.707288 \pm 39 \times10^{-6}$ (bed 357) at its uppermost part. Regarding to numerical ages, the ratios $^{87}Sr/^{86}Sr$ ratios indicate, respectively, a late Aptian (mean age of 115.90 Ma) and an early Albian (mean age of 112.70 Ma) age (Table 1 and Fig. 3). The middle part of the section records a minimum ratio of $0.707189 \pm 36\times10^{-6}$ (bed 235), which on average is slightly below the Aptian–Albian values (Howarth and McArthur, 1997; Jones and Jenkyns, 2001) and indicates an offset age. However, considering the error, the maximum value is rather similar to the lowest $^{87}Sr/^{86}Sr$ ratio occurring in the latest Aptian strontium-isotope record (0.707200, Kennedy et al., 2000; 0.70725, Jones and Jenkyns, 2001; 0.707221; Madhavaraju et al., 2013a; and 0.70722, McArthur et al., 2012), approximately

at 114 Ma (McArthur et al., 2012) (Fig. 3), as result of an increased pulse of mid-plate volcanic activity and the input of ^{86}Sr to the ocean during the emplacement of the Manihiki and the Southern Kerguelen Plateaus (Bralower et al., 1997; Erba et al., 2015).

Previous numerical ages are validated by the coherence with the constructed colomiellid biozonation scheme defining the Aptian–Albian boundary (with a $^{206}Pb/^{238}U$ age of 113.08 ± 0.07 Ma, according to Gradstein et al., 2012) (Fig. 3), and the previous report of the *Hypacanthoplites leanzae* ammonite zone at the base of the section (Barragán, 2000) (Fig. 3),equivalent to the latest late Aptian *Hypacanthoplites jacobi* Zone of the ammonite standard biozonation of the Mediterranean province (Reboulet et al., 2014). Nonetheless, the scarcity of ammonite fossils in the middle and upper part of the section does not allow the proper identification of the top of this zone. Furthermore, the reliability of the obtained numerical ages is verified by the trace element concentrations (Table 1). Mn (46–83 ppm) and Fe concentrations (26–75 ppm) are below the threshold value of 100 ppm considered for diagenesis (Steuber et al., 2005; Mutterlose et al., 2009). Likewise, the Mn/Sr ratios are below 2, thus pointing to an unaltered isotope signature (Kaufman et al., 1993; Jacobsen and Kaufman, 1999). These results imply that analyzed micritic calcite matrix can be accepted as near-primary calcite retaining the original seawater strontium-isotope composition.

4.3. Carbon geochemistry: $\delta^{13}C$ and TOC

Carbon stable isotope values of the carbonate fraction ($\delta^{13}C_{carb}$) vary between +0.51‰ and +3.60‰ with an average of +2.35‰ (Fig. 5). A relatively uniform trend defines the lowermost 14.3 m of the studied interval, with variations between +2.01‰ and +2.67‰. From 14.3 m there is a prominent long-term negative carbon-isotope excursion of 2.09‰ that ends at 40.8 m, forming a distinct negative peak of +0.51‰. This long-term negative excursion spans the upper part of the upper Aptian until the lower part of the lower Albian, and covers 26.5 m through the transition from microfacies association VI to VII. It also contains four negative spikes at 18.5 m (+1.46‰), 27.9 m (0.89‰), 34.7 m (+0.68‰) and 40.8 m (+0.51‰). The uppermost 14.4 m of the section records the return towards pre-excursion values and is defined by an overall positive trend in $\delta^{13}C_{carb}$, reaching a maximum value of +3.6‰ at 53.7 m.

In addition to the TOC values calculated herein, Figure 5 shows the TOC values determined by Barragán (2000). TOC values range between 0.1% and 7.5% (average 3.1%), with the higher values (>4%) recorded within the following levels: at 4.1 m (4.5%), 6.5 m (5.5%), 11.4 m (4.6%), 11.8 m (5.7%), 12.5-14.3 m (up to 5.0%), 25.0-26.1 (up to 6.0%), 32.2-35.4 m (up to 7.5%), and at 55.9 m (5.0%). Highest TOC values are observed within the studied interval coincide with the negative carbon-isotope excursion.

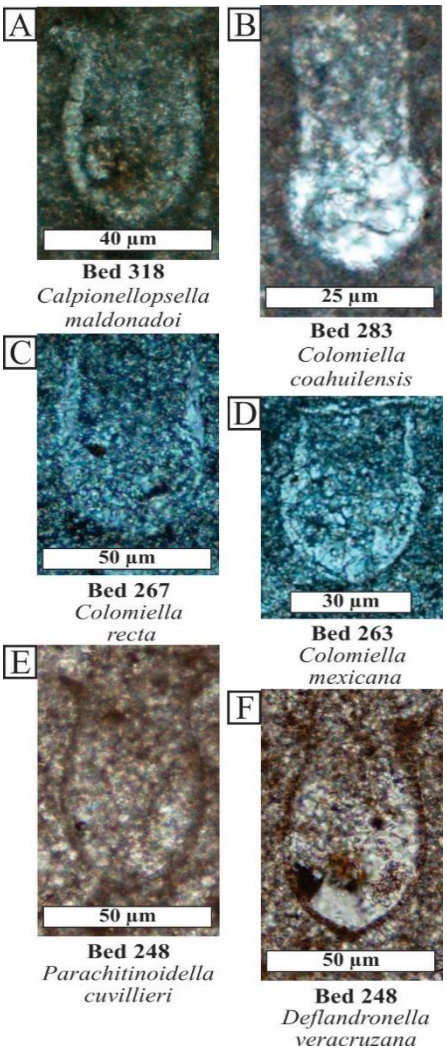

Fig. 4. Photomicrographs of colomiellids from the studied interval.

Table 1. Sr-isotopes and trace elements values of the analyzed samples from the FZD section and derived numerical ages.

Bed/ Sample	Distance base (m)	Mn (ppm)	Fe (ppm)	Sr (ppm)	$^{86}Sr/^{87}Sr$	±1SD ($\times 10^{-6}$)	Age	Age (Ma) Lower limit	Upper limit
FZD-357	102.3	67	41	450	0.707288	39	112.70	111.03	113.17
FZD-282	100.2	83	26	490	0.707278	36	112.87	112.45	113.29
FZD-235*	98.8	46	48	334	0.707189	36	–	–	–
FZD-191	97.9	51	75	288	0.707300	39	115.90	114.52	117.41
FZD-170	96.9	63	44	408	0.707295	29	115.66	114.57	116.92

4.4. Mineralogy

The bulk-rock mineralogy of the sediments in the studied interval is shown in Figure 5. It consists mainly of calcite (64–90%), quartz (5–17%), phyllosilicates (0–18%), and fluctuating presence of pyrite (0–9%). No feldspar is observed. Phyllosilicates and quartz are more abundant in the interval between 19 and 44 m. Distinctive abundance peaks are observed at 25 m (11%), 30.2 m (18%), 35.4 m (11%) and 43.8 m (14%) for phyllosilicates; and at 30.2 m (14%) and 34.0 m (17%) for quartz. Calcite content slightly decreases in this interval showing a minimum value of 64% at 30.2 m. The DI fluctuates from 0.08 to 0.50 and shows a stratigraphic variation comparable to that of phyllosilicates content (R^2 = 0.71). The highest DI values correspond to the negative $\delta^{13}C$ excursion interval (Fig. 5).

5. Discussion

5.1. Correlations based on carbon-isotope stratigraphy

Paleontological studies of ammonites (Barragán, 2000) and colomiellids (Figs. 3 and 4), together with numerical ages derived from strontium-isotope stratigraphy (Table 1) assigned an overall late Aptian–early Albian age to the studied succession. During the Aptian–Albian boundary, the $\delta^{13}C_{carb}$ curve exhibits a long-term negative carbon-isotope excursion of 2.09‰ in magnitude (down to +0.51‰) (Fig. 6). This negative shift correlates well with that observed globally, indicating that late diagenetic processes did not entirely perturb the original signal, and therefore suggesting a change in the carbon cycle during this transition.

Very similar trend and values have been also identified in the $\delta^{13}C$ profile from the Vocontian Basin in the northern Tethys (Herrle et al., 2004), which is used as a Tethyan time-calibrated reference curve for the Barremian–Albian interval. In that basin the long-term negative trend in $\delta^{13}C$ occurs between carbon-isotope segments Ap15 and Al5 (Fig. 6). It is temporally equivalent to the OAE 1b set of Föllmi et al. (2006) that includes the black shales representing the Jacob, Kilian, Paquier and Leenhardt events. Comparatively, the same $\delta^{13}C$ pattern is observed in the Pacific Realm (Resolution Guyot, Jenkyns and Wilson, 1999; Pulluicana–Huameripashga composite section, Navarro-Ramirez et al., 2015), the central Tethys (Piobicco composite section, Erbacher et al., 1996; Poggio le Guaine section in the Umbria–Marche Basin, Sabatino et al., 2015); the southern Tethys (Kuh-e Bangestan section, Vincent et al., 2010; Bangbu section, Li et al., 2015), and in the Santa Rosa Canyon (Bralower et al., 1999) also in northeastern Mexico (Fig. 6). A similar, somewhat negative trend, probably associated with OAE 1b set, is also documented in the Aptian–Albian carbon-isotope curve of terrestrial organic matter from USA (Price River section; Ludvigson et al., 2010) and China (Chong'an section; Hu et al., 2014). Other relatively poorly defined records link to the OAE 1b are reported from northern Mexico (Cerro Pimas and Cerro El Caloso-Pitaycachi sections; Madhavaraju et. al, 2013a, b) and in the Comanche platform of Texas at the upper part of the Pearsall Formation–lower part of the Glen Rose Formation (Magnolia-Mercer #1 Core; Phelps et al., 2015), both cases equivalent to the La Peña–Aurora formations transition of northeastern Mexico. These records are related with a positive carbon-isotope excursion; however, the $\delta^{13}C$ profile of the Comanche platform seems affected by local diagenesis.

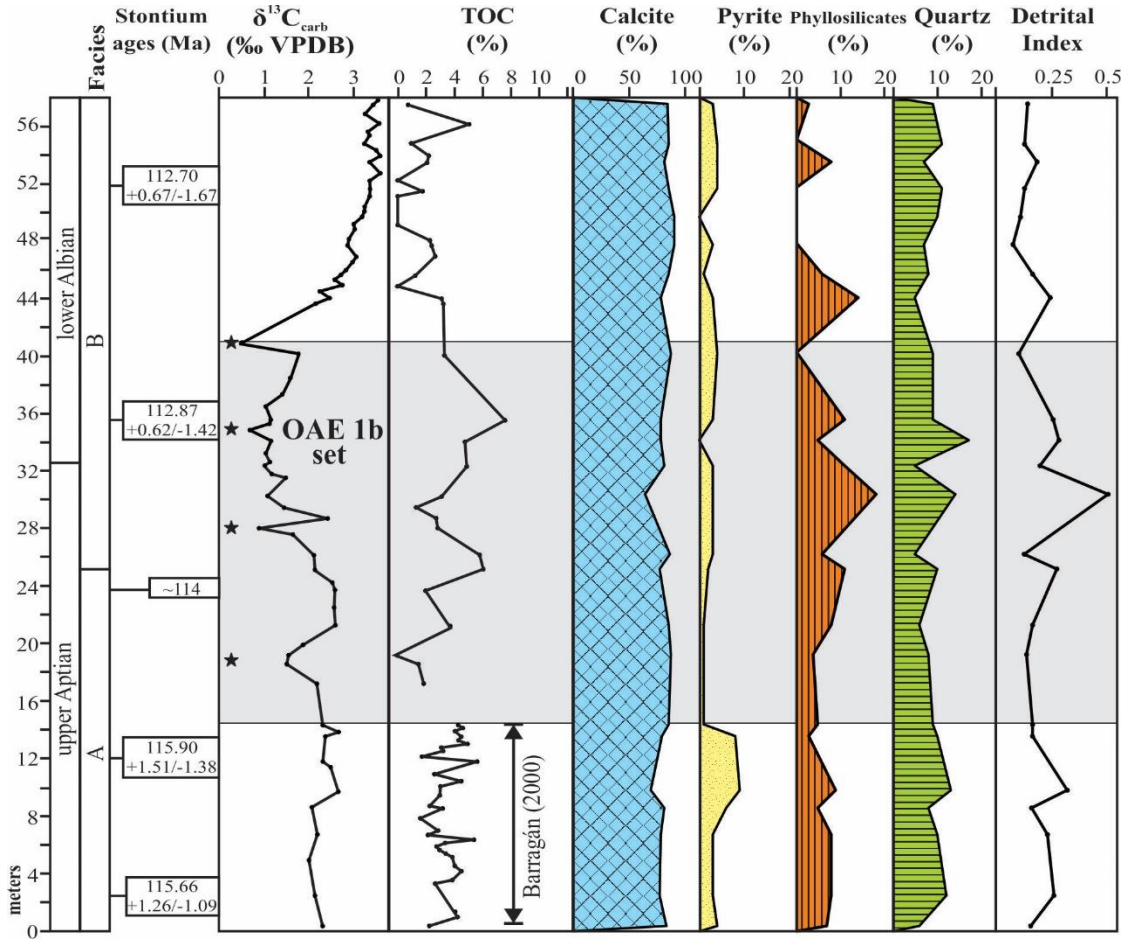

Fig. 5. $\delta^{13}C$, TOC, bulk-rock mineralogy and detrital index of the Francisco Zarco Dam section. Ages from strontium-isotopes are also shown. Marked organic-rich levels in the studied section have TOC content>4%. Short-term negative carbon-isotope spikes with values and positions similar to those associated with the Jacob, Kilian, Paquier and Leenhardt episodes are marked by black starts.

A remarkable feature of the $\delta^{13}C_{carb}$ curve of the studied interval is represented by the presence of a series of closely spaced negative spikes with values and a vertical distribution similar to those observed in the $\delta^{13}C_{carb}$ from the Vocontian Basin (Herrle et al., 2004), associated with the Jacob, Kilian, Paquier and Leenhardt episodes. This is in line with chemostratigraphic data from other North Atlantic sediments revealing that a $\delta^{13}C_{carb}$ negative shift is also associated with the Paquier event at Blake Nose (Erbacher et al., 2001) (although partially defined by a positive excursion in the bulk organic carbon; Kuypers et al., 2002; Trabucho Alexandre et al., 2011) and with the Kilian event at Mazagan Plateau (Wagner et al., 2007; Hofmann et al., 2008; Trabucho Alexandre et al., 2011). Unfortunately, our age resolution is not sufficient to properly identify each event.

5.2. Paleoenvironmental change during the late Aptian–early Albian interval

5.2.1. Climate conditions

The mineralogical composition of sediments and the DI provide important data regarding paleoenvironmental conditions such as sea-level fluctuation and climate change in source areas (e.g., Duchamp-Alphonse et al., 2011; Stein et al., 2012). Higher detrital mineral content —and DI values— reflect important delivery of terrigenous material from continental sources and/or decreased dilution by carbonate input. In the studied stratigraphic interval, the highest peaks in quartz and phyllosilicates abundance between 19 and 44 m (coinciding with a prominent increase in DI values), indicates a major

contribution of terrigenous material during this interval (Fig. 5). Given that the FZD section is characterized by a steady and long-term deepening of the depositional setting (Núñez-Useche et al., 2012), the observed mineralogical variations seem to reflect mainly paleoclimatic features rather than sea-level changes. Therefore, this higher proportion of detrital minerals may be the result of warm conditions that have led to intense biogeochemical weathering. A comparable higher supply of detrital components is also observed at Magazan Plateau during the Paquier event (Wagner et al., 2007; Hoffman et al., 2008). In the Umbria-Marche Basin, Tiraboschi et al. (2009) and Sabatino et al. (2015) documented several increases in proxies for detrital components (K/Al, Mg/Al, Ti/Al and Cr/Al) mostly related to the OAE 1b sub-events, thus indicating a major contribution of terrigenous material.

An increased contribution of terrigenous material is consistent with the extremely warm and humid conditions documented in the Blake Nose and the Mazagan Plateau sediments around the Aptian–Albian transition (Erbacher et al., 2001; Hofmann et al., 2008; Wagner et al., 2008; McAnena et al., 2013). An abrupt rise in sea surface temperature between ~3 and 4°C (up to ~31–32 °C) has been documented in those places on the basis of TEX86 data. In the studied interval of the FZD section, the absence of feldspars, a common detrital mineral in the lowermost 29.1 m of the La Peña Formation (up to 6.81%; Núñez-Useche et al., 2015), supports a warmer and more humid climate that favored the degradation of feldspars and formation of clay minerals. Indeed, the interval of the La Peña Formation investigated herein contains a higher proportion of phyllosilicates (up to 14%) when compared to the underlying interval (up to 5.4%; Núñez-Useche et al., 2015). The studied site and the proximal North American continental mass were both located within the northern edge of the tropical–equatorial hot arid climate belt of Chumakov et al. (1995), close to the latitudinal limit of the northern mid-latitude warm humid belt. However, the abundance of smectite (clay mineral associated with variation between dry and humid periods) in sediments of the Blake Nose (Pletsch et al., 1996; Rodríguez-López et al., 2008), together with our results, suggests less marked aridity for this source area. Thus, the prevailing climate in the adjacent landmass to the studied site caused high biogeochemical weathering and runoff.

5.2.2. A long-term carbon-isotope perturbation

Different studies suggest that $\delta^{13}C$ negative excursions that define OAE 1b sub-events are indeed primary global signals and propose heterogeneous mechanisms responsible for their occurrence. They include: (*a*) global cooling and consequent sea-level fall (Weissert and Lini, 1991; Kuypers et al., 2002; Herrle et al, 2004; Mutterlose et al., 2009; Trabucho Alexandre et al., 2011); (*b*) release of isotopically light CO_2 into the atmosphere link to the destabilization of gas hydrates (Wagner et al., 2007) and/or to the emplacement of the Kerguelen Plateau (Erba et al., 2015); (*c*) increase of continental runoff during warmer and more humid conditions and resulting amplified input of isotopically light terrestrial carbonate ions (Hofmann et al., 2008; McAnena et al., 2013; Sabatino et al., 2015). Indistinctly of the relatively instantaneous and extreme conditions that gave rise to these short-term negative spikes, certainly influenced by paleoceanographic local conditions, it is evident from Fig. 6 a long-term mechanism responsible for the continuous ^{13}C depletion in carbon pool and organic matter deposition throughout the Aptian–Albian boundary. This supports the proposal of Sabatino et al. (2015) regarding a unique, long-carbon cycle perturbation related to the OAE 1b, significant in terms of the global carbon cycle.

In the studied section, according to the ages inferred from strontium-isotopes (Fig. 2), the long-term negative carbon-isotope excursion interval is ~3-4 Myr long. This duration is comparable to that estimated by Sabatino et al. (2015) (~3.8 Myr) in the Umbria-Marche Basin. Although additional studies are required for a more convenient explanation, our results may provide some insight into the nature of this perturbation. Considering that in the studied interval the highest TOC and DI values occur within the OAE 1b set, we suggest that an increased runoff may have produced density stratification and consequent lower rates of deep water renewal, at this particular site of the North Atlantic during the Aptian–Albian transition. This could have resulted in

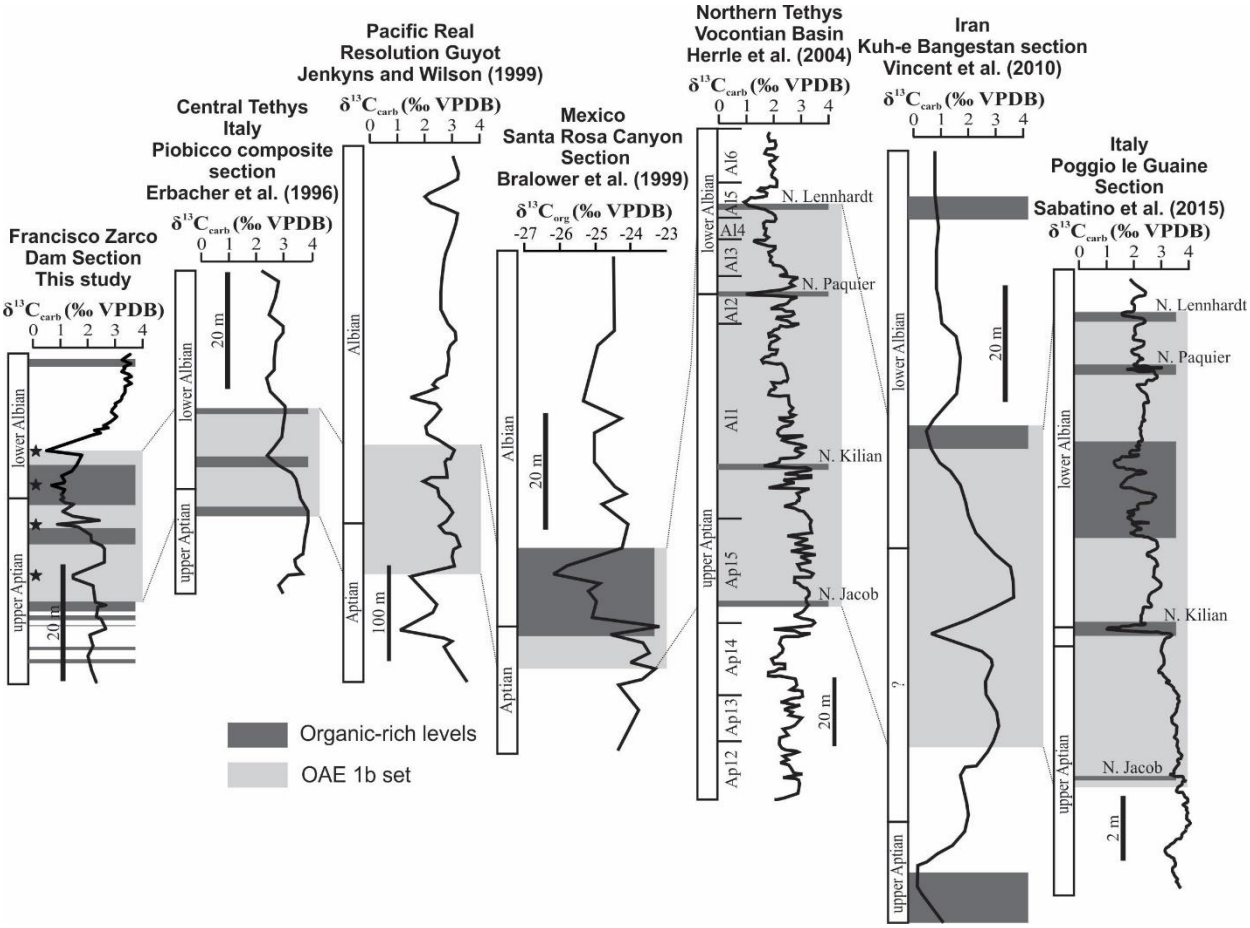

Fig. 6. $\delta^{13}C$ record of the Francisco Zarco Dam section (this study), correlated with other sections. Short-term negative carbon-isotope spikes with values and positions similar to those associated with the Jacob, Kilian, Paquier and Leenhardt episodes are marked by black starts.

an increase of the oceanic dissolved inorganic carbon leading to a consequent $\delta^{13}C$ decrease and bottom water anoxia favoring organic matter preservation in sediments.

6. Conclusions

Colomiellid biostratigraphy (*Deflandronella* to *Calpionellopsella* colomiellid subzones) together with strontium-isotope stratigraphy (~115–112 Ma) constrain the age of the studied sediments to the late Aptian–early Albian. The $\delta^{13}C$ curve reveals a long-term negative carbon-isotope excursion that concur with the carbon-isotope signature reported in other parts of the world during the Aptian–Albian boundary, assignable to the OAE 1b set. The increase in detrital minerals (phyllosilicates plus quartz) coupled with the absence of feldspar observed within the negative $\delta^{13}C$ excursion suggest that the sediments accumulated under warm and humid conditions leading to high biogeochemical weathering and runoff rates in the source area. This fits with n abrupt rise in sea surface temperature recorded in other Atlantic basins and also marked aridity in the North American adjacent landmass than previously reported. This study supports a long-carbon cycle perturbation related to the OAE 1b, punctuated by instantaneous and extreme events of accelerated global change that resulted in minor shifts in the $\delta^{13}C$ curve. Our results point to an increased runoff as the mechanism responsible for $\delta^{13}C$ decrease. This also explains density stratification and consequent organic matter preservation in sediments under oxygen-depleted bottom water conditions.

Acknowledgements

Funding was provided by the projects 177510 SEP-CONACyT and IN101914 (PAPIIT, UNAM). The authors gratefully acknowledge Teresa Pi for XRD analysis; Isaac Hernández Montero, Gabriela Solís Pichardo, Gerardo Arrieta and Teodoro Hernández Treviño for performing the strontium-isotope measurements; Edith Cienfuegos Alvarado, Francisco Javier Otero Trujano and Rafael Puente Martínez for carbon-isotope analysis; and Priyadarsi Debajyoti Roy who allowed the use of his research facilities for TOC determinations. Constructive comments of Patrick Zell and Karl Föllmi helped to improve this manuscript.

REFERENCES

Barragán, R., 2000, Ammonite biostratigraphy, lithofacies variations, and paleoceanographic implications for Barremian-Aptian sequences of northeastern Mexico. Ph.D. thesis, Miami, USA, Florida International University, 296 p.

Barragan, R., 2001. Sedimentological and paleocological aspects of the Aptian transgressive event of Sierra del Rosario, Durango, northeast Mexico. Journal of South American Earth Sciences 14, 189–202.

Barragán, R., Maurrasse, F.J-M.R., 2008. Lower Aptian (Lower Cretaceous) ammonites from the basal strata of the La Peña Formation of Nuevo León State, northeast Mexico: biochronostratigraphic implications. Revista Mexicana de Ciencias Geológicas 25, 145–157.

Blakey website. https://www2.nau.edu/rcb7/105_Cretaceous_2globes.jpg.

Bralower, T.J., CoBabe, E., Clement, B., Sliter,W.V., Osburn, C.L., Longoria, J., 1999. The record of global change in mid-Cretaceous (Barremian-Albian) sections from the Sierra Madre, northeastern Mexico. Journal of Foraminiferal Research 29(4), 418–437.

Bralower, T.J., Fullagar, P.D., Paull, C.K., Dwyer, G.S., Leckie, R.M., 1997. Mid-Cretaceous strontium-isotope stratigraphy of deep-sea sections. Geological Society of America Bulletin 109(11), 1421–1442.

Borza, K., 1979. Tintinnina aus dem oberen Apt und unteren Alb der Westkarpaten. Geologicky Zbornık Geologica Carpathica 30, 341–361.

Cantú-Chapa, A., 1989. La Peña Formation (Aptian): A condensed limestone-shale sequence from the subsurface of NE mexico. Journal of Petroleum Geology 12(1), 69–84.

Chung, F.H., 1974. Quantitative interpretation of X-ray diffraction patterns of mixtures. I. Matrix-flushing method for quantitative multicomponent analysis. Journal of Applied Crystallography 7(6), 519–525.

Chumakov, N.M., Zharkov, M.A., Herman, A.B., Doludenko, M.P., Kalandadze, N.M., Lebedev, E.L., Ponomareko, A.G., Rautian, A.S., 1995. Climatic belts of mid-Cretaceous time. Stratigraphical and Geological Correlation 3, 241–260.

Coccioni, R., Sabatino, N., Frontalini, F., Gardin, S., Sideri, M., Sprovieri, M., 2015. The neglected history of Oceanic Anoxic Event 1b: insights and new data from the Poggio le Guaine section (Umbria–Marche Basin). Stratigraphy 11, 245–282.

Conklin, J., Moore, C., 1977. Paleoenvironmental analysis of the Lower Cretaceous Cupido Formation, northeast Mexico, In: Bebout, D.G., Loucks, R.G. (Eds.), Cretaceous carbonates of Texas and Mexico. University of Texas Bureau of Economic Geology Report of Investigations 89, pp. 302–323.

Duchamp-Alphonse, S., Fiet, N., Adatte, T., Pagel, M., 2011. Climate and sea-level variations along the northwestern Tethyan margin during the Valanginian C-isotope excursion: mineralogical evidence from the Vocontian Basin (SE France). Palaeogeography, Palaeoclimatology, Palaeoecology 302(3), 243–254.

Erba, E., Duncan, R.A., Bottini, C., Tiraboschi, D., Weissert, H., Jenkyns, H.C., and Malinverno, A., 2015. Environmental consequences of Ontong Java Plateau and Kerguelen Plateau volcanism, in Neal, C.R., Sager, W.W, Sano, T., and Erba, E. (Eds.), The Origin, Evolution, and Environmental Impact of Oceanic Large Igneous Provinces, Geological Society of America Special Paper 511.

Erbacher, J., Thurow, J., Littke, R., 1996. Evolution patterns of radiolaria and organic matter variations: a new approach to identify sea-level changes in mid-Cretaceous pelagic environments. Geology 24(6), 499–502.

Erbacher, J., Hemleben, C., Huber, B.T., Markey, M., 1999. Correlating environmental changes during early Albian oceanic anoxic event 1B using benthic foraminiferal paleoecology. Marine Micropaleontology 38, 7–28.

Erbacher, J., Huber, B.T., Norris, R.D., Markey, M., 2001. Increased thermohaline stratification as a possible cause for an ocean anoxic event in the Cretaceous period. Nature 409(6818), 325–327.

Föllmi, K.B., 2012. Early Cretaceous life, climate and anoxia. Cretaceous Research, 35, 230–257.

Föllmi, K.B., Godet, A., Bodin, S., Linder, P., 2006. Interactions between environmental change and shallow water carbonate buildup along the northern Tethyan margin and their impact on the Early Cretaceous carbon isotope record. Paleoceanography, 21(4), , doi:10.1029/2006PA001313.

Goldhammer, R.K., Lehmann, P.J., Todd, R.G., Wilson, J.L., Ward, W.C., Johnson, C.R., 1991. Sequence stratigraphy and cyclostratigraphy of the Mesozoic of the Sierra Madre Oriental, Northeast Mexico, A field guidebook: Society of Economic Paleontologists and Mineralogists, Gulf Coast Section, pp. 1–84.

Goldhammer, R.K., 1999. Mesozoic sequence stratigraphy and paleogeographic evolution of northeast Mexico, In: Bartolini, C., Wilson J.L., Lawton, T.F. (Eds.), Mesozoic sedimentary and Tectonic History of North-Central Mexico, Boulder, Colorado, Geological Society of America, Special Paper 340, pp. 1–59.

Gradstein, F.M., Ogg, J.G., Schmitz, M., Ogg, G., 2012. The Geologic Time Scale. Elsevier, Amsterdam, The Netherlands, 1144 p

Herrle, J.O., Kößler, P., Friedrich, O., Erlenkeuser, H., Hemleben, C., 2004. High-resolution carbon isotope records of the Aptian to Lower Albian from SE France and the Mazagan Plateau (DSDP Site 545): a stratigraphic tool for paleoceanographic and paleobiologic reconstruction. Earth and Planetary Science Letters 218(1), 149–161.

Hillier, S., 2000. Accurate quantitative analysis of clay and other minerals in sandstones by XRD: comparison of a Rietveld and a reference intensity ratio (RIR) method and the importance of sample preparation. Clay Minerals 35(1), 291–302.

Hofmann, P., Stüsser, I., Wagner, T., Schouten, S., Damsté, J.S.S., 2008. Climate–ocean coupling off North-West Africa during the Lower Albian: the oceanic anoxic event 1b. Palaeogeography, Palaeoclimatology, Palaeoecology 262(3), 157–165.

Howarth, R.J., McArthur, J.M., 1997. Statistics for strontium isotope stratigraphy: a robust LOWESS fit to the marine Sr-isotope curve for 0 to 206 Ma, with look-up table for derivation of numeric age. Geology 105, 441–456.

Hu, G., Hu, W., Cao, J., Yao, S., Liu, W., Zhou, Z., 2014. Fluctuation of organic carbon isotopes of the Lower Cretaceous in coastal southeastern China: Terrestrial response to the Oceanic Anoxic Events (OAE 1b).Palaeogeography, Palaeoclimatology, Palaeoecology 399, 352–362.

Humphrey, W.E., Diaz, T., 2003. Jurassic and Lower Cretaceous stratigraphy and tectonics of northeastern Mexico. Bureau of Economic Geology, University of Texas at Austin, 152 p.

Jacobsen, S.B., Kaufman, A.J., 1999. The Sr, C and O isotopic evolution of Neoproterozoic seawater. Chemical Geology 161(1-3), 37–57.

Jenkyns, H.C., 1980. Cretaceous anoxic events: from continents to oceans. Journal of the Geological Society 137, 171–188.

Jenkyns, H.C., Wilson , P.A., 1999. Stratigraphy, paleoceanography, and evolution of Cretaceous Pacific gyots: Relics from a greenhouse Earth. American Journal of Science 299, 341–392.

Jones, C.E., Jenkyns, H.C., 2001. Seawater strontium isotopes, oceanic anoxic events, and seafloor hydrothermal activity in the Jurassic and Cretaceous. American Journal of Science 301(2), 112–149.

Kaufman, A.J., Jacobsen, S.B., Knoll, A.H., 1993. The Vendian record of Sr and C isotopic variations in seawater: Implications for tectonics and paleoclimate. Earth and Planetary Science Letters 120, 409–430.

Kennedy, W.J., Gale, A.S., Bown, P.R., Caron, M., Davey, R.J., Gröcke, D., Wray, D.S., 2000. Integrated stratigraphy across the Aptian-Albian boundary in the Marnes Bleues, at the Col de Pre-Guittard, Arnayon (Drome), and at Tartonne (Alpes-de-Haute-Provence), France: A candidate global boundary stratotype section and boundary point for the base of the Albian stage. Cretaceous Research 21(5), 591–720.

Kuypers, M.M., Pancost, R.D., Nijenhuis, I.A., Sinninghe Damsté, J.S., 2002. Enhanced productivity led to increased organic carbon burial in the euxinic North Atlantic basin during the late Cenomanian oceanic anoxic event. Paleoceanography 17(4), 1051, doi: 10.1029/2000PA000569.

Leckie, R.M., Bralower, T.J., Cashman, R., 2002. Oceanic anoxic events and plankton evolution: biotic response to tectonic forcing during the mid-Cretaceous. Paleoceanography 17(3), 1–29.

Lehmann, C., Osleger, D.A., Montañez, I.P., 1998. Controls on Cyclostratigraphy of Lower Cretaceous Carbonates and Evaporites, Cupido and Coahuila Platforms, Northeastern Mexico. Journal of Sedimentary Research 68(6), 1109–1130.

Lehmann, C., Osleger, D.A., Montañez, I.P., Sliter, W., Arnaud-Vanneau, A., Banner, J., 1999. Evolution of Cupido and Coahuila carbonate platforms, Early Cretaceous, northeastern Mexico. Geological Society of America Bulletin 111(7), 1010–1029.

Lehmann, C., Osleger, D.A., Montañez, I.P., 2000. Sequence stratigraphy of Lower Cretaceous (Barremian–Albian) Carbonate Platforms of Northeastern Mexico: Regional and Global correlations. Journal of Sedimentary Research 70(2), 373–391.

Li, Y.-X., Bralower, T.J., Montañez, I.P., Osleger, D.A., Arthur, M.A., Bice, D.M., Herbert, T.D., Erba, E., Premoli Silva, I., 2008. Toward an orbital chronology for the early Aptian Oceanic Anoxic Event (OAE1a, ~120 Ma). Earth and Planetary Science Letters 271, 88–100.

Li, X., Wei, Y., Li, Y., Zhang, C., 2015. Carbon isotope records of the early Albian oceanic anoxic event (OAE) 1b from eastern Tethys (southern Tibet, China). Cretaceous Research, In press.

Ludvigson, G.A., Joeckel, R.M., González, L.A., Gulbranson, E. L., Rasbury, E. T., Hunt, G.J., Kirland, J.I., Madsen, S., 2010. Correlation of Aptian-Albian carbon isotope excursions in continental strata of the Cretaceous foreland basin, eastern Utah, USA. Journal of Sedimentary Research 80(11), 955–974.

Madhavaraju, J., Lee, Y.I., León, C.M. G., 2013a. Diagenetic significance of carbon, oxygen and strontium isotopic compositions in the Aptian-Albian Mural Formation in Cerro Pimas area, northern Sonora, Mexico. Journal of Iberian Geology (39), 73–88.

Madhavaraju, J., Sial, A.N., González-León, C.M., Nagarajan, R., 2013b. Carbon and oxygen isotopic variations in early Albian limestone facies of the Mural Formation, Pitaycachi section, northeastern Sonora, Mexico. Revista Mexicana de Ciencias Geológicas 30(3), 526–539.

Maldonado, G.V., Tello, D.E., 1976. Identificación del modelo geológico del arrecife Cupido a partir de información sismológica. III Simposium de Geología de Subsuelo, Superintendencia General de Exploración, 179–191.

McAnena, A., Flögel, S., Hofmann, P., Herrle, J.O., Griesand, A., Pross, J., Tabolt, H.M., Rethemeyer, J., Wallmann, K., Wagner, T., 2013. Atlantic cooling associated with a marine biotic crisis during the mid-Cretaceous period. Nature Geoscience 6(7), 558–561.

McCrea, J.M., 1950. On the Isotopic Chemistry of Carbonates and a Paleotemperature Scale. The Journal of Chemical Physics 18, 849–857.

McArthur, J.M., Mutterlose, J., Price, G.D., Rawson, P.F., Ruffell, A., Thirlwall, M.F., 2004. Belemnites of Valanginian, Hauterivian and Barremian age: Sr-isotope stratigraphy, composition ($^{87}Sr/^{86}Sr$, $\delta^{13}C$, $\delta^{18}O$, Na, Sr, Mg), and palaeo-oceanography. Palaeogeography, Palaeoclimatology, Palaeoecology 202(3), 253–272.

McArthur, J.M., Howarth, R.J., Shields, G.A., 2012. Strontium isotope stratigraphy. In: Gradstein, F.M., Ogg, J.G., Schmitz, M., Ogg, G. (Eds.),

The Geologic Time Scale 2012. Elsevier Science Limited, 1144 p

Moreno-Bedmar, J.A., Barragán, R., Company, M., Bulot, L.G., 2013. Aptian (Lower Cretaceous) ammonite biostratigraphy of the Francisco Zarco Dam stratigraphic section (Durango State, Northeast Mexico). Journal of South American Earth Sciences 42, 150–158.

Mutterlose, J., Pauly, S., Steuber, T., 2009. Temperature controlled deposition of Early Cretaceous (Barremian–early Aptian) black shales in an epicontinental sea. Palaeogeography, Palaeoclimatology, Palaeoecology 273, 330–345.

Navarro-Ramirez, J.P., Bodin, S., Heimhofer, U., Immenhauser, A., 2015. Record of Albian to early Cenomanian environmental perturbation in the eastern sub-equatorial Pacific. Palaeogeography, Palaeoclimatology, Palaeoecology 423, 122–137.

Núñez-Useche, F., Barragán, R., 2012. Microfacies analysis and paleoenvironmental dynamic of the Barremian-Albian interval in Sierra del Rosario, eastern Durango state, Mexico. Revista Mexicana de Ciencias Geológicas 29(1), 204–218.

Núñez-Useche F., Moreno-Bedmar J.A., Company M. Barragán R., 2014. A negative carbon isotope excursion within the *Dufrenoyia furcata* Zone: proposal for a new episode for chemostratigraphic correlation in the Aptian. Carnets de Géologie [Notebooks on Geology] 14 (6), 129–137.

Núñez-Useche, F., Barragán, R., Moreno-Bedmar, J.A., Canet, C., 2015. Geochemical and paleoenvironmental record of the early to early late Aptian major episodes of accelerated change: Evidence from Sierra del Rosario, Northeast Mexico. Sedimentary Geology 324, 47–66.

Phelps, R.M., Kerans, C., Da-Gama, R.O., Jeremiah, J., Hull, D., Loucks, R.G., 2015. Response and recovery of the Comanche carbonate platform surrounding multiple Cretaceous oceanic anoxic events, northern Gulf of Mexico. Cretaceous Research 54, 117–144.

Pletsch, T., Daoudi, L., Chamley, H., Deconinck, J.F., Charroud, M., 1996. Paleogeographic controls on palygorskite occurrence in mid-Cretaceous sediments of Morocco and adjacent basins. Clay Minerals 31, 403–416.

Prokoph, A., Shields, G. A., Veizer, J., 2008. Compilation and time-series analysis of a marine carbonate $\delta^{18}O$, $\delta^{13}C$, $^{87}Sr/^{86}Sr$ and $\delta^{34}S$ database through Earth history. Earth-Science Reviews 87(3), 113–133.

Reboulet, S., Szives, O., Aguirre-Urreta, B., Barragán, R., Company, M., Idakieva, V., Ivanov, M., Kakabadze, M.V., Moreno-Bedmar, J.A., Sandoval, J., Baraboshkin, E.J., Çaglar, M.K., Főzy, I., GonzálezArreola, C., Kenjo, S., Lukeneder, A., Raisossadat, S.N., Rawson, P.F., Tavera, J.M., 2014. Report on the 5th International Meeting of the IUGS Lower Cretaceous Ammonite Working Group, the Kilian Group (Ankara, Turkey, 31st August 2013), Cretaceous Research 50, 126–137.

Rodríguez-López, J.P., Meléndez, N., de Boer, P.L., Soria, A.R., 2008. Aeolian sand sea development along the mid-Cretaceous western Tethyan margin (Spain): erg sedimentology and palaeoclimate implications. Sedimentology 55, 1253–1292.

Sabatino, N., Coccioni, R., Manta, D.S., Baudin, F., Vallefuoco, M., Traina, A., Sprovieri, M., 2015. High resolution chemostratigraphy of the late Aptian–early Albian oceanic anoxic event (OAE 1b) from the Poggio le Guaine section (Umbria–Marche Basin, central Italy). Palaeogeography, Palaeoclimatology, Palaeoecology 426, 319–333.

Schlanger, S.O., Jenkyns, H.C., 1976. Cretaceous oceanic anoxic events—causes and consequences. Geologie en Mijnbouw 55, 179–184.

Stein, M., Arnaud-Vanneau, A., Adatte, T., Fleitmann, D., Spangenberg, J.E., Föllmi, K.B., 2012. Palaeoenvironmental and palaeoecological change on the northern Tethyan carbonate platform during the Late Barremian to earliest Aptian. Sedimentology 59(3), 939–963.

Steuber, T., Korbar, T., Jelaska, V., Gušić, I., 2005. Strontium-isotope stratigraphy of Upper Cretaceous platform carbonates of the island of Brać (Adriatic Sea, Croatia): implications for

global correlation of platform evolution and biostratigraphy. Cretaceous Research 26, 741–756.

Tinker, S.W., 1982. Lithostratigraphy and Biostratigraphy of the Aptian La Peña Formation, northeast Mexico and south Texas, and depositional setting of the Aptian-Pearsall-La Peña Formations, Texas subsurface and northeast Mexico: Why is there not another Fairway Field?. M.S. thesis, Ann Arbor, Michigan, USA, University of Michigan, 80 p.

Tiraboschi, D., Erba, E., Jenkyns, H.C., 2009. Origin of rhythmic Albian black shales (Piobbico core, central Italy): Calcareous nannofossil quantitative and statistical analyses and paleoceanographic reconstructions. Paleoceanography 24(2), PA2222.

Trabucho Alexandre, J., Van Gilst, R.I., Rodríguez-López, J.P., De Boer, P.L., 2011. The sedimentary expression of oceanic anoxic event 1b in the North Atlantic. Sedimentology 58, 1217–1246.

Trejo, M., 1975. Tintinidos mesozoicos de Mexico (taxonomía y datos paleobiológicos). Boletín de la Asociación Mexicana de Geólogos Petroleros 1012, 329–449.

Tsikos, H., Karakitsios, V., Van Breugel, Y., Walsworth-Bell, B., Bombardiere, L., Petrizzo, M.R., Sinninghe Damsté, J.S., Schouten, S., Erba, E., Premoli Silva, I, Farrimond, P., Tyson, R.V., Jenkyns, H.C., 2004. Organic-carbon deposition in the Cretaceous of the Ionian Basin, NW Greece: the Paquier Event (OAE 1b) revisited. Geological Magazine 141(04), 401–416.

Veizer, J., 1989. Strontium isotopes in seawater through time. Annual Review of Earth and Planetary Sciences 17, 141–167.

Vincent, B., van Buchem, F.S., Bulot, L.G., Immenhauser, A., Caron, M., Baghbani, D., Huc, A.Y., 2010. Carbon-isotope stratigraphy, biostratigraphy and organic matter distribution in the Aptian–Lower Albian successions of southwest Iran (Dariyan and Kazhdumi formations). GeoArabia Special Publication 4(1), 139–197.

Wagner, T., Wallmann, K., Herrle, J.O., Hofmann, P., Stuesser, I., 2007. Consequences of moderate ~ 25,000 yr lasting emission of light CO_2 into the mid-Cretaceous ocean. Earth and Planetary Science Letters 259(1), 200–211.

Wagner, T., Herrle, J.O., Sinninghe Damsté, J., Schouten, S., Stuesser, I., Hofmann, P., 2008. Rapid warming and salinity changes of Cretaceous surface waters in the subtropical North Atlantic. Geology 36, 203–206.

Weissert, H., Lini, A., 1991. Ice age interludes during the time of Cretaceous greenhouse climate?, In: Müller, D.W., McKenzie, J.A. (Eds.), Controversies in Modern Geology: Evolution of Geological Theories in Sedimentology, Earth History and Tectonics, Academic, London, pp. 173–191.

Wilson, J.L., Pialli, G., 1977. A Lower Cretaceous shelf margin in northern Mexico, In: Bebout, D.G., Loucks, R.G. (Eds.), Cretaceous carbonates of Texas and Mexico: University of Texas Bureau of Economic Geology Report of Investigations 89, pp. 286–294.

Wilson, J.L., Ward, W.C., 1993. Early Cretaceous carbonate platforms of northeastern and east-central Mexico, In: Simo, J.A., Scott, R.W., Masse, J.-P. (Eds.), Cretaceous carbonate platforms. American Association of Petroleum Geologists Memoir 56, 35–50.

Yamamoto, K., Ishibashi, M., Takayanagi, H., Asahara, Y., Sato, T., Nishi, H., Iryu, Y., 2013. Early Aptian paleoenvironmental evolution of the Bab Basin at the southern Neo-Tethys margin: Response to global carbon-cycle perturbations across Ocean Anoxic Event 1a. Geochemistry, Geophysics, Geosystems 14(4), 1104–1130.

Appendix A. $\delta^{13}C_{carb}$, TOC, mineral composition and detrital index of the studied section.

Samples	Distance base (m)	$\delta^{13}C$ (‰ VPDB)	TOC (%)	Mineral composition obtained by XRD analysis				Detrital Index
				Phyllosilicates (%)	Pyrite (%)	Quartz (%)	Calcite (%)	
FZD-375	57.5	3.55						
FZD-374	57.2	3.44	0.8	3	3	9	84	0.14
FZD-373	56.5	3.26						
FZD-372	55.9	3.58	5.0					
FZD-371	55.3	3.33						
FZD-370	55.1	3.36						
FZD-369	54.4	3.24	0.9	0	4	11	85	0.13
FZD-368	54.0	3.51						
FZD-367	53.7	3.60	2.2					
FZD-366	53.2	3.36	2.1	8	4	7	81	0.19
FZD-363	52.5	3.60						
FZD-360	51.9	3.36	0.1					
FZD-357	51.4	3.37	1.8	0	4	11	85	0.13
FZD-354	50.9	3.36	0.1					
FZD-352	50.1	3.25						
FZD-351	49.8	3.25						
FZD-349	49.4	3.19		0	0	10	90	0.11
FZD-347	48.9	3.01	0.1					
FZD-344	48.6	3.03						
FZD-343	47.9	2.90	2.2					
FZD-340	47.5	2.87	2.3	0	3	7	90	0.08
FZD-337	46.7	3.07	2.7					
FZD-335	46.3	2.98						
FZD-334	45.7	2.83						
FZD-333	45.4	2.72	1.2	6	1	8	85	0.16
FZD-370	45.2	2.58						
FZD-331	44.8	2.75	0.1					
FZD-329	44.3	2.25						
FZD-327	43.8	2.47	3.1	14	3	5	78	0.24
FZD-325	43.4	2.16	3.2					
FZD-312	40.8	0.51						
FZD-309	39.9	1.79	3.3	0	4	9	87	0.10
FZD-300	38.3	1.60						
FZD-292	37.1	1.42						
FZD-285	36.3	1.04						
FZD-282	35.4	1.16	7.5	11	3	9	78	0.26
FZD-281	35.1	1.13						
FZD-280	34.7	0.68						
FZD-277	34.0	1.16	4.7	5	0	17	78	0.28
FZD-272	33.1	1.05						
FZD-268	32.5	1.14						
FZD-265	32.2	1.01	4.8	11	3	5	81	0.20
FZD-262	31.6	1.18						
FZD-261	31.4	1.49						
FZD-255	30.2	1.08	3.1	18	3	14	64	0.50
FZD-251	29.3	1.45	1.3					
FZD-247	28.6	2.41	2.7					
FZD-243	27.9	0.89	2.8					
FZD-242	27.5	1.65						
FZD-238	26.1	2.12	5.7	6	3	5	86	0.13
FZD-236	25.0	2.15	6.0	11	2	10	77	0.27
FZD-235b	24.2	2.50						
FZD-235a	23.6	2.55	2.0					
FZD-232b	22.4	2.57						
FZD-232a	21.2	2.58	3.7	8	1	6	85	0.16
FZD-230	19.8	2.60						
FZD-227	19.1	1.47	0.1	4	1	8	87	0.14

Samples	Distance base (m)	$\delta^{13}C$ (‰ VPDB)	TOC (%)	Mineral composition obtained by XRD analysis				
				Phyllosilicates (%)	Pyrite (%)	Quartz (%)	Calcite (%)	Detrital Index
FZD-224	18.5	1.46	1.4					
FZD-218	17.2	2.20	1.8					
FZD-202	14.3	2.26		5	1	9	85	0.16
FZD-200	13.8	2.67						
FZD-198	13.5	2.38		3	8	10	79	0.16
FZD-191	11.8	2.32						
FZD-190	11.4	2.50						
FZD-189	9.7	2.67		9	9	13	69	0.32
FZD-184	8.5	2.08		5	6	8	81	0.16
FZD-181	6.7	2.20		8	3	10	78	0.23
FZD-174	4.9	2.01						
FZD-170	2.5	2.14		8	3	12	77	0.26
FZD-168	0.4	2.32		7	4	6	83	0.16

Afloramiento de la Formación Agua Nueva en Xilitla, San Luis Potosí

CAPÍTULO

6

EL EVENTO ANÓXICO DEL CENOMANIANO–TURONIANO EN EL CENTRO DE MÉXICO

Artículo: **Núñez-Useche, F.**, Canet, C., Barragán, R., Alfonso P., 2016. Bioevents and redox conditions around the Cenomanian–Turonian anoxic event in Central Mexico. Aceptado en Palaeogeography, Palaeoclimatology, Palaeoecology.

Palaeogeography, Palaeoclimatology, Palaeoecology 449 (2016) 205–226

Contents lists available at ScienceDirect

Palaeogeography, Palaeoclimatology, Palaeoecology

journal homepage: www.elsevier.com/locate/palaeo

Bioevents and redox conditions around the Cenomanian–Turonian anoxic event in Central Mexico

Fernando Núñez-Useche [a,b,*], Carles Canet [b], Ricardo Barragán [c], Pura Alfonso [d]

[a] Posgrado en Ciencias de la Tierra, Universidad Nacional Autónoma de México, Del. Coyoacán, 04510 México D.F., Mexico
[b] Instituto de Geofísica, Universidad Nacional Autónoma de México, Del. Coyoacán, 04510 México D.F., Mexico
[c] Instituto de Geología, Universidad Nacional Autónoma de México, Del. Coyoacán, 04510 México D.F., Mexico
[d] Departament d'Enginyeria Minera i Recursos Naturals, Universitat Politècnica de Catalunya, Av. Bases de Manresa 61-73, 08242 Manresa, Spain

ARTICLE INFO

Article history:
Received 28 May 2015
Received in revised form 13 January 2016
Accepted 17 January 2016
Available online 24 January 2016

Keywords:
Cenomanian–Turonian
Organic-rich sediments
Anoxic/dysoxic bottom waters
Pyrite framboids
Bacterial sulfate reduction
Central Mexico

ABSTRACT

The Xilitla section of central Mexico (western margin of the proto-North Atlantic) is characterized by pelagic sediments enriched in marine organic matter. Using biostratigraphic and radiometric data, it was dated at the latest Cenomanian–earliest Turonian transition. We identified an interval coeval with the faunal turnover associated with the Oceanic Anoxic Event 2 (OAE 2), recording the *Heterohelix* shift and the "filament event" for the first time in Mexico. An integral analysis of sedimentary facies, pyrite and geochemical proxies reveals vertically variable redox conditions, with prevailing anoxic to dysoxic bottom waters. Along with phosphorous and manganese depletion, the highest content of total organic carbon and of certain redox-sensitive trace elements (RSTEs) is found during part of the anoxic event, confirming more uniform and constant oxygen-depleted conditions. This interval is also characterized by a significant enrichment in biogenic barium and elevated TOC/N_{TOT} ratios, suggesting a link between productivity and anoxia. Sulfur isotope fractionation has a maximum value within the anoxic event, favored by the increase in the flux of organic matter and intensified through sulfur recycling. Highly bioturbated beds representing short-lived episodes of oxic conditions are intermittent within the OAE 2 and become more frequent in the early Turonian. This study proposes a model similar to that of modern upwelling regions. High marine productivity controlled organic matter burial and oxygenation at the seafloor, varying between anoxic (laminated facies with small pyrite framboids) and dysoxic conditions (bedding-parallel bioturbated facies with inoceramid bivalves and large pyrite framboids), interrupted by short-term well-oxygenated episodes (thoroughly bioturbated facies with common benthic foraminifera). General low-oxygen conditions led to the formation of glauconite and pyrite (bacterially mediated); the enrichment of redox-sensitive trace elements in sediments (Cd, Zn, V and Cr scavenged by organic matter and Ni, Mo, Pb, Co and Re by pyrite) and resulted in Mn and P depletion.

1. Introduction

Throughout the Mesozoic, several short-lived episodes of marine anoxia caused profound imprints on life and the environment, termed Oceanic Anoxic Events (OAEs; Schlanger and Jenkyns, 1976). The Cenomanian–Turonian anoxic event (OAE 2) is one of the most dramatic episodes of accelerated global change to have occurred throughout the Cretaceous, during a major global sea-level rise. Water column oxygen depletion in the course of this event caused a significant faunal turnover and enhanced the deposition of organic-rich sediments leading to a prominent positive carbon isotope excursion (Leckie et al., 2002; Caron et al., 2006; Jiménez Berrocoso et al., 2008; Hetzel et al., 2009; Gambacorta et al., 2015). In addition to affecting the global carbon cycle, the increased delivery of organic carbon to the seafloor drove an expansion of the oxygen minimum zone, elevated trace metal abundance in sediments, and favored high bacterial sulfate reduction (BSR) rates that, in turn, increased sedimentary pyrite burial and led to important modifications in seawater sulfur isotope composition (Coccioni and Luciani, 2004; Denne et al., 2014; Lowery et al., 2014; Poulton et al., 2015; Reolid et al., 2015).

The precise driving mechanisms behind the OAE 2 are still under debate; however, proposed hypotheses for the widespread ocean anoxia/dysoxia related to this event include the release of large quantities of CO_2 into the atmosphere through massive submarine volcanic activity during the formation of the Caribbean Plateau. Seawater chemistry changed radically due to the introduction of large quantities of sulfate and biolimiting metals that enhanced primary marine productivity (Snow et al., 2005; Trabucho Alexandre et al., 2010). Additionally, the associated CO_2 outgassing favored global warming, thus accelerating the hydrological cycle and increasing continental runoff and nutrient delivery into surface waters, which also contributed to increase productivity. Moreover, enhanced recycling of phosphorous from sediments overlain

* Corresponding author at: Posgrado en Ciencias de la Tierra, Universidad Nacional Autónoma de México, Del. Coyoacán, 04510 México D.F., Mexico.
E-mail address: fernandonunezu@comunidad.unam.mx (F. Núñez-Useche).

http://dx.doi.org/10.1016/j.palaeo.2016.01.035
0031-0182/

by anoxic waters has likely been an active mechanism further sustaining marine productivity (Mort et al., 2007; Poulton et al., 2015). While this event is well recorded in the Tethys, Central Atlantic and the Western Interior Seaway (WIS) in North America (e.g., Hetzel et al., 2009; Bomou et al., 2013; Eldrett et al., 2014), it is poorly understood in the Mexican Sea, a key area representing the transition between the WIS and the open ocean.

The Xilitla section of the Tampico-Misantla Basin, central Mexico, contains organic-rich sediments of the Agua Nueva Formation. It offers a good opportunity to study paleoenvironmental response to OAE 2 global perturbation in this particular site of the western margin of the proto-North Atlantic. In the present study, we present a multi-proxy approach to the stratigraphic section, correlating information from biostratigraphy, sedimentary facies, pyrite framboids content and size, carbon and sulfur isotopes, and total organic carbon and redox-sensitive trace elements (RSTEs) contents. The goals of this contribution are to: (i) identify the bioevents linked to the global turnover across the Cenomanian–Turonian (C–T) transition, (ii) provide information illustrating the redox conditions of the depositional environment; (iii) decipher the causes of such conditions and explore their genetic link with OAE 2; and (iv) construct a general depositional model considering the analytical results of the different proxies. This investigation is critical to developing a better understanding of the impact of OAE 2 on the deposition and preservation of organic matter in the study area.

2. Geologic and physiographic setting

The Tampico–Misantla Basin (TMB) is the easternmost paleogeographic feature of a set of basins that once constituted the Cretaceous Mexican Sea along the western margin of the proto-North Atlantic (Fig. 1). The basin has a continental basement, and its Jurassic (continental clastic sediments) to Early Cretaceous (basinal carbonates) filling pattern was mainly controlled by sea level changes related to the passive-margin development that resulted from the opening of the proto-Gulf of Mexico (Goldhammer and Johnson, 2001). During the late Cenomanian–early Turonian interval, as a result of the maximum global sea level rise (Hardenbol et al., 1998), the Mexican Sea expanded greatly and connected with the Western Interior Seaway (WIS) and the deep-water pelagic limestone of the Agua Nueva Formation accumulated in the TMB. This event was contemporary with volcanic activity in the western Pacific Mexico province (Goldhammer and Johnson, 2001; Centeno-García et al., 2008). As a consequence of the Sevier and

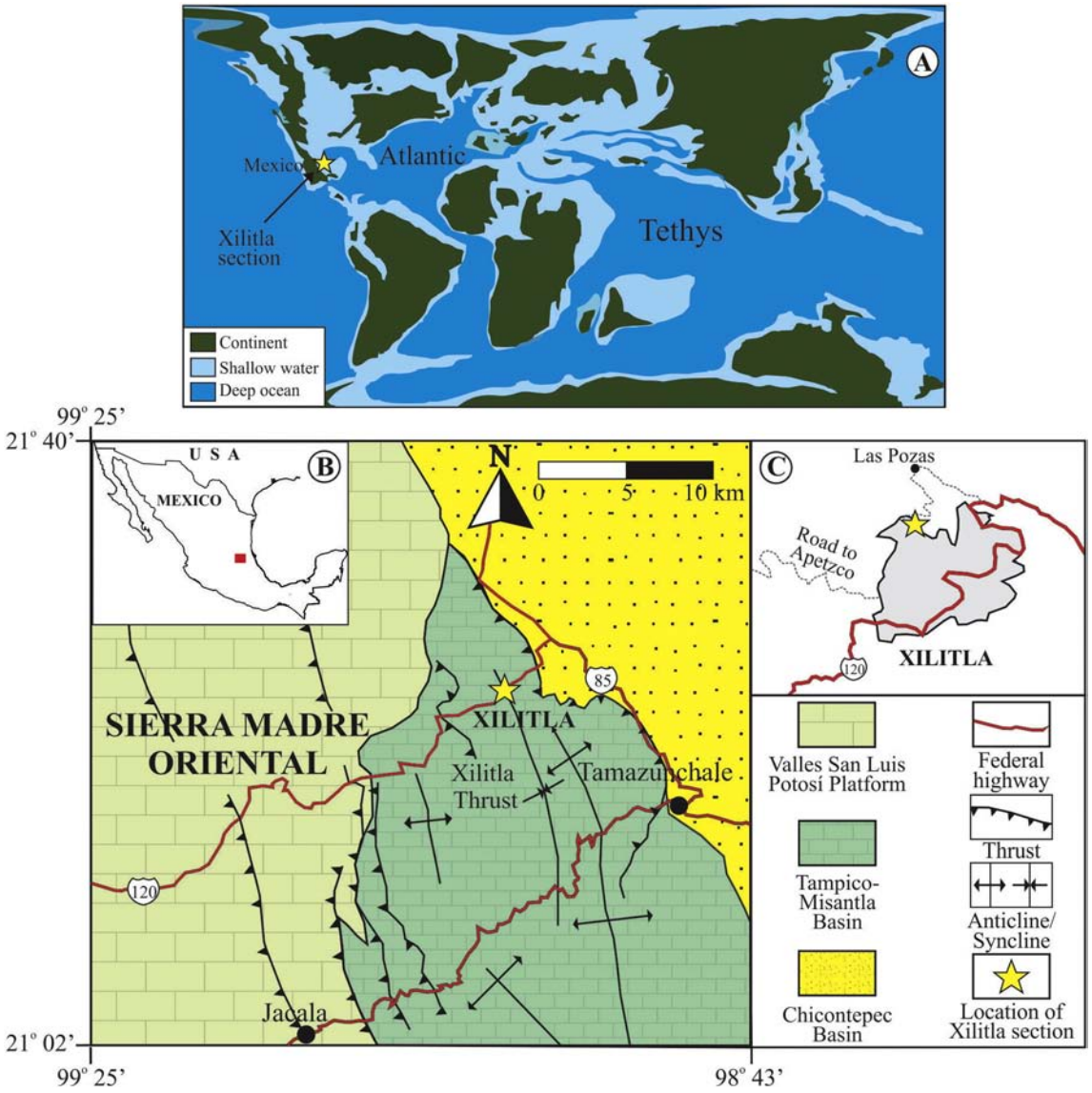

Fig. 1. (A) Paleoceanographic reconstruction of the Cenomanian–Turonian (http://jan.ucc.nau.edu/~rcb7/) showing the location of Mexico and the Xilitla section. (B). Central–northeastern portion of the Sierra Madre Oriental Fold-Thrust Belt with the major paleogeographic elements. (C) Schematic map of Xilitla.

Laramide orogenies and the resulting closure of the Mexican Sea in the Late Cretaceous, the TMB evolved into a flysch-filled foreland basin (Suter, 1984; Morán-Zenteno, 1994). The Xilitla section is situated on the west limb of a syncline fold in the footwall of the Xilitla Thrust (21° 23′ 47″ N, 98° 59′ 88″ W, base of the section) (Fig. 1). It is exposed on the northern edge of the village of the same name, along the road to Las Pozas connecting with federal highway 120 (Fig. 1). The continuous sedimentary succession is distributed along four small adjacent artisanal quarries, and comprises 29 m of pelagic sediments from the Agua Nueva Formation. They correspond to limestone with chert intercalated with thin calcareous shale and greenish bentonite horizons. Dark, laminated beds rich in organic matter and with well-preserved fossil-fish assemblages, tiny shells of bivalves and pyrite, alternating with bioturbated beds are reported in different studies (Blanco et al., 2010, 2011; Blanco-Piñón et al., 2008, 2009, 2012, 2014). Without the adequate biostratigraphic control necessary in this type of research, the aforementioned studies considered a C–T age for this unit and highlighted the potential link between the anoxic depositional environment and global OAE 2.

3. Materials and methods

3.1. Field and petrographic observations

The studied section was described and sampled bed-by-bed. Field descriptions focused on the color of the fresh and weathered rock, sedimentary structures, ichnofabric and fossil content. Colors were defined according to the Geological Society of America (GSA) Rock-Color Chart (Goddard et al., 1963). Furthermore, 120 thin sections of calcareous beds were petrographically analyzed under transmitted light microscopy (Olympus BX60) using the nomenclature of Dunham (1962). The microscopic study paid special attention to further descriptions of components and fabric type, as well as the presence/absence of bioturbation and early diagenetic minerals. The degree of bioturbation was described using the index proposed by Taylor and Goldring (1993). Facies are assigned a letter in the oxygen-restricted biofacies (ORB) scheme proposed by Reolid et al. (2010), which is slightly different from that originally presented by Wignall and Hallam (1991) and Wignall (1994). The petrographic analysis of thin sections was also applied in order to semi-quantitatively estimate the abundance of heterohelicids and bivalve filaments. Identification of index species of planktic foraminifera was based on the zonation scheme of Premoli Silva and Sliter (2002). The results of these studies provide information about age and sedimentary features, fossils and mineral composition, data that constitute the basis for facies characterization.

3.2. U–Pb geochronology

Selected individual homogenous grains were analyzed for U–Pb isotope analysis using Laser Ablation Inductively Coupled Plasma Mass Spectrometry (LA–ICP–MS) composed of a Resonetics M50 workstation coupled with a Thermo X Series II quadrupole ICPMS at the *Centro de Geociencias*, *Universidad Nacional Autónoma de México* (UNAM). Sample preparation and correction of results were performed according to the methodology described by Solari et al. (2009), which produced accuracy better than 0.5% and precision within the range of 2–3% 2σ error. Age was estimated considering the criteria of Jeffries et al. (2003) concerning the age of a single zircon, and of Gehrels et al. (2006) regarding a robust age based on a cluster of three or more zircons with similar ages. All calculations and graphs were made using Isoplot 3.00 by Ludwig (1991).

3.3. Analysis of pyrite grains

A statistical study of grain size was applied to pyrite framboids from twenty-two samples in order to assess their size distribution and content. This task entailed observation of polished sections under a reflected light with an Olympus BX60 microscope. All framboids contained in two ribbons parallel to the stratigraphic plane and separated between 0.5 and 0.8 mm were photographed and measured under maximum magnification (100×). For comparison, at least 55 framboids per sample were also measured under a scanning electron microscope (SEM) at the *Instituto de Geología* and the *Instituto de Ciencias del Mar y Limnología* (UNAM) using gold-coated rock chips. Framboid content is reported as the number of framboids per mm^2.

Wavelength dispersive spectrometry (WDS) and energy dispersive X-ray spectroscopy (EDS) analyses were carried out on both diagenetic pyrite framboids ~8 μm in diameter with no evidence of overgrowth (disseminated in the matrix and filling burrows) and crystals separated from laminated pyrite. This analysis was performed on thin, critically point-dried sections coated with a thin layer of gold, using a JEOL JXA-8900XR electron probe microanalyzer (EPMA) (*Instituto de Geofísica*, UNAM) and a model JSM 6300 SEM (*Instituto de Geología*, UNAM). This analysis provides data concerning the chemical composition of pyrite grains. EDS analysis focused on the content and distribution of carbon, whereas WDS analysis on the content of major and trace elements (Fe, S, V, Ni, Cr, Mo, U and Th).

Pyrite sulfur isotope composition was determined for fourteen grains, which were separated from laminae using a dental drill with a Tungsten Carbide end. These grains are composed of relatively intact pyrite microcrystals and were carefully hand-picked under a binocular microscope; those selected were free from visible sulfur minerals (including barite crystals). The analyses were performed with a Delta C Finnigan MAT continuous flow mass spectrometer, coupled with a TC-EA Carlo Erba 1108 elemental analyzer. Analyses were made following the methodology of Giesemann et al. (1994), at the *Centres Científics i Tecnològics* of the *Universitat de Barcelona* using 0.15–0.20 mg of sample material. Results are expressed using the $\delta^{34}S_{py}$ notation, in permil relative to the VCDT (Vienna Canyon del Diablo Troilite) standard, and have a standard deviation of ±0.2‰.

3.4. Carbonate carbon- and oxygen-isotope data

Carbon and oxygen isotope values on the carbonate fraction of the matrix ($\delta^{13}C_{carb}$ and $\delta^{18}O_{carb}$, respectively) were obtained from sixty samples extracted from micritic matrix of laminated and bioturbated limestone and shaly limestone fragments, with a dental drill (employing a Tungsten Carbide end), and avoiding veins and hydrocarbon impregnations. Orthophosphoric acid was added to about 0.9 mg of each sample at 25 °C and allowed to react for 54 h under vacuum, following the guidelines of McCrea (1950). The CO_2 released was analyzed with a Thermo Finnigan MAT 253 mass spectrometer coupled with Gas Bench II at the *Laboratorio Universitario de Geoquímica Isotópica* of the *Instituto de Geología* (UNAM). Carbon and oxygen isotope values are reported in permil relative to the VPDB (Vienna Pee Dee Belemnite) standard. Reproducibility of replicate analyses of samples was generally better than 0.2‰ for both carbon and oxygen isotope ratios.

3.5. Whole–rock geochemistry

Fresh limestone and shaly limestone chips of about 1–2 cm in length (free of veinlets, stylolites and hydrocarbons) were collected at a depth of at least 4–6 cm from the exposed surface, in order to avoid the effects of weathering. These were washed with distilled water and dried prior to being powdered with an agate pestle and mortar to <75 μm. Each sample was separated into aliquots for different whole-rock geochemical analyses.

In order to obtain information relevant to organic carbon content and the origin of organic matter, samples from the three major types of sedimentary facies (laminated and moderately/highly bioturbated calcareous beds) were analyzed through the application of various techniques. Determination of total organic carbon (TOC) was performed by measuring total carbon and total inorganic carbon at the *Laboratorio de*

Paleoambientes of the *Instituto de Geología* (UNAM). The measurements were taken using a HiperTOC solid analyzer (Thermo Scientific), which employs an infrared cell to measure the CO_2 produced by combustion. Total carbon concentration was measured by heating 10–20 mg of sample material to 980 °C, and total inorganic carbon was determined by acidifying the sediment with 10% H_3PO_4. TOC content was calculated by subtracting total inorganic carbon from total carbon. Accuracy and precision of both analyses are better than 5%. Total nitrogen (N_{TOT}) was also determined using 2.0 mg of sample material with a CHNS/O Perkin Elmer 2400 series II, mode CHN at the *Laboratorio de Edafología Ambiental* of the *Instituto de Geología* (UNAM). The carrier gas was He and the combustion and reduction temperatures were 980° and 640 °C, respectively.

Additionally, pyrolysis on samples with TOC values above 1% was performed using a model 6 turbo ROCK-EVAL analyzer, marketed by Vinci Technologies, at the *Laboratorio de Geoquímica y Petrografía Orgánicas* of the *Instituto Mexicano del Petróleo* (IMP). For this analysis, 100 mg of sample material was heated to 300 °C in order to release volatile hydrocarbons (S_1). Later, sample pyrolysis was performed at a rate of 25 °C per minute until reaching 600 °C to release pyrolytic hydrocarbons (S_2). The CO_2 released was trapped inside a thermal conductivity detector to quantify thermally produced (S_3) organic CO_2 (TOC). The hydrogen index (HI) was obtained by dividing $S_2 \times 100$ by TOC, and the oxygen index (OI) by dividing $S_3 \times 100$ by TOC (Espitalié et al., 1985). These parameters represent the amount of hydrogen and oxygen relative to the amount of organic carbon present in a sample, respectively.

Concentrations of major and trace elements were determined for twenty-nine samples from laminated and moderately bioturbated beds distributed along the entire stratigraphic column. These analyses were carried out at Activation Laboratories Ltd. (Actlabs) in Canada, through Inductively Coupled Plasma/Optical Emission Spectrometry (ICP-OES; Varian 735) and Inductively Coupled Plasma Mass Spectrometry (ICP-MS; Perkin Elmer Sciex ELAN 9000), after the digestion of 1.0 g of sample material using four different acids (HF, $HClO_4$, HNO_3 and HCl) (Package code Ultratrace 6). For evaluation of the analytical performance of the method, standards GXR-1, GXR-2, GXR-6, SAR-M, DNC-1 and SBC-1 of the United States Geological Survey, and DH-1a from the Canada Centre for Mineral and Energy Technology were analyzed at the beginning and end of each batch of samples. Percentages of the relative standard deviation were consistently below 10%, as corroborated by standards and analysis of replicate samples.

All elemental concentrations were normalized to aluminum content in order to remove the effect of variable terrigenous input, as well as to differentiate the authigenic contribution of redox-sensitive trace elements (RSTEs) (Calvert and Pedersen, 1993; Brumsack, 2006; Tribovillard et al., 2006; Reolid et al., 2015). Aluminum is commonly of detrital origin and is usually immobile during biological and diagenetic processes (e.g., Calvert and Pedersen, 1993). In addition, to compare the relative enrichment of RSTEs, we calculated the enrichment factor (EF) for a given element (X) relative to average shale value (Wedepohl, 1971): $EF_{element} = (X/Al)_{sample}/(X/Al)_{average\ shale}$. An EF > 3 represents detectable authigenic enrichment of the element over average shale concentration, and an EF > 10 represents a moderate to strong degree of authigenic enrichment (e.g. Tribovillard et al., 2006).

Biogenic barium (Ba_{bio}; a proxy for bio-productivity) was calculated using the normalized approach proposed by Dymond et al. (1992): $Ba_{bio} = Ba_{total} - (Al \times (Ba/Al)_{detrit}$. In this equation, the Ba/Al_{detrit} represents the Ba/Al ratio of the detrital fraction. As the composition of the detrital source was not available, we used the global average ratio (0.0037) proposed by Reitz et al. (2004).

Nine samples for X-ray powder diffraction analysis were ground with an agate pestle and mortar to <75 μm and mounted in aluminum holders for determining mineral composition. A Shimadzu XRD-6000 X-ray diffractometer equipped with a Cu tube and graphite monochromator was used at the XRD laboratory of the *Instituto de Geología*, *Universidad Nacional Autónoma de México* (UNAM). The analyses were applied to randomly oriented samples using the measurement range (2θ) of 4 to 70° at a speed of 1°/min.

All analytical and calculated data presented are available electronically in Supplementary Appendix A.

4. Results

4.1. Age of the Xilitla section

Previous studies close to the town of Xilitla (Blanco et al., 2011; Blanco-Piñón et al., 2008, 2014) have reported an age spanning the C–T transition for the Agua Nueva Formation, on account of the joint presence of the distinctive planktic foraminifera *Rotalipora cuhsmani* and the bivalve *Inoceramus labiatus*. Nonetheless, these studies do not provide a biostratigraphic framework that would allow a more precise constraint on the time of deposition. In this study, we use U–Pb zircon geochronology and bioevents to give more accurate information in this regard.

Zircons from sample Az (bed 11; at 1.7 m) (Figs. 2 and 3) give an age that varies between 89 and 100 Ma. The youngest concordant zircon age is 89 ± 0.7 Ma; however, an even more concordant zircon provides an age of 93 ± 1.0 Ma. The calculated age (TuffZirc algorithm) for a group of fourteen zircons is 95 ± 0.3 Ma. Based on the mean age of the seventeen most concordant zircons, an age of 94.1 ± 1.6 Ma was obtained. Considering these data, the latter age is regarded as being more robust.

Four important bioevents that are commonly recognized within the latest Cenomanian–earliest Turonian transition (Keller et al., 2004; Coccioni and Luciani, 2004; Caron et al., 2006; Robaszynski et al., 2010; Negra et al., 2011; Kędzierski et al., 2012; Bomou et al., 2013; Denne et al., 2014; Lowery et al., 2014; Reolid et al., 2015) were identified within the section studied (Fig. 2). From base to top they correspond to:

(i) The last occurrence of *Rotalipora cushmani* (Morrow) (top of the *R. cushmani* Total Range Zone), identified in bed 17 (at 2.8 m).
(ii) The *Heterohelix* shift, characterized by a peak in heterohelicid abundance (40–50% of allochems), identified in bed 29 (at 5.1 m).
(iii) The so-called "filament event", characterized by a peak in filament accumulation (30–40% of the allochems), identified in beds 93–95 (from 15.8 to 16.2 m). Filaments are translucent grains about 10–900 μm in length and 0.3–2 μm wide, and match known thin-shelled juvenile pelagic bivalves. Blanco-Piñón et al. (2014) had already reported the presence of these filaments in the Agua Nueva Formation of the Xilitla area.
(iv) The first occurrence of *Helvetoglobotruncana helvetica* (Bolli) (base of the *H. helvetica* Total Range Zone), identified in bed 106 (at 17.2 m).

It is noteworthy that the identification of the *Heterohelix* shift and the filament event is the first documentation of their presence in Mexico. Taking these four bioevents into account, the lower 2.8 m of the studied section belong to the top of the *R. cushmani* Total Range Zone, whereas the *Whiteinella archaeocretacea* Partial Range Zone spans from 2.8 to 17.2 m and the *H. helvetica* Total Range Zone starts at 17.2 m and extends above the top of the section (Fig. 2). The filament event occurs in other sections just above the C–T boundary, before or coeval with the first Turonian index ammonite *Watinoceras* (Caron et al., 2006; Negra et al., 2011). Building upon this consideration, we place the C–T boundary below bed 93 (at 15.8 m) in the studied section (Fig. 2).

4.2. Facies description and occurrence

At the field scale, the Xilitla section consists of an interbedded sequence of calcareous rocks and bentonites. The former corresponds to

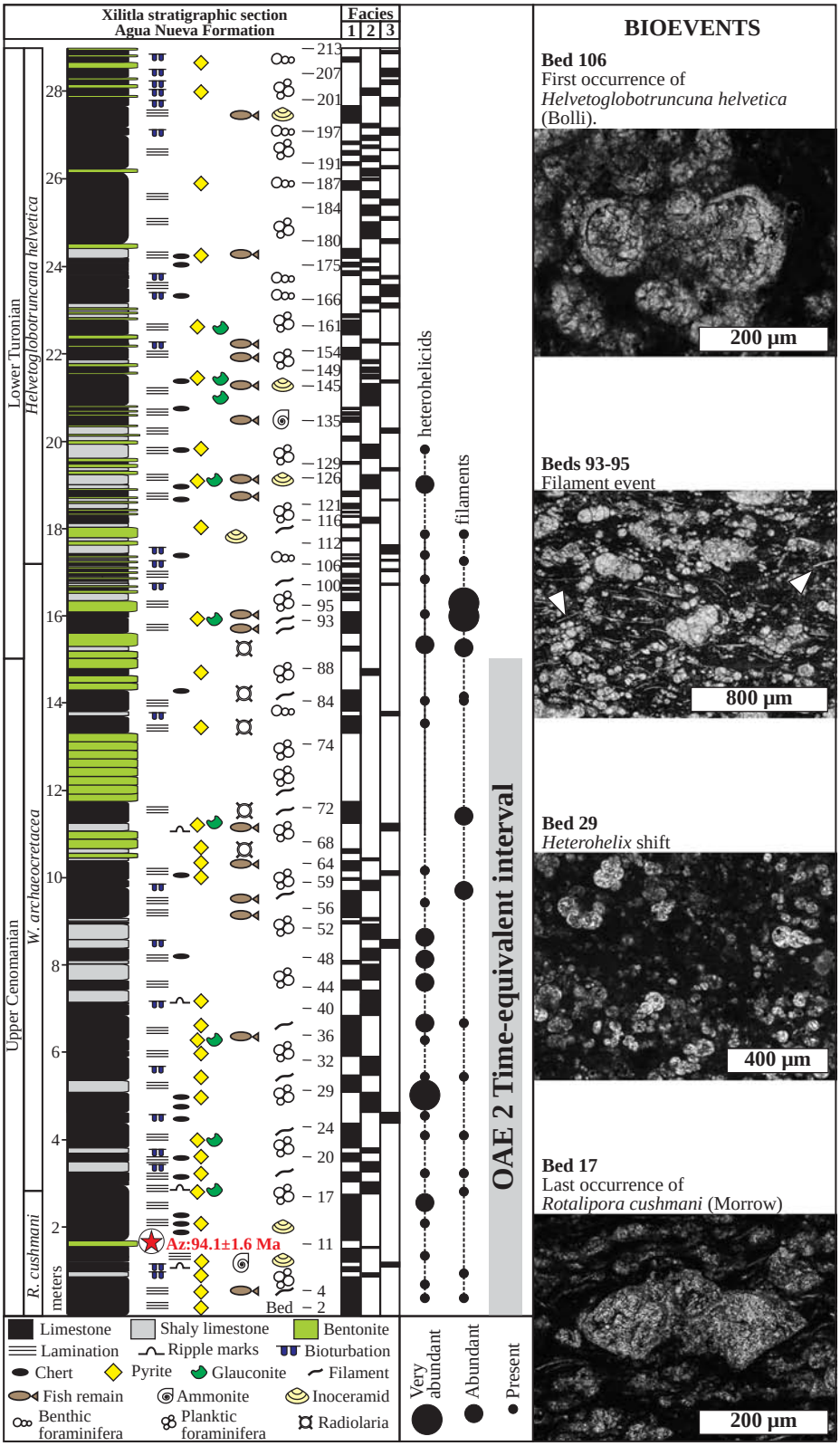

Fig. 2. Lithology, facies (F1 to F3) and age distribution of the Xilitla section. Bentonite beds are green and are wider than the other lithologies in order to make them stand out visually in the stratigraphic column. The right panel shows photomicrographs of the four indentified bioevents. (For interpretation of the references to color in this figure legend, the reader is referred to the web version of this article.)

fissile and shaly limestone displaying various shades of black and gray (N1 to N8) on fresh cuts, and dark yellowish orange (10YR 6/6) to pale yellowish orange (10YR 8/6) on weathered surfaces (Fig. 4A–B). These beds are essentially tabular and vary in thickness from 2 to 42 cm. They frequently contain layers (with a pinch-and-swell structure, Fig. 4C) and nodules of flint parallel to bedding, with various dimensions (centimeter-scale) and lenticular to irregular shape. Sets of fractures and stylolytes with oil stain are common at some calcareous

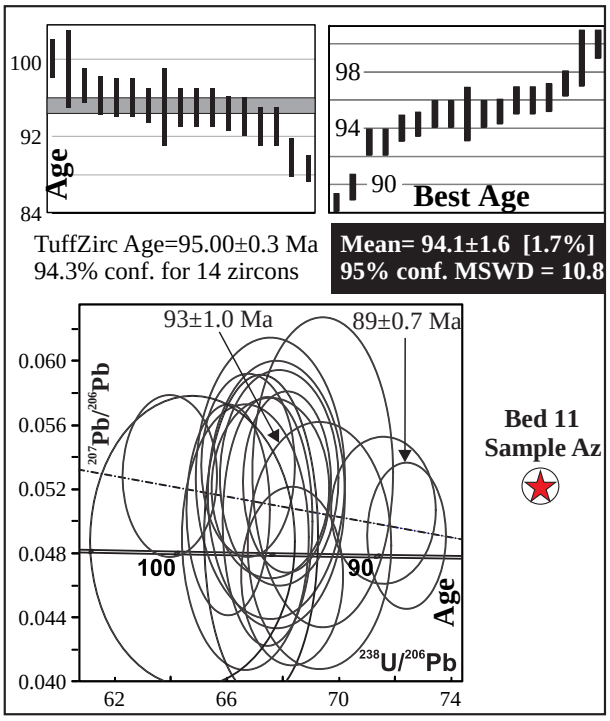

Fig. 3. LA-ICP-MS U–Pb analysis of zircons separated from bentonite sample Az, plotted on Tera–Wasserburg diagram. The TuffZirc age and best age are also plotted. See Fig. 2 for stratigraphic position of sample.

levels. On the other hand, bentonite beds are light olive gray (5Y 6/1) on fresh cuts (Fig. 4D) and moderate reddish orange on weathered surfaces (10R 6/6), vary in thickness from 2 to 20 cm, and are common from 10 m to the top of the section. Thick successions of bentonite beds can be observed between 12 and 16 m (Fig. 2). The most remarkable lithologic feature of the Xilitla section is the common presence of laminated beds containing pyrite (Fig. 4E–F), fish remains and inoceramid bilvalves, interspersed with bioturbated layers (Fig. 4F). Both field and petrographic observations allow for the discrimination of various redox facies deposited in a pelagic marine environment and which are described below.

4.2.1. Facies F1. Dark laminated/non-bioturbated mudstone/wackestone rich in pyrite and glauconite

This facies consists of dark gray (N3) to black (N1), thinly laminated beds with a low bioturbation index (0–1) (weak to absent bioturbation) (Figs. 4E–F and 5A–B). Pyrite laminae from 1 mm to 8 mm thick alternate with thinner layers of calcareous material (Fig. 5A–B). Pyrite occurs less commonly as nodules, including the variety called "*Pyrite Sun*" (Fig. 5C), which consists of a flat disk shape constituted of radiating, acicular crystals. This facies also contains common well-preserved fish remains (Fig. 5D–E) and scarce ammonites (Fig. 5F). Microscopically, this facies may be divided in two subfacies:

- *Subfacies F1A*: Mudstone and bioclastic wackestone with planar laminated (Fig. 6A) to anisotropic fabric (Fig. 6B); abundant planktic foraminifera (Fig. 6A–D); common fish remains (Fig. 6B) and bivalve fragments (Fig. 6C); rare ostracods, and echinoderm fragments. Micro-lamination is more accentuated in limestone and is defined by laminae with parallel boundaries, sometimes wavy, that differ in color and internal composition (Fig. 6A). Darker laminae are medium dark gray (N4) to dark gray (N3) micritic layers high in organic matter and clay concentration and contain few scattered fossils, whereas lighter laminae are fossiliferous. Millimetric laminae of bentonite alternating with calcareous/argillaceous laminae are rarely observed within the upper 10 m of the section. Subfacies F1A contains abundant disseminated pyrite framboids (Fig. 7A and E), in addition to frequent glauconite as infilling of foraminiferal tests or as cement within intergranular porosity (Fig. 6D). Subfacies F1A is the most dominant type of facies in the whole section, although it is more continuously present within the lowest 9 m (top *R. cushmani*–middle *W. archaeocretacea* zones) (Fig. 2).
- *Subfacies F1B*: This subfacies consists of wackestone with a grayish yellow (5Y 8/4) argillaceous matrix yielding abundant radiolarians, common fish remains, and is almost barren of planktic foraminifera (Fig. 6E). It shows some degree of anisotropic fabric and several stages of silicification and dolomitization that dim the presence of framboidal pyrite and glauconite. Subfacies F1B occurs in relatively short and intermittent episodes (discrete beds of 10–20 cm) solely between 10 and 16 m (middle *W. archaeocretacea*–base *H. helvetica* zones) (Fig. 2).

4.2.2. Facies F2. Poor to moderately bioturbated wackestone/packstone

It consists of medium gray (N5) to medium light gray (N6) laminated beds with a bioturbation index of 2–3 (poorly to moderately bioturbated). Burrows are mainly bedding-parallel (Fig. 5G–H) and mostly include *Planolites* (Fig. 5I) and *Chondrites* (Fig. 5J). Pyrite is disseminated, as laminae, or as burrow infill (Fig. 5G). Inoceramid bivalve shells (Fig. 5K–L) and fish remains (Fig. 5K) are frequent. Ripple marks are regularly present on the top surface of beds (Fig. 5M). Facies F2 is the second most dominant type of facies, occurring regularly throughout the stratigraphic section (Fig. 2).

Microscopically, this facies is related to silty bioclastic wackestone and packstone with a yellowish gray (5Y 8/1) micritic matrix (Fig. 6F–G). Planktic foraminifera are the dominant skeletal allochems and are commonly recrystallized and densely packed. Bivalve filaments are common and benthic foraminifera and ostracods are rarely present. Lamination is moderately preserved and usually interrupted by burrows with irregular outlines (Fig. 6F–G). Disseminated pyrite corresponds mainly to framboids (Fig. 7B–D and F). Glauconite is less common than in facies F1 and occurs mainly as cement infilling intergranular porosity.

Some scattered, straight to gently curved filaments (thin-shelled pelagic bivalves) are regularly present in both facies F1 and F2 between 0 and 18 m. An interval with a significant accumulation of these filaments (increase in 30–40%) can be observed in beds 93–95 (15.8–16.2 m) (filament event; Fig. 2).

4.2.3. Facies F3. Highly bioturbated, light-colored wackestone/packstone

This facies consists of thoroughly bioturbated limestone (bioturbation index mostly between 4 and 5), with no evidence of lamination or pyrite. Its distinguishing feature is the presence of vertical and oblique burrows with different cross-cutting relationships (Figs. 4F and 5N–Q).

Based on the contrast between burrows fills and the host sediment, this facies can be subdivided into two types: (i) light-on-dark (LOD) bioturbated facies, characterized by abundant trace fossils in a burrow-mottled and dark matrix (Fig. 5N); and (ii) dark-on-light (DOL) bioturbated facies with common overlapping burrows (Fig. 5O–P). Small *Chondrites* burrows and large *Zoophycos*-like trace fossils (Fig. 5N) occur in both patterns, as well as vertical and oblique burrows (Fig. 5O–Q). Facies F3 occur as short, isolated events within the lowest 16 m of the studied section, but become more common within the upper 12 m (especially in the uppermost 6 m) (*H. Helvetica* Zone) (Fig. 2).

Microscopic observations show that this facies consists of wackestone and packstone with a moderate yellow (5Y 7/6) micritic matrix containing abundant planktic foraminifera and common benthic foraminifera (Fig. 6H–I). These grains are highly recrystallized and packed. Lamination is not evident and samples exhibit a mottled

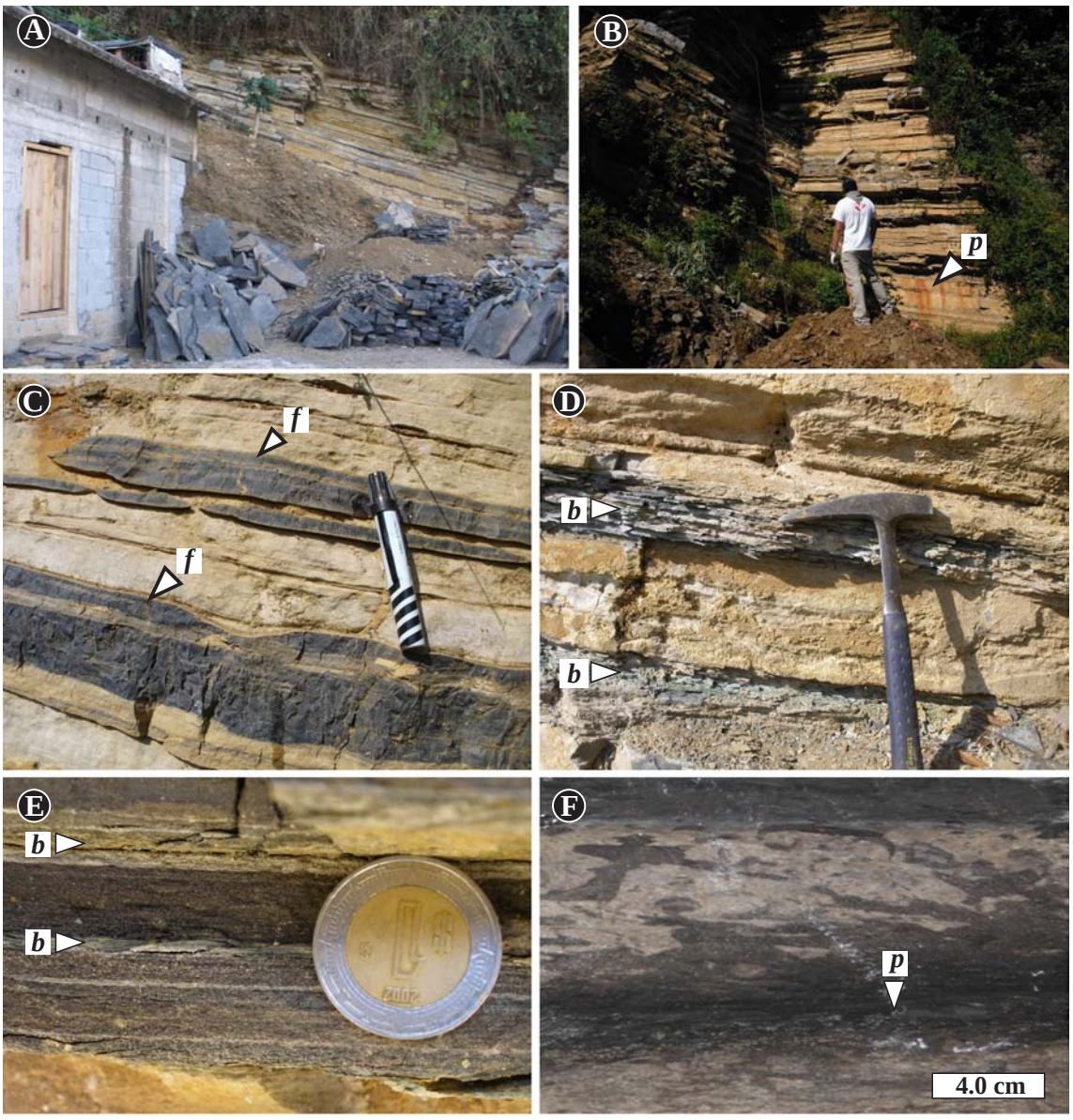

Fig. 4. Photographs illustrating the general characteristics of the outcrop: (A) Lower part of the Xilitla section (Quarry I). Several loose slabs of limestone can be observed in the front of the picture. (B) Notice the yellowish–reddish stains of some beds as a result of pyrite (*p*) weathering (Quarry III). (C) Layers of flint (*f*) with a pinch-and-swell structure (Pen size = 12 cm). (D) Interbedded limestones and bentonites (*b*) (Quarry III). (E) Laminated limestone bed with laminae of greenish bentonite (*b*). (F) Alternation of dark gray laminated limestone with pyrite (p), and light-colored bioturbated limestone (bed 197). (For interpretation of the references to color in this figure legend, the reader is referred to the web version of this article.)

appearance characterized by vertical burrows (Fig. 6I). Disseminated pyrite and glauconite are absent in this facies.

4.3. Pyrite framboid size distribution and content

Disseminated pyrite morphology in this study includes: (i) spherical framboids that consist of microcrystal pyrite aggregates, commonly with intercrystal porosity; (ii) irregular anhedral to subhedral masses; and (iii) euhedral pyrite grains. Of these, the framboids are the most common (Fig. 7). Preliminary observations of unpolished rock chips, under SEM, revealed the presence of different microcrystal size, form and organization inside the framboids (Fig. 7C–F). Although the morphology and size of the majority of framboids is clearly preserved, thus conducive to measurement, some of them have been partially or totally recrystallized (with minor internal porosity or as a pyrite spheroid) or show evidence of secondary growth.

Pyrite framboids only occur in facies F1 and F2, mainly within the lowest 11 m of the section. Their stratigraphic distribution and main statistical parameters of size and content are listed in Table 1 and depicted in Fig. 8. Although the size of framboids varies slightly from sample to sample, they are generally rather small, with mean diameters of between 5.0 μm in bed 30 (facies F1) and 7.6 μm in bed 152 (facies F2). The small-sized framboid population is recorded in beds 30, 35, 131 and 194 (facies F1), whereas framboids with diameters >10 μm are more common in the upper part of the stratigraphic section, mainly in beds 152 and 187 (facies F2), and bed 161 (facies F1). The highest framboid content occurs mainly in beds of facies F1 with values of 1213 per mm^2 (bed 210), 620 per mm^2 (bed 1) and 541 per mm^2 (bed 62). Of the analyzed beds included in facies F2, only bed 10 has a significant content of 558 per mm^2. The minimum number of framboids occurs in facies F2 with a value of 70 per mm^2 (beds 65 and 187).

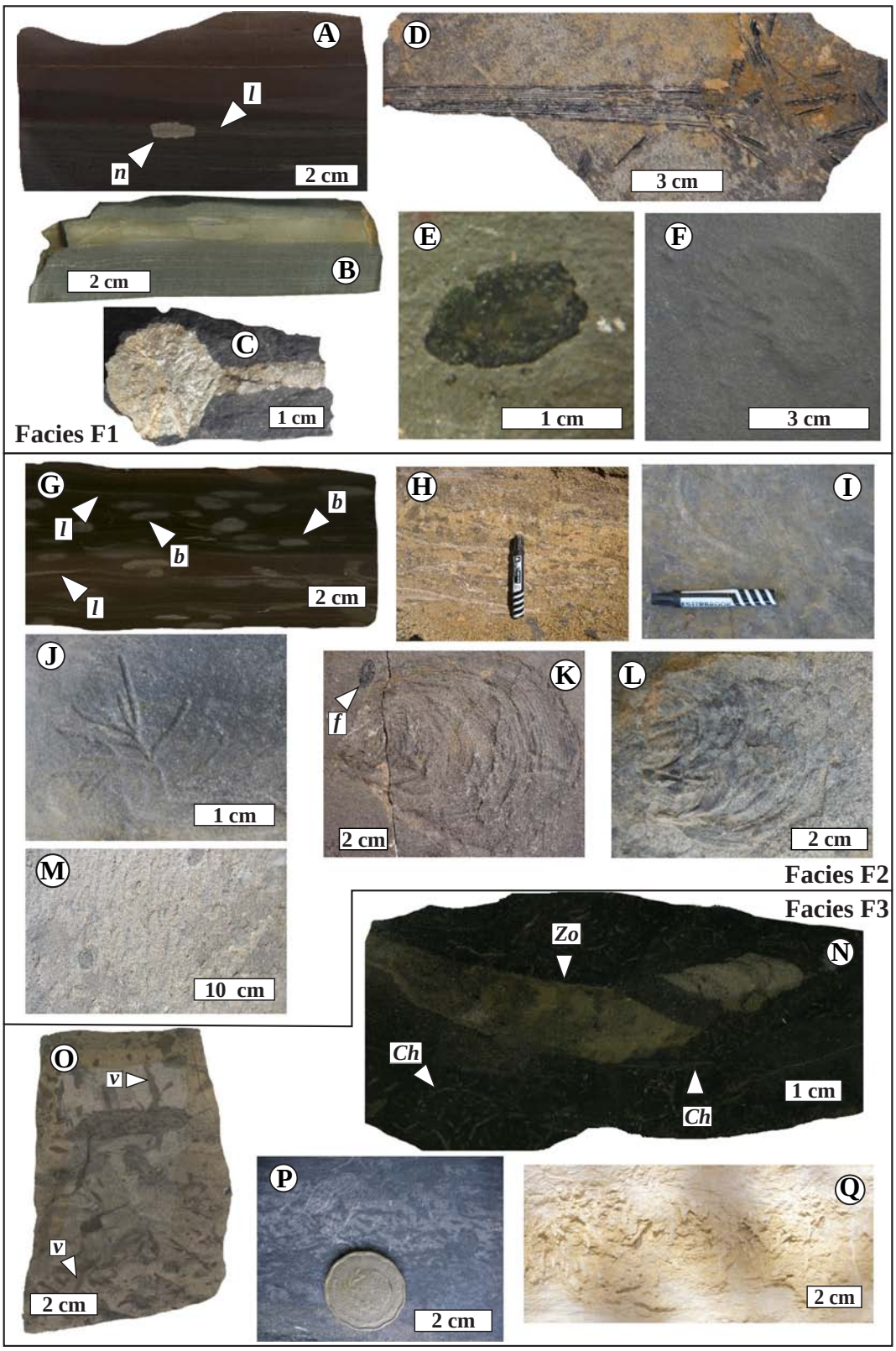

Fig. 5. General characteristics of the sedimentary facies. Facies F1: (A) Limestone with undisrupted laminated fabric and pyrite as laminae (*l*) and nodules (*n*) (bed 115). (B) Laminae of pyrite (bed 22). (C) Sun pyrite (bed 35). (D) Disarticulated remains of fish (bed 95). (E) Fish scale (bed 6). (F) Ammonite (bed 60). Facies F2: (G) Moderately bioturbated and laminated limestone. Pyrite is disseminated in bed-parallel burrows (*b*) and laminated (*l*) (bed 65). (H) Bedding-parallel burrows (bed 19) (Pen size = 12 cm). (I) *Planolites* (bed 7) (Pen size = 12 cm). (J) *Chondrites* (*bed 52*). (K) *Inoceramus cicloides* Wegner. Note the fish scale (*f*) (bed 12). (L) *Inoceramus* (*Mytiloides*) *labiatus* Schlotheim (bed 126). (M) Ripple marks caused by currents on the upper bed surface (top view, bed 18). Facies F3: (N) Bioturbated limestone with a LOD pattern. Small *Chondrites* (*Ch*) and large *Zoophycos*-like (*Zo*) (bed 207). (O). DOL bioturbated pattern. Note different cutting relationships between bioturbation and vertical burrows (*v*) (bed 212). (P) DOL bioturbated pattern. From bottom to top, there is an increase in bioturbation intensity (bed 205). (Q) Vertical mid-strata burrows (bed 108). See the position of beds in Fig. 2.

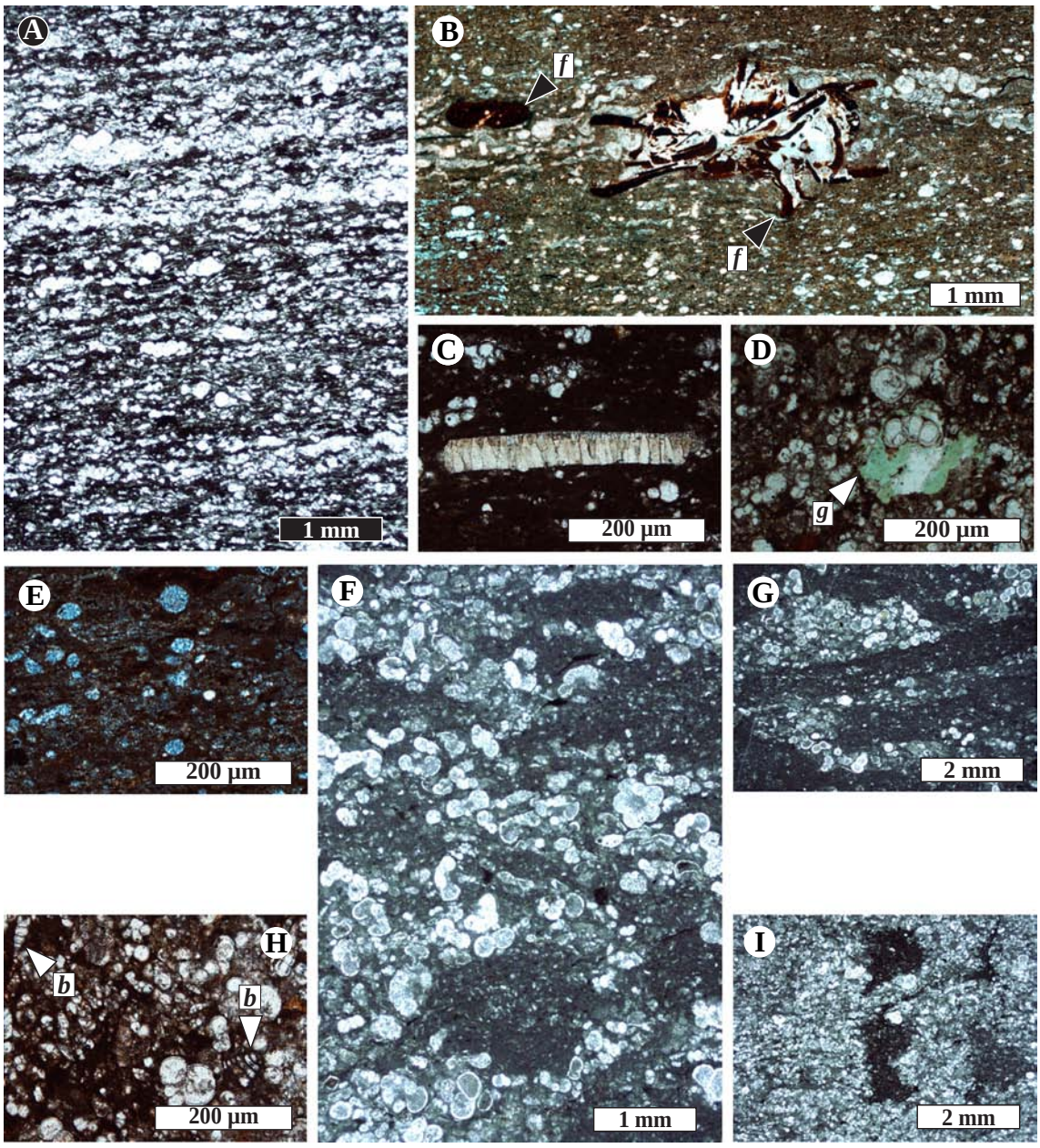

Fig. 6. Microscopic characteristics of the sedimentary facies. Facies F1: (A) Wackestone with planar laminated matrix and planktic foraminifera (bed 12). (B) Remains of fish (*f*) and planktic foraminifera in a wackestone with anisotropic fabric (bed 199). (C) Bivalve shell fragment (bed 30). (D) Authigenic glauconite (*g*) as cement and within planktic foraminifera (bed 161). (E) Subfacies F1B. Occasional radiolarian wackestone/packstone facies with no evidence of bioturbation (bed 87). Facies F2: (F) Disrupted lamination by horizontal–sub horizontal burrows (bed 204). (G) Bedding–parallel burrows (186). Facies F3: (H) Benthic foraminifera (*b*) in bioturbated facies (bed 50). (I) Vertical burrow filled with mudstone-type sediment (bed 80). See the position of beds in Fig. 2.

4.4. Stable isotopes and organic matter characterization

Carbon isotope values vary between −1.9 and +1.6‰ (Fig. 9 and Appendix B). The most striking feature of the $\delta^{13}C_{carb}$ curve is a distinct negative shift of 2.7‰ from 9.3 to 11.2, followed by a return to baseline values. Oxygen isotope data ($\delta^{18}O_{carb}$; Appendix B) show considerable variation across the whole section, fluctuating between −3.4‰ and −6.5‰ (−4.4‰ on average).

The TOC content fluctuates between 0.32 and 3.32%, with most of the samples rich in organic carbon recorded within the lowest 9 m of the section (top *R. cushmani*–middle *W. archaeocretacea* zones) (Fig. 10). In general, facies F3 shows low TOC values (consistently below 1%), while facies F1 and F2 have a higher content (ranging from 1 to 3.32%). The analyzed samples have a relatively high hydrogen index (HI; 276–468 mgH/g TOC) and low oxygen index (OI; 8–39 mg O/g TOC) values (Fig. 11). Total nitrogen concentration (N_{TOT}) ranges between 0.04 and 0.06%, leading to TOC/N_{TOT} ratios between 22.5 and 55.3 (Fig. 10). Low and high values of HI, OI and N_{TOT} are randomly distributed among sedimentary facies.

4.5. Major and trace elements

Al-normalized RSTEs contents are compared to TOC and total S (S_{TOT}) contents (Fig. 10 and Appendix B). In general, Cd, V, Zn and Cr display a decreasing trend with higher ratios in the lowest 9 m (top *R. cushmani*–middle *W. archaeocretacea* zones) of the section, where TOC reaches elevated values. Conversely, Ni, Co, Pb and Mo present a flat pattern with minor peaks at different levels. In detail, the interval

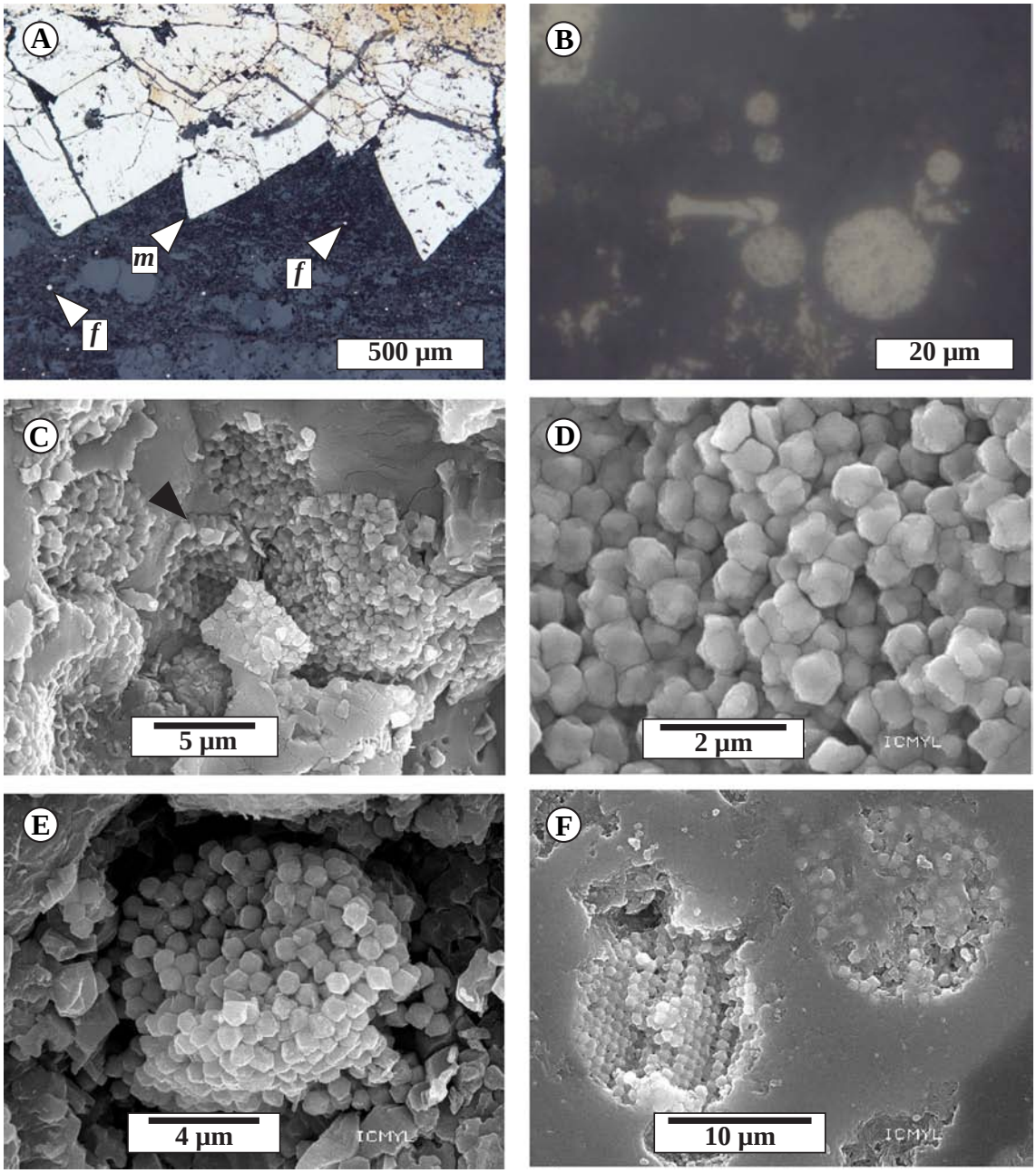

Fig. 7. Microscoptheic features of framboidal pyrite from the Xilitla section. Photomicrographs under reflected light microscope: (A) Massive (m) and framboidal (f) pyrite (bed 30). (B) Pyrite framboids in the calcareous matrix (bed 152). Photomicrographs under scanning electron microscope: (C) Framboids with disordered structure composed of randomly aggregated irregular microcrystals. In the center there is a framboid with hexagonal arrangement made up of octahedral microcrystals, all of which share a common morphological orientation (arrow) (bed 17). (D) Close–up of microcrystals of the framboid on the right in C. Note spherical clusters of poorly-formed octahedral particles. (E) Framboid with hexagonal arrangement composed of octahedral microcrystals with slight truncation and totally disoriented (bed 22). (F) To the left, there is a framboid with cubo–octahedral microcrystals in hexagonal arrangement and almost perfect orientation (bed 126).

between 1 and 9 m records maximum peaks of Cu/Al (164.84×10^{-4}) at 1.4 m; V/Al (404.08×10^{-4}) at 2.5 m; Fe/Al (0.96) and Zn/Al (426.61×10^{-4}) at 2.8 m; and U/Al (9.81×10^{-4}) at 4.8 m. This interval also shows a significant increase of Cr/Al (118.16×10^{-4}), as well as a moderate increase of Ni/Al (66.94×10^{-4}) at 2.5 m. Several pronounced peaks of Ba/Al with values of up to 438.46×10^{-4} can also be observed within the lower 9 m, where Mn/Al is consistently low (down to 104.86×10^{-4}). The interval between 9 and 29 m (middle *W. archaeocretacea–H. helvetica* zones) records moderate increases of Cd/Al (2.78×10^{-4}) and Zn/Al (341.06×10^{-4}) at 15.4 m; Cr/Al (90.68×10^{-4}), Ag/Al (1.73×10^{-4}) and Cu/Al (123.78×10^{-4}) at 17.1 m; and Cr/Al (153.69×10^{-4}), Co/Al (15.85×10^{-4}), Ag/Al (0.57×10^{-4}) and Cu/Al (64.62×10^{-4}) at 22.6 m.

Otherwise, S, Fe/Al, Co/Al, Pb/Al and Mo/Al exhibit a relatively flat pattern. Raw concentration of S presents dramatic increases at 10.1 m (7.43%) and 28.7 m (8.73%). In the latter stratigraphic position, the maximum peaks also occur for Fe/Al (18.24), Ni/Al (240.73×10^{-4}), Co/Al (28.54×10^{-4}), Pb/Al (57.07×10^{-4}), Ag/Al (2.12×10^{-4}), Mo/Al (40.24×10^{-4}) and Re/Al (0.154×10^{-4}), in addition to a moderate to slight peak of V/Al (270.73×10^{-4}) and Cr/Al (43.41×10^{-4}). The P/Al ratio exhibits low values in the lower 9 m of the section, with values between 0.03 and 0.09, and afterward increases slowly showing pronounced peaks at 22.6 m (0.12), 27.5 m (0.12), and 28.7 m (0.11).

The calculated EFs for trace elements are shown in Fig. 12. Analyzed samples are consistently enriched in RSTEs compared to the average shale. The largest mean EFs are recorded for Cd (167.06), Ag (69.89),

Table 1
Pyrite framboid size statistical parameters. N = Number of framboids in measured area, Min. F.D. = Minimum framboid diameter measured under optical microscope, Min. F.D. SEM = Minimum framboid diameter measured under SEM, Max. F.D. = Maximum framboid diameter measured under optical microscope. Underestimation of smallest framboids under reflected light affecting the calculated relative content can be ruled out because minimum framboid size estimated by SEM is similar to the minimum size determined with the optical microscope.

Bed	Facies	Mean (μm)	S.D.	Min F.D. (μm)	Min F.D. SEM (μm)	Max F.D. (μm)	Framboid content (number per mm^2)
210	1	6.1	2.8	1.6	1.8	29.1	1213
204	2	6.9	2.6	2.0	–	22.8	115
194	1	5.1	2.6	1.4	1.4	19.6	99
187	2	7.3	3.2	2.3	2.5	25.4	70
178	2	6.5	3.3	2.6	–	22.5	150
161	1	7.4	3.0	2.5	2.5	28.5	355
152	2	7.6	3.1	0.8	1.0	21.5	214
131	1	5.3	2.4	2.0	2.1	22.5	318
126	2	6.8	3.1	1.7	1.7	26.2	192
115	1	6.4	3.0	2.4	2.5	22.7	102
93	1	5.7	2.5	1.7	–	19.9	432
80	2	7.2	3.1	2.0	–	17.5	110
78	1	5.6	2.1	2.2	2.4	12.2	320
65	2	5.6	2.2	1.2	1.5	14.3	70
62	1	6.0	2.6	1.6	1.9	19.7	541
41	2	7.1	2.7	2.0	2.4	17.0	397
35	1	5.3	2.7	1.4	1.8	26.4	211
30	1	5.0	2.1	1.4	2.1	13.5	150
22	1	5.8	2.4	2.0	2.6	18.6	300
17	2	6.7	2.7	2.3	2.3	19.3	130
10	2	6.9	2.9	0.9	1.1	24.8	558
1	1	6.1	2.2	3.2	3.2	20.1	620

Re (37.22), Mo (16.80), Zn (10.31), V (8.72), U (8.07) and P (7.29). Fe, Cr, Ni, Co, Pb, Cu, and Mn record moderate to low EFs (mean EFs between 2.22 and 7.93). Note that mean EFs of Cd, Zn, V, Cr, Cu, U and Ba from the lowest 9 m are higher than those of the whole section.

Observations of thin rock sections and XRD analyses reveal that the detrital fraction of analyzed samples does not exceed 40%; indeed, they consist mainly of marine carbonate (65–92%, average 84.7%). This indicates that the Ba/Al ratio of Reitz et al. (2004) is valid for calculating reliable biogenic barium concentration. Accordingly, the Ba_{bio} content fluctuates between 472.53 (at 6.9 m, bed 39) and 1.9 ppm (at 5.4 m, bed 30) (with an average of 110.34 ppm) (Fig. 10).

4.6. Elemental and sulfur isotope composition of pyrite grains

The results of EDS and WDS analysis confirm that sulfides present in the studied sediments are pyrite. Under the SEM, a low density matrix occurs between pyrite microcrystals and/or enveloping the surface of the entire framboids (in both those disseminated in the matrix and those infilling burrows) (Fig. 13). EDS analysis on framboids reveals that such interstitial material is enriched in carbon, compared to pyrite crystals. Otherwise, the elemental data acquired through WDS analysis (Table 2) show that laminated and framboidal pyrite both contain significant quantities of Mo (~4500–6000 ppm) and lesser amounts of Ni (~200–400 ppm) and U (~220–2280 ppm). Regarding the sulfur isotope composition, $\delta^{34}S_{py}$ values of the analyzed grains (composed of pyrite microcrystals) are consistently negative, ranging from −5.2‰ (bed 106) to −51.2‰ (bed 13) (Fig. 14). The $\delta^{34}S_{py}$ profile displays an increasing trend from −51.2‰ at 1.9 m to −5.1‰ at 14.3 m.

5. Discussion

5.1. Correlations based on bioevents and definition of the OAE 2 time-equivalent interval

The OAE 2 time-equivalent interval is commonly delimited by a large positive carbon isotope excursion (with three distinctive peaks), both in marine inorganic carbonate (2–4‰) and organic matter (up to 6‰), interpreted to be the result of enhanced burial of ^{12}C-enriched organic matter (Keller et al., 2004; Caron et al., 2006; Bomou et al., 2013) (Fig. 9). However, in the $\delta^{13}C_{carb}$ profile (Fig. 9 and Appendix B) from the Xilitla section there is not a truly defined positive shift. Overall, the carbon isotope values are unusually lower in comparison to the Cretaceous $\delta^{13}C_{carb}$ database (Leckie et al., 2002; Föllmi, 2012). They are depleted by more than 1.5–3‰ compared to contemporaneous marine calcite. Likewise, the $\delta^{18}O_{carb}$ values (Appendix B) are also low compared to those found in Cretaceous pelagic sediments (Clarke and Jenkyns, 1999). This difference can be the result of both diagenetic effects and local conditions. For instance, alteration of the $\delta^{13}C$ is possibly linked to early diagenetic modification, as a result of the transfer of isotopically light carbon from bacterial degradation of organic matter to carbonate cement. Diagenetic effects during burial (pore water interaction and/or dissolution and recrystallization) can be also considered given the recrystallization of skeletal allochems.

Major biological changes across the C–T transition are also a useful tool to trace the OAE 2 time-equivalent facies (Coccioni and Luciani, 2004; Caron et al., 2006; Bomou et al., 2013; Reolid et al., 2015) (Fig. 9). Among planktic foraminifera, the onset of the global turnover associated with the anoxic event occurs mostly below the last occurrence of *R. cushmani*, marking the disappearance of planktic foraminifera of complex morphology and with a longer and deeper life-cycle (K-species like the rotaliporids), which have adapted to oligotrophic stable nutrient levels in deep and intermediate waters. They disappeared due to the oceanic perturbation of oxygen levels within the *W. archaeocretacea* Zone, conversely favoring the proliferation of species with a short and shallow life-cycle (r-selected species such as the heterohelicids and whiteinellids). The first occurrence of *H. helvetica* marks the reappearance of complex keeled morphotypes (K-selected species), thus reflecting the return to stable nutrient conditions and the end of the anoxic event.

In the studied section, within the *W. archaeocretacea* Zone, both the *Heterohelix* shift (bed 29, at 5.1 m) (Fig. 2) and the "filament event" (bed 93–9, 15.8–16.2 m) (Fig. 2) highlight environmental conditions of great stress during the turnover related to OAE 2. The rapid rise in the abundance of heterohelicids (surface-dweller opportunists) is associated to the better adaptation of these organisms to sudden environmental change (temperature, salinity, nutrient level), and commonly indicates a drop in water column oxygenation (e.g., Caron et al., 2006; Reolid et al., 2015). Otherwise, the abundance of filaments is interpreted as the result of the mass mortality of planktonic bivalve larvae (e.g., Caron et al., 2006; Kędzierski et al., 2012; Bomou et al., 2013) and/or the product of disintegration of pelagic bivalves during high-energy events (Negra et al., 2011). They are related to heightened marine productivity and oxygen-deficient water masses. Both bioevents have also been observed worldwide in a similar biostratigraphic position in the Western Interior Seaway (Pueblo section-GSSP, Caron et al., 2006; Atascosa and Karnes cores, Denne et al., 2014), and in the Tethys (Gongzha section-Tibet, Bomou et al., 2013; Rybie section-Poland; Kędzierski et al., 2012; wadi Bahloul-Tunisia, Caron et al., 2006 and Reolid et al., 2015) (Fig. 9). For the first time in Mexico, the record of the *Heterohelix* shift and the filament event is the expression of an effective connection between the Mexican Sea and the aforementioned oceanic basins during the C–T transition. Furthermore, the occurrence of the "filament event" below the base of the *H. helvetica* Zone supports the use of this bioevent as a global stratigraphic marker preceding the restoration of keeled planktonic foraminifera, in opposition to what is suggested by Desmares et al. (2007).

Considering the connection between the aforementioned bioevents and the main peaks in the $\delta^{13}C$ curve defining the anoxic event, the OAE 2 time-equivalent interval in the Xilitla section can be constrained to the lowermost 15.8 m (Fig. 9). This position for the OAE 2 interval is also supported by the robust radiometric age estimated from bentonite Az (94.1 ± 1.6 Ma) (Fig. 3). This result is compatible with the astronomically recalibrated radiometric age of 93.90 ± 0.15 Ma for the C–T boundary proposed by Meyers et al. (2012) (Fig. 9).

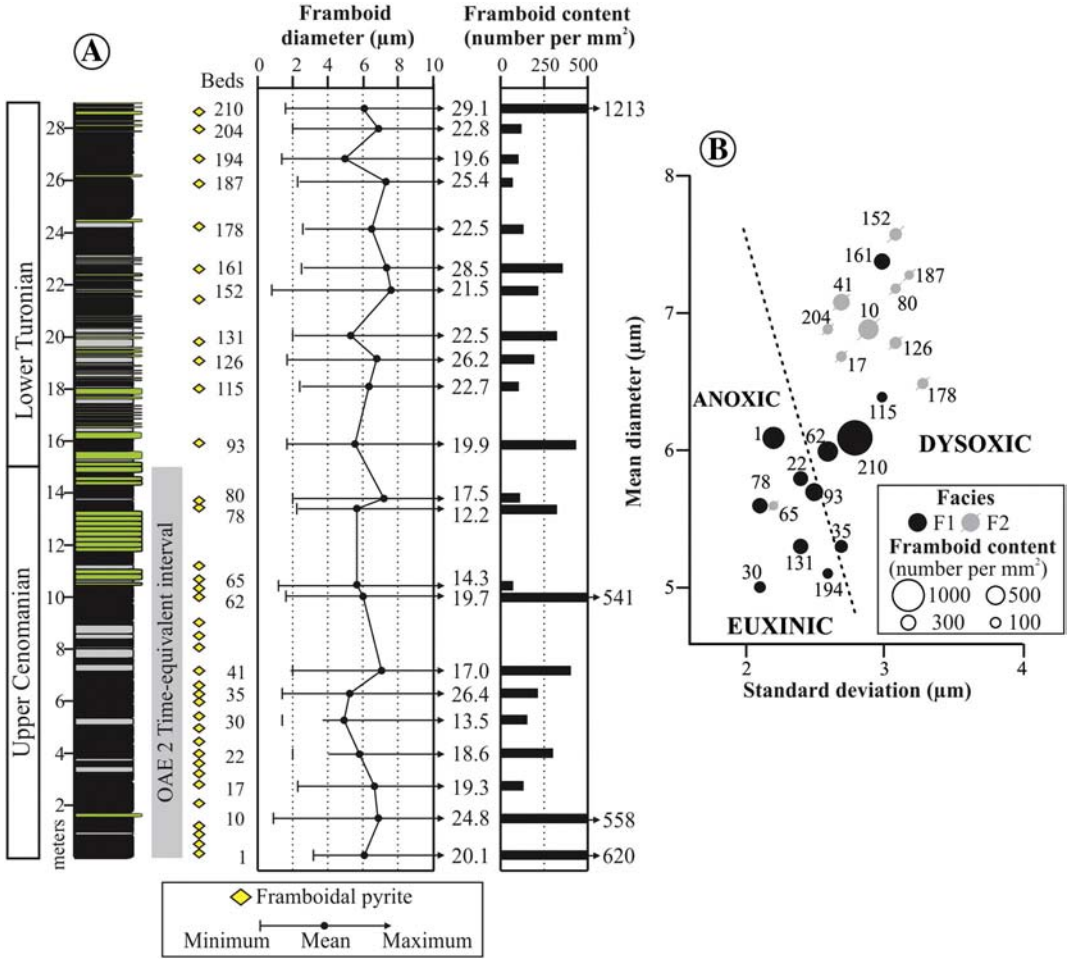

Fig. 8. Framboidal pyrite plots: (A) Stratigraphic distribution, diameter and content of framboidal pyrite. (B) Mean versus standard deviation plot of framboidal pyrite. The boundary between fields for euxinic, anoxic and dysoxic environments is that seen in modern depositional settings (from Wilkin et al., 1996). Size of circles is proportional to the estimated content of framboids. The color of the dots represents the sedimentary facies. (For interpretation of the references to color in this figure legend, the reader is referred to the web version of this article.)

5.2. Assessing redox conditions

5.2.1. Interpretation of sedimentary facies

- *Interpretation of facies F1*: The lack of bioturbation (Figs. 5A–B and 6A–B) and absence of benthic foraminifera are consistent with anoxic bottom-water conditions (ORB-A; Reolid et al., 2010). Such environment precluded burrowers and allowed the preservation of abundant disarticulated fish parts (Figs. 5D–E and 6B) that settled to the sediment from oxygenated upper water layers. The millimeter-scale fine lamination observed in this facies (Figs. 5A–B and 6A) implies deposition in a low-energy environment. The differences in laminae color and content reflect minor fluctuations in sedimentary conditions in the TMB. For instance, the planktonic-rich laminae may reflect short periods of high productivity conditions that sustained the proliferation of calcareous zooplankton. Currently, these blooms in foraminiferal productivity have been observed in certain areas of the Mediterranean (Rigual-Hernández et al., 2012) and North Atlantic Basin (Salmon et al., 2014), where they are associated with seasonal rise in sea surface temperature and nutrient conditions.

The radiolarian-rich beds in the middle part of the section (subfacies F1B) (Figs. 2 and 6E) fit in with the predominance of these organisms in other black shales representing the OAE 2, commonly interpreted as the regional renewal of nutrient-rich waters (Coccioni and Luciani, 2004; Caron et al., 2006; Kędzierski et al., 2012; Gambacorta et al., 2015). Such blooms of organisms with silica skeletons also supported ocean acidification during OAE 2, due to an increased uptake of CO_2 derived from massive volcanic eruptions of the Caribbean Plateau (Gebhardt et al., 2010; Du Vivier et al., 2015a). Under these conditions, planktic foraminifera biomass diminished due to low calcium carbonate availability; radiolarian, less affected by acidification, competed more efficiently and flourished. Considering that subfacies F1B is spatially and temporally associated with the thick successions of bentonite (Fig. 2), a local factor that may have accounted for the silica supply and probably enhanced seawater acidification and selective radiolarian proliferation was volcanic ash-fall in the TMB. It has been demonstrated that fall-out of volcanic ash in the ocean may induce a reduction of the surface water pH, which affects planktonic calcifying organisms (e.g., Cobianchi et al., 2015).

- *Interpretation of facies F2*: The poor-to-moderate degree of bioturbation of facies F2, coupled with the presence of very few benthic foraminifera suggests that this facies accumulated under dysoxic oxygen levels (ORB-B of Reolid et al., 2010). Dominance of horizontal burrows disrupting the original lamination (Figs. 5G–I and 6F–G), as well as the absence of vertical ones suggests that favorable oxygen conditions at the sediment–water interface allowed organism colonization and that anoxic conditions prevailed within the lower sediment layers. A striking feature of this facies which further reflects a slight concentration of oxygen at the seafloor is the common presence of inoceramid shells (Fig. 5K–L). These bivalves flourished under dysoxic bottom-water conditions in several mid-Cretaceous

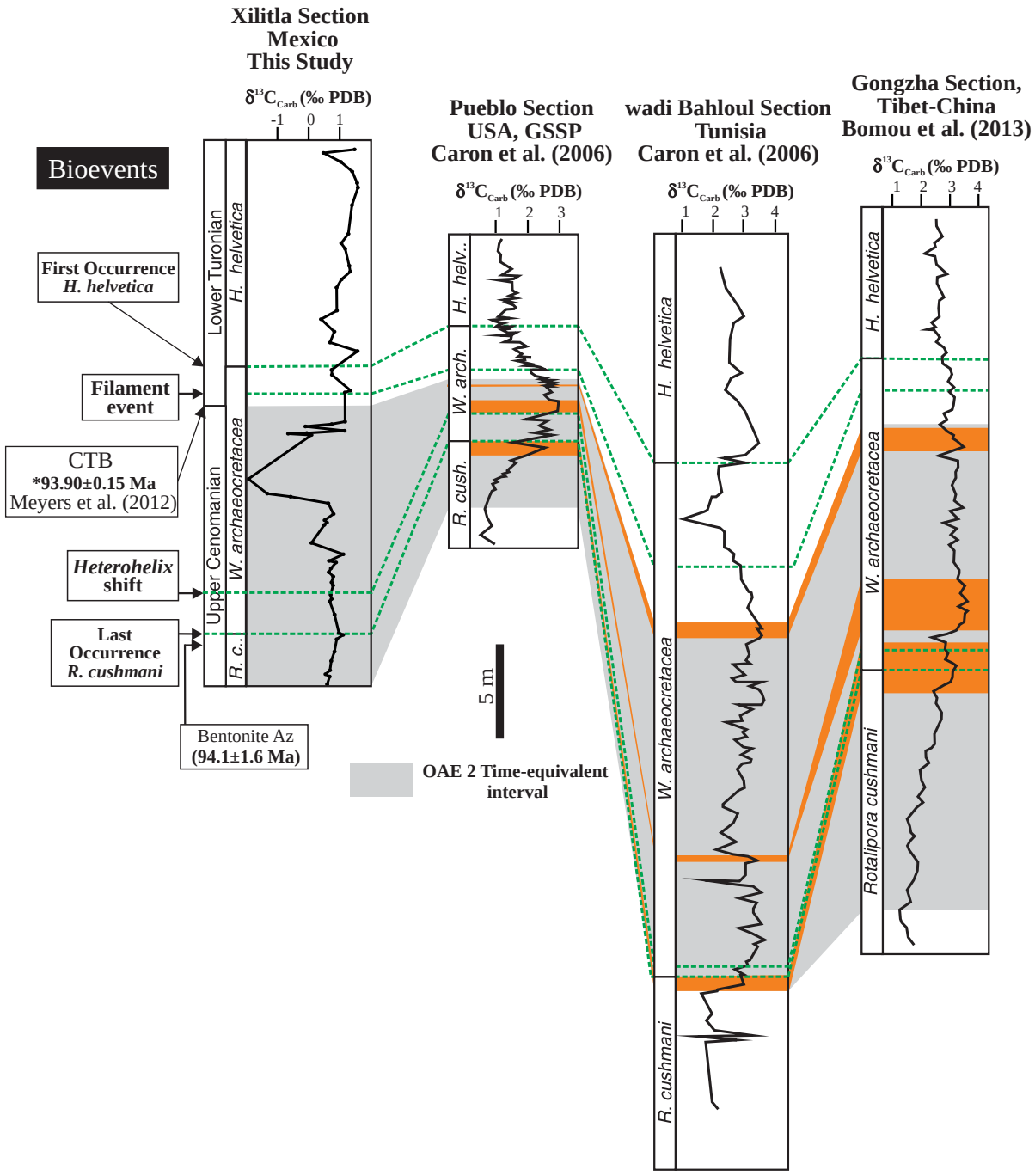

Fig. 9. Correlation of bioevents and carbon isotope events across the Cenomanian–Turonian transition between the Xilitla section (Mexico), and sections in Colorado—USA, Central Tunisia and Tibet—China. Notice that the $\delta^{13}C$ data from the Xilitla section do not record the typical features of the globally documented Cenomanian–Turonian positive excursion.

basins (Caron et al., 2006; Jiménez Berrocoso et al., 2008; Ifrim et al., 2011; Lowery et al., 2014). Ripple marks (Fig. 5M) associated with some beds provide evidence of periodic seafloor ventilation by bottom currents.

A high concentration of bivalve filaments in sediments, as observed in facies F1 and F2 (Fig. 2), is thought to be linked to episodes of high marine productivity (Caron et al., 2006; Kędzierski et al., 2012; Bomou et al., 2013). The presence of disseminated framboidal pyrite (Fig. 7) and glauconite (filling primary porosity) (Fig. 6D) in both facies also points towards reducing environments, in which these minerals formed as a syngenetic-early diagenetic phase in the iron reduction zone of the oxic–anoxic interface (e.g., Wilkin et al., 1996; Lowery et al., 2014).

- *Interpretation of facies F3*: The composite ichnofabric of this facies (Figs 5N–Q and 6I) indicates intense activity of organisms both at the seafloor surface and within the sediment, under relatively well-oxygenated conditions. Bottom waters with high oxygen concentrations are also suggested by the common presence of benthic foraminifera (Fig. 6H–I). Facies F3 is similar to ORB-D of the model of Reolid et al. (2010). An oxic environment may have heightened aerobic remineralization of organic matter, a process that commonly inhibits pyrite formation (e.g. Bond and Wignall, 2010) and accounts for the lack of pyrite in this facies.

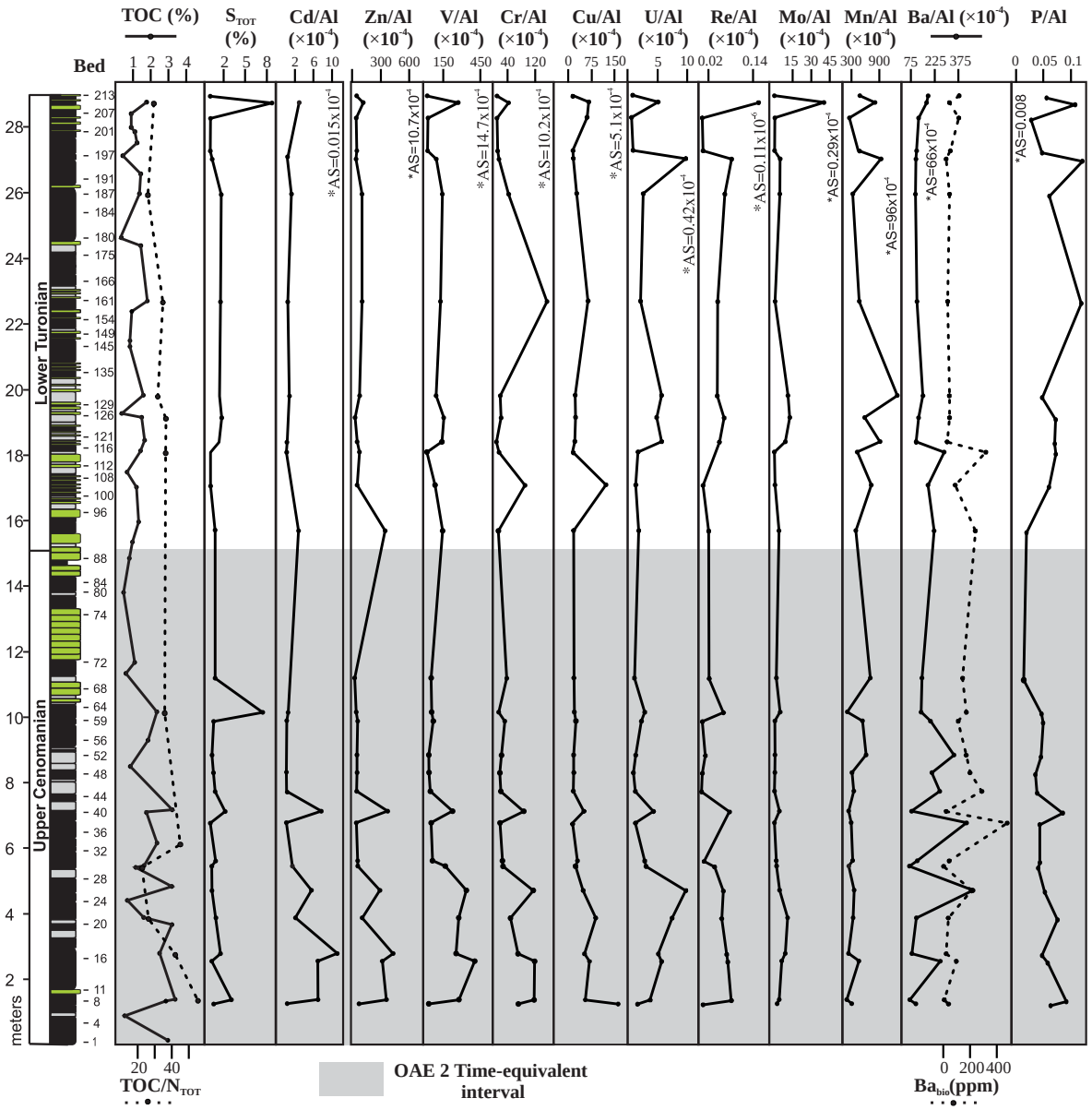

Fig. 10. Vertical profiles of TOC (%), TOC/N_{TOT}, S_{TOT} (%), Al-normalized RSTEs and Ba_{bio} (ppm) of the Xilitla section. The values with asterisk in the Al-normalized profiles represent concentrations of each corresponding normalized element in the average shale (AS) from Wedepohl (1971).

From facies F1 to F3 there is a clear progressive increase in the availability of oxygen at the bottom of the water column. Indeed, a higher TOC content in facies F1 and F2 (>0.51%) than in facies F3 (<1%) supports this interpretation. From observing the vertical distribution of said facies (Fig. 2), it is evident that oxygen deficiency was more uniform within the lowest 9 m of the section, during the lower part of the OAE 2 interval. Afterwards, the bottom-water redox conditions became more variable and oxygen increased progressively during relatively short and intermittent episodes, mainly in the post-OAE 2 interval.

5.2.2. Pyrite framboid size and content distribution

Many studies have shown that the size distribution and content of pyrite framboids are regulated by bottom-water redox conditions, which in turn are controlled by the position of the oxic–anoxic interface relative to the sediment–water interface (Wilkin et al., 1996; Bond and Wignall, 2010; Núñez-Useche et al., 2015). Oxygen-depleted (dysoxic) bottom waters, where the oxic–anoxic interface is close to the sediment–water interface, favor the formation of diagenetic framboids (>6 μm in diameter) at the sediment–water interface and within the sediment. Under more oxygen-restricted conditions, the oxic–anoxic interface moves upward and abundant syngenetic framboids are formed in the anoxic water column. Since they rapidly sink to the seafloor, syngenetic framboids are smaller (4–6 μm in diameter) and less variable in size than diagenetic framboids. Euxinic conditions (free H_2S) also produce populations of tiny syngenetic framboids (3–5 μm in diameter) within a narrow size range.

Mean vs. standard deviation plot of pyrite framboid data from Xilitla (Fig. 8 and Table 1) shows a distinction between anoxic and dysoxic conditions, quite consistent with the facies interpretation: framboids of anoxic facies F1 are smaller and less variable in size (mostly syngenetic; suggesting more oxygen-depleted conditions) than those of dysoxic facies F2 (mostly diagenetic).

Although most pyrite framboids in both facies indicate poorly-oxygenated bottom waters, all samples from facies F1 have a content of tiny framboids (<5 μm in diameter) higher than 18%—that may have resulted from intermittent euxinicity. This is more evident for samples 30, 131 and 194, which fall close to the euxinic field and exhibit a content of tiny framboids exceeding 40%. However, considering the low content

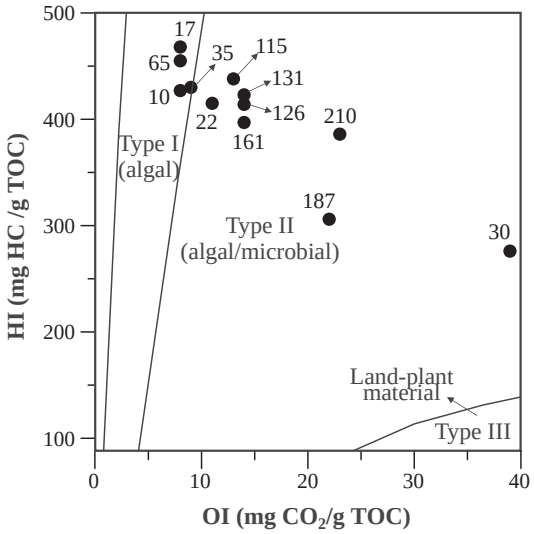

Fig. 11. Rock Eval data. Hydrogen index (HI) vs. oxygen index. Maturation paths shown for type I–II–III organic matter (modified pseudo-van Krevelen diagram, Tisot and Welte, 1984). Each sample is identified by the corresponding bed number. See the position of beds in Fig. 2.

of framboids in these samples, their framboid populations might reflect short-lived pulses of euxinia superimposed on longer term anoxic conditions, which may resulted in a time-averaged framboid population typical of anoxic environments (e.g., Bond and Wignall, 2010). The content of framboidal pyrite (Fig. 8 and Table 1) is less indicative of oxygen conditions. Many samples from dysoxic facies F2 have a greater framboid content than those from anoxic facies F1. This is probably because the bioturbated fabric of facies F2 favored upward diffusion of H_2S from underlying sediments, in which bacterial sulfate reduction (BSR) continued but iron limited pyrite formation, thus prompting framboid formation somewhat independently from redox conditions. This phenomenon has been invoked previously for sulfur excess in dysoxic facies with low TOC (e.g., Algeo and Maynard, 2004).

5.2.3. Redox control of trace element enrichment

Under oxygen-depleted bottom waters, certain RSTEs are less soluble and preferentially transferred from the water column into the sediment. Conversely, Mn is reduced to soluble forms (Mn^{2+} or $MnCl^{+}$) that are not readily taken up by organic matter; it diffuses upward out of sediment or from the sediment–water interface (Calvert and Pedersen, 1993; Canet et al., 2004; Algeo and Maynard, 2004; Tribovillard et al., 2006).

RSTEs/Al ratios of sediments from Xilitla are consistently above those of average shale (Fig. 10 and Appendix B). Their EFs values include the mean of the C–T black shales (Brumsack, 2006) and those from modern sediments underlying anoxic environments (Calvert and Pedersen, 1993) (Fig. 12). Several Al-normalized RSTEs ratios covary with TOC ($R_{Cd} = 0.72$, $R_{Zn} = 0.68$, $R_V = 0.67$, and $R_{Cr} = 0.61$) and S_{TOT} ($R_{Ni} = 0.73$, $R_{Mo} = 0.72$, $R_{Pb} = 0.68$, $R_{Co} = 0.67$, and $R_{Re} = 0.67$) (Table 3), suggesting that trace elements were mainly fixed in organic and authigenic Fe-sulfide phases, respectively. These correlations indicate that, despite the diagenetic overprint of the carbonate fraction affecting the $\delta^{13}C$ record, great alteration of the trace element data can be ruled out. This is because in organic-rich sediments the carbonate fraction exerts lesser control on the whole rock trace elements content than the organic and sulfide fractions do (Abanda and Hannigan, 2006; Xu et al., 2012).

Both correlation patterns agree with the known geochemical behavior of RSTEs under low oxygen conditions (Calvert and Pedersen, 1993; Algeo and Maynard, 2004; Brumsack, 2006; Tribovillard et al., 2006). In the sediments studied, the peaks of Cd/Al and Zn/Al (elements generally incorporated into marine plankton biomass) may record episodes of intensive primary production. Correlation of Al-normalized concentrations of V and Cr with TOC and not with S_{TOT} reflect the preferential incorporation of these elements into organic matter. Conversely, correlation of Mo/Al, Co/Al, Ni/Al and Re/Al with S_{TOT} reflect the higher degree of pyritization of these trace elements. The presence of Mo and

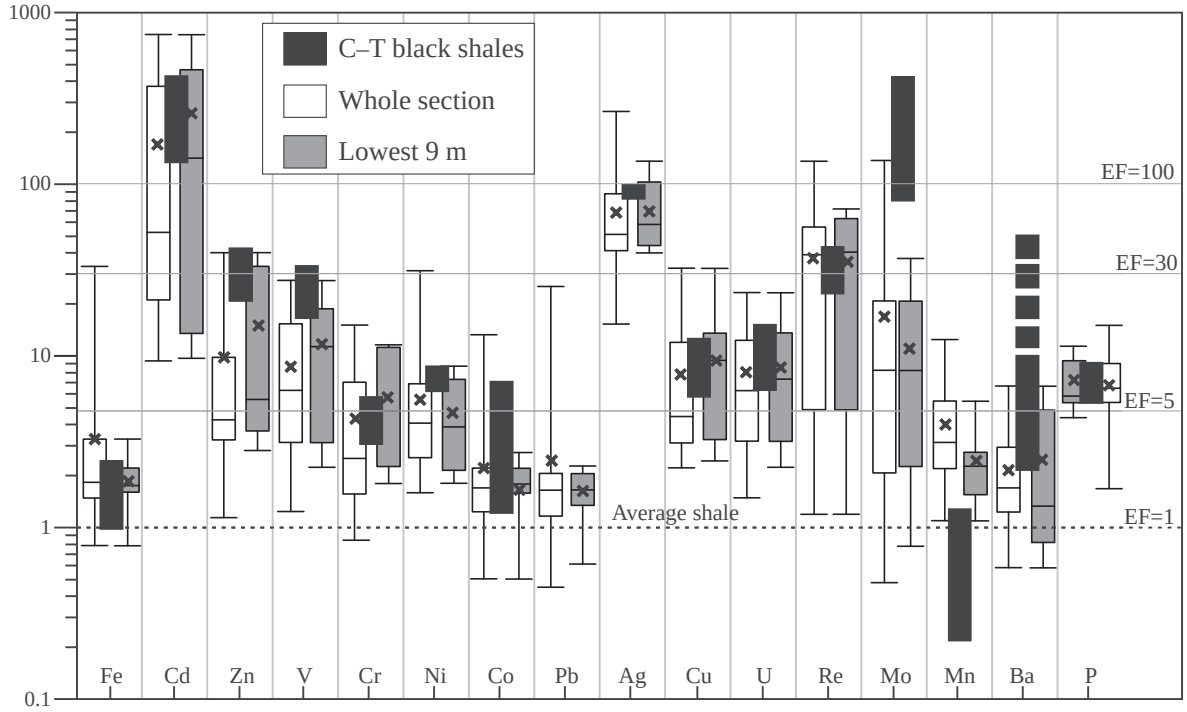

Fig. 12. Calculated enrichment factors (EFs; note logarithmic scale) for RSTEs measured in the Xilitla section. All measurements (white box-plot) and lowest 9 m values (light gray box-plot) are compared to the mean of the Cenomanian–Turonian (C–T) black shales from various locations by Brumsack (2006) (black box-plot). The line in the middle of the boxes is plotted at the median, and "x" represents the mean. The horizontal dashed line indicates the value for which there is no enrichment/depletion with regards to average shale composition.

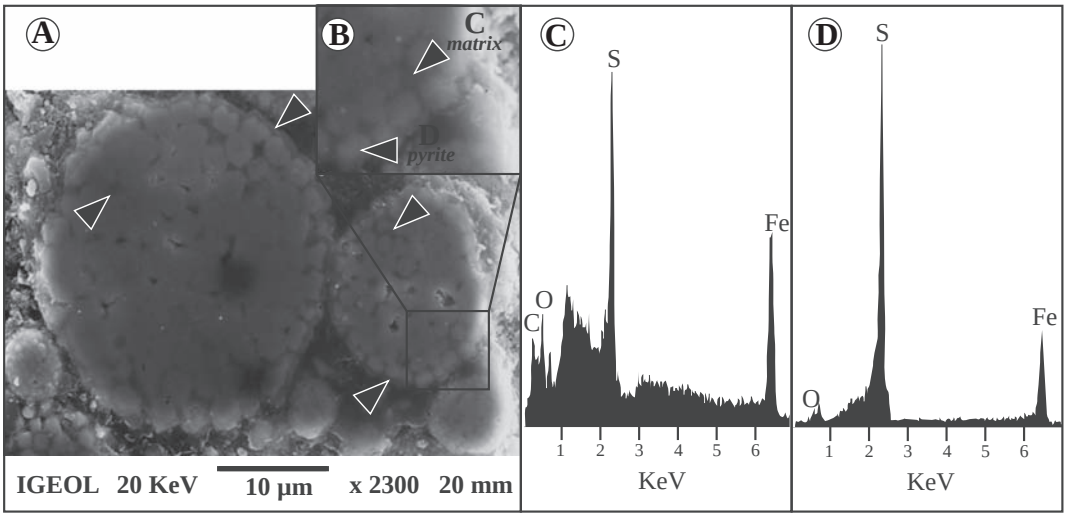

Fig. 13. Results of EDS analysis on pyrite framboids (A) Scanning electron micrograph of pyrite framboids. Note the dark matrix between microcrystals and enveloping the framboids (arrows). (B) Enlarged image of the boxed area in (A). EDS analysis on the internal matrix (C) and a single microcrystal (D) shows that carbon is present in the former. Both analyzed areas are shown by arrows in (B).

Ni in both laminated and framboidal pyrite (Table 2) corroborates their incorporation into pyrite (probably taken up in solid solution), and supports reduced conditions in pore waters under which these elements are absorbed by pyrite. Although Pb is commonly removed as an independent sulfide phase rather than in solid solution in pyrite, high levels of Pb pyritization are also reported in anoxic-sulfidic sediments.

Worthy of note is that the RSTE data do not allow differentiation between anoxic facies F1 and dysoxic facies F2. This is because under regular re-oxygenation of the bottom waters RSTEs behavior is less predictable and they are less consistent as indicators of oxygen levels (e.g, Algeo and Maynard, 2004). Despite this, higher mean EFs for Cd, Zn, V, Cr, Cu and U (Fig. 12), along with the lowest Mn/Al concentration (Fig. 10) and a negative TOC–Mn correlation ($R = -0.1$) within the lowest 9 m of the section, indicate that more severe and constant oxygen deficiency prevailed during deposition of this stratigraphic interval. From 9 to 10 m upward, concurrent slight to moderate increases in different RSTEs point to short-lived episodes of low oxygen conditions. Nevertheless, the overall decrease in TOC and certain Al-normalized RSTEs content (Fig. 10) suggests that oxygen deficiency was less severe and more variable within this interval. This interpretation is supported by the gradual increase of the Mn/Al ratio between 10 and 19.8 m (Fig. 10).

Besides local redox conditions, we suggest an important event controlling the RSTEs distribution patterns in the organic-rich sediments from Xilitla. The higher RSTEs concentrations within the lowest 9 m of the section seem to indicate the introduction of large amounts of trace metals (e.g., Co, Cu, Zn, Fe, V, Mo) into the ocean, a phenomenon associated with the submarine volcanism of the Caribbean Plateau, which commenced between 95 and 92 Ma (Snow and Duncan, 2001; Leckie et al., 2002; Snow et al., 2005; Trabucho Alexandre et al., 2010). This is in agreement with the synchronous increase in unradiogenic seawater-osmium at 94.44 ± 0.14 and 94.28 ± 0.25 Ma (close to the OAE 2 onset) found by Du vivier et al. (2015b) in proto-Pacific sections, linked to the basaltic eruptions of said plateau. The radiometric age determined in this study close to the base of the section (94.1 ± 1.6 Ma) (Fig. 3) is in the range of those ages. Accordingly, the decrease trend in certain RSTEs (Cd, V, Zn, Cr and, and to a lesser extent, Cu, U and Re) (Fig. 10 and Appendix B), similar to the one found in other oxic and anoxic sediments (Elrick et al., 2009, Bomou et al., 2013; Eldrett et al., 2014), may reflect the gradual global drawdown of the trace metal reservoir due to widespread deposition of organic-rich sediments in the Tethys and proto-North Atlantic during OAE 2.

To summarize, our sedimentary, pyrite framboid and geochemical data indicate more permanent reducing environments within the lowest 9 m of the section, likely reflecting oxygen deficient conditions associated with OAE 2, superimposed to the anoxic/dysoxic bottom-water regime inherent to the TMB. Such conditions are comparable to those reported for northern Mexico (Duque-Botero et al., 2009) and Demerara Rise (southern North Atlantic; Hetzel et al., 2009; Trabucho Alexandre et al., 2010), where anoxia was intense. This suggests that the Xilitla section placed close to the core of an oxygen-minimum zone. However, these conditions contrast with the oxygenated regime within OAE 2 found in the northern Tethyan pelagic zone (Chrummflueschlucht section; Westermann et al., 2010), the Gamba-Tingri Basin (Gongzha section; Bomou et al., 2013), and in some areas of the Western Interior Seaway (Shell Iona-1 core; Eldrett et al., 2014). Within this poorly-oxygenated regime associated with OAE 2, there were episodes of intermittent oxic conditions reflected by the regular presence of thoroughly bioturbated beds with common benthic foraminifera (facies F3). This indicates a more dynamic benthic environment related to fluctuations of the oxygen-minimum zone. Similar intermittent suboxic conditions

Table 2
Chemical composition of pyrite in the analyzed samples (WDS analysis data).

Bed	Pyrite Texture	S	Fe	V	Ni	Th	Mo	U	Total	S	Fe	V	Ni	Th	Mo	U
		wt. (%)								(ppm)						
210	Framboid	53.159	45.732	–	0.017	–	0.451	–	99.359	531,590	457,320	–	170	–	4510	–
210	Laminated	53.303	46.636	–	–	–	0.524	0.015	100.478	533,030	466,360	–	–	–	5240	300
161	Framboid	53.147	46.311	0.29	0.034	0.017	0.498	0.013	100.31	531,470	463,110	5800	340	170	4980	260
126	Framboid	52.905	47.084	–	0.015	0.043	0.591	0.011	100.649	529,050	470,840	–	150	430	5910	220
126	Laminated	52.681	46.176	–	0.038	0.006	0.541	0.114	99.556	526,810	461,760	–	380	60	5410	2280
30	Framboid	52.668	46.293	–	0.034	–	0.471	–	99.466	526,680	462,930	–	340	–	4710	–
22	Framboid	54.028	47.385	–	–	0.114	0.524	–	102.051	540,280	473,850	–	–	1140	5240	–
22	Laminated	54.019	46.986	–	0.016	–	0.568	0.042	101.631	540,190	469,860	–	160	–	5680	840

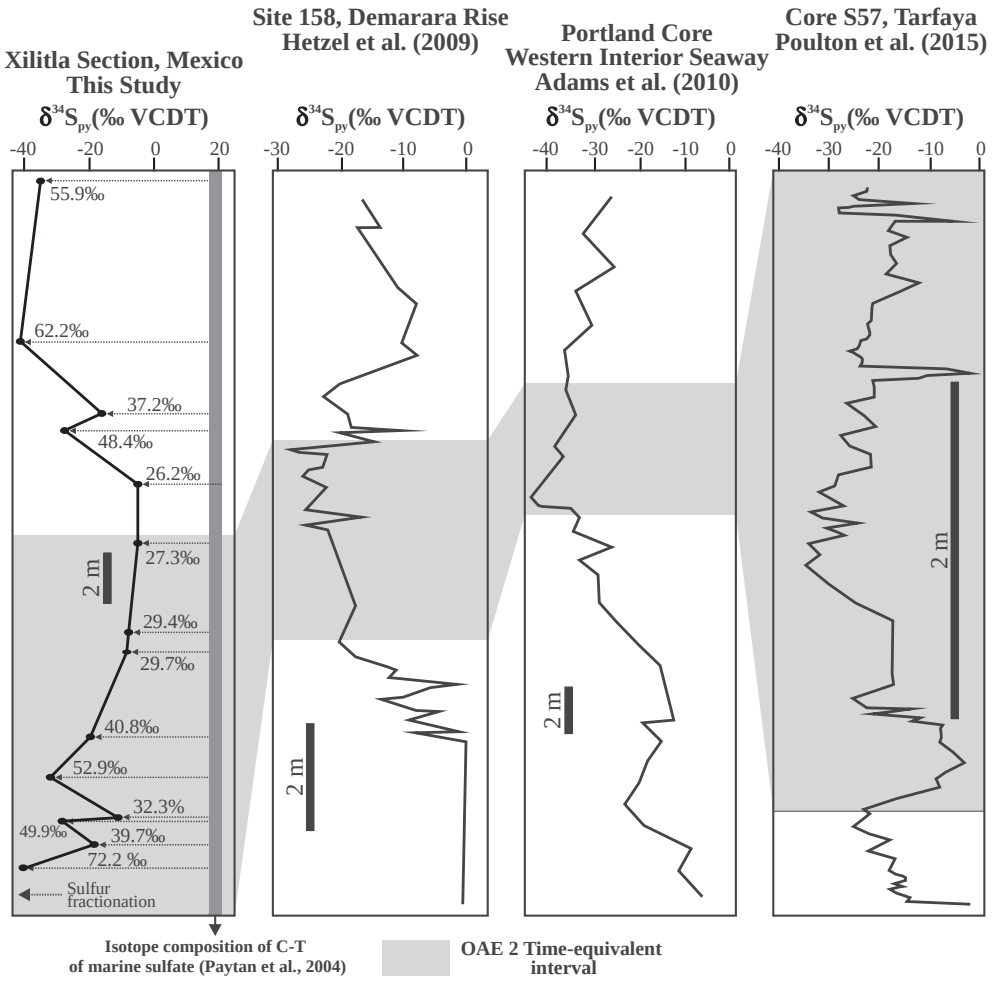

Fig. 14. The evolution of the $\delta^{34}S_{py}$ observed in the Xilitla section compared to that from Site 158, Portland Core and Core S57.

have also been documented in the Tarfaya Basin (Kuhnt et al., 2009), the Silesian Basin (Rybie section; Uchman et al., 2013) and in the Central Tunisian Platform (the Oued Bahloul section; Reolid et al., 2015). These variable OAE 2 redox regimes, observed worldwide, point towards strong local influence on both oxygen conditions and the accumulation of organic-rich sediments in marine basins.

From 9 m upward in the sequence, oxygen deficiency was less severe and more variable, and was controlled mainly by local redox conditions. Oxygen-depleted conditions during the early Turonian have been also reported for southern and northern Mexico during the deposition of the Mexcala Formation (Guerrero-Morelos Platform; Hernández-Romano et al., 1997; Elrick et al., 2009) and the Indidura Formation (Parras Basin; Duque-Botero et al., 2009), respectively. Therefore, a regional control of redox conditions during the early Turonian is suggested for this part of the proto-North Atlantic Basin, possibly associated with the intermittent permanence of a weaker oxygen-minimum zone.

Table 3
Correlation coefficients (*R*) between Al-normalized trace elements and TOC-S_{TOT}.

Trace element/Al	TOC *R* (n = 19)	S_{TOT} *R* (n = 29)	Trace element	TOC *R* (n = 19)	S_{TOT} *R* (n = 29)
Fe/Al	0.05	0.8	Ag/Al	0.17	0.50
Cd/Al	0.72	0.08	C/Al	0.23	0.04
Zn/Al	0.68	0.09	U/Al	0.38	0.14
V/Al	0.67	0.24	Re/Al	0.45	0.67
Cr/Al	0.61	0.04	Mo/Al	0.06	0.72
Ni/Al	0.16	0.73	Mn/Al	−0.43	0.03
Co/Al	0.06	0.67	Ba/Al	0.15	0.21
Pb/Al	0.02	0.68	P/Al	0.28	0.33

5.3. Sea-level variation

A major global sea-level rise is known to have occurred during the C–T transition (Hardenbol et al., 1998). In the context of this eustatic fluctuation, the filament event is related to an interval close to the end of the transgressive interval, heralding the transition to normal marine conditions (Negra et al., 2011; Kędzierski et al., 2012). In the Xilitla section, no significant stratigraphic features constrain the extent of said transgressive phase; however, considering the position of the filament event, the transgressive phase could be attributed to the lower part of the section. High sea-level conditions for this interval matches more uniform oxygen-depleted conditions that favored organic-rich sediment formation, mainly in the lowermost 9 m. Above this bioevent, the abundance of limestone beds, relative to shaly limestone beds, progressively increases upward within the section. This limestone-dominated interval may reflect a long-term decrease in detrital influx linked to the global sea-level change, such as is observed at Pueblo (USA), Eastbourne (UK) and Ghonza (China) (Bomou et al., 2013) sections.

5.4. Link between marine productivity and anoxia: geochemical evidence

5.4.1. Biogenic barium

Barium is an important tracer of marine productivity (Dymond et al., 1992; Tribovillard et al., 2006; Hetzel et al., 2009). In organic-rich sediments underlying areas of high productivity, bio-induced formation of barite ($BaSO_4$) occurred within organic particles in reducing environments. Intense bacterial sulfate reduction (BSR) may cause sulfate depletion and mobilization of Ba (Dymond et al., 1992); however, the

highly negative pyrite $\delta^{34}S$ values from Xilitla suggest that such did not occur in the sediments studied. Therefore, Ba can be reasonably used as a proxy for productivity. Fig. 12 shows that the studied section have a moderate enrichment of Ba in relation to the average shale and comparable to the C–T mean values (Brumsack, 2006). This is indicative of fertile water masses. Since Ba content can be influenced by other sources (e.g., detrital aluminosilicates, hydrothermal precipitates, secretion by benthic organisms) (Dymond et al., 1992), a more reliable evaluation of productivity is achieved using biogenic barium (Ba_{bio}) (Fig. 10). The Ba_{bio} content represents between 3.8 and 91% (63.1% in average) of the Ba total. Therefore, a considerable part of the Ba total is composed of biogenic barium, confirming high productivity. As shown in Fig. 10, both Ba/Al and Ba_{bio} are relatively enriched in the lowest 9 m, thus indicating recurrent intensification of productivity during the deposition of this interval.

5.4.2. Phosphorus content

Phosphorous is an important biolimiting nutrient modulating marine productivity (Tribovillard et al., 2006; Bomou et al., 2013). Dissolved P delivery to the ocean, mostly by continental runoff, is carried to the seafloor by organic matter, clay particles and manganese oxyhydroxides. Under reducing conditions, P diffuses upward from the sediment and returns to the water column, increasing primary productivity (e.g., Mort et al., 2007). Fig. 10 shows a clear enrichment of P compared to average shale in the Agua Nueva Formation that points towards high productivity, analog to modern coastal upwelling areas in Peru (Böning et al., 2004) and Namibia (Brumsack, 2006). The minor enrichment in P within the lowermost 9 m suggests partial loss of P linked to more uniform oxygen-depleted conditions. This scenario fits that observed for basins of the Tethys and Atlantic during OAE 2, where anoxia increased P remobilization from sediments to sustain productivity (Mort et al., 2007; Hetzel et al., 2009; Poulton et al., 2015). P availability in this part of the proto-North Atlantic Basin may also have been controlled by both a climate change towards more arid conditions and a long-term sea-level rise, decreasing continental biogeochemical weathering rates, as is observed in Tethyan and Atlantic sections (Bomou et al., 2013).

5.4.3. Elevated TOC/N_{TOT} ratios

In the pseudo-van Krevelen-type diagram (Fig. 11), analyzed samples fall into fields of type I (algal) and type II (algal/microbial) organic matter. This marine origin is not consistent with the obtained TOC/N_{TOT} values (22–55), suggesting a terrestrial source (TOC/N_{TOT} >20; Meyers et al., 2006). Nonetheless, similar unusual TOC/N_{TOT} ratios have also been reported for marine organic matter deposited under areas of high productivity. For instance, values between 10 and 22 were measured by Bouloubassi et al. (1999) in the Mediterranean sapropels. Most of the black shales deposited during mid-Cretaceous OAEs display values of between 25 and 50 (e.g., Meyers et al., 2006). Thus, TOC/N_{TOT} ratios obtained in this study fit highly eutrophic conditions. These anomalous values are a result of the loss of nitrogen during oxygen stress periods linked to high productivity (e.g., Twichell et al., 2002; Van Mooy et al., 2002).

Remarkably, marine productivity was higher within the lowest 9 m, where there were more stable and severe anoxic/dysoxic conditions. This supports a positive feedback loop among high productivity, deposition of organic matter and oxygen depleted conditions—at least during part of the OAE 2 (Mort et al., 2007; Hetzel et al., 2009; Lowery et al., 2014; Reolid et al., 2015). Based on the regular presence of volcanic ash, we suggest that there was a link between local volcanic input and high productivity. Ash particles can induce natural fertilization by supplying large amounts of bio-available Fe to the ocean (Duggen et al., 2010; Langmann et al., 2010). However, since bentonite beds are rare in the lowest 9 m (Fig. 2), we suggest that the increase in nutrient conditions was mainly driven by the release of biolimiting elements (e.g., Fe, P) into the global ocean, triggered by the coeval volcanic eruptions of the Caribbean Plateau (Snow et al., 2005; Trabucho Alexandre et al., 2010).

5.5. Control of bacterial sulfate reduction and sulfate availability on the sulfur isotope record

The $\delta^{34}S_{py}$ curve from the Xilitla section displays an increasing trend from −51.2‰ (bed 13) to −5.2‰ (bed 106) during and immediately after OAE 2 (Fig. 14). This trend is similar to that found in Demerara Rise (Site 1258; Hetzel et al., 2009), the Western Interior Seaway (Portland Core; Adams et al., 2010), and in shelf sediments from Tarfaya (Core S57; Poulton et al., 2015). In all cases, the $\delta^{34}S_{py}$ reaches a minimum value within the anoxic event and gradually returns to higher values afterwards (Fig. 14). This similarity supports a common mechanism driving the global sedimentary sulfur isotope signal during OAE 2. According to Adams et al. (2010), the sulfur isotope record during the anoxic event was greatly influenced by more availability of seawater sulfate concentration, prompted by the release of sulfur by massive volcanism that progressively declined. Under anoxic conditions, sulfate-reducing bacteria obtain energy by oxidizing organic compounds while reducing marine sulfate to hydrogen sulfide, preferentially incorporating ^{32}S. Therefore, higher sulfate levels during this event must favored a greater fractionation of sulfur through bacterial sulfate reduction (BSR), resulting in lighter $\delta^{34}S$ pyrite.

Interestingly, the Xilitla section shows a minimum $\delta^{34}S_{py}$ value within OAE 2—quite isotopically lighter compared to that of the aforementioned sites (Fig. 14). Taking the sulfur isotope composition of C–T marine sulfate to be between +17 and +21‰ (average around +19‰; Paytan et al., 2004), and assuming that bottom waters and/or pore waters in sediments were derived from coeval open marine waters, then an overall sulfur isotope fractionation of 26.2 to 72.2‰ during OAE 2 is estimated for the Xilitla section (Fig. 14). In some cases, these values match those found in laboratories by BSR of 4 to 46‰ (Ohmoto et al., 1990; Canfield, 2001). However, higher values can be explained only through an additional fractionation of the sulfide pool during the oxidative phase of the sulfur cycle, in which oxidation of bacterial HS^- to elemental S or other intermediate oxidized S species is followed by the bacterial disproportionation into isotopically lighter sulfide and heavier sulfate (Habicht and Canfield, 1997; Passier et al., 1997). This process has been invoked by Passier et al. (1997) to explain fractionation values of 57.9 to 70.2‰ in the eastern Mediterranean sapropels.

In either case, the large sulfur fractionation in the studied section hints to a dramatic increase in relative seawater sulfate concentration in the TMB during the anoxic event. This increase could be the result of both (i) the compelling variable redox conditions causing increased diffusion of sulfate to lower sediment layers through bioturbation during dysoxic periods, and (ii) bottom currents (as evidenced by ripple marks; Fig. 5M) that contributed to the replenishment of the sulfate reservoir through the mixing of sediment and ambient waters. Both bioturbation and bottom currents might provide the O_2 required for the oxidation of primary pyrite and sulfur recycling. The decrease in sulfur fractionation through the anoxic event in the Xilitla section (Fig. 14) is apparently linked to a decline in burial efficiency of organic matter. This is evident from the inverse relationship between $\delta^{34}S_{py}$ and TOC values observed in the lowermost 18 m. Above this interval, $\delta^{34}S_{py}$ values become lighter in the *H. helvetica* Zone in spite of moderate TOC concentration. This return to lighter values is an isotope signature not observed in other sites (Fig. 14), and implies a different mechanism that, once again, contributed to the increase in sulfate concentration and the extent of sulfur fractionation by BSR.

Evidence of bacterial activity in the TMB is confirmed by EDS analysis revealing the presence of a carbon-rich matrix coating the outer surface of both individual microcrystals and pyrite framboids (Fig. 13). This envelope can be interpreted as a remnant of the organic material that constituted an original bacterial biofilm and provided the structural framework for the clustering of pyrite microcrystals. According to

several research projects, this carbon-rich component is mainly produced by extracellular bacterial polysaccharides and is stretched during framboid maturation (e.g., Rickard, 2012).

5.6. Depositional model

The multiproxy approach applied here shows that the organic-rich sediments of the Agua Nueva Formation display vertically variable sedimentary facies, and predominantly provides evidence of oxygen-depleted conditions in bottom waters interrupted by punctuated, short-lived oxic episodes. Based on the correlation of several proxies, we proposed a model to explain these episodically dysaerobic conditions.

As shown in Fig. 15, a layer of oxygen-depleted seawater developed just at the seafloor, as a consequence of oxygen consumption by decaying marine organic matter from high biologically productive surface waters; this is similar to the scenario encountered in modern coastal upwelling areas. Above this layer, there was greater oxygen availability, coinciding with the presence of abundant fish and ammonite remains. Variations in total primary production controlled the supply of organic matter to the seafloor, thus producing redox variations in bottom waters mostly from anoxic (facies F1) to dysoxic (facies F2) conditions. Under anoxic conditions (Fig. 15A), the oxic–anoxic interface was located above the sediment–water interface. Such conditions precluded colonization by benthic fauna and preserved finely-laminated fabric. Diagenetic and syngenetic pyrite framboid formation through BSR took place at both the anoxic water column and the sediment–water interface. The increase in oxygen content of bottom waters caused the deepening of the oxic–anoxic interface, which placed at the sediment–water interface or just beneath it (Fig. 15B). Therefore, dysoxic conditions developed close to the sediment–water interface and within the uppermost sediments, whereas anoxic conditions persisted in pore waters within the lower sediments. Sporadic bottom currents favored mixing with oxygenated water and contributed to sustaining dysoxic conditions. This scenario allowed the colonization of the seafloor by inoceramid bivalves and other low-oxygen tolerant benthic taxa (including benthic foraminifera) that burrowed into the sediment and disrupted lamination. Pyrite framboids were diagenetically formed—mainly in the uppermost sediment. Influx of H_2S from the underlying sediments, provided by BSR and favored by the bioturbated fabric, may have stimulated additional diagenetic framboid formation. In the model, overall low oxygen levels (anoxic and dysoxic) promoted glauconite formation and the scavenging of trace elements and their incorporation to sediments. Whereas Cd, Zn, V and Cr were mainly fixed in organic matter and Ni, Mo, Pb, Co and Re were scavenged by pyrite, Mn and P diffused out of the sediments. Biogenic barium became enriched in sediments linked to organic matter decay. Bioturbation and bottom currents played an important role in enhancing the diffusion of sulfate to lower sediment for BSR and providing the O_2 for sulfur recycling.

During periods of low productivity and low export of organic matter from marine surface, the oxic–anoxic interface deepened below the sediment–water interface (Fig. 15C). This caused oxic conditions at both the seafloor and the upper sediments (facies F3), which allowed intense bioturbation and the establishment of benthic foraminifera, as well as anoxic/dysoxic conditions in the lower sediments.

6. Conclusions

Biostratigraphic and radiometric data reveal that the Xilitla section spans the latest Cenomanian–earliest Turonian interval. Four important global bioevents, which from base to top are (i) the last occurrence of *R. cushmani*, (ii) the *Heterohelix* shift, (iii) the filament event, and (iv) the first occurrence of *H. helvetica* mark the biotic turnover associated with oxygen-depleted conditions during OAE 2 in the Tampico–Misantla Basin. The occurrence of these bioevents suggests inter-

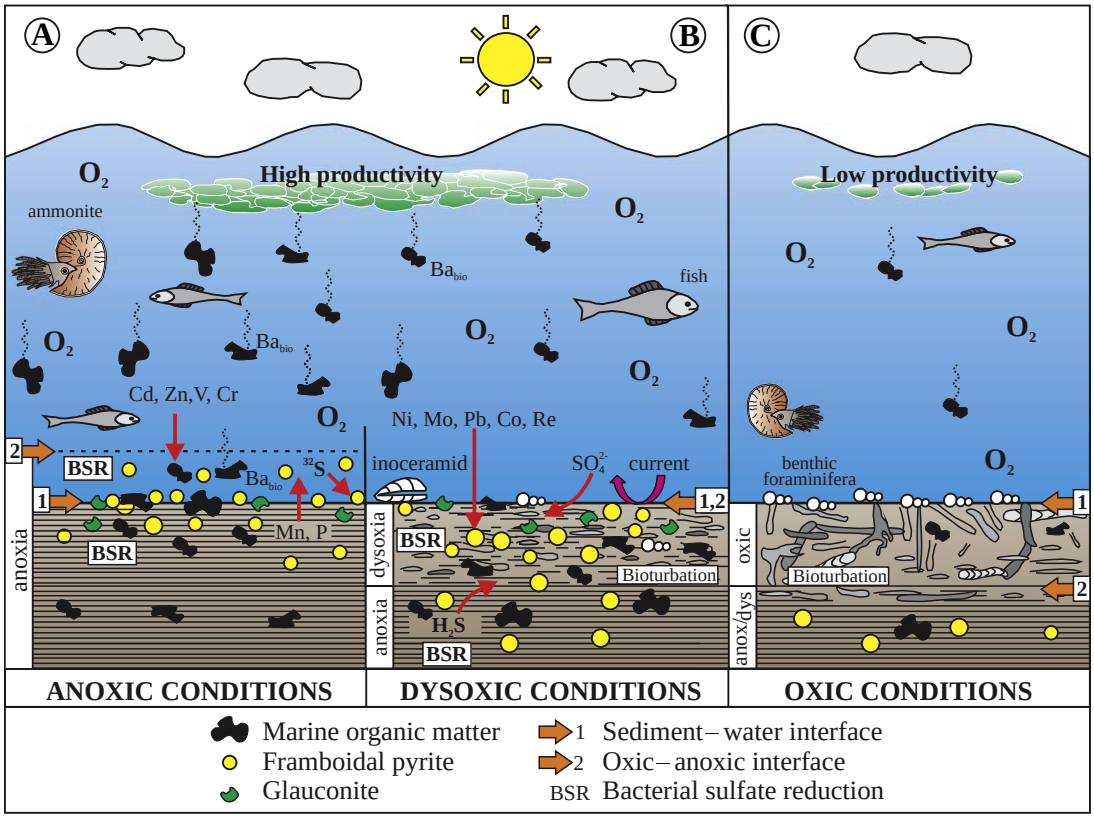

Fig. 15. Proposed model of bottom-water conditions during the deposition of the Agua Nueva Formation at Xilitla. The position of the oxic–anoxic interface in regards to the sediment–water interface determined the variations between anoxic to dysoxic and oxic bottom-water conditions.

ocean connections of this part of the western margin of the Proto-North Atlantic with the Tethys Sea and the Western Interior Seaway.

According to the constructed model, high marine productivity was associated with organic matter burial and oxygen depletion in the Tampico–Misantla Basin, analogous to that occurring in modern coastal upwelling areas. Fluctuations in primary production controlled bottom-water oxygen conditions at the seafloor, which remained mostly oxygen-deficient (anoxic–dysoxic) and were interrupted by punctuated, short-lived oxic events.

The regular presence of the facies of anoxic settings, the higher enrichment in TOC and selected RSTEs, and the depletion in Mn and P suggest that more constant and severe oxygen deficiency occurred within the lowest 9 m of the studied section, during part of the OAE 2. Similar conditions have been found in central and southern Tethys; however, they contrast with oxygenated bottom waters observed in part of the Western Interior Seaway and northern Tethyan margin. This points to local mechanisms operating in different parts of the global ocean, producing dissimilar redox conditions during OAE 2. As indicated by the more constant occurrence of well-oxygenated facies, increase in TOC and RSTEs content and the decrease in Mn and P concentration, oxygen deficiency was less severe from 9 m upward.

Marine productivity was triggered by nutrient fertilization from intrabasinal volcanic ash-fall. However, higher eutrophic conditions in the lowest 9 m of the section may have been reinforced by P recycling from sediments, along with the release of biolimiting metals into the global ocean during coeval massive volcanic eruptions of the Caribbean Plateau. This submarine volcanism apparently influenced trace element availability and burial in sediments: higher within the lowest 9 m, and declining progressively afterward.

A positive trend in the stable sulfur isotope curve with minimum values within OAE 2 indicates that highest isotope fractionation was related to organic matter burial. This pattern is similar to the one observed at other sites, thus suggesting globally controlled changes in the overall sulfur cycle, likely from the release of sulfur by massive volcanism. Locally, a greater availability of both seawater sulfate concentration in sediments (as a result of bioturbation and/or bottom currents) and organic matter (favored by high primary production) enhanced BSR and increased the extent of sulfur fractionation during pyrite formation. Sulfur recycling favored by variable redox conditions account for the highly negative $\delta^{34}S$ values for pyrite.

Supplementary data to this article can be found online at http://dx.doi.org/10.1016/j.palaeo.2016.01.035.

Acknowledgments

This paper is part of the Ph.D. dissertation of the first author (F. Núñez-Useche), who gratefully acknowledges a fellowship from the *Consejo Nacional de Ciencia y Técnología*-Mexico to study at the *Instituto de Geología*—UNAM. This research was sponsored by projects PAPIIT IN 109912, DGAPA, UNAM and CONACYT-SEP 177510. Other funds included a Grant-in-Aid from the Geological Society of America, and the R. Dana Russell Memorial Grant from the American Association of Petroleum Geologists Grant-in-Aid program, both provided to the first author. Sulfur isotope analyses were financed by project 2009GR-0044, *Generalitat de Catalunya*. Rock-Eval analyses were subsidized by the *Coordinación Tecnológica de Geociencias—Instituto Mexicano del Petróleo*. The authors express their gratitude to the following members of the *UNAM*: Josep Moreno-Bedmar, Rafael López-Martínez and Fabian Durán Aguilar for their support in the field; David Zamudio and Ana Luisa Carreño for assisting in the identification of planktic foraminifera; Blanca Estela Buitrón for identification of inoceramid bivalves; Priyadarsi D. Roy for allowing us to use his facilities for TOC analysis; Mario Ramos for his assistance with U–Pb zircon geochronology; and Margarita Reyes Salas, Sonia Ángeles García, Yolanda Hornelas Orozco and Carlos Linares López for their assistance with SEM and EPMA equipment. The English manuscript was proofread by Sonia Helen Ponce Wainer.

References

Abanda, P.A., Hannigan, R.E., 2006. Effect of diagenesis on trace element partitioning in shales. Chem. Geol. 230, 42–59.
Adams, D.D., Hurtgen, M.T., Sageman, B.B., 2010. Volcanic triggering of a biogeochemical cascade during Oceanic Anoxic Event 2. Nat. Geosci. 3, 201–204.
Algeo, Th.J., Maynard, J.B., 2004. Trace-element behavior and redox facies in core shales of Upper Pennsylvanian Kansas-type cyclothems. Chem. Geol. 206, 289–318.
Blanco, A., Zavala, F.J., Hernández-Ávila, J., Maurrasse, F., Duque-Botero, F., Ramírez-Cardona, M., 2010. Microbial preservation in sedimentary pyrite from Cretaceous organic-matter-rich carbonate mudstone: a preliminary report. Lunar and Planetary Science Conference, p. 2487.
Blanco, A., Maurrasse, F.J., Duque, F., Delgado, A., 2011. Anoxic–dysoxic–oxic conditions in the Cenomanian Agua Nueva Formation (Upper Cretaceous) in Central Mexico, and their relation to Oceanic Anoxic Event 2 (OAE 2). Geol. Soc. Am. Abstr. Programs 43, 421.
Blanco-Piñón, A., Maurrasse, F.J.-M.R., Rojas-León, A., Duque-Botero, F., 2008. Cyanobacteria/Foraminifera association from anoxic/dysoxic beds of the Agua Nueva Formation (Upper Cretaceous–Cenomanian/Turonian) at Xilitla, San Luis Potosi, Central Mexico (summary). EOS Trans. Am. Geophys. Union 89 (23) (Jt. Assem. Suppl., Abstract pp. 24 A-04, The meeting of the Americas: Fort Lauderdale, FL, USA).
Blanco-Piñón, A., Zavala-Diaz de la Serna, F.J., Hernandez-Avila, J., Maurrasse, F., Duque-Botero, F., 2009. Microscopic bioforms in pyritic layers from the Cenomanian/Turonian (Upper Cretaceous) Agua Nueva Formation, Xilitla, Central Mexico: a preliminary description. Geol. Soc. Am. Abstr. Programs 41, 82.
Blanco-Piñón, A., Ángeles-Trigueros, S.A., Hernández-Ávila, J., Zavala-Díaz de la Serna, F.J., 2012. SEM imaging of biostructures in Upper Cretaceous sedimentary pyrite: an astrobiological approach. Geol. Soc. Am. Abstr. Programs 44, 75.
Blanco-Piñón, A., Maurrasse, F.J.-M.R., Zavala Díaz-de la Serna, F.J., López-Doncel, R.A., Ángeles-Trigueros, S.A., Hernández-Avila, J., Juárez Arriaga, E., 2014. Evidencias petrográficas de estructuras de origen algal/bacteriano en carbonatos de la Formación Agua Nueva (Cenomaniano/Turoniano: Cretácico Superior) en Xilitla, S. L. P. México Central. Bol. Soc. Geol. Mex. 66, 397–412.
Bomou, B., Adatte, T., Tantawy, T., Mort., H., Fleitmann, D., Huang, Y., Föllmi, K.B., 2013. The expression of the Cenomanian–Turonian oceanic anoxic event in Tibet. Palaeogeogr. Palaeoclimatol. Palaeoecol. 369, 466–481.
Bond, D.P.G., Wignall, P.B., 2010. Pyrite framboid study of marine Permian–Triassic boundary sections: a complex anoxic event and its relationship to contemporaneous mass extinction. Geol. Soc. Am. Bull. 122, 1265–1279.
Böning, P., Brumsack, H.J., Böttcher, M.E., Schnetger, B., Kriete, C., Kallmeyer, J., Borchers, S.L., 2004. Geochemistry of Peruvian near-surface sediments. Geochim. Cosmochim. Acta 68 (21), 4429–4451.
Bouloubassi, I., Rullkötter, J., Meyers, P.A., 1999. Origin and transformation of organic matter in Pliocene–Pleistocene Mediterranean sapropels: organic geochemical evidence reviewed. Mar. Geol. 153, 177–197.
Brumsack, H.-J., 2006. The trace metal content of recent organic carbon-rich sediments: implications for Cretaceous black shale formation. Palaeogeogr. Palaeoclimatol. Palaeoecol. 232, 344–361.
Calvert, S.E., Pedersen, T.F., 1993. Geochemistry of Recent oxic and anoxic marine sediments: implications for the geological record. Mar. Geol. 113, 67–88.
Canet, C., Alfonso, P., Melgarejo, J.C., Belyatsky, B.V., 2004. Geochemical evidences of sedimentary-exhalative origin of the shale-hosted PGE–Ag–Au–Zn–Cu occurrences of the Prades Mountains (Catalonia, Spain): trace-element abundances and Sm–Nd isotopes. J. Geochem. Explor. 82, 17–33.
Canfield, D.E., 2001. Isotope fractionation by natural populations of sulfate-reducing bacteria. Geochim. Cosmochim. Acta 65, 1117–1124.
Caron, M., Dall'Agnolo, S., Accarie, H., Barrera, E., Kauffman, E.G., Amédro, F., Robaszynski, F., 2006. High-resolution stratigraphy of the Cenomanian–Turonian boundary interval at Pueblo (USA) and wadi Bahloul (Tunisia): stable isotope and bioevents correlation. Geobios 39, 171–200.
Centeno-García, E., Guerrero-Suastegui, M., Talavera-Mendoza, O., 2008. The Guerrero Composite Terrane of Western Mexico: collision and subsequent rifting in a supra-subduction zone. Geol. Soc. Am. Spec. Pap. 436, 279–308.
Clarke, L.J., Jenkyns, H.C., 1999. New oxygen isotope evidence for long-term Cretaceous climatic change in the Southern Hemisphere. Geology 27, 699–702.
Cobianchi, M., Mancin, N., Lupi, C., Bordiga, M., Bostock, H.C., 2015. Effects of oceanic circulation and volcanic ash-fall on calcite dissolution in bathyal sediments from the SW Pacific Ocean over the last 550 ka. Palaeogeogr. Palaeoclimatol. Palaeoecol. 429, 72–82.
Coccioni, R., Luciani, V., 2004. Planktonic foraminifera and environmental changes across the Bonarelli Event (OAE2, latest Cenomanian) in its type area: a high resolution study from the Tethyan reference Bottaccione section (Gubbio, Central Italy). J. Foraminifer. Res. 34, 109–129.
Denne, R.A., Hinote, R.E., Breyer, J.A., Kosanke, T.H., Lees, J.A., Engelhardt-Moore, N., Spaw, F.M., Tur, N., 2014. The Cenomanian–Turonian Eagle Ford Group of South Texas: insights on timing and paleoceanographic conditions from geochemistry and micropaleontologic analyses. Palaeogeogr. Palaeoclimatol. Palaeoecol. 413, 2–28.
Desmares, D., Grosheny, D., Beaudoin, B., Gardin, S., Gauthier-Lafaye, F., 2007. High resolution stratigraphic record constrained by volcanic ash beds at the CenomanianeTuronian boundary in the Western Interior Basin, USA. Cretac. Res. 28, 561–582.
Du Vivier, A.D.C., Jacobson, A.D., Lehn, G.O., Selby, D., Hurtgen, M.T., Sageman, B.B., 2015a. Ca isotope stratigraphy across the Cenomanian–Turonian OAE 2: links between volcanism, seawater geochemistry, and the carbonate fractionation factor. Earth Planet. Sci. Lett. 416, 121–131.

Du Vivier, A.D.C., Selby, D., Condon, D.J., Takashima, R., Nishi, H., 2015b. Pacific $^{187}Os/^{188}Os$ isotope chemistry and U–Pb geochronology: synchroneity of global Os isotope change across OAE 2. Earth Planet. Sci. Lett. 428, 204–216.
Duggen, S., Olgun, N., Croot, P., Dietze, H., Delmelle, P., Teschner, C., 2010. The role of airborne volcanic ash for the surface ocean biogeochemical iron-cycle: a review. Biogeosci. Discuss. 7, 827–844.
Dunham, R.J., 1962. Classification of carbonate rocks according to depositional textures. In: Ham, W.E. (Ed.), Classification of Carbonate Rocks a Symposium. American Association of Petroleum Geologists Memoir 1, pp. 108–121.
Duque-Botero, F., Maurrasse, F.J.-M.-R., Hickey-Vargas, R., Melinte, M., Jaffe, R., Lopez-Oliva, J.G., 2009. Microspheroids accumulation and geochemistry of an anoxic basin of the Cenomanian/Turonian: the record of the Indidura Formation, NE Mexico. Geologic Problem Solving with Microfossils: A Volume in Honor of Garry D. Jones. Society for Sedimentary Geology, Society of Sedimentary Geology Special Publication 93, pp. 171–186.
Dymond, J., Suess, E., Lyle, M., 1992. Barium in deep-sea sediment: a geochemical proxy for paleoproductivity. Paleoceanography 7, 163–181.
Eldrett, J.S., Minisini, D., Bergman, S.C., 2014. Decoupling of the carbon cycle during ocean anoxic event 2. Geology 42, 567–570.
Elrick, M., Molina-Garza, R., Duncan, R., Snow, L., 2009. C-isotope stratigraphy and paleoenvironmental changes across OAE 2 (mid-Cretaceous) from shallow-water platform carbonates of Southern Mexico. Earth Planet. Sci. Lett. 277, 295–306.
Espitalié, J., Deroo, G., Marquis, F., 1985. La pyrolyse Rock-Eval et ses applications. Rev. Inst. Fr. Pétrol. 40, 563–579.
Föllmi, K.B., 2012. Early Cretaceous life, climate and anoxia. Cretac. Res. 35, 230–257.
Gambacorta, G., Jenkyns, H.C., Russo, F., Tsikos, H., Wilson, P.A., Faucher, G., Erba, E., 2015. Carbon-and oxygen-isotope records of mid-Cretaceous Tethyan pelagic sequences from the Umbria–Marche and Belluno Basins (Italy). Newsl. Stratigr. 48 (3), 299–323.
Gebhardt, H., Friedrich, O., Schenk, B., Fox, L., Hart, M., Wagreich, M., 2010. Paleoceanographic changes at the Northern Tethyan margin during the Cenomanian–Turonian Oceanic Anoxic Event (OAE-2). Mar. Micropaleontol. 77 (1), 25–45.
Gehrels, G., Valencia, V., Pullen, A., 2006. Detrital zircon geochronology by laser ablation multicollector ICPMS at the Arizona LaserChron Center. In: Olszewski, T. (Ed.), Geochronology: Emerging Opportunities. Paleontological Society Papers 12, pp. 67–76.
Giesemann, A., Jäger, H.J., Norman, A.L., Krouse, H.R., Brand, W.A., 1994. Online sulfur-isotope determination using an elemental analyzer coupled to a mass spectrometer. Anal. Chem. 66, 2816–2819.
Goddard, E.N., Trask, P.D., De Ford, R.K., Rove, O.N., Singewald, J.T., Overbeck, R.M., 1963. Rock-Color Chart. Distributed by the Geological Society of America, New York (16 pp).
Goldhammer, R., Johnson, C., 2001. Middle Jurassic–Upper Cretaceous Paleogeographic Evolution and sequence-stratigraphic framework of the Northwest Gulf of Mexico Rim. The Western Gulf of Mexico Basin: tectonics, sedimentary basins, and petroleum systems. AAPG Mem. 75, 45–81.
Habicht, K.S., Canfield, D.E., 1997. Sulfur isotope fractionation during bacterial sulfate reduction in organic-rich sediments. Geochim. Cosmochim. Acta 61, 5351–5361.
Hardenbol, J., Thierry, J., Farley, M.B., de Graciansky, P.C., Vail, P.P., 1998. Mesozoic and Cenozoic sequence chronostratigraphic framework of European basins. In: de Graciansky, P.C., Hardenbol, J., Jacquin, T., Vail, P.P. (Eds.), Mesozoic and Cenozoic Sequence Stratigraphy of European Basins. Society of Economic Paleontologists and Mineralogists Special Publication 60, pp. 3–13.
Hernández-Romano, U., Aguilera-Franco, N., Martínez-Medrano, M., Barceló-Duarte, J., 1997. Guerrero-Morelos Platform drowning at the Cenomanian–Turonian boundary, Huitziltepec area, Guerrero State, Southern Mexico. Cretac. Res. 18, 661–686.
Hetzel, A., Böttcher, M.E., Wortmann, U.G., Brumsack, H.-J., 2009. Paleo-redox conditions during OAE 2 reflected in Demerara Rise sediment geochemistry (ODP Leg 207). Palaeogeogr. Palaeoclimatol. Palaeoecol. 273, 302–328.
Ifrim, C., Götz, S., Stinnesbeck, W., 2011. Fluctuations of the oxygen minimum zone at the end of Oceanic Anoxic Event 2 reflected by benthic and planktic fossils. Geology 39, 1043–1046.
Jeffries, T., Fernández-Suárez, J., Corfu, F., Gutiérrez-Alonso, G., 2003. Advances in U–Pb geochronology using a frequecy quintupled Nd:YAG based laser ablation system (lambda = 213 nm) and quadrupole based ICP-MS. J. Anal. At. Spectrom. 18, 847–855.
Jiménez Berrocoso, Á., MacLeod, K.G., Calvert, S.E., Elorza, J., 2008. Bottom water anoxia, inoceramid colonization, and benthopelagic coupling during black shale deposition on Demerara Rise (Late Cretaceous western tropical North Atlantic). Paleoceanography 23, PA3212.
Kędzierski, M., Machaniec, E., Rodríguez-Tovar, F.J., Uchman, A., 2012. Bio-events, foraminiferal and nannofossil biostratigraphy of the Cenomanian/Turonian boundary interval in the Subsilesian Nappe, Rybie Section, Polish Carpathians. Cretac. Res. 35, 181–198.
Keller, G., Berner, Z., Adatte, T., Stueben, D., 2004. Cenomanian–Turonian and $\delta^{13}C$, and $\delta^{18}O$, sea level and salinity variations at Pueblo, Colorado. Palaeogeogr. Palaeoclimatol. Palaeoecol. 211, 19–43.
Kuhnt, W., Holbourn, A., Gale, A., Chellai, E., Kennedy, W.J., 2009. Cenomanian sequence stratigraphy and sea-level in the Tarfaya Basin (SW Morocco). Geol. Soc. Am. Bull. 1695–1710.
Langmann, B., Zakšsek, K., Hort, M., Duggen, S., 2010. Volcanic ash as fertiliser for the surface ocean. Atmos. Chem. Phys. Discuss. 10, 711–734.
Leckie, R.M., Bralower, T.J., Cashman, R., 2002. Oceanic anoxic events and plankton evolution: biotic response to tectonic forcing during the mid-Cretaceous. Paleoceanography 17 (13–1 to 13–29).
Lowery, C.M., Corbett, M.J., Leckie, R.M., Watkins, D., Romero, A.M., Pramudito, A., 2014. Foraminiferal and nannofossil paleoecology and paleoceanography of the Cenomanian–Turonian Eagle Ford Shale of Southern Texas. Palaeogeogr. Palaeoclimatol. Palaeoecol. 413, 49–65.
Ludwig, K.R., 1991. A plotting and regression program for radiogenic-isotope data; version 2.53. U.S. Geological Survey Open-File Microsoft excel. Berkeley Geochronological Center Special Publication 4a.
McCrea, J.M., 1950. On the isotopic chemistry of carbonates and a paleotemperature scale. J. Chem. Phys. 18, 849–857.
Meyers, P.A., Bernasconi, S.M., Forster, A., 2006. Origins and accumulation of organic matter in expanded Albian to Santonian black shale sequences on the Demerara Rise, South American margin. Org. Geochem. 37, 1816–1830.
Meyers, S.R., Siewert, S.E., Singer, B.S., Sageman, B.B., Condon, D.J., Obradovich, J.D., Jicha, B,.R., Sawyer, D.A., 2012. Intercalibration of radioisotopic and astrochronologic time scales for the Cenomanian–Turonian boundary interval, Western Interior Basin, USA. Geology 40 (1), 7–10.
Morán-Zenteno, D., 1994. The geology of the Mexican Republic. AAPG Stud. Geol. 39, 160.
Mort, H.P., Adatte, T., Föllmi, K., Keller, G., Steinmann, P., Matera, V., Berner, Z., Stüben, D., 2007. Phosphorus and the roles of productivity and nutrient recycling during Oceanic Anoxic Event 2. Geology 35, 483–486.
Negra, M.H., Zagrarni, M.F., Hanini, A., Strasser, A., 2011. The filament event near the Cenomanian–Turonian boundary in Tunisia: filament origin and environmental signification. Bull. Soc. Geol. Fr. 182 (6), 507–519.
Núñez-Useche, F., Barragán, R., Moreno-Bedmar, J.A., Canet, C., 2015. Geochemical and paleoenvironmental record of the early to early late Aptian major episodes of accelerated change: evidence from Sierra Del Rosario, Northeast Mexico. Sediment. Geol. 324, 47–66.
Ohmoto, H., Kaiser, C.J., Geer, A., 1990. Systematics of sulphur isotopes in recent marine sediments and ancient sediment-hosted base metal deposits. In: Herbert, H.K., Ho, S.E. (Eds.), Stable Isotopes and Fluid Processes in Mineralization. University of Western Australia Publ 23, pp. 70–120.
Passier, H.F., Middelburg, J.J., de Lange, G.J., Böttcher, M.E., 1997. Pyrite contents, microtextures, and sulfur isotopes in relation to formation of the youngest Eastern Mediterranean sapropel. Geology 25, 519–522.
Paytan, A., Kastner, M., Campbell, D., Thiemens, M.H., 2004. Seawater sulfur isotope fluctuations in the Cretaceous. Science 304, 1663–1665.
Poulton, S.W., Henkel, S., März, C., Urquhart, H., Flögel, S., Kasten, S., Jaap, S., Sinninghe, S., Wagner, T., 2015. A continental-weathering control on orbitally driven redox-nutrient cycling during Cretaceous Oceanic Anoxic Event 2. Geology 43 (11), 963–966.
Premoli Silva, I., Sliter, W.V., 2002. Practical manual of Cretaceous planktonic foraminifera. In: Premoli Silva, I., Rettori, R. (Eds.), International School on Planktonic Foraminifera, 1st Course. University of Perugia, Italy, p. 462.
Reitz, A., Pfeifer, K., de Lange, G.J., Klump, J., 2004. Biogenic barium and the detrital Ba/Al ratio: a comparison of their direct and indirect determination. Mar. Geol. 204, 289–300.
Reolid, M., Nagy, J., Rodríguez-Tovar, F.J., 2010. Ecostratigraphic trends of Jurassic agglutinated foraminiferal assemblages as a response to sea-level changes in shelf deposits of Svalbard (Norway). Palaeogeogr. Palaeoclimatol. Palaeoecol. 293 (1), 184–196.
Reolid, M., Sánchez-Quiñónez, C.A., Alegret, L., Molina, E., 2015. Palaeoenvironmental turnover across the Cenomanian–Turonian transition in Oued Bahloul, Tunisia: foraminifera and geochemical proxies. Palaeogeogr. Palaeoclimatol. Palaeoecol. 417, 491–510.
Rickard, D., 2012. Sulfidic sediments and sedimentary rocks. In: Van Loon, A.J. (Ed.), Developments in Sedimentology. Elsevier, p. 801.
Rigual-Hernández, A.S., Sierro, F.J., Bárcena, M.A., Flores, J.A., Heussner, S., 2012. Seasonal and interannual changes of planktic foraminiferal fluxes in the Gulf of Lions (NW Mediterranean) and their implications for paleoceanographic studies: two 12-year sediment trap records. Deep-Sea Res. I Oceanogr. Res. Pap. 66, 26–40.
Robaszynski, F., Zagrarni, M.F., Caron, M., Amédro, F., 2010. The global bio-events at the Cenomanian–Turonian transition in the reduced Bahloul Formation of Bou Ghanem (Central Tunisia). Cretac. Res. 31, 1–15.
Salmon, K.H., Anand, P., Sexton, P.F., Conte, M., 2014. Upper ocean mixing controls the seasonality of planktonic foraminifer fluxes and associated strength of the carbonate pump in the oligotrophic North Atlantic. Biogeosci. Discuss. 11, 12223–12254.
Schlanger, S.O., Jenkyns, H.C., 1976. Cretaceous oceanic anoxic events—causes and consequences. Geol. Mijnb. 55, 179–184.
Snow, L., Duncan, R.A., 2001. Hydrothermal links between ocean plateau formation and global anoxia. Eos Trans. AGU 82 (47) (Fall Meet. Suppl., abstract OS41A-0437).
Snow, L.J., Duncan, R.A., Bralower, T.J., 2005. Trace element abundances in the Rock Canyon Anticline, Pueblo, Colorado, marine sedimentary section and their relationship to Caribbean plateau construction and oxygen anoxic event 2. Paleoceanography 20, PA3005.
Solari, L.A., Gómez-Tuena, A., Bernal, J.P., Pérez-Arvizu, O., Tanner, M., 2009. U–Pb zircon geochronology with an integrated LA-ICP-MS microanalytical workstation: achievements in precision and accuracy. Geostand. Geoanal. Res. 34, 5–18.
Suter, M., 1984. Cordilleran deformation along the eastern edge of the Valles–San Luis Potosí carbonate platform, Sierra Madre Oriental fold-thrust belt, east-central Mexico. Geol. Soc. Am. Bull. 95, 1387–1397.
Taylor, A.M., Goldring, R., 1993. Description and analysis of bioturbation and ichnofabric. J. Geol. Soc. Lond. 150, 141–148.
Trabucho Alexandre, J., Tuenter, E., Henstra, G.A., van der Zwan, K.J., van de Wal, R.S.W., Dijkstra, H.A., de Boer, P.L., 2010. The mid-Cretaceous North Atlantic nutrient trap: Black shales and OAEs. Paleoceanography 25, PA4201.
Tribovillard, N., Algeo, T.J., Lyons, T., Riboulleau, A., 2006. Trace metals as paleoredox and paleoproductivity proxies: an update. Chem. Geol. 232, 12–32.
Twichell, S.C., Meyers, P.A., Diester-Haass, L., 2002. Significance of high C/N ratios in organic-carbon-rich Neogene sediments under the Benguela Current upwelling system. Org. Geochem. 33, 715–722.

Uchman, A., Rodríguez-Tovar, F.J., Machaniec, E., Kędzierski, M., 2013. Ichnological characteristics of Late Cretaceous hemipelagic and pelagic sediments in a submarine high around the OAE-2 event: a case from the Rybie section, Polish Carpathians. Palaeogeogr. Palaeoclimatol. Palaeoecol. 370, 222–231.

Van Mooy, B.A.S., Keil, R.G., Devol, A.H., 2002. Impact of suboxia on sinking particulate organic carbon: enhanced carbon flux and preferential degradation of amino acids via denitrification. Geochim. Cosmochim. Acta 66, 457–465.

Wedepohl, K.H., 1971. Environmental influences on the chemical composition of shales and clays. Phys. Chem. Earth 8, 305–333.

Westermann, S., Caron, M., Fiet, N., Fleitmann, D., Matera, V., Adatte, T., Föllmi, K.B., 2010. Evidence for oxic conditions during oceanic anoxic event 2 in the Northern Tethyan pelagic realm. Cretac. Res. 31, 500–514.

Wignall, P.B., 1994. Black Shales. Geology and Geophysics Monographs 30. Oxford University Press, Oxford (130 p.).

Wignall, P.B., Hallam, A., 1991. Biofacies, stratigraphic distribution and depositional models of British onshore Jurassic black shales. Geol. Soc. Lond. Spec. Publ. 58, 291–309.

Wilkin, R.T., Barnes, H.L., Brantley, S.L., 1996. The size distribution of framboidal pyrite in modern sediments: an indicator of redox conditions. Geochim. Cosmochim. Acta 60, 3897–3912.

Xu, G., Hannah, J.L., Bingen, B., Georgiev, S., Stein, H.J., 2012. Digestion methods for trace element measurements in shales: paleoredox proxies examined. Chem. Geol. 324, 132–147.

Supplementary Appendix A.

LA–ICP–MS analysis of volcanic zircons from bentonite sample Az (bed 11)*.

	CORRECTED RATIOS												CORRECTED AGES (Myr)									
	U (ppm)	Th (ppm)	Th/U	$^{207}Pb/^{206}Pb$	±1s	$^{207}Pb/^{235}U$	±1s	$^{206}Pb/^{238}U$	±1s	$^{208}Pb/^{232}Th$	±1s	Rho	$^{206}Pb/^{238}U$	±1s	$^{207}Pb/^{235}U$	± 1s	$^{207}Pb/^{206}Pb$	±1s	$^{208}Pb/^{232}Th$	± 1s	Best age (Myr)	±1s	disc %
Zircon_45_061	863	613	0.63	0.0491	0.0019	0.0942	0.0037	0.01	0.00011	0.0041	0.00011	0.2	88.7	0.7	91	3	152	82	82	2	89	0.7	2.5
Zircon_42_058	441	219	0.44	0.0507	0.0019	0.098	0.0038	0.01	0.00015	0.0043	0.00014	0.28	89.8	1	95	3	227	80	87	3	90	1	5.5
Zircon_39_054	288	225	0.69	0.0485	0.0032	0.0958	0.0064	0.01	0.00022	0.0044	0.00022	0.23	93	1	93	6	124	134	89	4	93	1	0
Zircon_31_B_04 5	276	148	0.47	0.0531	0.004	0.1058	0.0086	0.01	0.00021	0.0045	0.00007	0.3	93	1	102	8	332	165	91	1	93	1	8.8
Zircon_46_063	368	195	0.47	0.0466	0.0023	0.0942	0.0047	0.01	0.00016	0.0046	0.00013	0.23	94	1	91	4	28	96	92	3	94	1	-3.3
Zircon_44_060	830	510	0.54	0.0524	0.0023	0.1065	0.0051	0.01	0.00014	0.0046	0.00004	0.28	94.3	0.9	103	5	304	94	93.2	0.8	94	0.9	8.4
Zircon_43_059	228	130	0.5	0.0517	0.0034	0.1064	0.0072	0.01	0.00022	0.0046	0.00018	0.22	95	1	103	7	272	140	93	4	95	1	7.8
Zircon_49_066	284	102	0.32	0.0521	0.0023	0.1067	0.0049	0.01	0.00019	0.0052	0.00024	0.28	95	1	103	4	289	94	105	5	95	1	7.8
Zircon_32_046	259	89	0.3	0.0527	0.0036	0.1077	0.0075	0.01	0.00024	0.0044	0.00018	0.23	95	2	104	7	315	151	89	4	95	2	8.7
Zircon_51_069	213	111	0.46	0.0527	0.0027	0.1079	0.0058	0.01	0.00019	0.0046	0.0002	0.24	95	1	104	5	316	110	92	4	95	1	8.7
Zircon_33_047	466	181	0.34	0.05	0.0032	0.1026	0.0068	0.01	0.00015	0.0047	0.00012	0.2	95.2	0.9	99	6	195	134	95	2	95	0.9	3.8
Zircon_34_048	181	97	0.47	0.049	0.0034	0.1013	0.0071	0.02	0.00021	0.0046	0.00023	0.2	96	1	98	7	149	142	93	5	96	1	2
Zircon_35_049	510	251	0.43	0.0491	0.0041	0.101	0.0089	0.01	0.00019	0.0047	0.00025	0.3	96	1	98	8	151	173	95	5	96	1	2
Zircon_37_052	1019	793	0.69	0.0535	0.0023	0.1109	0.0054	0.02	0.00015	0.0047	0.00004	0.32	96.2	1	107	5	349	92	94.9	0.9	96	1	10.1
Zircon_36_051	370	233	0.55	0.0507	0.0027	0.1063	0.0057	0.02	0.00014	0.0052	0.00024	0.17	97.2	0.9	103	5	229	113	104	5	97	0.9	5.6
Zircon_48_065	184	115	0.55	0.0488	0.0037	0.1028	0.0082	0.02	0.00036	0.0049	0.00018	0.29	99	2	99	8	136	157	99	4	99	2	0
Zircon_50_067	565	428	0.67	0.0528	0.0021	0.1141	0.0046	0.02	0.00017	0.005	0.00013	0.27	100	1	110	4	322	82	101	3	100	1	9.1

*The bentonite sample was crushed and separated granulometrically. Separation of heavy minerals was carried out using a Wilfley Table, and then a Franz Magnetic separator at the Instituto de Geología (UNAM). Euhedral zircon crystals were hand-picked and then mounted in epoxy, sanded and polished to expose a transverse section. They were photographed using reflected light and scanning electron microscope-cathodoluminescence (SEM-CL) in order to select homogenous grains and avoid the detection of inherited ages by core relicts.

Supplementary Appendix A.

Isotopic data ($\delta^{13}C$, $\delta^{18}O$, $\delta^{34}S$), Rock–eval pyrolysis data and N_{TOT}.

Samples	Distance (m)	$\delta^{13}C$ (‰ VPDB)	$\delta^{18}O$ (‰ VPDB)	$\delta^{34}S$ pyrite (‰ VCDT)	TOC (%)	HI (mg H/g	OI (mg O/g TOC)	N_{TOT} (%)
212	28.9	1.5	-3.8					
210	28.7	0.5	-5.4	-34.9	1.77	386	23	0.06
207	28.4	1	-5		0.93			
205	27.7	1.4	-3.9					
203	28				0.9			
201	27.8				1.11			
200	27.1	1.6	-4					
199	27				1.21			
197	26.8	1.6	-4.1		0.46			
192	26.7				1.53			
187	25.9	1.4	-4		1.38	306	22	0.05
180	24.5				0.32			
179	24.4	1.3	-4.4					
173	23.9	1	-4.4					
169	23.6	1.2	-5					
166	23.3				1.42			
161	22.6	1.3	-5.4	-41.2	1.81	397	14	0.05
159	22.3	1.3	-5.2					
157	22.2				0.95			
152	21.9	1	-4.9					
147	21.5	0.9	-3.4					
146	21.4				0.85			
145	21.3				0.85			
135	20.2	0.9	-4					
131	19.8	0.4	-3.8	-16.2	1.59	423	14	0.05
127	19.3				0.43			
126	19.1	0.8	-4.4	-27.4	1.5	414	14	0.04
121	18.5	0.7	-3.8					
120	18.4				1.65			
115	18.1	1.6	-4.1		1.42	438	13	0.04
110	17.4				0.64			
106	17.1	0.7	-3.8	-5.2	1.18			
101	16.8	0.7	-4.5					
93	15.9	1.3	-5.3		1.32			
92	15.8	1.2	-4.5					
90	15.3				1.01			
88	14.9				0.82			
86	14.3	1.2	-5.1	-6.3				
84	14.1	0.7	-4.9					
82	14	-0.1	-4.5					
80	13.9				0.51			
79	13.8	1.1	-5					

Samples	Distance (m)	$\delta^{13}C$ (‰ VPDB)	$\delta^{18}O$ (‰ VPDB)	$\delta^{34}S$ pyrite (‰ VCDT)	TOC (%)	HI (mg H/g	OI (mg O/g TOC)	N_{TOT} (%)
78	13.7	-0.1	-5.2					
77	13.6	-0.7	-6.5					
76	13.5	0.1	-4.5					
72	11.6				1.11			
70	11.2	-1.9	-4.2	-8.4	0.65			
65	10.1	-1.3	-4.7	-8.7	2.33	455	8	0.06
63	10.2	-0.6	-4.9					
59	9.9	0.6	-4.4					
56	9.3	0.8	-3.9		1.85			
53	8.9	0.5	-4					
52	8.8	0.6	-4.2					
51	8.7	0.5	-4.6					
50	4.5				0.95			
45	7.7	0.1	-4.5					
41	7.1	1.1	-5.1	-19.8	3.15			
40	7				1.75			
39	6.9	0.7	-3.8					
38	6.7	0.9	-3.9					
36	6.4	0.7	-4					
35	6.2	0.6	-4.4		2.34	430	9	0.05
33	5.9	0.8	-4.2					
31	5.6	0.7	-3.8					
30	5.4	0.8	-4.5	-31.9	1.24	276	39	0.05
28	4.9	0.7	-3.8					
27	4.8	0.7	-4.1		3.11			
26	4.6	0.7	-4.2					
25	4.4				0.76			
22	3.9	0.8	-4.2	-11.3	1.61	415	11	0.06
21	3.7			-28.9				
20	3.6				3.15			
18	2.9	1	-3.9					
17	2.8	1.1	-4.3	-18.7	2.48	468	8	0.06
16	2.5	0.9	-4					
13	1.9	0.8	-3.7	-51.2				
10	1.5	0.7	-5.4		3.32	427	8	0.06
8	1.2				2.8			
6	0.9	0.7	-3.6		0.58			
5	0.7	0.5	-4.4					
4	0.5	0.7	-3.9					
1	0.1	0.6	-4.6		2.95			

Supplementary Appendix A.

Concentrations of major and trace elements measured in selected samples of the Xilitla section.

Samples	Distance base (m)	Al (%)	Fe (%)	S (%)	Cd (ppm)	Zn (ppm)	V (ppm)	Cr (ppm)	Ni (ppm)	Co (ppm)	Pb (ppm)	Ag (ppm)	Cu (ppm)	U (ppm)	Re (ppm)	Mo (ppm)	Th (ppm)	Mn (ppm)	Ba (ppm)	P (%)
212	28.9	0.98	0.8	0.16	< 0.1	33.3	20	9.9	19.2	2.6	4	0.12	11.1	0.8	< 0.001	0.2	0.4	379	153	0.054
210	28.7	0.41	7.48	8.73	1.2	42.9	111	17.8	98.7	11.7	23.4	0.87	27.3	2.1	0.063	16.5	0.9	292	60	0.044
207	28.4	1.92	1.11	0.18	< 0.1	56.8	51	19.1	25	4.3	11.6	0.24	117	1.2	0.006	1.1	1	310	185	0.052
201	27.8	1.11	0.61	0.14	< 0.1	39.9	26	13.2	17.4	1.5	3.3	0.18	15.1	1	0.006	0.4	0.9	388	93	0.052
199	27.5	0.49	0.58	0.43	0.2	13.6	46	7.7	25.8	2	1	0.18	7.4	4.8	0.04	2.4	0.4	414	39	0.059
187	25.9	1.18	1.89	1.68	1.5	108	168	51.5	58.2	6.5	3.1	0.48	31.1	3.1	0.075	5.4	0.7	276	90	0.071
161	22.6	0.65	1.68	1.55	0.3	60.2	83	99.9	38.2	10.3	4.5	0.37	42	1.4	0.029	0.5	0.5	243	56	0.077
131	19.8	0.51	1.34	1.44	0.4	33.9	47	10	24.5	1.8	1.2	0.17	10.8	2.9	0.022	5.7	0.6	609	63	0.024
126	19.1	0.78	1.44	1.72	< 0.1	13.1	121	17.1	41.1	3.1	2.9	0.27	17.6	3.8	0.048	9.9	0.8	382	75	0.056
120	18.4	0.63	1.27	1.37	0.2	24.7	88	5.4	39	2.6	2.4	0.38	12.8	3.6	0.031	5.7	0.7	518	51	0.044
115	18.1	1.43	1.54	0.17	0.2	91	26	22.8	17.5	2.2	4.5	0.33	16.6	2.5	< 0.001	0.2	1	473	367	0.103
106	17.1	0.74	0.63	0.17	< 0.1	29	62	67.1	18.1	2.7	4.7	1.28	91.6	1	0.004	0.5	0.7	468	115	0.044
90	15.4	1.51	0.94	0.84	4.2	515	219	21.2	38.2	2.9	3.8	1.13	23.8	2.8	0.031	5.9	1.6	453	292	0.028
70	11.2	1.78	1.36	0.84	< 0.1	21.7	93	67.9	55.4	9.5	1.8	0.23	29.8	2	0.039	3.2	0.7	1090	208	0.024
65	10.1	2.26	6.24	7.43	1.3	67.2	127	33.8	83.2	7.4	5.6	0.74	41.5	6.5	0.135	11.1	2.7	264	253	0.104
59	9.9	0.82	0.76	0.63	0.2	37.1	57	26.7	21.7	2.7	3.6	0.55	19.5	1.9	0.003	0.5	0.8	364	140	0.04
52	8.9	0.6	0.58	0.38	< 0.1	22.5	20	13.9	17.8	2.4	2.7	0.28	9.5	0.8	0.007	0.4	0.4	313	191	0.027
49	8.3	1.38	1.01	0.58	0.2	54	48	25.4	19.2	4.7	4.2	0.58	22.9	1.3	0.005	0.8	0.7	301	248	0.048
45	7.7	1.48	1.31	0.82	0.3	51.2	68	31.2	22.5	3.6	6.8	0.78	21.7	1.9	0.002	0.4	1.1	378	339	0.056
41	7.1	1.38	1.98	2.2	10.6	508	311	120	60.2	6	4.1	0.97	69.7	6	0.105	5.9	1	203	72	0.117
39	6.9	1.31	1.32	0.14	0.2	39.4	69	24.6	21	3	6.1	0.46	16.3	1.7	< 0.001	0.3	1	260	521	0.056
31	5.6	0.84	1.02	0.88	< 0.1	37.6	53	21.6	21.7	3	4.1	0.28	24.3	2.4	0.007	1.4	0.5	195	74	0.036
30	5.4	1.3	0.56	0.34	1.9	60.4	216	35.7	21.5	1.4	1.8	0.42	29.3	4	0.047	2.6	0.8	194	50	0.052
27	4.8	0.52	0.54	0.39	2.9	148	175	59.5	29.6	2	1.8	0.2	25	5.1	0.031	2.3	0.5	137	228	0.027
22	3.9	0.8	0.64	0.9	1.7	74.7	220	39	39.8	4.7	2.1	0.66	71.8	6	0.044	8.7	0.9	193	66	0.06
17	2.8	1.24	1.19	1.58	13.8	529	315	87.3	69.5	5.9	6.4	1.35	65.2	6.4	0.085	11.2	1.6	176	67	0.058
16	2.5	0.49	0.47	0.35	3.4	152	198	57.9	32.8	1.9	2.1	0.23	33.9	2.8	0.035	3	0.6	179	114	0.028
10	1.5	1.85	3.33	3.09	12.9	657	512	216	95.8	9.2	6.4	1.87	101	7	0.15	7.6	5.3	194	76	0.169
9	1.4	0.91	1.11	0.61	0.3	54.3	30	65	22.2	3.1	3.4	0.29	150	1.5	0.005	2.2	2.6	192	72	0.057

Supplementary Appendix A.

Al-normalized values and enrichment factors (EFs) of selected major and trace elements measured in the Xilitla section, and calculated values of the biogenic barium used in this study.

Samples	Distance base (m)	Fe/Al	Cd/Al ($\times10^{-4}$)	Zn/Al ($\times10^{-4}$)	V/Al ($\times10^{-4}$)	Cr/Al ($\times10^{-4}$)	Ni/Al ($\times10^{-4}$)	Co/Al ($\times10^{-4}$)	Pb/Al ($\times10^{-4}$)	Ag/Al ($\times10^{-4}$)	Cu/Al ($\times10^{-4}$)	U/Al ($\times10^{-4}$)	Re/Al ($\times10^{-4}$)	Mo/Al ($\times10^{-4}$)	Mn/Al ($\times10^{-4}$)	Ba/Al ($\times10^{-4}$)	P/Al	Ba_{bio} (ppm)
212	28.9	0.82	-	33.98	20.41	10.1	19.59	2.65	4.08	0.12	11.33	0.82	-	0.2	386.73	156.12	0.06	116.74
210	28.7	18.24	2.93	104.63	270.73	43.41	240.73	28.54	57.07	2.12	66.59	5.12	0.154	40.24	712.2	146.34	0.11	44.83
207	28.4	0.58	-	29.58	26.56	9.95	13.02	2.24	6.04	0.13	60.94	0.63	0.003	0.57	161.46	96.35	0.03	113.96
201	27.8	0.55	-	35.95	23.42	11.89	15.68	1.35	2.97	0.16	13.6	0.9	0.005	0.36	349.55	83.78	0.05	51.93
199	27.5	1.18	0.41	27.76	93.88	15.71	52.65	4.08	2.04	0.37	15.1	9.8	0.082	4.9	844.9	79.59	0.12	20.87
187	25.9	1.6	1.27	91.53	142.37	43.64	49.32	5.51	2.63	0.41	26.36	2.63	0.064	4.58	233.9	76.27	0.06	46.34
161	22.6	2.58	0.46	92.62	127.69	153.69	58.77	15.85	6.92	0.57	64.62	2.15	0.045	0.77	373.85	86.15	0.12	31.95
131	19.8	2.63	0.78	66.47	92.16	19.61	48.04	3.53	2.35	0.33	21.18	5.69	0.043	11.18	1194.12	123.53	0.05	44.13
126	19.1	1.85	-	16.79	155.13	21.92	52.69	3.97	3.72	0.35	22.56	4.87	0.062	12.69	489.74	96.15	0.07	46.14
120	18.4	2.02	0.32	39.21	139.68	8.57	61.9	4.13	3.81	0.6	20.32	5.71	0.049	9.05	822.22	80.95	0.07	27.69
115	18.1	1.08	0.14	63.64	18.18	15.94	12.24	1.54	3.15	0.23	11.61	1.75	-	0.14	330.77	256.64	0.07	314.09
106	17.1	0.85	-	39.19	83.78	90.68	24.46	3.65	6.35	1.73	123.78	1.35	0.005	0.68	632.43	155.41	0.06	87.62
90	15.4	0.62	2.78	341.06	145.03	14.04	25.3	1.92	2.52	0.75	15.76	1.85	0.021	3.91	300	193.38	0.02	236.13
70	11.2	0.76	-	12.19	52.25	38.15	31.12	5.34	1.01	0.13	16.74	1.12	0.022	1.8	612.36	116.85	0.01	142.14
65	10.1	2.76	0.58	29.73	56.19	14.96	36.81	3.27	2.48	0.33	18.36	2.88	0.06	4.91	116.81	111.95	0.05	169.38
59	9.9	0.93	0.24	45.24	69.51	32.56	26.46	3.29	4.39	0.67	23.78	2.32	0.004	0.61	443.9	170.73	0.05	109.66
52	8.9	0.97	-	37.5	33.33	23.17	29.67	4	4.5	0.47	15.83	1.33	0.012	0.67	521.67	318.33	0.05	168.8
49	8.3	0.73	0.14	39.13	34.78	18.41	13.91	3.41	3.04	0.42	16.59	0.94	0.004	0.58	218.12	179.71	0.03	196.94
45	7.7	0.89	0.2	34.59	45.95	21.08	15.2	2.43	4.59	0.53	14.66	1.28	0.001	0.27	255.41	229.05	0.04	284.24
41	7.1	1.43	7.68	368.12	225.36	86.96	43.62	4.35	2.97	0.7	50.51	4.35	0.076	4.28	147.1	52.17	0.08	20.94
39	6.9	1.01	0.15	30.08	52.67	18.78	16.03	2.29	4.66	0.35	12.44	1.3	-	0.23	198.47	397.71	0.04	472.53
31	5.6	1.21	-	44.76	63.1	25.71	25.83	3.57	4.88	0.33	28.93	2.86	0.008	1.67	232.14	88.1	0.04	42.92
30	5.4	0.43	1.46	46.46	166.15	27.46	16.54	1.08	1.38	0.32	22.54	3.08	0.036	2	149.23	38.46	0.04	1.9
27	4.8	1.04	5.58	284.62	336.54	114.42	56.92	3.85	3.46	0.38	48.08	9.81	0.06	4.42	263.46	438.46	0.05	208.76
22	3.9	0.8	2.13	93.38	275	48.75	49.75	5.88	2.63	0.83	89.75	7.5	0.055	10.88	241.25	82.5	0.08	36.4
17	2.8	0.96	11.13	426.61	254.03	70.4	56.05	4.76	5.16	1.09	52.58	5.16	0.069	9.03	141.94	54.03	0.05	21.12
16	2.5	0.96	6.94	310.2	404.08	118.16	66.94	3.88	4.29	0.47	69.18	5.71	0.071	6.12	365.31	232.65	0.06	95.87
10	1.5	1.8	6.97	355.14	276.76	116.76	51.78	4.97	3.46	1.01	54.59	3.78	0.081	4.11	104.86	41.08	0.09	7.55
9	1.4	1.22	0.33	59.67	32.97	71.43	24.4	3.41	3.74	0.32	164.84	1.65	0.005	2.42	210.99	79.12	0.06	38.33

Supplementary Appendix A.

Mineral composition obtained by XRD analysis

Samples	Distance base (m)	Calcite (%)	Quartz (%)	Mica-Illite (%)	Potassium Feldspar (%)	Dolomite (%)	Kaolinite (%)	Hematite (%)	Clorite (%)	Plagioclase (%)
210	28.7	83	6	1	1	1	5	1	0	2
187	25.9	89	4	2	1	0	0	0	0	4
161	22.6	89	7	1	0	0	0	0	0	3
131	19.8	73	13	2	1	0	0	1	1	9
126	19.1	92	3	1	0	0	0	0	0	4
115	18.1	92	3	1	1	0	0	0	0	3
65	10.1	65	10	7	3	6	1	1	2	5
30	5.4	88	1	4	1	0	1	0	0	5
22	3.9	92	1	1	1	0	0	0	0	5

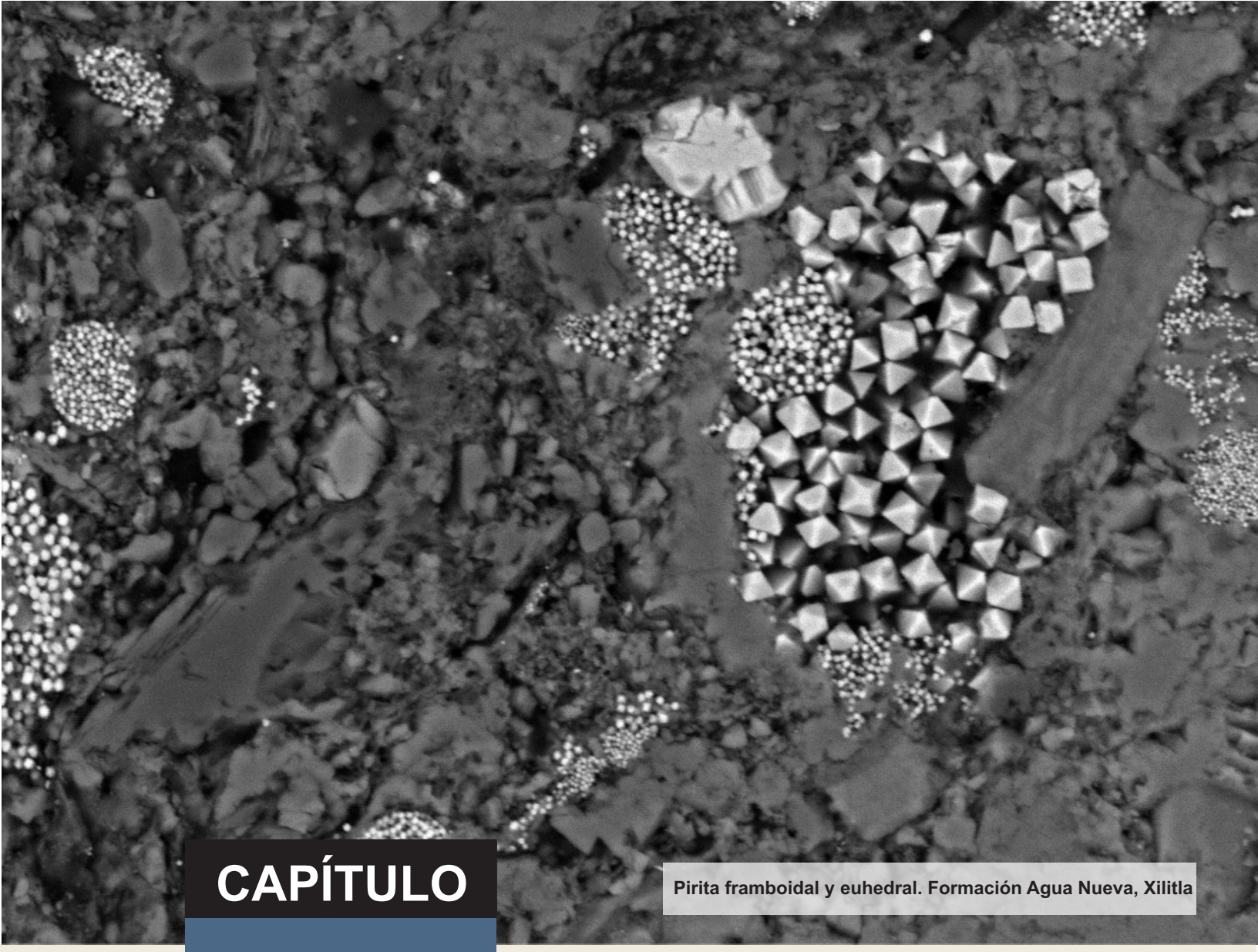

Pirita framboidal y euhedral. Formación Agua Nueva, Xilitla

CAPÍTULO 7

DISCUSIÓN Y CONCLUSIONES

DISCUSIÓN Y CONCLUSIONES

Este trabajo documenta varios episodios cretácicos de cambio global acelerado (Figs 4 y 5) . De igual forma, caracteriza las condiciones paleoambientales que persistieron durante su ocurrencia y descifra las condiciones globales/locales que condujeron al depósito de materia orgánica en los intervalos estratigráficos asociados con algunos de estos eventos.

En el norte del México, el estudio de la sucesión carbonatada de las formaciones Cupido y La Peña en la sección estratigráfica de la Presa Francisco Zarco arrojó los siguientes resultados:

- A nivel mundial, la mayoría de las plataformas carbonatadas del Tetis fueron ahogadas antes del OAE 1a o experimentaron un decremento en la producción carbonatada durante el evento. En el norte de México, el inicio del ahogamiento de la plataforma Cupido ocurrió durante el Barremiano tardío-Aptiano temprano, precediendo también a dicho a evento anóxico, con la transformación de una plataforma bordeada por un margen arrecifal y barras de arena a una rampa (unidad Cupidito) , y el subsiguiente cambio en la producción carbonatada de fotosintética a heterotrófica (Fig. 5A) . El OAE 1a (Aptiano temprano) está registrado en la parte superior de la Formación Cupido, más exactamente dentro de la unidad Cupidito. Corresponde a 30.6 m de facies lagunares hacia la base y de barras de ooides hacia la cima, está definido por los segmentos C3 (excursión isotópica negativa de carbono de 2.86‰) y C4-C6 (excursión isotópica positiva de carbono de 3.25‰) de Menegatti, y coincide parcialmente con un intervalo de sedimentos enriquecidos en materia orgánica (TOC= 1.13-5.15%) (Fig. 5B) . En la laguna Cupidito, este evento no se asocia con un cambio significativo en la producción carbonatada, pues durante su ocurrencia continuó el mismo modo heterotrófico. La crisis de biocalcificación (acidificación oceánica global) asociada con el segmento isotópico C3 que se registra a nivel mundial, y también durante la transición entre las formaciones Tamaulipas Inferior y la Peña en secciones de cuenca (Cañón Santa Rosa) , no se registra en las facies Cupidito de la sección estudiada. No obstante, es probable que la facies de grainstone de ooides en la parte superior del OAE 1a corresponda con una subsiguiente fase de alcalinidad desarrollada a expensas de la disminución de los niveles de CO_2 por el enterramiento de materia orgánica. Aunque esta fase no ha sido reportada en otras regiones durante el OAE 1a, un mecanismo similar si se ha propuesto para otros OAEs. Esto favoreció la agradación del material carbonatado, sirviendo como un mecanismo de defensa de la plataforma Cupido ante el ahogamiento.

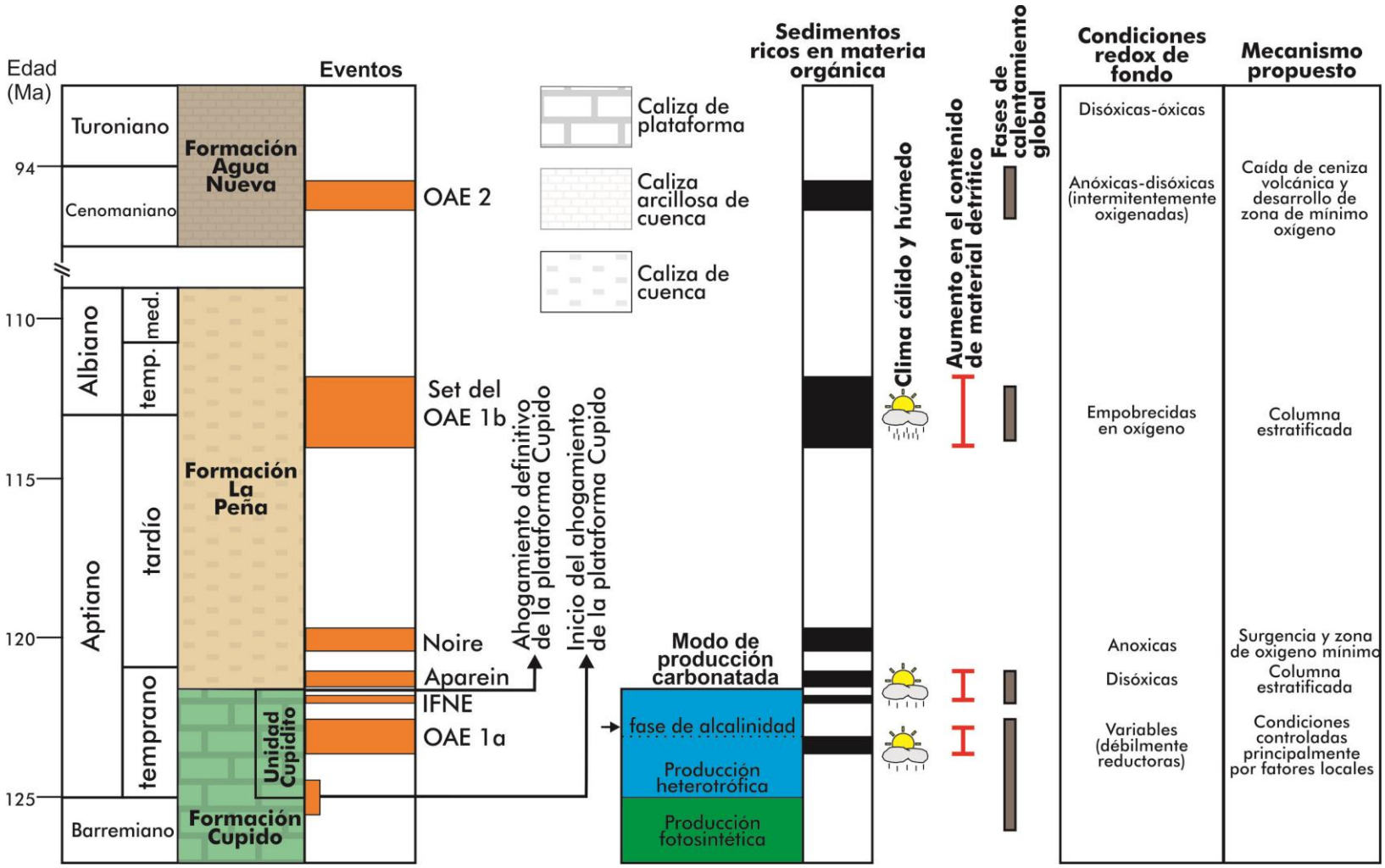

Figura 4. Diagrama sintético que muestra los principales eventos cretácicos de cambio global acelerado identificados en este trabajo, las condiciones paleoambientales y los mecanismos asociados a su desarrollo.

- Antes y durante el desarrollo de la parte baja del OAE 1a es evidente el incremento episódico en el arribo de material detrítico, tal como lo evidencian múltiples incrementos coincidentes en Al, Zr, Ti y K, con una buena correlación (Fig. 5B) . Altos valores de CIA y CIW' sugieren que durante estos intervalos intermitentes tuvo lugar un aumento del intemperismo biogeoquímico en la zona continental bajo condiciones climáticas más cálidas y de mayor humedad, coincidentes con un intervalo de calentamiento global intenso durante el Barremiano tardío-Aptiano temprano. La buena correlación positiva entre las concentraciones de Fe y P con el contenido de Al sugieren que estos elementos biolimitantes fueron suministrados principalmente por el influjo continental durante el depósito de la unidad Cupidito. Una vez incorporados a la superficie marina, estos elementos dispararon la productividad en la superficie marina. Además de este mecanismo local, se sugiere que durante el OAE 1a la introducción al océano de elementos biolimitantes relacionada con la actividad magmática submarina de la Provincia Ígnea de Ontong-Java fue un factor global que influyó en las condiciones de fertilidad. Durante el evento anóxico, el enriquecimiento simultáneo de Mn y otros elementos traza redox-sensibles (U, V, Ni, Cr, Co, Pb, Zn, Cu, Pb, Zn y Mo) , así como la presencia de foraminíferos bentónicos y de niveles bioturbados sugieren que las condiciones redox del fondo de la laguna Cupidito fueron variables y débilmente reductoras. La interfase óxico-anóxica residió principalmente en el sedimento, y durante cortos periodos de tiempo se posicionó cerca de la interfase sedimento-agua. De esta forma, condiciones reductoras propicias para la preservación de materia orgánica prevalecieron principalmente en el sedimento y un régimen óxico-disóxico favorable para la fauna bentónica predominó cerca de la interfase sedimento-agua. Este delicado balance de las condiciones redox estuvo determinado por: (i) el grado de intercambio de oxígeno entre la atmósfera y la superficie marina, (ii) el influjo de material continental y el desarrollo de una superficie de salinidad baja que controló el flujo horizontal de la masa de agua, (iii) la productividad marina y el enterramiento de materia orgánica estacional, y (iv) la restricción de la laguna que reguló el intercambio con el mar abierto y la renovación de oxígeno. Dadas las débiles y fluctuantes condiciones reductoras en la laguna Cupidito, la abundancia de elementos traza redox-sensibles en el intervalo estratigráfico equivalente al OAE 1a parece excesiva. Es posible que esto se deba a una mayor disponibilidad global de estos elementos en el océano, asociada con las erupciones volcánicas de la meseta de Ontong-Java.

- La producción heterotrófica continuó después del OAE 1a; sin embargo, la presencia de fragmentos de rudistas en la parte superior de la unidad Cupidito sugiere que ecosistemas fotosintéticos persistieron en partes internas de la rampa. Este tipo de producción estuvo favorecida por la reducción de las tasas de intemperismo en los periodos fríos y secos, lo que disminuyó los niveles de nutrientes en la superficie marina. Dichos periodos resultaron de la disminución de los niveles de CO_2 relacionados con el enterramiento de materia orgánica durante el evento anóxico. El ahogamiento definitivo de la plataforma Cupido durante el Aptiano temprano tardío estuvo marcado por un incremento periódico en el arribo de material detrítico y nutrientes bajo un clima más cálido

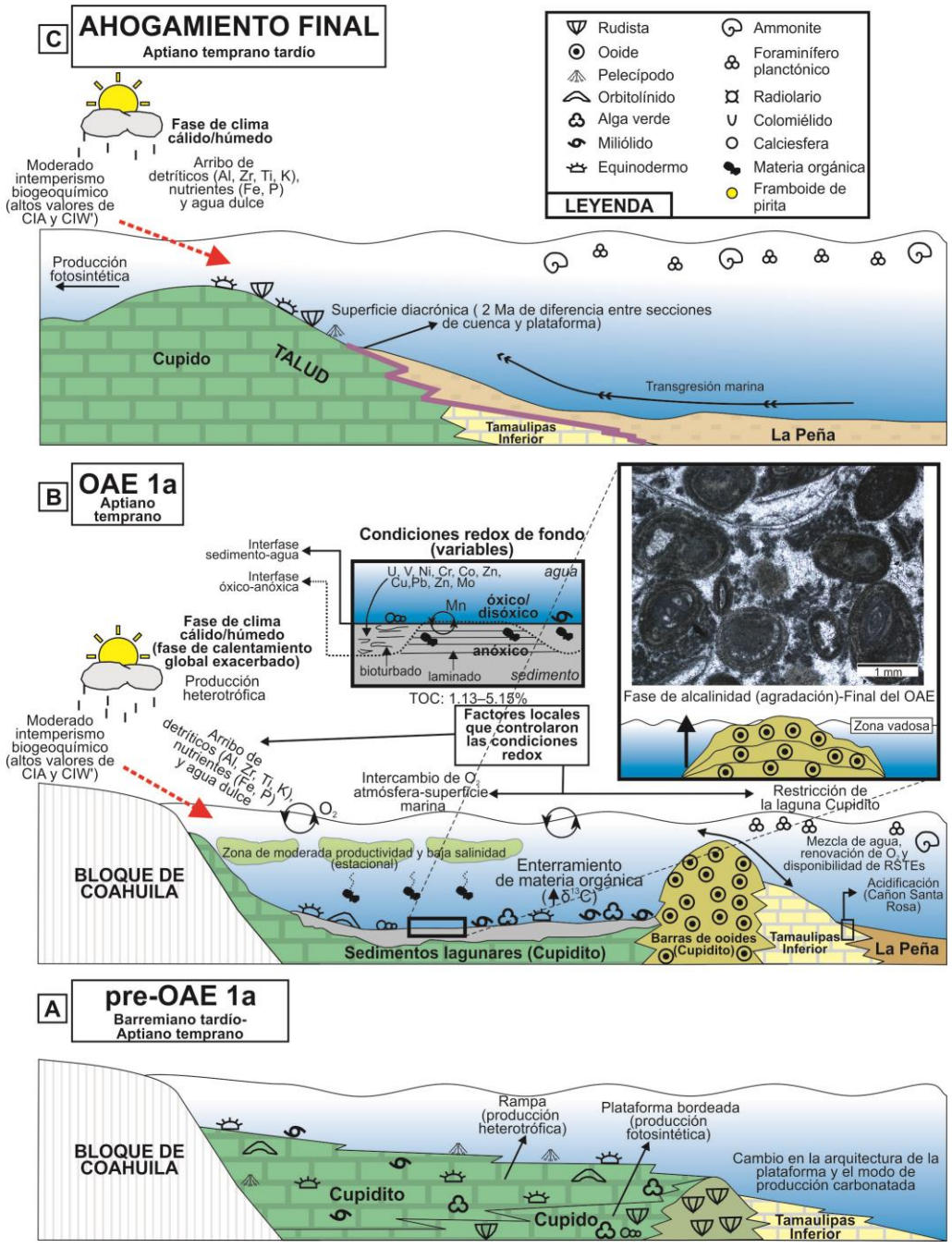

Figura 5. Modelo que resume las condiciones paleoambientales y paleoceanográficas para los distintos eventos documentados en este estudio.

y húmedo, tal como lo demuestra el incremento en el contenido de elementos detríticos (Al, Zr, Ti y K) y los altos valores de CIA y CIW' que persisten en la parte alta y cerca del techo de la unidad Cupidito (Fig. 5C) . Esto concuerda con una fase intensa de calentamiento global durante el Aptiano temprano tardío. Junto a la transgresión marina, el aumento de detritos incrementó las condiciones de estrés de la producción carbonatada y fue un detonante para la desaparición final de la plataforma. El evento de terminación de la

plataforma Cupido fue diacrónico: mientras en secciones estratigráficas de cuenca como el Cañón Santa Rosa ocurrió aproximadamente durante el inicio del OAE 1a, en secciones someras como la PFZ sucedió posteriormente durante la parte alta de la Biozona de amonites *Dufrenoyia furcata*, lo que explica la distinta posición litoestratigráfica del OAE 1a.

- La cima de la Formación Cupido, asignable a la Biozona de amonites *Dufrenoyia furcata*, registra una excursión isotópica negativa de carbono de 0.7‰ dentro del segmento isotópico C7 de Menegatti. Por su posición y amplitud, esta variación es correlacionable con la excursión nombrada en este estudio como Intra-Furcata Negative Excursion (IFNE; Aptiano temprano tardío) . La misma surge de la revisión de la curva isotópica de carbono del Aptiano de varias localidades alrededor del mundo, y corresponde al sub-segmento C7b de la división cuadripartita aquí propuesta del segmento C7 para el Dominio Prebético en España. La IFNE se define como una excursión isotópica negativa menor en la mitad inferior del segmento C7 y correlacionable con la zona de amonites *Dufrenoyia furcata*. Esta se propone como un nuevo marcador quimio-estratigráfico para el Aptiano.

- En la base de la Formación la Peña ocurre un intervalo de aproximadamente 9 m de sedimentos ricos en materia orgánica (TOC de hasta 8.72%) (Fig. 5D) . Por su posición en la parte superior de la Biozona de amonites *Dufrenoyia furcata*, (Aptiano temprano tardío) , este intervalo es equivalente en tiempo con el nivel Aparein (final del Aptiano temprano) reportado en España y otros niveles con alto contenido de TOC documentados en Italia. No obstante, el nivel mexicano difiere de los europeos por su posición respecto a los segmentos isotópicos de carbono de Menegatti: la base de la Formación La Peña se ubica en la transición entre los segmentos C7 y C8, y el nivel Aparein corresponde a una excursión isotópica negativa por encima del segmento C8. Por esto, la correlación entre estos niveles no puede establecerse aún con claridad. En cualquier caso, estos depósitos se enmarcan en una fase de condiciones anóxicas identificada a nivel global luego del OAE 1a, durante el Aptiano temprano tardío. El intervalo en la base de la Formación La Peña corresponde a un episodio de aumento sostenido en el contenido de elementos detríticos (Al, Zr, Ti y K) (Al, Ti y K con una buena correlación) y caracterizado por altos valores de CIA y CIW'. Esto evidencia que su depósito ocurrió durante una fase de condiciones más cálidas y húmedas que empezó desde la cima de la Formación Cupido, coincidente con una fase intensa de calentamiento global durante el Aptiano temprano tardío.

- La distribución de la abundancia de elementos traza redox-sensibles (U, V, Ni, Cr, Co, Pb, Zn, Cu, Pb, Zn y Mo) sugiere que durante el depósito de la base de la Formación La Peña prevalecieron condiciones reductoras poco variables sobre el suelo marino; hecho que también es inferido a partir de la baja y poco variable concentración de Mn y la drástica disminución en la abundancia de foraminíferos bentónicos (Fig. 5D) . Datos de framboides de pirita indican que la interfase óxico-anóxica se localizó dentro del sedimento o cerca de la interfase sedimento-agua, lo que resultó en condiciones disóxicas-anóxicas de fondo propicias para la conservación de la materia orgánica. En este intervalo,

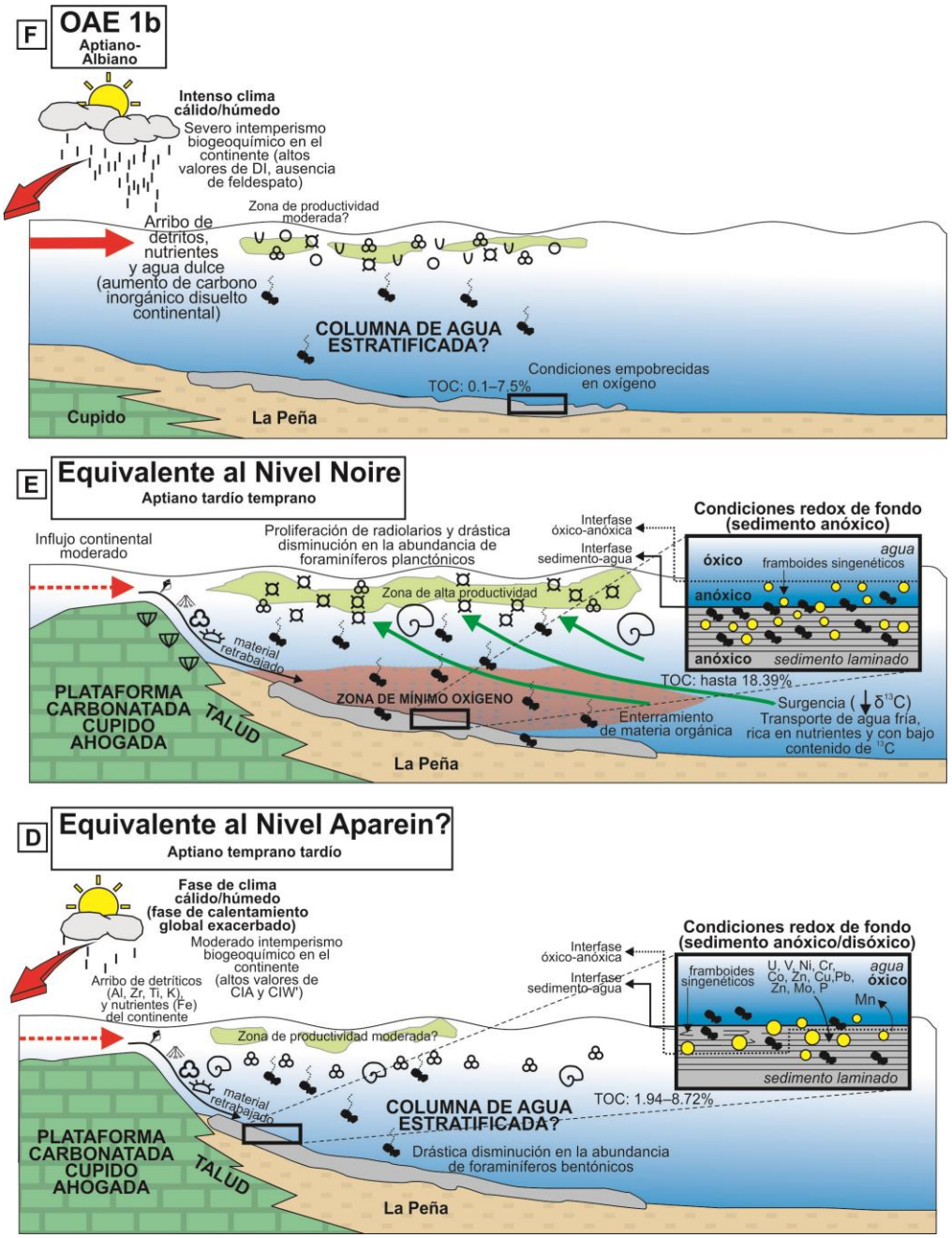

Figura 5. Continuación. Modelo que resume las condiciones paleoambientales y paleoceanográficas para los distintos eventos documentados en este estudio

la correlación positiva entre el contenido de Al y Fe señala que este elemento biolimitante fue introducido a la cuenca marina junto con el material detrítico. Una vez incorporado, el Fe detonó una moderada productividad marina en la superficie que generó materia orgánica autóctona. Por otro lado, la falta de correlación entre el contenido de P y las concentraciones de Al y Fe indican que el fósforo presente en los sedimentos residió principalmente en la fase orgánica, y su abundancia señala la existencia de algún

mecanismo que limitó su reciclaje bajo condiciones reductoras. En este sentido, la estratificación de la columna de agua asociada con el arribo de detritos y agua dulce puede ser invocada como la responsable.

- Coincidiendo con el segmento isotópico C8 de Menegatti y la Biozona de amonites *Epicheloniceras martini* (Aptiano tardío temprano) , hacia la parte inferior de la Formación La Peña se localiza otro intervalo de sedimentos ricos en materia orgánica (TOC de hasta 18.39%) , equivalente en tiempo con el nivel Noire de la Cuenca Vocontiana (Fig. 5E) . Este intervalo se correlaciona con un descenso en los valores isotópicos de carbono, un drástico aumento en la abundancia de radiolarios y una abrupta disminución en el contenido de foraminíferos planctónicos, rasgos que probablemente resultaron de la acción de un sistema de surgencia. Al transportar agua fría enriquecida en nutrientes y con una baja concentración de ^{13}C hacia la superficie, estas corrientes pudieron detonar condiciones eutróficas, elevar la producción de materia orgánica y contribuir a la generación y expansión de una zona de oxígeno mínimo. Puesto que estos sedimentos presentan una abundancia de minerales detríticos similar a la encontrada en los depósitos ricos en materia orgánica de la base de la Formación La Peña, es probable que el arribo de nutrientes desde el continente también haya contribuido, aunque de forma secundaria, a incrementar la fertilidad marina. La diminuta población de framboides de pirita presente en estos sedimentos es típica de condiciones anóxicas, por lo que durante su depósito la interfase óxico-anóxica se ubicó principalmente por debajo de la interfase sedimento-agua.

- Combinando bioestratigrafía de colomiélidos y edades numéricas derivadas de la estratigrafía isotópica de estroncio, se identificó un intervalo hacia la parte media de la Formación La Peña que corresponde a la transición Aptiano-Albiano. Los sedimentos de este intervalo presentan un alto contenido de materia orgánica (TOC= 0.1–7.5%) , y coinciden con una excursión isotópica negativa de carbono (amplitud de 2.09‰) con una duración aproximada de ~3-4 millones de años y que es correlacionable con el set de eventos del OAE 1b. Este es uno de los primero registros detallados de este evento en esta parte del mundo. Internamente, esta excursión exhibe variaciones isotópicas negativas menores que por su amplitud y distribución son comparables con los eventos Jacob, Kilian, Paquier y Leenhardt. La alta concentración de minerales detríticos y los elevados valores de índice detrítico que caracterizan esta parte de la Formación La Peña muestran que su depósito ocurrió bajo condiciones climáticas más cálidas y húmedas (Fig. 5F) . De hecho, la ausencia de feldespatos y la mayor abundancia de filosilicatos en relación a los sedimentos subyacentes de la misma unidad sugieren un régimen climático agresivamente más húmedo y un mayor intemperismo biogeoquímico en la zona continental. Esto evidencia una menor aridez para la zona continental de Norte América que la propuesta anteriormente por otros trabajos. Es probable que durante el OAE 1b el mayor influjo de material continental aumentara la productividad marina y ocasionara la estratificación de la columna de agua y la disminución de los valores isotópicos de carbono. Bajo ese escenario, el enterramiento de materia orgánica pudo ser favorecido por el desarrollo de condiciones empobrecidas en oxigeno sobre el suelo marino asociadas con la estratificación de la columna de agua.

Respecto a la sección de Xilitla (Cuenca Tampico-Misantla) y el registro del OAE 2, los principales resultados son:

- Usando geocronología U-Pb de circones magmáticos procedentes de bentonitas (ver fechamiento adicional en el Anexo A de este capítulo) y bioeventos faunísticos característicos se localizó un intervalo estratigráfico dentro de los sedimentos ricos en materia orgánica marina (TOC= 0.32–3.32%; kerógeno tipo I y II) de la Formación Agua Nueva que contiene la transición Cenomaniano-Turoniano. Además, se identificaron las facies temporalmente equivalentes al OAE 2. Dada la alteración de la señal isotópica de carbono que presentan los sedimentos de esta unidad, el reconocimiento del cambio en la abundancia de los heterohelícidos y del evento de filamentos por primera vez en México fue clave para ubicar el evento anóxico. Junto con la última aparición de *Rotalipora cushmani* (Morrow) y la primera aparición de *Helvetoglobotruncana helvetica* (Bolli) , estos bioeventos sugieren la existencia de conexiones de la Cuenca Mesozoica del Centro de México con el proto-Atlántico Norte abierto y el Mar Interior Occidental.

- Parte del intervalo que corresponde al OAE 2 se caracteriza por la presencia más regular de facies sedimentarias asociadas con condiciones anóxicas y disóxicas, los contenidos más altos de materia orgánica (TOC hasta 3.32%) y las concentraciones más elevadas de varios elementos traza redox-sensibles (Cd, Zn, V, Cr, Cu, U, Re, Ba y Ba biogénico) y las más bajas de Mn (Fig. 5G) . Sin embargo, la presencia de niveles bioturbados con foraminíferos bentónicos (facies asociadas a condiciones oxigenadas) indica que las condiciones redox de fondo, aunque en general empobrecidas en oxígeno, fueron más dinámicas. Estos eventos intermitentes de oxigenación han sido reportados en otras partes del mundo dentro del OAE 2; sin embargo, si se compara con otras cuencas, el registro redox del evento anóxico a nivel global es bastante variable (desde totalmente oxigenado a severamente anóxico-euxínico) , lo que sugiere una fuerte influencia de las condiciones locales sobre las condiciones de oxigenación. El empobrecimiento en oxígeno sobre el suelo oceánico fue menos severo y más variable durante la parte final del OAE 2 y posterior a él, tal como lo evidencia la mayor presencia de facies oxigenadas, el decremento en la concentración de TOC y elementos traza redox-sensible y el aumento en el contenido de Mn y P. Condiciones post-OAE 2 similares a estas han sido documentadas también en otras partes de México.

- Varios indicadores geoquímicos (contenido de P y Ba biogénico y valores anómalos de la relación TOC/N_{TOT} para sedimentos con materia orgánica marina) y paleontológicos (abundancia de filamentos e intervalos dominados por radiolarios) sugieren que una alta productividad en la superficie marina tuvo lugar durante el depósito de la Formación Agua Nueva, particularmente durante el OAE 2. Estas condiciones de fertilidad marina se asociaron con la introducción de elementos biolimitantes derivados de la caída de ceniza volcánica en la cuenca y probablemente de la construcción de la Provincia Ígnea del Caribe. Usando los indicadores estudiados se propone un modelo

paleoceanográfico similar al de las zonas de surgencia actuales (Fig. 5G) . En este, condiciones eutróficas en la superficie marina originaron el desarrollo de una zona de oxígeno mínimo. Variaciones en la productividad superficial y en el enterramiento de materia orgánica marina controlaron el régimen episódicamente disaeróbico sobre el suelo marino. Condiciones de fondo anóxicas, disóxicas y óxicas, determinadas por la fluctuación entre la posición de las interfases sedimento-agua y óxico-anóxica, fijaron la fábrica del sedimento, el tipo de organismo presente, la formación de minerales diagenéticos y singenéticos y la tasa de preservación de la materia orgánica y de enterramiento de elementos redox-sensibles.

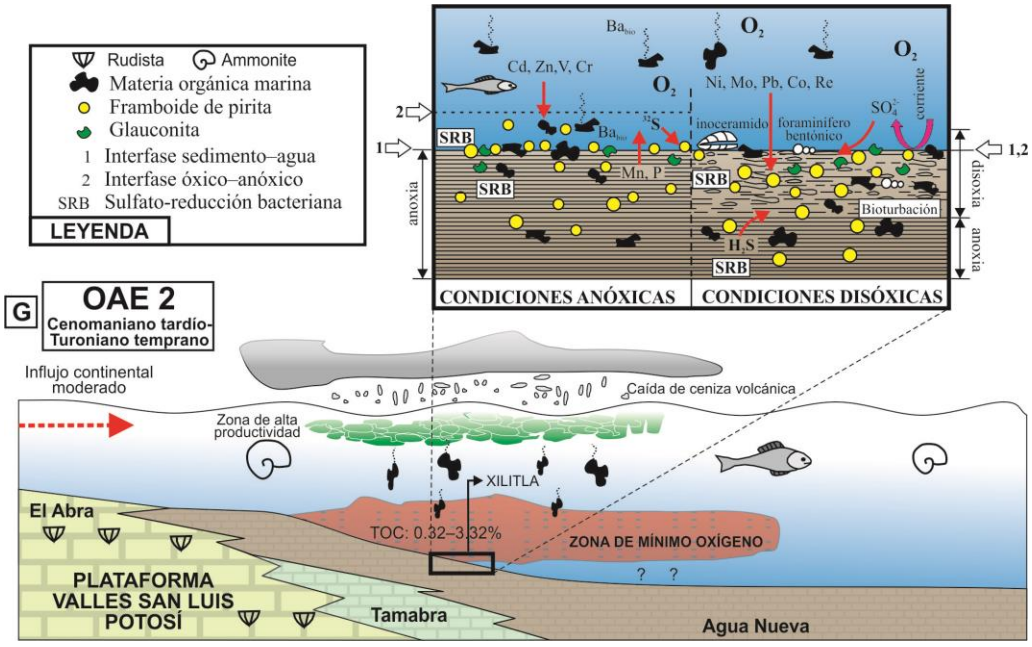

Figura 5. Continuación. Modelo que resume las condiciones paleoambientales y paleoceanográficas para los distintos eventos documentados en este estudio

- El fraccionamiento isotópico de azufre indica que la formación de pirita en los sedimentos de la Formación Agua Nueva tuvo lugar mediante sulfato-reducción bacteriana y probablemente a través del reciclaje de azufre. Este último proceso pudo estar favorecido por la bioturbación y las corrientes de fondo. La acción bacteriana es confirmada mediante el hallazgo de una membrana carbonosa alrededor de los microcristales y de los framboides de pirita. Esta representa el remanente del material extracelular producido durante la formación de los framboides. Al igual que en otras secciones alrededor del mundo, los valores isotópicos de azufre son mínimos dentro del OAE 2 y posteriormente aumentan de forman gradual, hecho que sugiere la acción de un mecanismo global que controló la señal isotópica del azufre durante el evento anóxico. Esto podría estar relacionado con la mayor disponibilidad de sulfato en el océano global que resultó de la liberación de azufre durante el vulcanismo submarino de la meseta del Caribe.

CONCLUSIONES GENERALES

- Mediante un estudio multidisciplinario, en este trabajo se documentan los intervalos equivalentes al OAE 1a (Aptiano temprano) y al evento IFNE (Aptiano temprano tardío; propuesto como un nuevo marcador quimio-estratigráfico para el Aptiano) en la unidad Cupidito, así como uno correlacionable aparentemente con el nivel Aparein (Aptiano temprano tardío) y otros correspondientes al nivel Noire (Aptiano tardío temprano) y al OAE 1b (Aptiano-Albiano) dentro de la Formación La Peña. En el centro de México, en la Cuenca de Tampico-Misantla se registra el intervalo equivalente al OAE 2 (Cenomaniano-Turoniano) dentro de la Formación Agua Nueva. Estos intervalos coindicen con sedimentos enriquecidos en materia orgánica.

- Durante la fase previa e inicial del OAE 1a y el depósito de los intervalos equivalentes al probable nivel Aparein y al OAE 1b condiciones globales de calentamiento global establecieron un clima más húmedo y cálido en el norte de México, que incrementó la tasas de intemperismo biogeoquímico en la zona continental, la escorrentía superficial, el arribo de nutrientes a las cuenca marina y la productividad. Por otro lado, el depósito del intervalo equivalente al nivel Noire tuvo lugar bajo la acción de un sistema local de surgencia que incrementó la fertilidad marina. El OAE 2 en el centro del país tuvo lugar durante una fase de actividad volcánica, y la caída de ceniza volcánica estimuló la productividad. Tanto el registro del OAE 1b como el del OAE 2 fueron aparentemente influenciados por las enorme erupciones volcánicas submarinas asociadas a las Grandes Provincias Ígneas.

- Las condiciones redox de fondo de la laguna Cupidito fueron variables y débilmente reductoras, durante el OAE 1a (principalmente anóxicas en el sedimento, y óxico-disóxicas en la interfase-sedimento agua) , controladas principalmente por factores locales. Para el probable nivel Aparein y el nivel Noire se evidenciaron condiciones de fondo disóxicas y anóxicas, respectivamente. Estancamiento de la columna de agua y expansión de una zona de oxígeno mínimo se proponen como los mecanismos responsables de dichas condiciones en cada caso. Un régimen empobrecido en oxígeno, asociado con la estratificación de la columna de agua, también prevaleció en la interfase-sedimento agua durante el OAE 1b. Durante el OAE 2, la productividad marina de la Cuenca de Tampico-Misantla fue el factor que determinó las condiciones de oxigenación de fondo, asociadas al desarrollo de una zona de mínimo oxígeno. Estas fueron principalmente anóxicas y disóxicas (con intervalos oxigenados cortos) durante el inicio de evento y menos reductoras durante la parte final y luego de su ocurrencia.

Anexo A (Capítulo 7).
Análisis adicional de U-Pb en circones detríticos.

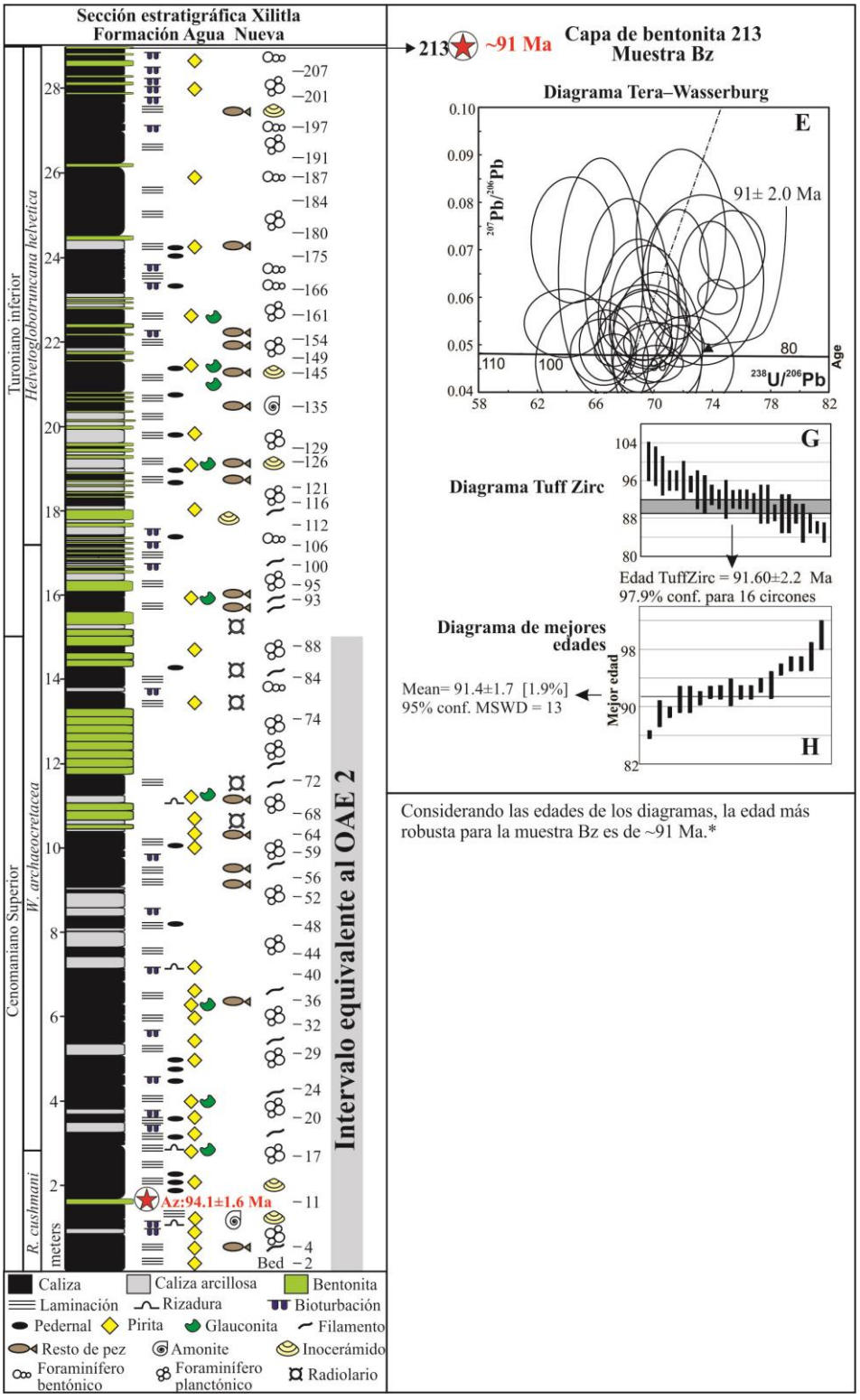

Anexo A (Capítulo 7).

Análisis LA-ICP-MS de los circones volcánicos de la muestra de bentonita Bz (capa 213).

	CORRECTED RATIOS												CORRECTED AGES (Myr)										
	U (pp	Th (ppm)	Th/ U	$^{207}Pb/^{206}Pb$	±1s	$^{207}Pb/^{235}U$	±1s	$^{206}Pb/^{238}U$	±1s	$^{208}Pb/^{232}Th$	±1s	Rho	$^{206}Pb/^{238}U$	±1s	$^{207}Pb/^{235}U$	± 1s	$^{207}Pb/^{206}Pb$	±1s	$^{208}Pb/^{232}Th$	± 1s	Best age	±1s	disc %
Zircon_05_013	1485	2714	1.61	0.0601	0.0015	0.1111	0.0029	0.01	0.0001	0.0042	0.0001	0.3	86.1	0.6	107	3	608	48	86	2	86	0.6	19.5
Zircon_18_029	403	586	1.28	0.0461	0.0041	0.0879	0.0088	0.01	0.00024	0.0044	0.00013	0.32	89	2	86	8	5	182	89	3	89	2	-3.5
Zircon_15_025	859	1097	1.13	0.0498	0.0018	0.0958	0.0036	0.01	0.00013	0.0044	0.00011	0.27	89.2	0.8	93	3	187	81	89	2	89	0.8	4.1
Zircon_22_034	249	135	0.48	0.0461	0.0035	0.0906	0.0075	0.01	0.00025	0.0046	0.00029	0.25	91	2	88	7	5	156	92	6	91	2	-3.4
Zircon_29_042	225	130	0.51	0.0485	0.0069	0.0953	0.0143	0.01	0.00026	0.0045	0.00043	0.24	91	2	92	13	125	269	91	9	91	2	1.1
Zircon_19_030	677	624	0.81	0.0461	0.0016	0.0905	0.0035	0.01	0.00015	0.0046	0.00011	0.27	91.2	1	88	3	2	67	93	2	91	1	-3.6
Zircon_28_041	771	1027	1.17	0.0503	0.002	0.0996	0.004	0.01	0.00014	0.0045	0.00011	0.25	92	0.9	96	4	208	88	91	2	92	0.9	4.2
Zircon_06_015	241	203	0.74	0.0533	0.0034	0.1035	0.0067	0.01	0.00023	0.0045	0.00016	0.24	92	1	100	6	341	129	90	3	92	1	8
Zircon_01_A_009	143	77	0.47	0.0548	0.0032	0.1083	0.0067	0.01	0.00026	0.005	0.00018	0.3	92	2	104	6	404	119	100	4	92	2	11.5
Zircon_14_024	201	112	0.49	0.0543	0.0031	0.1077	0.0063	0.01	0.00017	0.0045	0.00019	0.21	92	1	104	6	382	115	91	4	92	1	11.5
Zircon_26_039	244	169	0.61	0.0565	0.0059	0.112	0.0124	0.01	0.00022	0.0045	0.0001	0.2	92	1	108	11	472	230	90	2	92	1	14.8
Zircon_17_028	174	164	0.83	0.0511	0.0029	0.1024	0.006	0.01	0.00022	0.0045	0.00017	0.26	93	1	99	6	245	127	92	3	93	1	6.1
Zircon_27_040	876	1201	1.21	0.0562	0.0066	0.1125	0.0142	0.01	0.00024	0.0045	0.00008	0.18	93	2	108	13	461	253	91	2	93	2	13.9
Zircon_13_023	1133	623	0.48	0.0489	0.0014	0.1	0.0029	0.01	0.00012	0.0049	0.00013	0.27	95.2	0.8	97	3	144	59	98	3	95	0.8	1.9
Zircon_11_021	340	309	0.8	0.0486	0.0028	0.1006	0.0067	0.02	0.00021	0.0048	0.00008	0.31	96	1	97	6	126	117	96	2	96	1	1
Zircon_23_035	288	256	0.79	0.0499	0.003	0.1033	0.0068	0.02	0.00016	0.0047	0.00007	0.19	96	1	100	6	192	135	96	1	96	1	4
Zircon_03_011	528	743	1.24	0.0463	0.0055	0.0971	0.0132	0.02	0.00036	0.0049	0.00017	0.47	97	2	94	12	13	211	98	3	97	2	-3.2
Zircon_08_017	265	172	0.57	0.0546	0.003	0.1176	0.0067	0.02	0.00028	0.0056	0.00022	0.32	100	2	113	6	395	110	112	4	100	2	11.5
Zircon_21_033	188	114	0.54	0.0618	0.0078	0.125	0.0167	0.01	0.00025	0.0045	0.0001	0.2	94	2	120	15	666	273	91	2	94	2	21.7
Zircon_25_037	933	1622	1.53	0.0631	0.0053	0.1177	0.011	0.01	0.00017	0.0042	0.00004	0.31	87	1	113	10	711	179	83.8	0.	87	1	23
Zircon_20_031	2341	5945	2.24	0.0637	0.0073	0.1198	0.0161	0.01	0.00032	0.0042	0.00006	0.48	87	2	115	15	732	245	84	1	87	2	24.3
Zircon_02_010	215	122	0.5	0.0646	0.0102	0.1342	0.0223	0.02	0.00027	0.0046	0.00013	0.29	96	2	128	20	761	307	93	3	96	2	25
Zircon_12_022	224	147	0.58	0.0649	0.0056	0.1249	0.0114	0.01	0.00017	0.0043	0.00006	0.25	89	1	120	10	772	164	86	1	89	1	25.8
Zircon_09_018	791	1775	1.98	0.0701	0.0034	0.1283	0.0064	0.01	0.00016	0.0043	0.00018	0.25	85	1	123	6	930	89	87	4	85	1	30.9
Zircon_24_036	193	118	0.54	0.0721	0.0054	0.1574	0.0121	0.02	0.00028	0.0074	0.0005	0.23	99	2	148	11	990	151	148	10	99	2	33.1
Zircon_04_012	209	174	0.73	0.0735	0.0073	0.141	0.0152	0.01	0.00024	0.0042	0.00008	0.35	89	2	134	14	1027	183	85	2	89	2	33.6

*The bentonite sample was crushed and separated granulometrically. Separation of heavy minerals was carried out using a Wilfley Table, and then a Franz Magnetic separator at the Instituto de Geología (UNAM). Euhedral zircon crystals were hand-picked and then mounted in epoxy, sanded and polished to expose a transverse section. They were photographed using reflected light and scanning electron microscope-cathodoluminescence (SEM-CL) in order to select homogenous grains and avoid the detection of inherited ages by core relicts.